Y 3. At 7:
36/7-4

POWER REACTOR TECHNOLOGY

A Quarterly Technical Progress Review

Prepared for DIVISION OF TECHNICAL INFORMATION, USAEC, by
W. H. ZINN and J. R. DIETRICH, GENERAL NUCLEAR ENGINEERING CORPORATION

ILLINOIS STATE LIBRARY
NOV 30 1964

Fall 1964

● VOLUME 7

● NUMBER 4

TECHNICAL PROGRESS REVIEWS

To meet the needs of industry for concise summaries of current atomic developments, the Atomic Energy Commission is publishing this series, Technical Progress Reviews. Issued quarterly, each of the reviews digests and evaluates the latest findings in a specific area of nuclear technology and science.

The five journals published in this series are:

Isotopes and Radiation Technology, P. S. Baker, A. F. Rupp, and associates, Oak Ridge National Laboratory

Nuclear Safety, Wm. B. Cottrell, W. H. Jordan, and associates, Oak Ridge National Laboratory

Power Reactor Technology, W. H. Zinn and J. R. Dietrich, General Nuclear Engineering Corporation

Reactor Fuel Processing, Stephen Lawroski and associates, Chemical Engineering Division, Argonne National Laboratory

Reactor Materials, R. W. Dayton, E. M. Simons, and associates, Battelle Memorial Institute

Each journal may be purchased from the Superintendent of Documents, U. S. Government Printing Office, Washington, D. C., 20402. *Isotopes and Radiation Technology* at $2.00 per year for subscription or $0.55 for individual issues; the other four journals at $2.50 per year and $0.70 per issue. See back cover for remittance instructions and foreign postage requirements.

The views expressed in this publication do not necessarily represent those of the United States Atomic Energy Commission, its divisions or offices, or of any Commission advisory committee or contractor.

Availability of Reports Cited in This Review

Unclassified AEC reports are available for inspection at AEC depository libraries and are sold by the Office of Technical Services, Department of Commerce, Washington, D. C., 20230. Some of the reports cited are not available owing to their preliminary nature; however, the information contained in them will eventually be made available in formal progress or topical reports.

Unclassified reports issued by other Government agencies or private organizations should be requested from the originator.

Unclassified British and Canadian reports may be inspected at AEC depository libraries. British reports are sold by the British Information Service, 45 Rockefeller Plaza, New York, N. Y.; Canadian reports (AECL series) are sold by the Scientific Document Distribution Office, Atomic Energy of Canada, Ltd., Chalk River, Ontario, Canada.

Classified U. S. and foreign reports identified in this journal as Classified may be purchased by properly cleared Access Permit Holders from the Division of Technical Information Extension, U. S. Atomic Energy Commission, P. O. Box 1001, Oak Ridge, Tenn., 37831. Such reports may be inspected at classified AEC depository libraries.

POWER REACTOR TECHNOLOGY

A REVIEW OF RECENT DEVELOPMENTS

Prepared for DIVISION OF TECHNICAL INFORMATION, USAEC,
by W. H. ZINN and J. R. DIETRICH,
GENERAL NUCLEAR ENGINEERING CORPORATION

FALL 1964

VOLUME 7

NUMBER 4

Foreword

This quarterly review of reactor development has been prepared at the request of the Division of Technical Information of the U. S. Atomic Energy Commission. Its purpose is to assist interested organizations in the task of keeping abreast of new results in reactor technology for civilian application.

Power Reactor Technology contains reviews of selected recently published reports that are judged noteworthy in the fields of power-reactor research and development, power-reactor applications, design practice, and operating experience. It is not meant to be a comprehensive abstract of all material published during the quarter, nor is it meant to be a treatise on any part of the subject. However, related reports from different sources are often treated together to yield reviews having some breadth of scope, and background material may be added to place recent developments in perspective. Occasionally the reviews are written by guest authors. Reviews having unusual breadth or significance are placed at the front of the issue as Feature Articles.

The intention is to cover the various areas of reactor development from the general viewpoint of the reactor designer rather than from the more detailed points of view of specialists in the individual areas. To whatever extent the coverage of *Power Reactor Technology* may occasionally overlap the fields of the other Technical Progress Reviews, the overlaps will be motivated by this objective of viewing current progress through the eyes of the reactor designer.

A degree of critical appraisal and some interpretation of results are often necessary to define the significance of reported work. Any such appraisal or interpretation represents only the opinion of the reviewer and (in the usual case, when the review is written by General Nuclear Engineering Corporation staff) the Editor. When the review is predominantly interpretive the reviewer is named; unless identified as a guest author, he is a member of the General Nuclear Engineering Corporation staff. Readers are urged to consult the original references to obtain all the background of the work reported and to obtain the interpretation of the results given by the original authors.

For timely coverage, *Power Reactor Technology* must often review fragmentary material. The fixed subject headings listed below have been adopted in the hope of maintaining some continuity and order in the material from one issue to another: all reviews except Feature Articles will be arranged under these headings. A particular issue will not necessarily contain all the headings but only those under which material is reviewed.

Economics, Applications, Programs
Resources and Fuel Cycles
Physics
Fluid and Thermal Technology
Fuel Elements
Materials
Control and Dynamics
Containment, Radiation Control, and Siting
Systems Technology
Components
Design and Construction Practice
Operating Experience
Specific Reactor Types
Specific Applications
Unconventional Approaches

W. H. Zinn, President
J. R. Dietrich, Vice-President and Editor
General Nuclear Engineering Corporation

Contents

Foreword

I Physics 329
Doppler Effect 329
Control-Rod Programming 330
Short Notes 331
References 333

II Fluid and Thermal Technology . . 335
Burnout in Steam-Water Mixtures . . 335
References 352

III Fuel Elements 354
Stainless-Steel-Cladding Failures in VBWR 354
Fission-Product Helium 355
Steel-Lined Zircaloy-2-Clad Fuel Elements 356
Boron-Containing Fuel Elements . . 356
Electron-Beam Welding 358
Irradiation Effects in UO_2 359
References 363

IV Materials 365
Boron for Control Rods 365
Transition Joints of Zircaloy to Stainless Steel 368
References 369

V Containment, Radiation Control, and Siting 370
Effect of Fission-Product Release . . 370
Effect of Temperature on Fission-Product Deposition 371
References 371

VI Components 372
Pumps 372
Heat Exchangers 374
References 375

VII Design and Construction Practice 376
EGCR Control Rods 376
SRE Rod Drop-Time Measurement . . 377
Pressure-Tube Reactor Components . 379
Systems Design 384
References 384

VIII Operating Experience 385
Moderator-Level Control 385
References 399

IX Specific Reactor Types 401
Heavy-Water Reactors 401
Pressurized-Water Reactors: Chemical Shim 411
Pressurized-Water Reactors: Natural-Circulation Startup 421
Pressurized-Water Reactors: The Large Power Reactor Program . . 422
References 431

Index, Volume 7 433

Issued quarterly by the U. S. Atomic Energy Commission. Use of funds for printing this publication approved by the Director of the Bureau of the Budget on October 14, 1963.

Y 3.At 7:
36/7-4

Section

I

Power Reactor Technology

Physics

Doppler Effect

Results of recent transient tests on oxide-fueled cores in the SPERT reactor[1,2] have proved the efficacy of the Doppler effect — more specifically the Doppler broadening of neutron-absorption resonances — as a shutdown agency in the event of accidental power excursions. The phenomenon is, of course, important only if strong resonance absorption is present in the reactor (usually absorption by a fertile isotope, ^{238}U, or thorium) and if the substantial increase of fuel temperature which is necessary to increase the Doppler broadening by a significant amount can be tolerated. The slightly enriched oxide fuels usually meet the requirements. However, even with these fuels the temperature margin available for Doppler shutdown may not be large if the hypothetical accident occurs when the reactor is already operating at a power level high enough to cause fuel temperatures near the permissible limit. For this reason, the evaluation of the Doppler effect as a protective mechanism in practical cases requires considerable attention to detail and particular attention to the evaluation of the effects of temperature distribution — both the gross distribution from fuel element to fuel element and the local distribution within individual elements — on the amount of reactivity compensation available before destructive temperatures are reached. Similar considerations of detail are involved in the evaluation of the Doppler contribution to the power coefficient of reactivity.

Recent work that is applicable to practical Doppler evaluations is reported in Refs. 3 and 4. References 5 to 36 constitute a short bibliography of background material on the Doppler effect and related questions of resonance absorption in thermal and fast reactors.

Reference 1 describes the detailed mathematical methods developed for analysis of temperature effects on the Doppler coefficient of reactivity and the resonance capture probability, including the important cases of a nonuniform temperature distribution in fuel rods arrayed in a reactor lattice. The analytical techniques used for solution of this problem consist in: (1) transformation of the Boltzmann equation, which describes the steady-state transport of neutrons, into an integral equation whose solution can be expressed as a Neumann series; and (2) establishment of a relation between Monte Carlo histories and the Neumann series to determine the proper form for the random variables that depend on the paths of the neutron histories. By application of this technique, it is possible to evaluate the various reactor parameters and their derivatives, e.g., the Doppler coefficient, by a new and direct method that has not been utilized before.

On the basis of the new method, a computer program, REPAD, was written for a cylindrical lattice cell containing a centrally located cylindrical fuel rod with an arbitrary radial temperature distribution. Several specific cases for different fuel temperatures were investigated with REPAD, using water moderator and UO_2 fuel; both uniform and radially parabolic fuel-temperature distributions were treated. For each case, 12,000 histories were used. Running time on the IBM-709 is about 0.01 min per history for uniform fuel temperature and 0.02 min per history for nonuniform fuel temperature. In the latter case, 24 temperature regions in the fuel were used.

In the interpretation of the specific results obtained in the investigation, it is instructive to define

$$T_{av} = \frac{T_s + T_p}{2}$$

and $$T_{rm} = \left(\frac{\sqrt{T_s} + \sqrt{T_p}}{2}\right)^2$$

where T_s is the surface temperature and T_p is the peak temperature at the center line of the fuel rod. Also, an effective temperature, T_{eff}, is defined as that spatially constant fuel temperature which gives the same value of the reactor parameter (in this case the Doppler coefficient of reactivity or the resonance capture probability) as obtained for a parabolic temperature distribution in the fuel. It is not expected that T_{eff} for the resonance capture probability $(1-p)$ will be the same as T_{eff} for the Doppler coefficient of reactivity, $(1/p)(\partial p/\partial T)$. Values of T_{eff} calculated for two cases of parabolic fuel-temperature distribution are tabulated as follows:

T_s, °K	T_p, °K	T_p/T_s	T_{av}, °K	T_{rm}, °K	T_{eff}, °K
840	2800	3.34	1820	1670	1520 for $(1-p)$ 1400 for $(1/p)(\partial p/\partial T)$
1820	3780	2.08	2800	2720	2730 for $(1-p)$ 2800 for $(1/p)(\partial p/\partial T)$

For the higher temperature case, the parabolic temperature distribution can be characterized by the average temperature, because T_{av}, T_{rm}, and T_{eff} appear to give the same values of $(1-p)$ and $(1/p)(\partial p/\partial T)$ within the limits of statistical error. However, for the lower temperature run, which corresponds more nearly to practical operating fuel temperatures in a power reactor, the average temperature is a poorer approximation to the effective temperature. Use of the average temperature to characterize the parabolic distribution would, in this case, cause the following errors:

T_s, °K	T_p, °K	Parameter	Percentage error caused by replacing T_{eff} with: T_{av}	T_{rm}
840	2800	$(1-p)$	1.7	1.0
		$(1/p)(\partial p/\partial T)$	−9.0	−6.5

A qualitative explanation in Ref. 3 gives reasons why the average temperature appears to be a much better approximation to the effective temperature for the case at the higher temperatures.

Tabular data of the Doppler-broadened neutron cross sections of ^{241}Pu below 11 ev are given in Ref. 4 for temperatures ranging from 27 to 3000°C. The capture, fission, and scattering cross sections represent theoretical predictions based on the resonance parameters obtained from a multilevel analysis of the ^{241}Pu total cross sections. The total cross-section data fitted in the analysis are those measured by Simpson and Schuman in 1960, as tabulated in Ref. 37. More recent measurements of the fission cross section of ^{241}Pu by T. Watanabe and O. D. Simpson [*Phys. Rev.* (to be published)] and of the total cross section of ^{241}Pu by N. J. Pattenden and by D. S. Craig and C. H. Westcott (unpublished) indicate that the older data of Simpson and Schuman, which were fitted in the analysis, are not accurate over the peaks of the narrow resonances. For the fission cross section, the recent fission measurements indicate that the theoretical fission data, i.e., as predicted from the total cross-section data, are in agreement with the experimental fission data to the order of 10 to 20%. No experimental data are available to enable a similar comparison for the capture and scattering cross sections of ^{241}Pu.

Control-Rod Programming

Calculational work performed in obtaining a control-rod program for a large multiregion core of the pressurized-water reactor type is summarized in Ref. 38. The purpose was to predict the limitations on power when a given group of control rods is moved or to ascertain which control rods can be moved when the maximum reactor power is limited to a given value. The control rods are arranged in subgroups that can be moved independently, and there are many different orders in which the subgroups can be withdrawn. However, the rod-withdrawal programs considered involved only sequential withdrawals from one rod pattern to a successive pattern in such a way that any rod, once withdrawn from the core, need never be inserted again.

The core used as a model for the study was an 8-ft-diameter 3-region core. It was loaded

nonuniformly in the radial direction to give the most uniform radial power distribution when chemical shim was used for control. The additional restriction was imposed that the ^{235}U loading used be the greatest that could be controlled by movable cruciform control rods. This method of choosing the loading for the chemical-shim core was employed to provide a backup to the chemical-shim control concept in the event that movable control rods would be necessary for reactor operation. For the case of the core controlled by movable control rods, two concepts were studied: (1) partial control by chemical shim and 44 movable control rods, and (2) control by 44 movable control rods plus 8 fixed shims.

In the development of a suitable rod-withdrawal program, consideration was given to the restrictions imposed by the limiting peak-to-average power-density ratio in the core corresponding to full-power rating. A restriction imposed upon the rod-withdrawal program is that the nuclear radial peak-to-average power-density ratio must never exceed 2.30. The resulting permissible axial power distribution then imposes the restriction that the worth of any rod subgroup used cannot be greater than 2.5%; otherwise the perturbation of the axial power distribution would restrict the power capability of the core.

Reference 4 describes the method of analysis and results obtained in arriving at a control-rod-withdrawal program (with partial chemical shim and fixed shims) which satisfies restrictions and considerations imposed as basic ground rules for the study. First, the number of control rods needed to shut down the reactor is determined for the case in which the most reactive rod is stuck in its fully withdrawn position. Various orders of rod withdrawal are then investigated, and the two-dimensional power distributions are compared to obtain the most desirable ratio of peak-to-average power. Effects on power distribution of nonuniform build-up of plutonium and fission products and of fuel depletion are not considered. The rod-withdrawal program resulting from the study is displayed in Fig. I-1. Also given are the reactivity associated with each control-rod subgroup that is withdrawn (k) and the radial power-peaking factor associated with the pattern of rods remaining in the core (F). Figure I-1 applies to control by 44 movable control rods plus chemical shim for equilibrium xenon. If control were effected by 44 rods and 8 fixed shims, reactivities would be about 3% higher than values shown in Fig. I-1. When operating with fixed shims, the vessel would be opened when the 16-rod pattern was reached for removal of the shims. After shim removal 44 rods would be employed for control.

Short Notes

Results of a survey of experimental cross sections and other nuclear data for zirconium are presented in Ref. 39. The sources of information are given, and the interpretations made to produce a tabulation of nuclear data for use in neutronic calculations are described.

Measurements in water of the age of fission neutrons to indium resonance energy (1.46 ev) are described in Ref. 40. The measurements utilized a finite plane fission source and essentially infinite plane detectors so as to be equivalent to a measurement using axial detectors and an infinite plane source. The advantage of this experimental approach is that the measured results do not require calculated corrections to extrapolate to infinite source geometry, as is the case in measurements using axial detectors with a finite plane or point source. The remaining corrections to the data are small and well understoood. The reference describes the details of the experimental setup, experimental procedures, and methods of data reduction. The fission-neutron age measured in the experiment (to 1.46 ev) was 26.45 ± 0.32 cm^2 at a water density of 1.0 g/ml. For comparison, the comparable calculated age is given, as obtained with the Monte Carlo computer code TYCHE[41] which includes the effects of both inelastic scattering and anisotropic elastic scattering in oxygen. The calculated age is 25.62 ± 0.24 cm^2.

A review of neutron thermalization in Ref. 42 describes briefly the various techniques developed, their relation to one another, and their applications. Emphasis is placed on those aspects which are closely related to reactor design and, since digital computer codes are frequently used, to the numerical methods and codes that have been developed. The individual methods are surveyed in just sufficient detail to reveal the essential physics or the key to each method. An extensive bibliography is included, and it covers specific topics related to the neutron thermalization problem.

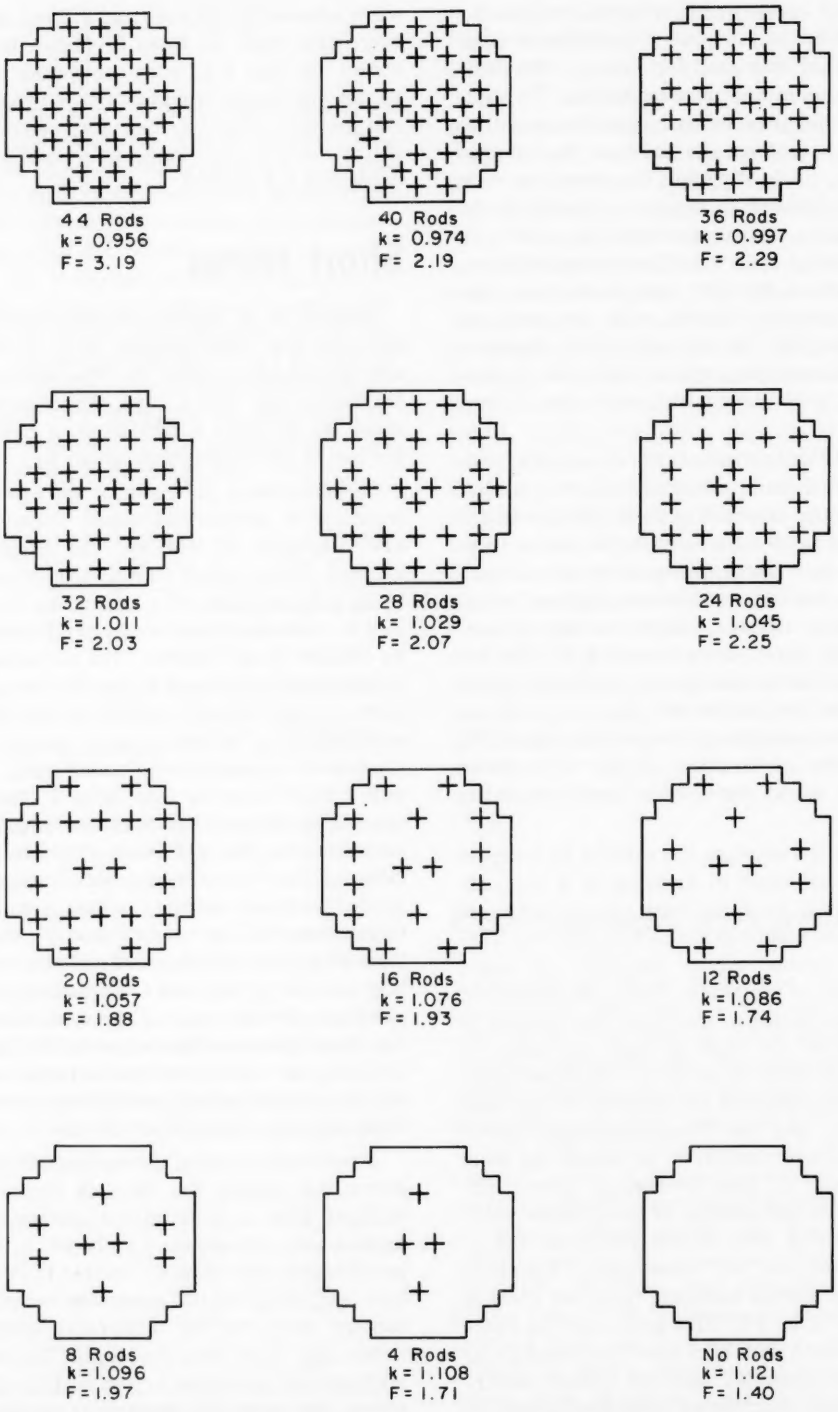

Fig. I-1 Control-rod-withdrawal program.[6] Here k is the neutron multiplication factor, hot at zero power, with boron to control the equilibrium xenon swing, and F is the radial peak-to-average power factor.

References

1. A. H. Spano, Self-Limiting Power Excursion Tests of a Water-Moderated Low-Enrichment UO_2 Core, *Nucl. Sci. Eng.*, 15(1): 37 (January 1963).
2. A. H. Spano, J. E. Barry, L. A. Stephan, and J. C. Young, Self-Limiting Power Excursion Tests of a Water-Moderated Low-Enrichment UO_2 Core in SPERT I, USAEC Report IDO-16751, Phillips Petroleum Co., 1962.
3. J. E. Olhoeft, The Doppler Effect for a Non-Uniform Temperature Distribution in Reactor Fuel Elements, USAEC Report WCAP-2048, Westinghouse Electric Corp., Atomic Power Division, July 1962.
4. N. H. Marshall and O. D. Simpson, Doppler Broadening of the Total Fission, Capture, and Scattering Neutron Cross Sections of Pu-241, USAEC Report IDO-16954, Phillips Petroleum Co., Dec. 16, 1963.
5. E. Creutz, H. Jupnik, T. Snyder, and E. P. Wigner, Review of the Measurements of the Resonance Absorption of Neutrons by Uranium in Bulk, *J. Appl. Phys.*, 26: 257 (1955).
6. E. Hellstrand, Measurements of the Effective Resonance Integral in Uranium Metal and Oxide in Different Geometries, *J. Appl. Phys.*, 28: 1493 (1957).
7. R. M. Pearce and D. H. Walker, A Direct Measurement of the Uranium Metal Temperature Coefficient of Reactivity, *Nucl. Sci. Eng.*, 2(1): 24-32 (February 1957).
8. J. Chernick and A. R. Vernon, Some Refinements in the Calculation of Resonance Integrals, *Nucl. Sci. Eng.*, 4(5): 649 (November 1958).
9. F. T. Adler, G. W. Hinman, and L. W. Nordheim, The Quantitative Evaluation of Resonance Integrals, in *Proceedings of the Second United Nations International Conference on the Peaceful Uses of Atomic Energy, Geneva, 1958*, Vol. 16, p. 142, United Nations, Geneva, 1958.
10. R. D. Richtmyer, R. Van Norton, and A. Wolfe, The Monte Carlo Calculation of Resonance Capture in Reactor Lattices, in *Proceedings of the Second United Nations International Conference on the Peaceful Uses of Atomic Energy, Geneva*, 1958, Vol. 16, p. 180, United Nations, Geneva, 1958.
11. L. Dresner, *Resonance Absorption in Nuclear Reactors*, Pergamon Press, Inc., New York, 1960.
12. W. H. Arnold, Jr., and R. A. Dannels, The Doppler Coefficient of $U^{238}O_2$, *Trans. Am. Nucl. Soc.*, 3(1): 229 (1960).
13. W. H. Arnold, Jr. and R. A. Dannels, Westinghouse Electric Corp., 1960. (Unpublished).
14. A. R. Vernon, Calculation of the Effective Resonance Integral of U^{238}, *Nucl. Sci. Eng.*, 7(3): 252 (March 1960).
15. M. Wagner, Spatial Distribution of Resonance Absorption in Fuel Elements, *Nucl. Sci. Eng.*, 8(3): 278 (September 1960).
16. E. Hellstrand, P. Blomberg, and S. Horner, The Temperature Coefficient of the Resonance Integral for Uranium Metal and Oxide, *Nucl. Sci. Eng.*, 8(6): 497 (December 1960).
17. L. W. Nordheim, The Contribution of the Individual Resonances to the Resonance Integrals in Uranium and Thorium, USAEC Report GA-2563, General Dynamics Corp., General Atomic Division, Oct. 26, 1961.
18. E. Hellstrand and J. Weitman, The Resonance Integral of Thorium Metal Rods, *Nucl. Sci. Eng.*, 9(4): 507 (April 1961).
19. R. M. Pearce, The Doppler Effect in Thermal Reactors, *J. Nucl. Energy, Pt. A*, 13: 150 (1961).
20. L. Dresner, Some Remarks on the Effect of a Non-uniform Temperature Distribution on the Temperature Dependence of Resonance Absorption, *Nucl. Sci. Eng.*, 11(1): 39 (September 1961).
21. R. Goldstein and E. R. Cohen, Theory of Resonance Absorption of Neutrons, *Nucl. Sci. Eng.*, 13(2): 132 (June 1962).
22. J. H. Ferziger, Resonance Absorptions in Lumps with Nonuniform Temperature Distributions, *Nucl. Sci. Eng.*, 14(3): 244 (November 1962).
23. E. Hellstrand and G. Lundgren, The Resonance Integral for Uranium Metal and Oxide, *Nucl. Sci. Eng.*, 12(3): 435 (March 1962).
24. L. W. Nordheim, A New Calculation of Resonance Integrals, *Nucl. Sci. Eng.*, 12(4): 457 (April 1962).
25. G. W. Hinman, G. F. Kuncir, J. B. Sampson, and G. B. West, Accurate Doppler Broadened Absorption, *Nucl. Sci. Eng.*, 16(2): 202 (June 1963).
26. M. M. Levine, Resonance Integral Calculations for U^{238} Lattices, *Nucl. Sci. Eng.*, 16(3): 271 (July 1963).
27. S. Iijima, Resonance Absorption and the Resonance Disadvantage Factor, *Nucl. Sci. Eng.*, 17(1): 42 (September 1963).
28. A. Reichel, The Temperature Dependence of Effective Resonance Integrals, *J. Nucl. Energy, Pt. A & B*, 17(7): 281 (September 1963).
29. H. Feshbach, G. Goertzel, and H. Yamauchi, Estimation of Doppler Effect in Fast Reactors, *Nucl. Sci. Eng.*, 1(1): 4-19 (March 1956).
30. H. A. Bethe, On the Doppler Effect in Fast Reactors, USAEC Report APDA-119, Atomic Power Development Associates, Inc., Mar. 11, 1957.
31. R. B. Nicholson, The Doppler Effect in Fast Neutron Reactors, USAEC Report APDA-139, Atomic Power Development Associates, Inc., June 1960.
32. P. Greebler, B. A. Hutchins, and J. R. Sueoka, Calculations of Doppler Coefficient and Other Safety Parameters for a Large Fast Oxide Reactor, USAEC Report GEAP-3646, General Electric Compnay, Atomic Power Equipment Department, Mar. 23, 1961.
33. P. Greebler and B. A. Hutchins, The Doppler Effect in a Large Fast Oxide Reactor, Its Calculation and Significance for Reactor Safety, in

Proceedings of the Seminar on the Physics of Fast and Intermediate Reactors, Vienna, Austria, August 3-11, 1961, Vol. III, p. 121, IAEA, Vienna, 1962.

34. M. G. Bhide and H. H. Hummel, Calculations of the Doppler Coefficient of Large Ceramic-Fueled Fast Reactors, USAEC Report ANL-6601, Argonne National Laboratory, August 1962.
35. P. Greebler and E. Goldman, Doppler Calculations for Large Fast Ceramic Reactors — Effects of Improved Methods and Recent Cross Section Information, USAEC Report GEAP-4092, General Electric Company, Atomic Power Equipment Department, Dec. 19, 1962.
36. Proceedings of the Conference on Breeding, Economics, and Safety in Large Fast Power Reactors, October 7–10, 1963, USAEC Report ANL-6792, Argonne National Laboratory, December 1963:
    a. B. Wolfe, N. Friedman, and D. Riley, Influence of the Doppler Effect on the Meltdown Accident, pp. 170-190.
    b. J. Codd and P. J. Collins, Some Calculations Concerning the Influence of Resonance Overlapping on the Doppler Effect in a Dilute Fast Reactor, pp. 711-724.
    c. R. N. Hwang, An Improved Method of Doppler-Effect Calculation for Fission Materials in the Intermediate Energy Region, pp. 727-742.
    d. H. H. Hummel and A. L. Rago, Effect of Parameter Variation in Doppler Effect Calculations, pp. 747-761.
    e. R. Froelich, K. Ott, and J. J. Schmidt, Calculation of Doppler Coefficients of Dilute Fast Reactors, pp. 777-789.
    f. C. Graves, Methods of Evaluation of Effective Cross Section for Doppler Coefficient Calculation in Large Fast Breeder Reactors, pp. 791-802.
    g. E. A. Fossoul, Doppler Effect in Fast Reactors for Nonuniform Heating and Temperature Distribution, pp. 803-819.
37. O. D. Simpson and N. H. Marshall, Doppler Broadening of the Low Energy Total Neutron Cross Section of Pu-241, USAEC Report IDO-16679, Phillips Petroleum Co., Aug. 4, 1961.
38. D. L. Miller, Control Rod Programming in a Large Multiregion Core, USAEC Report WCAP-3719, Westinghouse Electric Corp., Atomic Power Division, October 1962.
39. P. J. Hemmings, A Compilation of Nuclear Data for Natural Zirconium, British Report AHSB(S)-R-62, 1963.
40. R. K. Paschall, The Age of Fission Neutrons to Indium Resonance Energy in Water, Part I, Experiment, USAEC Report NAA-SR-8621, Atomics International, Nov. 30, 1963.
41. H. Alter, The Age of Fission Neutrons to Indium Resonance Energy in Water, Part II, Theoretical, USAEC Report NAA-SR-8662, Atomics International (to be published).
42. H. C. Honeck, A Review of the Methods for Computing Thermal Neutron Spectra, USAEC Report BNL-821 (T-319), Brookhaven National Laboratory, June 1963.

Section

II

Power Reactor Technology

Fluid and Thermal Technology

Burnout in Steam-Water Mixtures

By John S. Wiley

The DNB-2 Curve and Its Significance

The first article in this series on two-phase burnout, Sec. III, *Power Reactor Technology*, 7(1), presented data (Figs. III-6 and III-7 of that article) showing lines arbitrarily called DNB-1 and DNB-2. The discussion in the succeeding two articles was directed to typical DNB-1 behavior; the purpose of this review is to discuss the significance of the DNB-2 line. The terms "DNB-1" and "DNB-2" were coined by Levedahl,[1] who first published burnout data on a steam-energy flow (SEF) plot.* The application of the terms to the constant inlet-temperature data shown in Fig. II-1, however, is somewhat arbitrary since the data indicate a transition zone between the DNB-1 and DNB-2 curves. Data taken at an inlet subcooling (SC) or 62°F, for example, plot in a nearly vertical curve.

When DNB data are considered on an SEF plot, remember that the abscissa and ordinate of the plot are always related by the heat balance

$$\phi = D/4L_T[\text{SEF} + G(H_f - H_{\text{in}})] \qquad (1)$$

$$= D/4L_T\,(\text{SEF} + G\Delta H_{sc}) \qquad (2)$$

The experimenter may take data on burnout heat flux by setting G, for example, and varying H_{in}, or he may vary G at given values of H_{in}. Figure II-1 illustrates burnout data at 2000 psia from Table 21 of Ref. 2. The way the data are presented in the table suggests that the DNB points were established by making a series of runs with varying mass flow and constant inlet temperature, and the solid lines on Fig. II-1 depict this method of operation. The dashed lines, which are cross plotted, suggest that the experiments could have been run equally well by setting the mass flow at a constant value and varying the inlet temperature to find the DNB point. Thus DNB-2 lines on Fig. II-1 do not appear unique and could have been obtained by cross-plotting data taken at constant mass flow. The question this review attempts to answer, therefore, is whether the DNB-2 curves ever do represent some unique behavior that would contribute to our understanding of burnout phenomena.

Figure II-2 illustrates additional 2000-psia data appearing in Table 10 of Ref. 2. The few points were taken at a mass flow of about 0.5×10^6 lb/(hr)(sq ft), and a possible "best-fit" curve through the several points is shown as curve A in Fig. II-2. If curve A did represent the behavior of ϕ_{BO} with SEF at constant mass flow, then the deviation of the runs from the curve could be attributed to statistics. If more Table 10 data were plotted,* however, it would become evident that curve A is not really the best-fit curve and that the data could be better represented by DNB-1 and DNB-2 curves. If a constant-G curve is drawn on Fig. II-2, it takes a nose dive, as shown by curve B. This sort of behavior is not what is observed in Fig. II-1, where the constant-G curves are all quite straight. The writer therefore concludes that at least two different burnout mechanisms are il-

*Steam-energy flow is the product $Gx_e h_{fg}$, where G is the mass flow in pounds per hour per square foot, x_e is the exit quality, and h_{fg} is the vaporization enthalpy in British thermal units per hour per square foot.

*A presentation of Table 10 data is shown in Fig. III-7, *Power Reactor Technology*, 7(1).

lustrated in Fig. II-2, whereas the burnouts plotted in Fig. II-1 probably were all caused by a single mechanism. This argument is not particularly convincing at present because only a few points are shown on Fig. II-2. Further data, from experiments at 1000 psia, will be considered in an attempt to substantiate that burnouts giving DNB-2 lines can be caused by a different burnout mechanism than burnouts giving DNB-1 lines.

It is instructive to assume that one has available a number of test sections, of a given diameter but a variety of lengths, and to proceed to conduct, conceptually, a number of experiments to determine the burnout heat flux. Such programs have, in fact, been carried out many times in laboratories all over the world. Typical data for a test section having a length of 17 in. and an inside diameter of 0.220 in. are shown in Fig. II-3. These are data of Lee and Obertelli[3] and were taken at a nominal pressure of 1000 psia. It is evident that data taken at subcoolings from about 10 to 135°F plot on a single DNB-1 line.

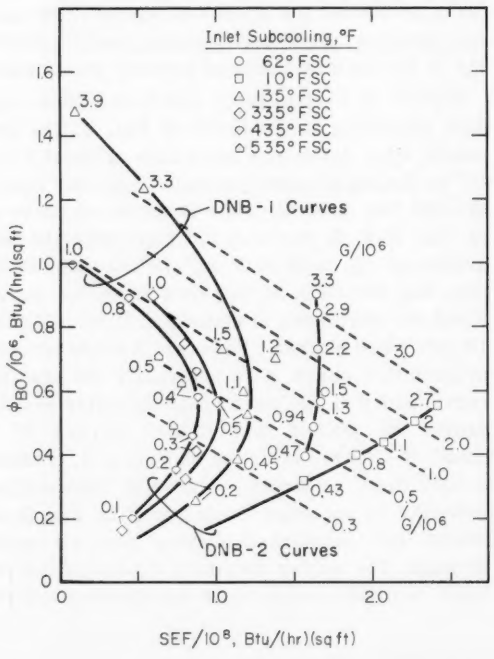

Fig. II-1 Steam-energy flow plot of data from Table 21 of Ref. 2. Pressure = 2000 psia, L_T = 27 in., and flow-channel thickness = 0.097 in.

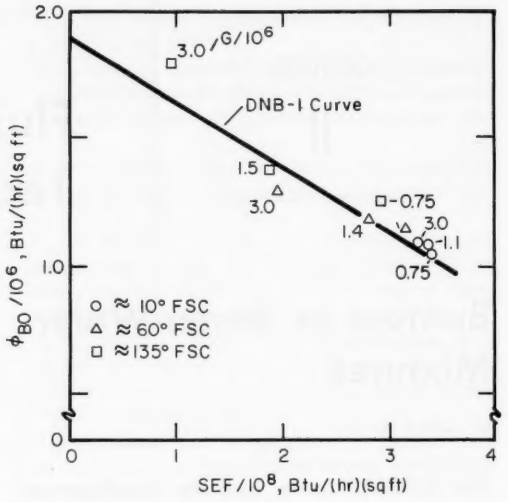

Fig. II-2 Steam-energy flow plot of burnout data from Table 10 of Ref. 2. $G/10^6 \cong 0.5$ lb/(hr)(sq ft) and pressure = 2000 psia.

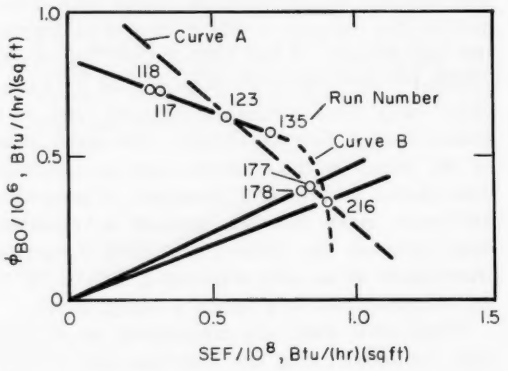

Fig. II-3 Steam-energy flow plot of runs 56 to 90 of Ref. 3. Pressure = 1000 psia (nominal), L_T = 17.0 in., and D = 0.220 in.

As tube length is increased to 34 in., the data take the appearance shown in Fig. II-4. The DNB-1 line is depressed, and this length effect has been discussed in Sec. III of *Power Reactor Technology*, 7(3). As the tube is lengthened to 53.5 in., data plotted in Fig. II-5 are obtained. At first glance the DNB-2 data plotted in Fig. II-5 suggest no unusual behavior and, indeed, look quite similar to data shown in Fig. II-1. The spread of the data seems to call for some attention, however, for at 1000 psi the SEF plot

ordinarily pulls together the data for a tubular test section, so that data for a rather wide range of mass flows falls on a single line, at least in the DNB-1 range.

Figure II-6 compares Lee-Obertelli data with data appearing in Ref. 4, which reports work done by the Centro Informazioni Studi Esperienze (CISE). The particular Ref. 4 data plotted were taken with a steam-water mixture fed to the test section, and, if burnout is independent of upstream history, then the 31.4-in. CISE test section should be equivalent to the last few feet of the 79-in. Lee-Obertelli test section.* Curves, arbitrarily called DNB-2′, have been placed through the CISE data (neglecting, for the moment, the portion labeled "instability branch"), and it is evident that they coincide fairly well with the Lee-Obertelli data at the corresponding mass flows. The DNB-2′ curves have been extrapolated to the DNB-1 curve with a shape suggested by data appearing in Ref. 5. The vertical, extrapolated portion of the DNB-2′ curves plotted on Fig. II-5 represent what Collier[5] calls "dryout," where the heat-transfer coefficient is reduced from a high value in the forced convective region to a value near that

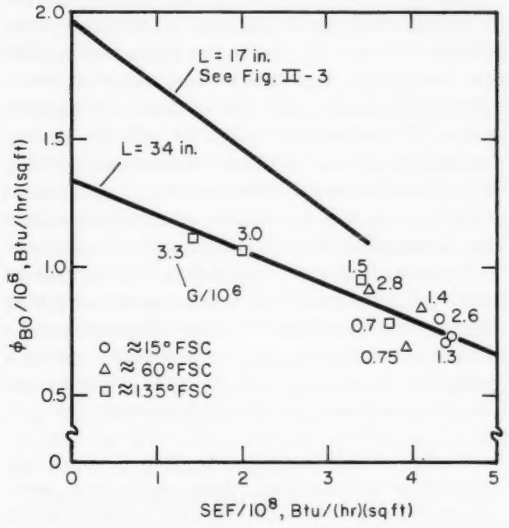

Fig. II-4 Steam-energy flow plot of runs 117 to 134 of Ref. 3. Pressure = 1000 psia (nominal), L_T = 34.0 in., and D = 0.220 in.

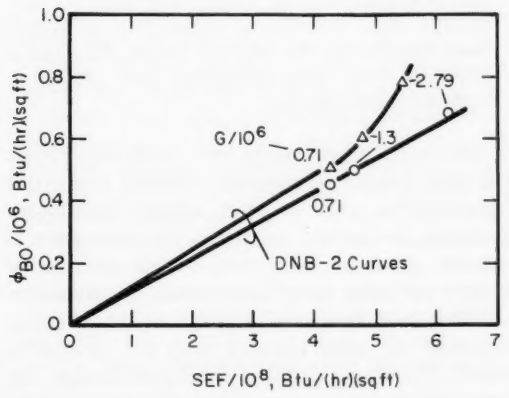

Fig. II-5 Steam-energy flow plot of runs 135 to 152 of Ref. 3. Pressure = 1000 psia (nominal), L_T = 53.5 in., and D = 0.220 in.

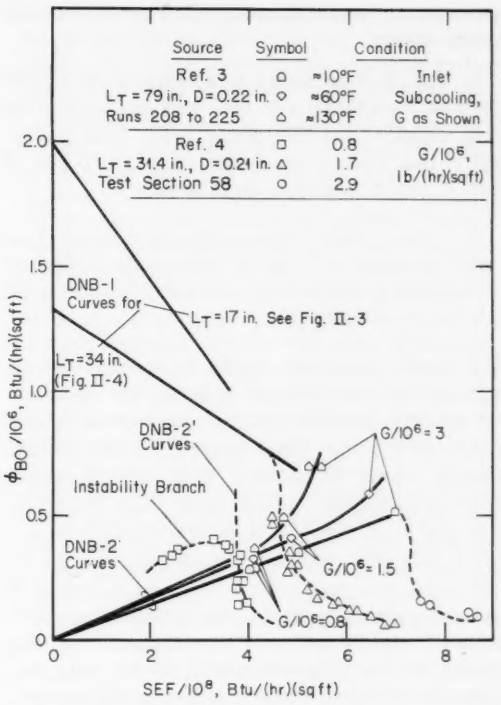
Source Symbol Condition
Ref. 3 ○ ≈10°F
L_T = 79 in., D = 0.22 in. ◇ ≈60°F Inlet Subcooling,
Runs 208 to 225 △ ≈130°F G as Shown
Ref. 4 □ 0.8 G/10⁶,
L_T = 31.4 in., D = 0.21 in. △ 1.7 lb/(hr)(sqft)
Test Section 58 ○ 2.9
DNB-1 Curves for L_T = 17 in. See Fig. II-3
L_T = 34 in. (Fig. II-4)
DNB-2′ Curves
G/10⁶ = 3
Instability Branch
DNB-2′ Curves
G/10⁶ = 1.5
G/10⁶ = 0.8
$\phi_{BO}/10^6$, Btu/(hr)(sqft)
SEF/10⁸, Btu/(hr)(sqft)

Fig. II-6 Comparison of data in Ref. 3 (Lee and Obertelli) and Ref. 4 (CISE data). Pressure = 1000 psia (nominal).

*The test sections used to take burnout data reported in Ref. 3 had lengths of 3.9, 8.3, 15.8, and 31.4 in. Although there is a length effect observable in the SEF plots of CISE data, changing the length from 15.8 to 31.4 in. has but little effect on the positions of the DNB-2′ curves.

expected for heat transfer by forced convection to dry steam.

In Fig. II-6 is shown an attempt to reconcile burnout data taken with test sections employing both single- and two-phase feed. This possibility has been considered on page II-184 of Ref. 4, which is quoted as follows:

> ... experiments in the quality region carried out with subcooled water at the inlet, cannot be directly compared with data taken with water and steam entering the test section...

The above quotation might be interpreted as stating that it is difficult to obtain the complete set of DNB curves with but one test section of given dimensions. For example, the DNB-1 data usually come from low L/D test sections, whereas the DNB-2 data come from high L/D test sections. As L and D are changed to explore different regions, they in themselves affect ϕ_{BO}, and, until the effects of L and D on ϕ_{BO} are known precisely, this confounding effect makes analyses difficult. The importance of this should not be underestimated, for it acts as a restraint of great binding power on the experimenter. Suppose, for example, the objective is to determine the position of the DNB-1 line with a test section having an L_T/D of 300 and mass flows of about 1 million lb/(hr)(sq ft). Experience indicates that ϕ_{BO} will be of the order of 1 million Btu/(hr)(sq ft) at a value of SEF = 0. If these numbers are put into Eq. 1, it can be shown that the experiment must be conducted with the water at an inlet subcooling of about 1200 Btu/lb. To avoid working with cryogenic fluids, the experimenter must therefore explore the DNB-1 region with test sections of low L/D. However, he then is unable to explore the DNB-2 region without using two-phase feed to the test section. Accordingly the constant-G curves implied in Fig. II-6 will probably be difficult to obtain with a single test section of given dimensions employing only single-phase feed.

Figure II-6 bears a striking resemblance to curve B of Fig. II-2 with respect to the "droop" in the constant-G curves and lends credibility to the hypothesis that some DNB-2 type burnouts are caused by a different burnout mechanism than that operating to cause DNB-1 type burnouts. Unfortunately a discussion of burnout mechanisms usually is of a qualitative nature, and the state of the art is such that it would be hazardous to say which burnout mechanism was responsible for the termination of a given burnout experiment.

From the standpoint of simplifying the variables that must be considered by the designer, it would be fortunate if all DNB-2 type burnouts at the pressure under consideration (1000 psia) were caused by a single mechanism. Unfortunately there appears to be at least one other mechanism that gives burnout data which, when plotted on an SEF plot, exhibits curves of the DNB-2 type. This is labeled "instability branch" in Fig. II-6. This particular set of data is typical of behavior experienced in a relatively large number of runs at pressures from 580 to 1200 psia (nominal) and mass flow rates of about 0.8×10^6 lb/(hr)(sq ft). The region of the intersection of the instability branch with the appropriate DNB-2′ curve line is discussed in Ref. 4 and is termed the "maximum ϕ_{BO}," although it pertains only to a particular value of mass flow. The authors of Ref. 4 state that this maximum in burnout heat flux is related to a change in flow and heat-transfer mechanisms, and they suggest that the behavior near the maximum is related to some kind of instability due to a change in flow pattern at the inlet of the heated tube. The following is quoted from Ref. 4:

> Rather strong pressure oscillations were observed at low qualities. These oscillations, much more relevant at low flowrates, are probably due to flow instabilities; it must however be noted that the efficiency of the pressure control loop decreases with flowrate. The oscillations were seen both at the absolute and at the differential manometers; no quantitative measurements were made of their amplitude, frequency and of the flow conditions at which they appeared. Usually, experiments were not performed when oscillations higher than ±1 kg/cm^2 were detected at the absolute manometer, and in this case more stable conditions were reached by increasing inlet quality.

Not many experiments have been reported in the open literature wherein carefully controlled observations were made to explore oscillatory behavior in heated sections. The designer is usually given burnout data, which consists of values of mass flow, inlet enthalpy, pressure, burnout heat flux, and exit quality at burnout. Because the experimenter does not ordinarily know the more detailed conditions inside the tube at burnout, such as phase distributions and burnout mechanisms, this information is not presented. The method of detecting burnout varies widely, and the final value of ϕ_{BO} set

down by the experimenter in his data table may involve subjective considerations.* Often the experimental equipment is not set up to detect fast transients in flow, pressure drop, or wall temperature. These considerations lead the designer to apply relatively large safety factors on burnout because the experimental data, when reduced to a correlation, may not be particularly applicable to his case; for example, hydraulic instability rather than steam blanketing of heat-transfer surfaces may be the limit on his particular design, whereas the correlation he is using may pertain to burnout caused by transition to film boiling.

Accordingly the experiments of Quandt[6] are of interest because they are one of the few reported studies on flow oscillations in a test section producing a steam-water mixture. The experimental equipment used was modified to make it more suitable for measurement of flow oscillations. Special high-speed instrumentation was employed to measure test-section flow and pressure drop, overall pressure drop, total pressure, inlet plenum temperature, and test-section outside wall temperature. Tests were run in Bettis High-Pressure Loop No. 23, which was modified; a high-flow bypass was used in parallel with the test section to ensure a constant overall pressure drop.

The following quotation[6] serves to define what was observed during the course of burnout runs:

Experimental Observations of Flow Oscillations

This discussion will supplement the quantitative data previously presented with a qualitative description of an oscillation test conducted at constant over-all pressure drop and increasing heat flux. First the total pressure drop was established at a zero power condition corresponding to the desired initial flow. From this point the heat flux was increased in small steps with steady-state conditions being established after each step in order to record the flow decrease and the various test section and coolant temperatures. Since the flow through the unheated by-pass was about 20-30 times the heated-section flow, minor adjustments were sufficient to maintain a constant over-all pressure drop. During this increase in power, the fast-response instruments showed relatively steady flows and pressure drops with a normal amount of noise appearing on the traces due to turbulent flow (approximately 15-25% of the reading and at roughly the natural frequency of the transducer system ...). Due to this rather high noise level the fast-response instruments were not used to measure absolute values.

When the flux was high enough for the channel to be near an oscillating condition the increments in power from one steady-state point to another were reduced to 2% of the existing flux. Eventually a steady-state condition was reached where the normal small drift of loop variables such as inlet temperature, total pressure, heat flux, etc., was sufficient to cause the flow and channel pressure drop to begin a well-defined sinusoidal oscillation, die out, and start again. These "incipient oscillations" would appear with amplitudes roughly 30% of the average flow reading, while the other variables which were being recorded with high-speed instruments showed no variation other than normal noise. If, at this point the flux was increased by 2%, self-sustained flow oscillations of constant amplitude would result. If the flux was lowered by 2%, the flow would resume the normal noise pattern. Therefore it was possible to determine rather precisely the conditions at which flow oscillations began. Upon further small increases in heat flux the amplitude of the flow oscillation increased rapidly, then leveled out with the instruments showing an extremely reproducible, and now nonlinear, oscillation of definite frequency. At this point both heated channel flow and pressure drop showed the oscillations while the over-all pressure drop, channel outside wall temperatures, and inlet temperature remained steady.

Continuing increases in heat flux finally caused the over-all pressure drop and the test-section-wall temperature to pick up the oscillation. Hence the oscillation had become strong enough to influence the external loop and the test section inside surface was passing in and out of a burnout condition every cycle. Continued increases in heat flux caused the inlet water temperature to begin to oscillate, indicating that the flow had begun to pulse out the inlet of the channel. This last point might occur at 10-20% higher power than the point of initial oscillation. Further increases in heat flux resulted finally in a wall-temperature excursion (burnout) superimposed on top of the oscillation. In some runs burnout occurred before any of the secondary oscillations began, and this complete pattern did not occur.

Results of the experiments are plotted in Fig. II-7. These data are called "values at last stable condition" and presumably correspond to data taken at the point (in time) "at which flow oscillations began." The data line up nicely into DNB-2 curves with the exception of the two 1200-psia runs at a subcooling of 115°F. Their behavior suggests that they may lie on a DNB-1

*Pages II-174 to II-177 of Ref. 4 contain an excellent description of the problems besetting the determination of which value of ϕ represents ϕ_{BO}.

curve or at least near the intersection of the DNB-1 and DNB-2 curves. The data in Fig. II-7 are replotted in Figs. II-8 to II-10; however, in these curves, instead of ϕ_{BO}, the fractionable length of the test section undergoing boiling at burnout, $(L_B/L_T)_{BO}$ is plotted as a function of mass flow with inlet subcooling as a parameter.

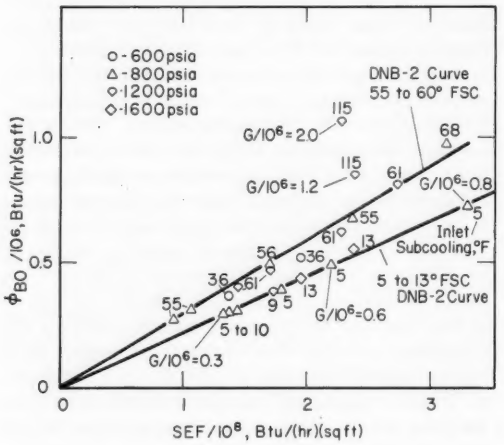

Fig. II-7 Steam-energy flow plot of data from Quandt.[6] Pressure, mass flow, and inlet subcooling as indicated.

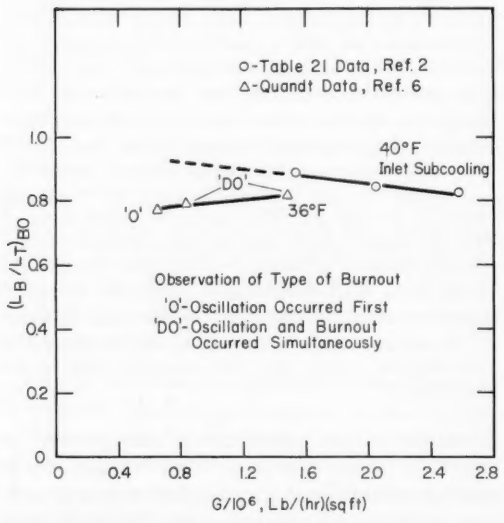

Fig. II-8 Fractional length of test section undergoing boiling at point of burnout vs. mass flow. Comparison of data in Refs. 2 and 6. Pressure = 600 psia and inlet subcooling as indicated.

The call-outs "D," "DO," and "O" signify whether the runs were terminated by burnout occurring first, burnout and oscillation occurring simultaneously, or an oscillation occurring first, respectively. These results were taken from Table 1 of Ref. 6. Also plotted on Figs. II-8 to II-10 are data taken from Table 21 of Ref. 2. The Table 21 data were taken in a test section whose nominal dimensions were the same as those of the of the test section used to take the Ref. 6 data, and the data originally appeared in Refs. 7 to 9. The latter references suggest that the Table 21 data were taken in test loops without a parallel channel flow, although the loops

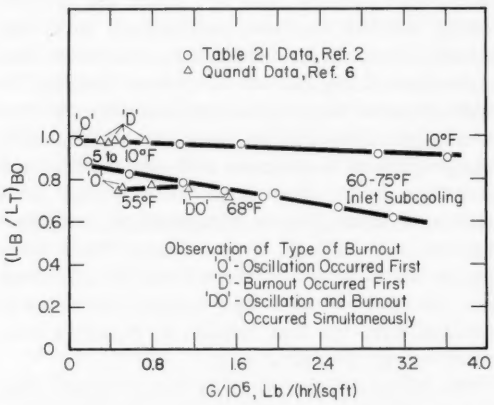

Fig. II-9 Fractional length of test section undergoing boiling at point of burnout vs. mass flow. Comparison of data in Refs. 2 and 6. Pressure ~800 psia and inlet subcooling as indicated.

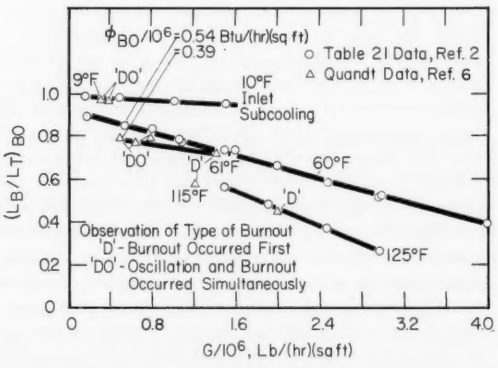

Fig. II-10 Fractional length of test section undergoing boiling at point of burnout vs. mass flow. Comparison of data in Refs. 2 and 6. Pressure = 1200 psia and inlet subcooling as indicated.

utilized could have provided an alternate flow path.

It is of interest to speculate as to whether the same instability or oscillatory behavior was operating in the Table 21 experiments as in those of Quandt. Figure II-8 reveals some disparity between the $(L_B/L_T)_{BO}$ values from Table 21 and those from Quandt. In the Quandt runs, which exhibited some sort of oscillatory behavior, burnout always occurred at lower values of $(L_B/L_T)_{BO}$ than in the Table 21 runs. This is also true at the higher pressures (Figs. II-9 and II-10), although at low subcooling the difference is minor. Values of ϕ_{BO} are indicated for two of the runs plotted in Fig. II-10. Whatever was happening within the Table 21 test section for the burnout run with $\phi_{BO} = 0.54 \times 10^6$ Btu/(hr)(sq ft), it represents a 38% increase in heat flux compared to the corresponding value observed by Quandt of 0.39×10^6 Btu/(hr)(sq ft).

An interesting series of experiments is described in Ref. 10. The authors had noticed that values of ϕ_{BO} taken in various laboratories exhibited "very considerable divergences." Although test sections of different lengths were utilized for the various runs, the divergences were greater than could reasonably be assigned to the effect of that variable. Accordingly a test loop was fabricated which produced feed for the test section by condensing high-pressure steam, as shown schematically in Fig. II-11. It was discovered that ϕ_{BO} (or q_{cr} in the terminology usually used in Russian heat-transfer literature) depended on which valve was used to throttle the high-pressure steam. This is illustrated in Fig. II-12. Burnout was indicated by reddening of the test section, and the authors state that they believe the lower branch of the burnout curve was due to the presence of pulsations. Traces of flow-time curves shown in the reference illustrate the oscillatory behavior of the coolant flow rate upon approaching burnout with the flow rate controlled by valve No. 1 (Fig. II-11). Similar behavior was evidenced when the compressible volume shown in Fig. II-11 was filled with steam or water with a temperature above 572°F. In Figs. II-13 and II-14 are shown the results of hundreds of runs leading to burnout in pulsating and nonpulsating systems.

The variety of DNB-1 lines shown in Fig. II-13 is interesting. At qualities less than zero, q_{cr} is length independent; this could be the region where film boiling causes burnout, as it would seem reasonable that formation of a patch of steam over a local, heated area would be independent of upstream conditions. In the quality region, q_{cr} becomes length dependent, suggest-

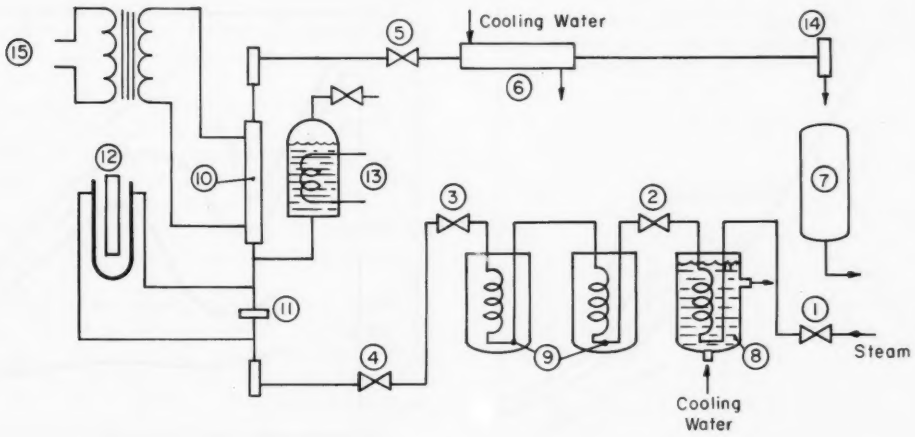

Fig. II-11 Schematic of experimental apparatus used to take data reported in Ref. 10.

1 to 5	Throttling valves	11	Measuring orifice
6	Condenser	12	Differential manometer
7	Weighing tank	13	Electrically heated buffer volume
8	Vapor cooler	14	Thermocouple wells
9	Coils	15	Power supply
10	Test section		

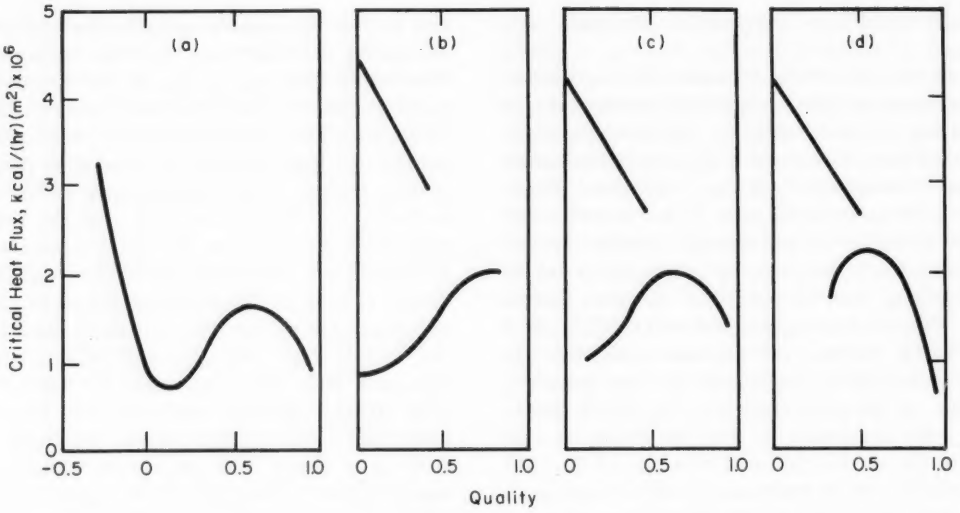

Fig. II-12 Critical burnout heat flux vs. quality.[10] Pressure = 100 atm abs., mass flow = 400 kg/(m^2)(sec), tube inside diameter = 8 mm, and L_T/D = 20. (Data not shown.)

Fig. II-12 part	Valve used for flow control (see Fig. II-11)	Volume upstream of test section, liters
a	1	1.87
b	2	1.41
c	3	0.56
d	4	0.05

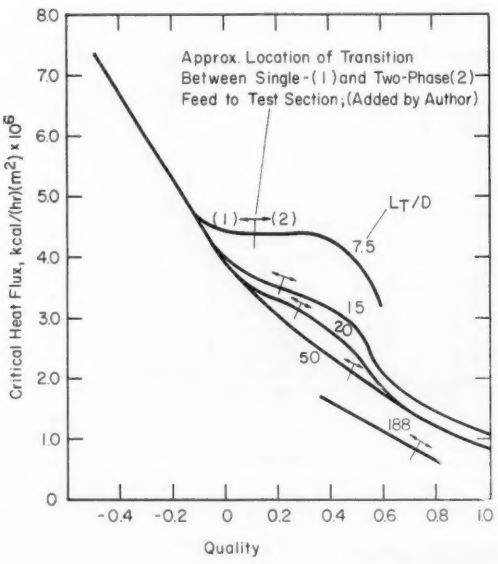

Fig. II-13 Critical burnout heat flux vs. quality for a nonpulsating system.[10] Pressure = 100 atm abs., mass flow = 750 kg/(m^2)(sec), tube inside diameter = 8 mm, and L_T/D is as indicated. (Data not shown.)

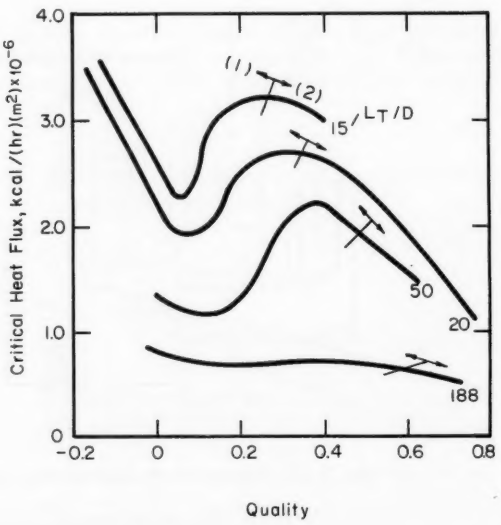

Fig. II-14 Critical burnout heat flux vs. quality for a pulsating system.[10] Pressure = 100 atm abs., mass flow = 750 kg/(m^2)(sec), tube inside diameter ~8 mm, and L_T/D is as indicated. (Data not shown.)

ing that an entrance effect is important, although it certainly extends to large values of L_T/D. Tick marks are shown on the curves to show the transition point from single-phase to two-phase feed to the test section. These tick marks were added by the reviewer. A relatively large number of "instability branches" are shown in Fig. II-14, all arising from runs with single-phase feed.

The "stabilizing" of an otherwise unstable burnout is discussed in Ref. 11. This consists in orificing the test section between its inlet and the expander (Fig. II-11). The following is quoted from Ref. 11:

> ... The throttles between the expander and heated channel do not always exclude the undesired conditions as transition from type 1 to type 2 can be effected only if the pressure drop in the throttle separating the heated channel from the preceding section is rather substantial. Thus, for example, in runs ... at $P = 100$ atm and $W_g = 400$ kg/m^2 sec the pressure drop needed amounted to about 10 kg/cm^2 ...

A pressure drop through an inlet orifice of about 140 psi is considerably more than design practice would dictate in this country, and it is of interest to note that orifices with a resistance of about 30 psi were used in the Russian First Atomic Power Station for the boiling channels.[12]

> ... Successful working in the boiling regime made it possible towards the middle of 1957 to transfer more than half of the channels of the reactor (70), into the boiling regime.
>
> Beginning at that time, spent channels were replaced by channels with the resistance disk at the entrance end of the fuel element. The resistance of the disk was 2 atm at a flow 250 kg/hr. Lengthy operation of the majority of the channels in the boiling regime showed that no hydraulic pulsation or instability of flow would occur under these conditions.
>
> Working in the boiling regime gives typically a steam content at the exit end of the channels of 5-25 wt.% with thermal ratings of $0.6\text{-}1.3 \times 10^6$ kcal/m^2 hr with water flows along the channel of 0.7-1 m/hr at a pressure of 100 atm and a temperature at the inlet end of 190°C.

The First Atomic Power Station is a pressure-tube graphite-moderated reactor.

In summary, the DNB-2 lines are of little use for design purposes. Some DNB-2 type burnouts are caused by instabilities within the test section, but it is difficult to apply these data to reactor design. Some DNB-2 type burnouts appear to be caused by a different burnout mechanism than DNB-1 type burnouts, but in any case little is known about the details of what happens within the test section. Possibly the best use of the DNB-2 line is as a signal to the experimenter that, if his data fall on DNB-2 curves, he may be generating ambiguous information, which will probably prove difficult for the designer to use with confidence.

Burnout in Nonuniformly Heated Channels

Much information is available on the burnout of channels of various shapes for an axially uniform power-generation rate, but axial uniformity is never encountered in actual nuclear reactors. Several reports have been written about burnout in connection with nonuniform axial power generation,[13–15] and this section will review those publications.

Work done at General Electric's Atomic Power Equipment Department (GEAP) utilized a heated rod in annular geometry. Test sections were fabricated to give both a cosine and truncated cosine distribution of heat flux. This was accomplished by a technique of axially varying the wall thickness of the tube, and the method was common to experiments done at the other laboratories. The relative heat generation in the cosine and truncated cosine rods is shown in Figs. II-15 and II-16. A number of thermocouples were spot welded to the inside diameter of the test section and served as temperature or

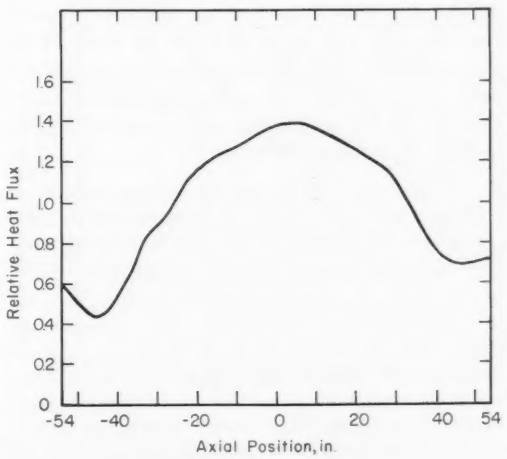

Fig. II-15 Relative heat-flux distribution—cosine rod No. 4.[13]

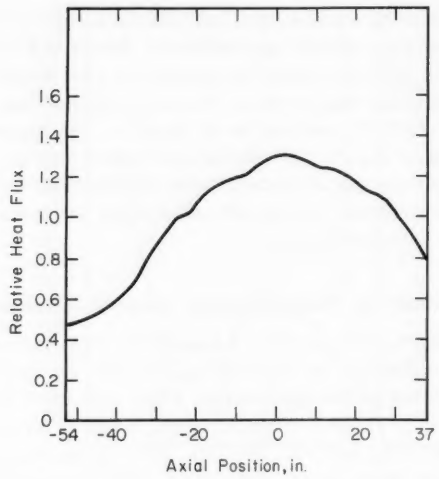

Fig. II-16 Relative heat-flux distribution — truncated cosine rod No. 20.[13]

voltage detection devices. Burnout was detected by a bridge that measured imbalance in the resistance of two adjacent segments of the heated rod and with the thermocouples. Details of the apparatus and other parameters of interest are shown in Table II-1.

Reference 13 gives the test-section average heat flux and exit quality at burnout-detector trip and the local heat flux and quality for those thermocouple positions at which a temperature rise was indicated.* The local data are plotted in Figs. II-17 to II-19, where they are compared with data for a similar test section heated uniformly. The data for the uniformly heated test section are from Ref. 16. In Ref. 13 the conclusion is that the nonuniformly heated rod data averaged 9 to 20% low compared to a correlation of the uniformly heated rod data given in Ref. 16. It was concluded[13]

> ... that the uniform rod burnout correlation can be used to predict burnout for cosine heat flux distribution. It is tacit in this conclusion that burnout depends only on local conditions of quality and flow ... The nonuniform rod data points averaged 9 to 20 percent low. The magnitude of this deviation is considered small, and of the same order as that for the uniform rod data upon which the correlation was originally based.

Figures II-20 and II-21 show the average heat flux at burnout plotted as a function of the exit quality at burnout. This particular method of showing nonuniform heat-flux burnout data is recommended in another reference and will be discussed later. Also plotted in Figs. II-20 and II-21 are the results of the uniformly heated test-section burnout runs. A difference is evident between the burnout data, for example Fig. II-17, from the uniformly and nonuniformly heated test sections. Whether this is due to the

Table II-1 CONDITIONS FOR GEAP BURNOUT TESTS[13]

Rod outside diameter, in.	0.540
Flow-tube inside diameter, in.	0.875
Hydraulic diameter, in.	0.335
Heated length, in.	
Cosine rod	108
Truncated cosine rod	91
Pressure, psia	1000
Flow rates, lb/(hr)(sq ft) × 10^{-6}	0.84 to 1.40
Exit quality range, %	12 to 35
Peak to average power generation (approx.)	
Cosine rod	1.4
Truncated cosine rod	1.3

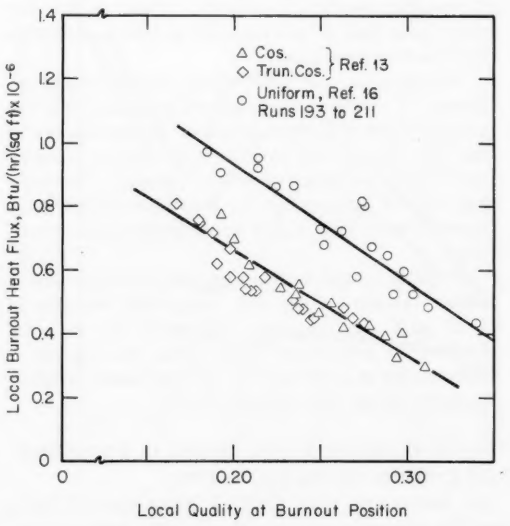

Fig. II-17 Comparison of uniformly and nonuniformly heated test-section burnout data. Pressure = 1000 psia and mass flow = 0.84 × 10^6 lb/(hr)(sq ft).

*The thermocouples were positioned at finite locations along the heated length of the test section, and there would seem to be no guarantee that burnout would take place at a position immediately adjacent to a thermocouple. This source of error is not discussed in the reference. Possibly it is a minor one, because in many runs wall-temperature increases were observed by several thermocouples simultaneously.

nonuniform shape of the heat-generation rate is not necessarily obvious, for other variables may be involved. An indication of another variable is given by the series of cosine rod-burnout data, starting with run 16 and terminating with run 23; these runs are shown in Figs. II-19 and II-21. Runs 16 to 20 utilized heated rod No. 59, which was destroyed during run 20 by a burnout. Rod No. 42 was then employed for runs 21 to 23, which were close duplicates of the mass flow, inlet subcooling, and pressure of runs 17, 18, and 16, respectively. These duplicate runs are marked on Fig. II-19 with dashed connecting curves, and it can be seen that runs 21 to 23 produced slightly different results than runs 16 to 18. This is particularly evident in Fig. II-21. Test section 59 had been used for at least 15

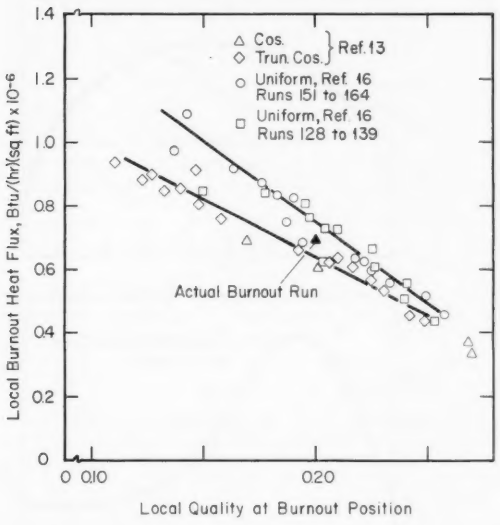

Fig. II-18 Comparison of uniformly and nonuniformly heated test-section burnout data. Pressure = 1000 psia and mass flow = 1.1×10^6 lb/(hr)(sq ft).

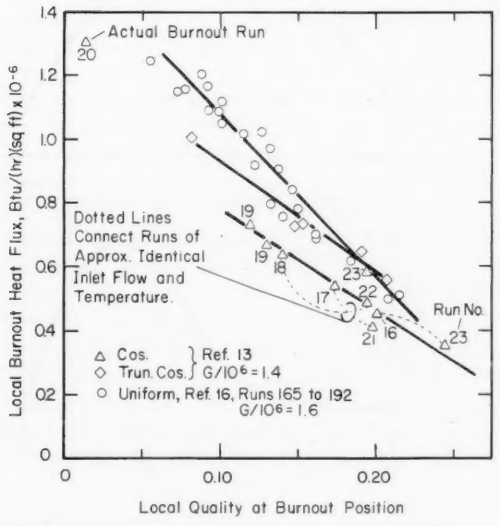

Fig. II-19 Comparison of uniformly and nonuniformly heated test-section burnout data. Pressure = 1000 psia and mass flow is as indicated.

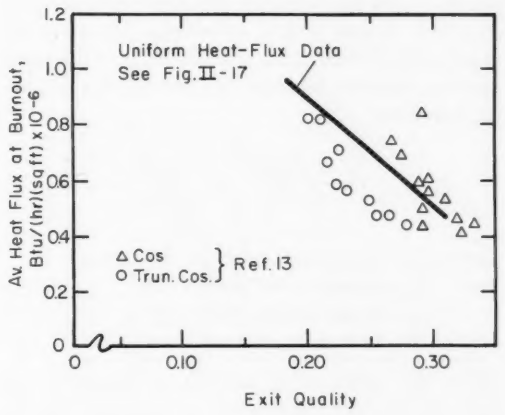

Fig. II-20 Comparison of uniformly and nonuniformly heated test-section burnout data. Pressure = 1000 psia and mass flow = 0.84×10^6 lb/(hr)(sq ft).

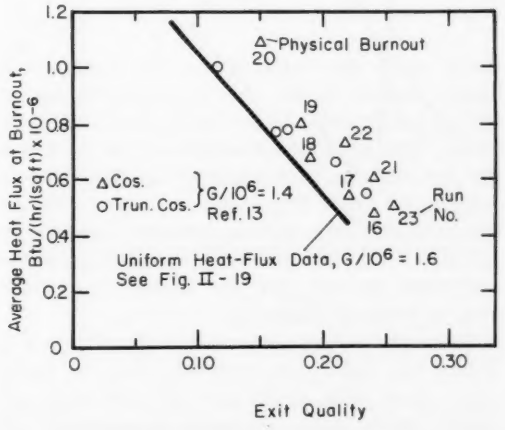

Fig. II-21 Comparison of uniformly and nonuniformly heated test-section burnout data. Pressure = 1000 psia and mass flow is as indicated.

runs prior to run 16; thus there may have been some "aging" effect, as reported by Zenkevich et al.[17] A further difference was that test section 59 was fabricated of type 347 stainless steel, whereas test section 42 was fabricated of Incoloy.

The reference concludes with a discussion of a prediction of the power level and position of burnout for a nonuniformly heated rod. It is assumed that the burnout heat flux is a linear function of quality, e.g.,

$$\phi_{BO} = A - Bx \tag{3}$$

where ϕ_{BO} is the burnout heat flux, x is the quality, and A and B are constants. If $f(y)$ is the relative heat flux along the length, y, of the tube, then the burnout location is given by the following relation:

$$\left[\frac{d \ln f(y)}{dy}\right]_{y=y_1} = -\frac{B\pi D_1}{\dot{W} h_{fg}} \tag{4}$$

where y_1 = location of position of burnout
D_1 = diameter of heated tube
h_{fg} = vaporization enthalpy
$\dot{W}$ = flow rate, lb/unit time

After the position of burnout is obtained, the test-section average power at burnout can be determined:

$$\bar{\phi}_{BO} = \frac{1}{f(y)_{y=y_1}} \left[\frac{A + B\dfrac{\Delta h_s}{h_{fg}}}{\dfrac{B\pi D_1}{\dot{W} h_{fg}} \dfrac{\int_{y_0}^{y_1} f(y)\, dy}{f(y)_{y=y_1}}}\right] \tag{5}$$

where y_0 is the value of y at the entrance to heated portion of the test section, and Δh_s is the inlet subcooling in British thermal units per pound. The predicted average burnout heat flux for the several runs reported in Ref. 13 was determined from Eq. 5 and compared with the experimental data, and the agreement was within +11 to −2.5%. Unfortunately the authors of the reference do not give the values of A and B used in their calculations.

The experiments performed at The Babcock & Wilcox Co. (B&W) are reported in Ref. 14. These were done with uniformly and nonuniformly heated tubes having an inside diameter of 0.41 to 0.45 in. and a heated length of 72 in. The pressure was 2000 psia, and the various nonuniform axial power-generation profiles used are shown in Fig. II-22. The test sections were fabricated from type 304 stainless steel, and a number of thermocouples were fastened to the exterior of the test section for detection of burnout by means of temperature fluctuations or ex-

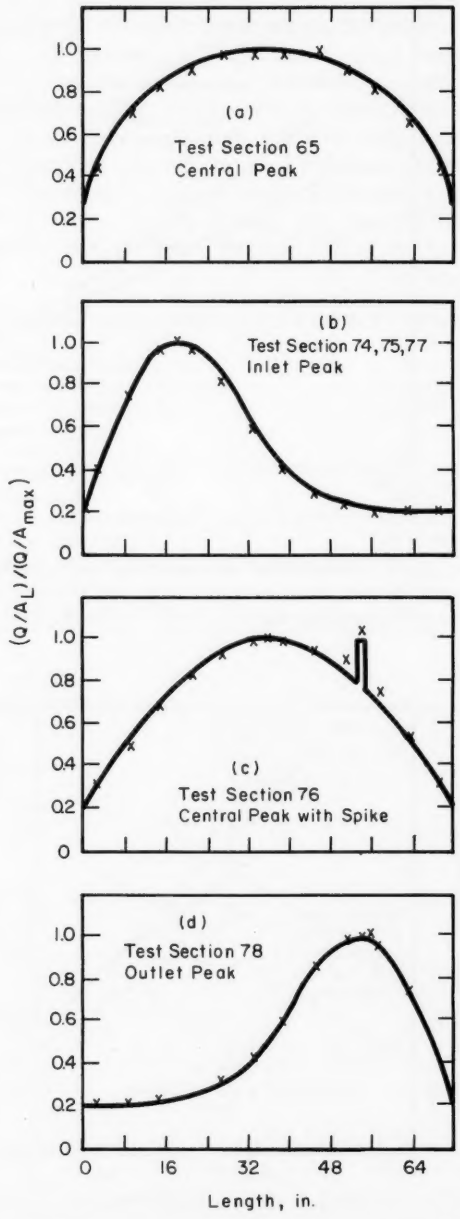

Fig. II-22 Axial power profiles of various test sections used to take data appearing in Ref. 14. Crosses on figures indicate test results.

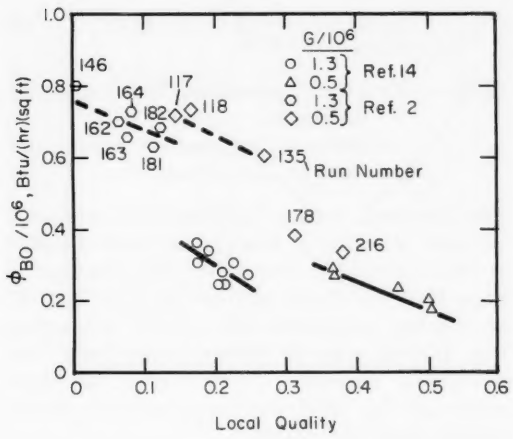

Fig. II-23 Comparison of burnout data from Ref. 14 and Table 10 of Ref. 2. Pressure = 2000 psia. Test-section dimensions are as follows:

Ref.	Inside diameter, in.	Length, in. (heated)
14	~0.41	72
2	0.306	23.25

cursions. Runs were accomplished at mass flows of 0.5, 0.7, 1.0, and 1.3×10^6 lb/(hr)(sq ft) and varying inlet subcooling.

Data taken with the uniformly heated* test section are shown in Fig. II-23 for mass flow of 0.5 and 1.3×10^6 lb/(hr)(sq ft). Also plotted on Fig. II-23 are data from Table 10 of Ref. 2.

It is evident that the Table 10 data plotted in Fig. II-23 lie above the Ref. 14 data. This could be explained by the fact that the test section used to take the Table 10 data had a length of about 24 in., whereas the test section used to take the Ref. 14 data had a length of about 72 in. The effect of length is an important one and was discussed in Sec. III of *Power Reactor Technology*, 7(3). However, on an SEF plot, runs 178 and 216 are on a DNB-2 line (Fig. II-2), and it is possible that the B&W data shown in Fig. II-23 also would plot on DNB-2 lines. The DNB-2 lines are best obtained by plotting constant inlet-temperature data. Unfortunately most of the B&W experiments were not done at constant inlet temperature, and only a few runs can be exhibited on an SEF plot. These will be presented later.

The data are presented[14] in terms of burnout heat flux vs. quality plots. Part *a* of Fig. II-24 shows local heat flux vs. local quality, and part

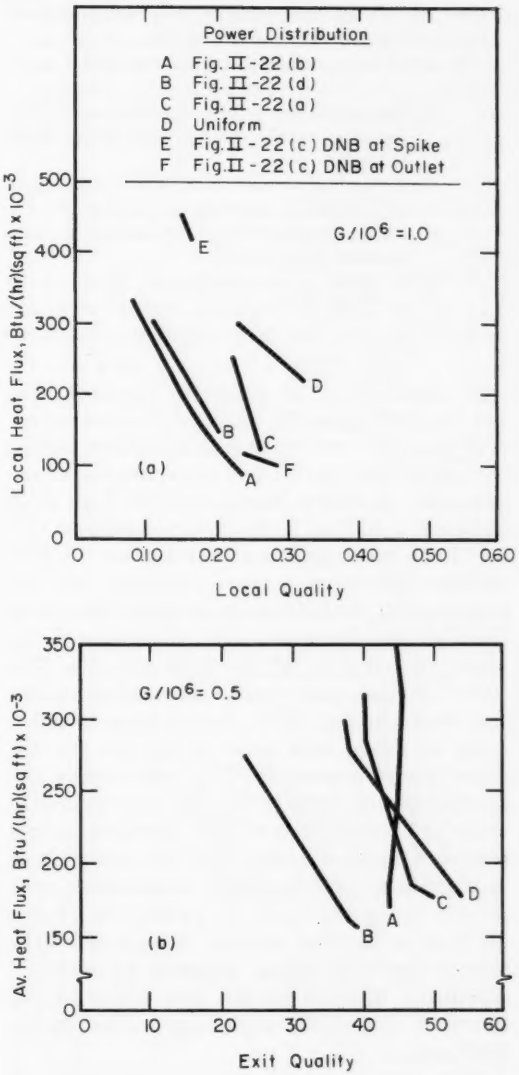

Fig. II-24 Comparison of effects of axial heat-flux distribution and burnout heat flux vs. quality.[14] Pressure = 2000 psia and mass flow is as indicated. The average heat flux plotted on the ordinate of (*b*) is defined as

$$\text{Average heat flux} \equiv \frac{1}{L_T} \int_0^{L_T} \phi(x)\, dx$$

*The uniformly heated test sections burned out 1 to 2 in. upstream of their ends; the use of local quality for the uniformly heated test sections introduces negligible differences compared to the use of exit quality.

b of Fig. II-24 shows average heat flux vs. exit quality. The authors conclude that:

> 2 For a given enthalpy at the point of DNB, the nonuniform heat-flux distributions have lower allowable local heat flux than does the uniformly heated tube. However, on very small areas of the heat-transfer surface (heat-flux spikes smaller than 1 sq in.), it appears possible to approach or even exceed the heat flux that would normally result in DNB with uniform heated flux.
>
> 3 For a given enthalpy at the outlet of the channel:
>
> (a) The outlet peak flux distribution has the lowest channel power at DNB for all mass velocities tested.
>
> (b) At the lower mass velocities, higher channel power is permissible with inlet peak and central peak flux distributions than with uniform distribution.
>
> (c) At higher mass velocities the channel power at DNB for inlet peak, central peak, and uniform flux distribution has nearly the same value.

A comparison of the 1000-psia data just cited and the 2000-psia data under discussion is impressive. The test sections used in the APED and B&W work have about the same length and hydraulic diameter. Comparison of Fig. II-18 and part *a* of Fig. II-24, however, shows that the 2000-psia operation results in a much greater difference between the uniformly and nonuniformly heated test-section data than does the 1000-psia operation. Also, the values of ϕ_{BO} shown in part *a* of Fig. II-24 are quite low. The B&W test loop was conceptually similar to the one shown in Fig. II-11. Steam from a boiler could be mixed with water to provide the desired inlet temperature. The experiments described in Ref. 14 were all done with subcooled water at the test-section inlet, but the reference does not state whether this was achieved by mixing steam with relatively cooler water or by merely using the boiler to produce hot water for feed to the test section. If the boiler were used to generate steam, possibly the same instabilities that led to the low values of ϕ_{BO} shown in Fig. II-12 were also present in the B&W runs.

SEF plots were made for some of the data in Ref. 14 at subcoolings of about 12 to 60°F. These plots are shown in Figs. II-25 and II-26; only runs that burned out with L_{BO} greater than 66 in. are plotted in these figures. Because the SEF plot is intimately tied into the heat-balance equation, the ordinate of Fig. II-25 is $(q/A)_{av.}$, defined as follows:

$$(q/A)_{av.} = \frac{1}{L_{BO}} \int_0^{L_{BO}} (q/A)\, dx \qquad (6)$$

where q/A = axially dependent heat flux, Btu/(hr)(sq ft)
x = distance along heated channel, ft
L_{BO} = value of x at burnout, ft

The inlet-peak section exhibited many upstream burnouts about 33 in. downstream from the point of start of heating. These data are presented in Figs. II-27 and II-28. Also included in Fig. II-27 are the two runs for the central-peak-with-spike test section wherein burnout occurred at the position of the spike (L = 54 in.), and the curve shown in Fig. II-27 was arbitrarily drawn through these two points.

In considering Figs. II-27 and II-28, the reviewer was impressed not so much by the difference in heat flux at which the uniformly and nonuniformly heated test sections exhibited burnout (for given inlet conditions), but rather by the difference in local qualities at burnout. Figure II-25 illustrates that at an inlet subcooling of about 10°F the data group into a DNB-2 curve; variation of mass flow moves the SEF at burnout over a rather wide range for the uniformly heated tube, but the tube with the outlet peak exhibits burnout at roughly a constant value of SEF, namely, ~0.9×10^6 Btu/(hr)(sq ft). When subcooling is increased to about 60°F

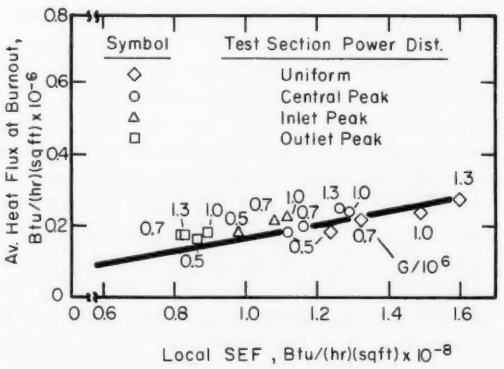

Fig. II-25 Steam-energy flow plot of data from Ref. 14. Pressure = 2000 psia, inlet subcooling = ~12°F, and mass flow is as indicated. The average heat flux plotted on ordinate is defined as

$$\text{Average heat flux} \equiv \frac{1}{L_{BO}} \int_0^{L_{BO}} \phi(x)\, dx$$

Runs shown were terminated by burnout at $L_{BO} \cong 69$ in.

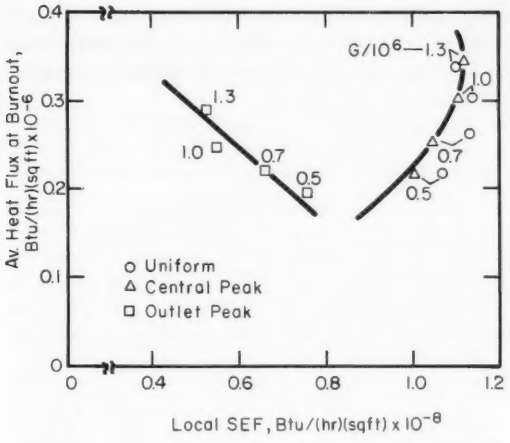

Fig. II-26 Steam-energy flow plot of data of Ref. 14. Pressure = 2000 psia, mass flow is as indicated, inlet subcooling = 60°F (approximately), L_{BO} = 66 to 69 in., and the average heat flux at burnout is defined as in Fig. II-25.

(Fig. II-26), the uniformly heated test section and the test section with the central peak exhibit burnout at almost identical values of $\phi_{BO_{ab.}}$ and SEF_{local}. Only when the power distribution is peaked toward the outlet does the character of the burnout curve change, and then it takes a characteristic DNB-1 shape.

Reference 15, which contains nonuniformly heated test-section data, is a companion to Ref. 3. A total of four nonuniformly heated test sections were utilized with an axial heat-generation rate given by Eq. 7.

$$\phi = \phi_{max} \cos \frac{\pi x}{L_T} \qquad (7)$$

where ϕ_{max} is the heat flux at the center of the test section in British thermal units per hour per square foot, x is the length along the test section measured from the center in feet, and L_T is the extrapolated length in feet. Two of the test sections, Mark I and II, had the wall-thickness variations accomplished by a series of "steps," each 4 in. long, machined on the outside. Test sections III and III*a* were machined to give a smooth variation in wall thickness rather than a series of steps. One inside diameter was 0.383 in.; other pertinent data are given in Table II-2.

Burnout was detected by a bridge type detector with one lead each connected to the center and exit of the tube and with the third lead positioned to give approximately equal resistances in each arm of the bridge. Several runs were made with thermocouples to detect temperature increases:

> ... these showed that within ¼ of a second a temperature excursion could be taking place over several zones of the tube and, within this time scale, not starting at one unique point and spreading along the tube. The series of tests on the Mk I tube was concluded by isolating the detector and allowing the tube to overheat sufficiently to rupture the tube: this confirmed that the power previously indicated

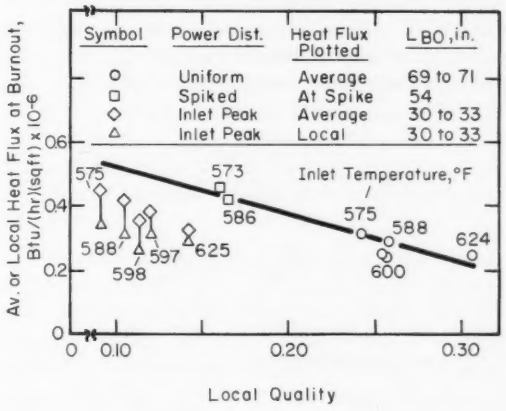

Fig. II-27 Burnout heat flux vs. quality; Ref. 14 data. Pressure = 2000 psia, inlet temperature is as indicated, and mass flow = 1×10^6 lb/(hr)(sq ft).

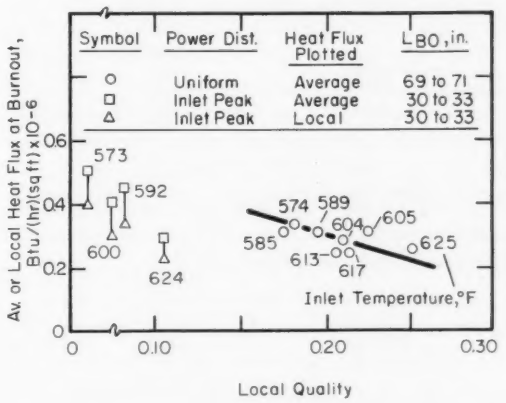

Fig. II-28 Burnout heat flux vs. local quality; Ref. 14 data. Pressure = 2000 psia, inlet temperature is as indicated, mass flow = 1.3×10^6 lb/(hr)(sq ft), and the average heat flux at burnout is defined as in Fig. II-25.

at trip-off would have resulted in a substantial rise of temperature.

Runs were made at 560, 1000, and 1600 psia, with mass velocities from 0.75 to 3.0×10^6 lb/(hr)(sq ft) and inlet subcoolings from 0 to 250 Btu/lb. Data presented in tabular form include the burnout power, mean exit quality, and axial zone wherein burnout occurred, as well as inlet pressure, mass velocity, and inlet subcooling.

A number of methods are considered to correlate the nonuniform flux data with uniform flux data. Three sources of uniform flux burnout data are considered: data in Ref. 3, calculated values of ϕ_{BO} using Barnett's equation,[19] and calculated values using the round-tube best-fit equation of Ref. 2. Barnett's correlation* is as follows, using the nomenclature of Ref. 3:

$$\phi = \frac{A + \left(\frac{DGC}{4}\Delta H_i\right)}{1 + CL}$$

$$= A - \left(\frac{DGC}{4} h_{fg}\right)\frac{x}{100}$$

where $A = \alpha D^a G^b$ and $C = \beta D^c G^d$. Here α, β, a, b, c, and d are dependent on pressure as follows:

	560 psia	1000 psia	1600 psia
α	1.507	0.994	0.790
a	−0.724	−0.555	−0.42
b	−0.419	−0.161	0.079
β	0.0144	0.00841	0.0101
c	−1.471	−0.430	−1.606
d	−0.819	−0.490	0.0715
No. of experiments	135	317	97
Rms, % error	4.76	5.36	2.26
Max. errors, %	+17, −16	+24, −17	+6, −7

*For a pressure of 1000 psia and a tube inside diameter of 0.18 in., Barnett's correlation can be shown to have the following form:

Mass flow, lb/(hr)(sq ft) $\times 10^{-6}$	Correlation
1.0	$\phi_{BO} = 2.58 \times 10^6 - 0.0044$ SEF
4.0	$\phi_{BO} = 2.06 \times 10^6 - 0.0022$ SEF

These correlations can be compared with the ones shown in Table III-6 and III-7, *Power Reactor Technology*, 7(3).

With these sources of uniformly heated test-section burnout data, three recipes were tried to see how closely each would duplicate the nonuniform burnout data:[15]

Methods A, B and C (Overall Length Concept)

The basis of these three methods is to use the overall channel length of the cosine flux tube as the length of the uniform flux tube: using uniform flux data, a, b and c above, comparison being then made of the burnout power or average flux over the whole channel length in each case, regardless of the position of burnout. This method has been suggested by others to give fair agreement for tubes at 2000 p.s.i.(7)[†] and 1000 p.s.i.(8). Comparison of cosine flux and uniform flux data (9, 10) for an annular section at 1000 p.s.i. confirms this hypothesis. It is appreciated that this is somewhat empirical since no account is taken of the location of burnout. These methods are subsequently referred to as the "overall length concept".

Methods D, E and F (Local Length Concept)

These three methods consider the possibility of burnout at a series of stations along the cosine flux tube: at each point considered, the distance, l, from the inlet is used as the length of tube with uniform flux, which from data a, b, or c above, and the same inlet condition, gives the predicted burnout flux at that point. By varying the distance l, the burnout line AB ... is plotted and the particular value of l, at which burnout takes place is where the cosine flux profile is tangential to the line AB. In evaluating the tests, the point at the end of each zone is considered. These methods are subsequently referred to as the "local length concept".

Methods G and H (Equivalent Length Concept)

These two methods are similar to D, E, and F in that they enable the burnout line AB to be plotted and hence the predicted burnout flux to be determined. In place of the actual distance of any point from inlet, however, an associated "equivalent length, L_e", is considered, defined as follows:-

$$L_e = \frac{1}{\phi_1}\int_0^1 \phi\, dl$$

where ϕ_1 = local value of flux on the cosine profile distance l from inlet.

†Numbers in parentheses refer to references in the original article.

The recommended method of predicting the magnitude of ϕ_{BO} and the location of burnout is quoted as follows:[15]

> If the requirement is for the prediction of burnout power regardless of the accuracy of predicting its location along the channel, then the local length concept using Barnett's equation for uniform flux data is recommended.
>
> If, however, accuracy of predicting the location of burnout has to be considered, as might well be the case when the channel length differs from available test data, then the recommendation is to use the equivalent length concept with Barnett's equation for uniform flux data. This, in general, gives a predicted burnout power higher than the local length concept and an allowance — say a reduction of 10% in the predicted power should then be made.
>
> For an approximate estimate, however, the burnout power can be predicted by considering the power on a uniform flux tube of same overall length and diameter. The experimental burnout power was then found to be predicted well at 560 p.s.i., to be 10-15% lower than the predicted power at 1000 p.s.i. and 0-10% higher at 1600 p.s.i.

Figure II-29 illustrates Lee-Obertelli uniformly and nonuniformly heated burnout data for nearly identical test sections. The average test-section heat flux at burnout is plotted against the steam-energy flow calculated using the exit quality at burnout. Although only a relatively small sample of the Lee-Obertelli data is shown in Fig. II-28, it is interesting to note that Ref. 15 contains DNB-2 type burnout data. A few runs in Fig. II-29 are plotted from Table 10 of Ref. 2, and it is evident that the Table 10 data plot above the Lee-Obertelli data (similar to the behavior shown in Fig. II-23). This is probably a length effect because the 1000-psia data shown in Fig. II-29 were taken in a test section having a length of 76 in. and an inside diameter of 0.540 in. These data from the 76-in. test section are from Ref. 19 and are plotted in Fig. III-12, *Power Reactor Technology*, 7(3). The Ref. 19 data in Fig. II-29 fall somewhat under the Mark I test-section data, but this is probably the effect of a slightly bigger inside diameter.

Discussion and Conclusions

The most direct way to treat nonuniformly heated test sections is possibly by Methods A, B, and C of Lee and Obertelli. This is based on treating the nonuniformly heated test section as one operating at the average heat flux and neglects the position of burnout. The results of this method are illustrated in Figs. II-20, II-21, part *b* of II-24, and II-29. With the exception of the data for the outlet-peak distribution in part *b* of Fig. II-24, this method is not as much in error as might be expected. Several of the inlet-peak and central-peak runs fell below the uniformly heated test-section results (part *b* of Fig. II-24), although the shape of curve *A* in that figure suggests rather peculiar behavior in any event.

The other somewhat obvious method of treating nonuniformly heated test sections is that of considering only local conditions — quality, mass flow, and heat flux. Figures II-17 to II-19 substantiate that this is not a bad approximation, although at lower mass flows (Fig. II-17) the data derived from the nonuniformly heated test section diverge significantly from data from uniformly heated test sections. Local conditions at burnout are not listed in Ref. 15, although the Lee-Obertelli Methods D, E, and F appear to be based on this concept and are recommended by them. Those runs (listed in Ref. 14) exhibiting burnout near the end of the test section are illustrated in Figs. II-25 and II-26. Although there are differences between the uniformly and nonuniformly heated test-section data, these are most noticeable with the outlet-peak test section (Fig. II-26). Figures II-27 and II-28 il-

Table II-2 DESIGN DATA ON TEST SECTIONS USED IN REF. 15

Designation	Flux profile	Ratio of maximum to average flux	Ratio of maximum to minimum flux	Heated length, in.	Extrapolated length, in.
Mark I	Stepped	1.25	2.4	72	100
Mark II	Stepped	1.43	8.0	72	78.8
Mark III	Smooth	1.45	9.7	72	76.8
Mark III*a*	Smooth	*	*	60	76.8

*The Mark III*a* tube was the Mark III tube with no power applied to the last foot of the tube.

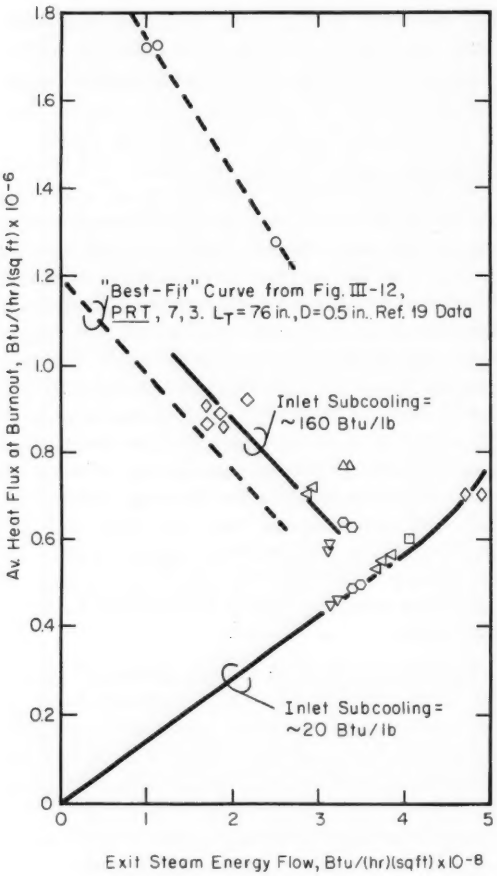

Fig. II-29 Steam-energy flow plot of data from Refs. 2, 3, 15, and 19. Pressure = 1000 psia, mass flow is as indicated, and the average heat flux is defined as in Fig. II-24.

lustrate the burnout data for those nonuniformly heated test sections exhibiting burnout well upstream of the exit. It is difficult to compare these upstream burnout data with uniformly heated test-section data because a substantial extrapolation of the uniformly heated data given in Ref. 14 is necessary. Burnout data from other sources for long, cylindrical test sections at 2000 psia were not readily available to the reviewer, although they may exist.

When the preceding data are considered, it appears that the designer is forced to a rather large degree of conservatism in trying to assess the effect of nonaxial power distributions in a reactor. Some of the uncertainty may be inevitable, but the situation might be helped by experiments designed to study the DNB-2 region in detail.

References

1. W. J. Levedahl, Application of Steam Energy Flow to Reactor Design, *Trans. Am. Nucl. Soc.*, 5(1): 149-150 (June 1962).
2. R. A. DeBortoli, S. J. Green, B. W. LeTourneau, M. Troy, and A. Weiss, Forced-Convection Heat Transfer Burnout Studies for Water in Rectangular Channels and Round Tubes at Pressures Above 500 psia, USAEC Report WAPD-188, Westinghouse Electric Corp., Bettis Plant, October 1958.
3. D. H. Lee and J. D. Obertelli, An Experimental Investigation of Forced Convection Burnout in High Pressure Water. Part I. Round Tubes with Uniform Flux Distribution, British Report AEEW-R-213, August 1963.
4. A Research Program in Two-Phase Flow, CISE (Centro Informazioni Studi Esperienze), Segrate (Milano), Italy, Jan. 31, 1963.
5. J. G. Collier, Heat Transfer and Fluid Dynamic Research as Applied to Fog Cooled Power Reactors, Canadian Report AECL-1631 (CRARE-1108), June 1962.
6. E. R. Quandt, Analysis and Measurement of Flow Oscillations, in *Heat Transfer—Buffalo, Chem. Eng. Prog. Symp. Ser.*, 57(32): 111 (1961).
7. M. Troy, Upflow Burnout Data for Water at 2000 psia in 0.097 in. × 1 in. × 27 in. Long Rectangular Channels, USAEC Report WAPD-TH-340, Westinghouse Electric Corp., Bettis Plant, July 1957.
8. H. S. Jacket, J. D. Roarty, and J. E. Zerbe, Investigation of Burnout Heat Flux in Rectangular Channels at 2000 psia, USAEC Report WAPD-AIW(IM)-3, Westinghouse Electric Corp., Bettis Plant, Dec. 5, 1955.
9. M. Troy, Upflow Burnout Data for Water in Rectangular Channels at Pressures from 600 to 1870 psia, USAEC Report WAPD-TH-321, Westinghouse Electric Corp., Atomic Power Division, September 1957.
10. M. A. Styrikovich et al., Effect of Upstream Elements on Critical Boiling in a Vapor Generating Pipe, USAEC Translation AEC-tr-4740 [*Teploenerg.*, 7(5): 81-87 (1960)].
11. I. T. Aladyev, Z. L. Miropolsky, V. E. Doroshchuk, and M. A. Styrikovich, Boiling Crisis in Tubes, in *International Developments in Heat Transfer*, Part II, pp. 237-243, American Society of Mechanical Engineers, 1961.
12. Yu. V. Evdokimov, V. Ya. Kozlov, V. G. Konochkin, L. A. Kocheltkov, A. K. Krasin, V. V. Litkin, V. S. Severyanov, B. A. Semenov, and G. N. Ushakov, Experience in the Operation of the First Atomic Power Station, *J. Nucl. Energy: Pts. A & B*, 18(3): 148-155 (March 1964).

13. E. Janssen and J. A. Kervinen, Burnout Conditions for Nonuniformly Heated Rod in Annular Geometry, Water at 1000 psia, USAEC Report GEAP-3755, General Electric Company, Atomic Power Equipment Department, June 1963.
14. H. S. Swenson, J. R. Carver, and C. R. Kakarala, The Influence of Axial Heat-Flux Distribution on the Departure from Nucleate Boiling in a Water-Cooled Tube, ASME Paper 62-WA-297, Nov. 25, 1962.
15. D. H. Lee and J. D. Obertelli, An Experimental Investigation of Forced Convection Burnout in High Pressure Water. Part II. Preliminary Results for Round Tubes with Non-uniform Axial Heat Flux Distribution, British Report AEEW-R-309, November 1963.
16. E. Janssen and J. A. Kervinen, Burnout Conditions for Single Rod in Annular Geometry, Water at 600 to 1400 psia, USAEC Report GEAP-3899, General Electric Company, Atomic Power Equipment Department, February 1963.
17. Letter to the Editors: Critical Heat Fluxes for a Bundle of Tubes Cooled in Pressurized Water, *J. Nucl. Energy: Pt. B*, 1(3): 197 (March 1960).
18. P. G. Barnett, An Investigation into the Validity of Certain Hypotheses Implied by Various Burnout Correlations, British Report AEEW-R-214, June 1963.
19. R. R. Hood and L. Isakoff (Comps.), Heavy Water Moderated Power Reactors Progress Report, May–June 1963, USAEC Report DP-855, E. I. du Pont de Nemours & Co., Inc., August 1962.

Section

III

Power Reactor Technology

Fuel Elements

Stainless-Steel-Cladding Failures in VBWR

The fuel elements under irradiation in the Vallecitos Boiling-Water Reactor (VBWR) as part of the AEC-sponsored Fuel-Cycle Program were described in *Power Reactor Technology*, 7(1) (see Table IV-1, page 28, of that issue and the accompanying description). These fuel elements comprised 50 assemblies, each made up of 16 metal-jacketed rods containing pressed and sintered UO_2 pellets of 0.376-in. diameter. The jackets were all designed to be free-standing. Twenty-four of the assemblies employed Zircaloy jackets 22 mils thick, and the remainder employed 20-mil annealed 304 stainless steel (10 assemblies) or 15-mil cold-worked 304 stainless steel (16 assemblies). A recent paper[1] describes the condition of these elements at the end of operation of the VBWR in December 1963, after the irradiation program had run for three years. The findings are summarized in Table III-1.

The two failures listed in Table III-1 for Zircaloy-jacketed rods appeared to be incidental; one was attributed to fretting wear and the other to some unknown cause. The larger number of failures of steel-jacketed rods, on the other hand, apparently resulted from some specific failure process. A performance limit apparently existed[1] for the 304-stainless-steel-jacketed rods at an exposure level of about 2.6×10^{20} fissions/cm^3. According to Ref. 1, cracking of the jackets caused the failures, which consistently occurred in the peak flux zone. Typically, the cold-worked material cracked longitudinally, whereas the annealed material cracked mostly in the circumferential direction and usually at pellet interfaces.

In Ref. 2 the failures are characterized as intergranular corrosion. The authors state that the characteristic failure is not limited to the elements tested under the Fuel-Cycle Program, but has been observed in essentially all the types of stainless-steel-clad elements irradiated in the VBWR. The cause of the cracking has not yet been determined, but evaluation of the data thus far indicates[2] that it results from a stress-assisted corrosion attack of the grain boundaries and that the mechanism becomes operative only after a long time in the reactor environment. The latter observation suggests that either a long crack-nucleation stage is involved or a material change takes place as a result of radiation damage or coolant environment which eventually makes the material sensitive to cracking. The occurrence of both circumferential ridging and cracking at the pellet interfaces of annealed cladding points to a relation between localized high stresses and strains and susceptibility to cracking. It is also stated in Ref. 2 that this is similar to cracking experienced in a pressurized-water-reactor environment, in which intergranular cracking occurred in unsensitized type 304 stainless steel that had been stressed beyond the yield point.*

Whether or not the cracking phenomenon is understood completely, a question of great practical importance is the extent to which the experience in VBWR is typical. Steel-jacketed elements are performing satisfactorily in the Yankee reactor, in which jackets of type 348 stainless steel are used. Thus we can ask whether the difference in behavior of the steel jackets results from typical differences between the boiling-water and the pressurized-water environments, whether it results from inci-

*Reference 2 cites the following report: T. J. Pashos, Experience with Stainless Steel as a Fuel Clad Material in Water-Cooled Power Reactors, Report APED-4260, September 1963.

Table III-1 FUEL-ELEMENT FAILURES OBSERVED IN VBWR UNDER THE FUEL-CYCLE PROGRAM[5]

Cladding material	Type designation	Cladding thickness, cm	No. of rods irradiated	No. of failures detected: Assembly sipping*	No. of failures detected: Rods visual	Type of failure	Probable cause of failure	Average exposure, fissions/cm^3 × 10^{-20} (Mwd/ton): Failed assembly	Lead assembly	Group average
Zircaloy-2	J	0.0588	381	1	1	Small hole	Fretting wear	2.41 (8358)	2.78 (9643)	1.8 (6250)
Zircaloy-4	J	0.0588	5	1	1	Small hole	Unknown	1.66 (5774)	Same	Same
Type 304 S.S., cold worked (75,000 psi yield strength at room temperature)	I	0.0381	252	1	1	Longitudinal crack 18 cm long	Intergranular corrosion	2.38 (8252)	2.65 (9193)	1.92 (6780)
				1	1	Longitudinal crack 1 cm long		2.03 (7044)		
				1	†	Unknown		2.65 (9193)		
				1	†	Unknown		2.32 (9042)		
Type 304 S.S., annealed (40,000 psi yield strength at room temperature)	H	0.0507	160	1	1	Circumferential cracks	Intergranular corrosion	2.24 (7770)	2.48 (8599)	2.13 (7400)
				1	1	Circumferential cracks		2.48 (8599)		
				1	2	Circumferential cracks		2.44 (8485)		

*Coolant water surrounding the fuel rods in an assembly is trapped and a sample withdrawn. The sample is analyzed for fission-product iodine and compared to results obtained from a nondefective assembly sampled in a similar manner. A higher concentration of radioactive iodine is interpreted as being indicative of a failure in the fuel-rod cladding.

†Inspection not yet performed.

dental differences in fuel-element design or operating conditions (such as the heat-flux level), or whether it is representative of the difference between types 304 and 348 stainless steels. The VBWR experience focuses interest on the fuel performance of the boiling reactors that do utilize steel-jacketed elements, notably Humboldt Bay, Big Rock Point, and Elk River. The first two reactors use type 304 stainless steel, whereas the Elk River reactor uses type 304 with an admixture of 600 ppm of boron as burnable poison.

Fission-Product Helium

As reported in a Westinghouse paper[3] presented at the June meeting of the American Nuclear Society, helium is in some cases one of the major gaseous constituents within the void spaces of irradiated oxide fuel rods. The gas has been found in fuel elements that have had no opportunity to acquire helium as part of the fabrication process. In some irradiated elements that have operated with UO_2 center temperatures below that at which equiaxed grain growth occurs (1500 to 1700°C), the helium has been found to be more abundant than the fission-product gases xenon and krypton in the void spaces. In these low-temperature cases, the fractional release of xenon and krypton from the UO_2 was less than 0.5%.

The primary source of helium is the ternary fission of ^{235}U, thus giving an alpha particle plus two larger fission fragments. The helium resulting from such ternary fissions has a reported[4] fission yield of about 0.3%, whereas the fission yield of xenon plus krypton ranges from 25 to 30%. The high fractional content of helium in the free gases within the elements is explained as the result of a high diffusivity of the helium in UO_2. As stated in Ref. 3, the observed fractional release of helium from UO_2 during irradiation of various experimental fuel rods ranges from about 10 to almost 100%, but no clear-cut correlation has been found between the fractional release and UO_2 temperature or burnup level. To account for the concentration

of helium relative to xenon and krypton in fuel elements operating at low temperature (less than 1500°C center temperature), the rate of diffusion of helium in UO_2 must be about 100 times greater than that of xenon and krypton. The helium phenomenon is thought to be significant as a contribution to the internal pressure within fuel-element jackets, and possibly, in some cases, as a contribution to the thermal conductivity of the gases in the pellet-jacket gap.

Steel-Lined Zircaloy-2-Clad Fuel Elements

The extensive fuel-element development programs at General Electric's Atomic Power Equipment Department (APED) were reviewed in Sec. IV of *Power Reactor Technology*, 7(1). One of the elements fabricated for irradiation in the VBWR under the Fuel-Cycle Program incorporated fuel rods clad with stainless-steel-lined Zircaloy-2. Reference 5 details the techniques used for fabrication of these rods.

Reasons for development of the lined Zircaloy-2-clad rods are briefly as follows. Early experiences at APED indicated that Zircaloy-2-clad rods were susceptible to failure by attack by fluorides contained as an impurity in the UO_2 fuel pellets and by hydrogen liberated in a chemical reaction within leaking fuel elements. It was postulated that a stainless-steel-lined Zircaloy-2 fuel rod would solve the hydriding and fluoride problems by interposing a nonreactive barrier (the stainless steel) between the fuel and cladding. Subsequent research, however (since 1961), indicated that defected Zircaloy-clad fuel rods could operate satisfactorily for long periods of time provided the UO_2 contained less than 35 ppm of fluoride.[5] Development work was, nevertheless, continued on the fabrication of lined elements and culminated in the VBWR irradiations.

The lined fuel rods contained pressed and sintered UO_2 pellets centerless ground to a diameter of about 0.37 in. The tubing was produced by a subcontractor using coextrusion; the fabrication involved the following steps:

a. Zircaloy-2 and 304L stainless-steel sleeves of the appropriate size were prepared and cleaned.

b. Mild steel canning components, which completely enveloped the stainless steel and Zircaloy, were prepared.

c. The various components were assembled and the mild steel can was welded shut, except for the opening in the evacuation tube.

d. The mild steel can was evacuated and sealed.

e. The assembled parts were then heated to 871 C (1600 F) and extruded, using an extrusion force of 136 to 182 metric tons and an extrusion ratio of 15.7 to 1.

f. The carbon steel canning was removed and the tubing was etched to remove any surface contamination.

g. The tubing was visually inspected, and prepared for shipping. No other inspection was performed...

The tubing was ordered early in 1961, and it is stated in Ref. 5 that commercial processes for the production of this type of tubing were not available at that time. Imperfections of various sorts were noted, but only 3 tubes out of the 20 received were bad enough to be rejected. The lining, which was type 304 stainless steel, had thicknesses varying from about 2 to 6 mils. It was metallurgically bonded to the Zircaloy-2, although the reaction zone was not extensive. Some blisters, which did not interfere with pellet loading, were noted on the inside diameter of the tubes where bonding had not taken place; the nominal cladding-to-pellet gap was about 0.004 in. Calculational techniques for sizing the cladding thickness and for the plenum design are presented.[5]

Irradiation of the lined fuel rods ended with the shutdown of the VBWR in December of 1963. At that time the rods had received an average exposure of about 6700 Mwd/ton, and no failures have been reported.

Boron-Containing Fuel Elements

The use of boron as a burnable poison in power-reactor cores usually involves a problem of how to incorporate the boron in the core composition. In a number of cases discrete shim strips containing boron have been installed specifically for the purpose, but a more desirable approach usually is to add the boron to one of the normally present core materials. This has been done in the Elk River reactor, which is supplied with 600 ppm of boron as an admixture to the type 304 stainless steel used for the fuel-element jackets. However, this approach has not yet been proved out by ex-

perience. Several recent reports describe development work at the General Electric Company[6] and at Combustion Engineering, Inc.,[7–10] on the incorporation of boron in fuel-element jackets and in the uranium oxide fuel material. The experimental fuel elements produced at General Electric have been previously cited in *Power Reactor Technology*, 7(1): 34-35 (Table IV-8) in the discussion of the Fuel-Cycle Program at General Electric. These fuel elements were incorporated in the Special Assembly 12L described in that program.

Special Assembly 12L contained some fuel elements with boron in the cladding and some with boron in the UO_2, as well as some elements without boron, for purposes of comparison. The borated cladding consisted of type 304 stainless-steel tubing, in either the annealed or the cold-worked condition and contained either 500 or 750 ppm of natural boron. The fuel was in the form of sintered pellets of UO_2 or in the form of powder, placed by vibratory compaction. The fabrication of the fuel rods with the borated stainless steel appeared to involve no special problems except the welding of the upper end-plug closure seal. Cracks appeared at the center of the weld bead due to the hot short condition of the high-boron alloy. The cracking was eliminated by a redesign of the weld configuration to control the stresses during the cooling period and by modifying the welding procedure to cause dilution of the weld metal to reduce the overall boron content.

The fuel rods fabricated with the burnable poison within the UO_2 fuel material are somewhat more interesting. Before the start of the in-pile test program, laboratory studies showed boron to have a migratory behavior at temperatures greater than 1000°F. Migration is undesirable because it results in changes in the self-shielding of the boron, or otherwise modifies the neutron flux level seen by the boron, and hence changes the reactivity worth and the rate of boron burnup. The APED experimenters therefore utilized boron as zirconium diboride, either as a fine, uncoated powder (−325 mesh) or as larger sintered particles sized between 100 and 200 μ and coated individually with a film of molybdenum metal or BeO.

The designs of two types of fuel rods (designated F and G) containing poisoned oxide are shown in Fig. III-1. The poison-bearing fuel was loaded into the tubes by vibratory compaction, and, as illustrated in the figure, three

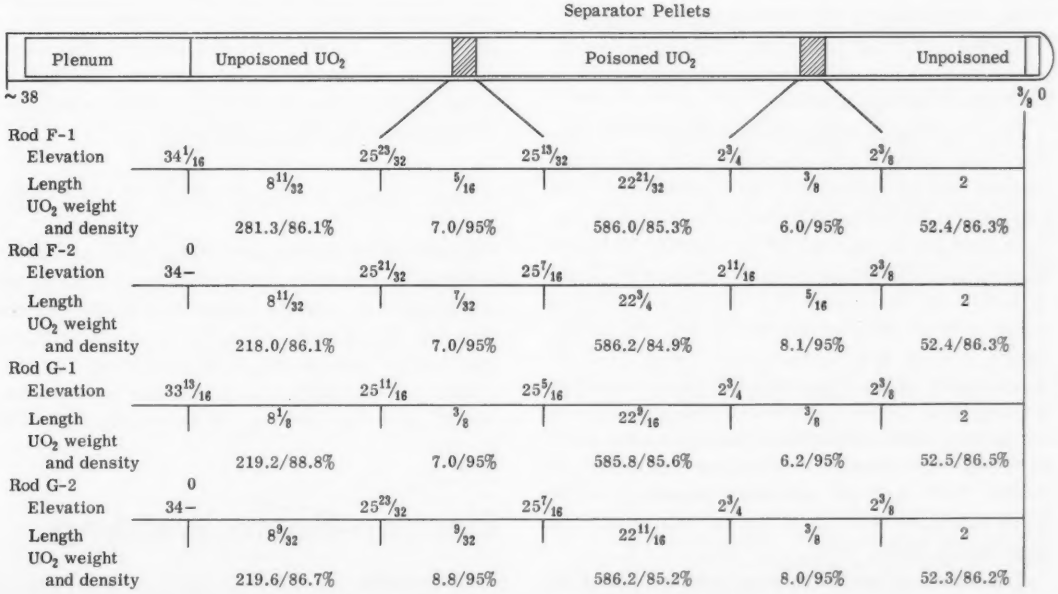

Fig. III-1 Locations and dimensions of fuel sections in rods[6] with poison in the UO_2. (Elevation and length are in inches.)

axial zones were provided. An additional two rods (designated type E) were fabricated of UO_2 containing BeO-coated ZrB_2 powder, but at the time of writing of Ref. 6 these rods had not been completed. The zoned loading indicated in Fig. III-1 was begun by filling and compacting the lower portion of the cladding tube. A $\frac{1}{4}$-in. sintered UO_2 pellet was then placed on top of the lower portion to act as a separator, and the fuel containing a mixture of UO_2 and coated or uncoated poison particles was compacted in place. Low g-level vibration was used during the initial loading of the poisoned zone to lock the sintered pellet in place and prevent its relative motion. After compaction of the middle zone, another separator was seated and the upper regions of the tube interior were cleaned of traces of poisoned fuel by means of a suction probe and swabs. The top zone was then loaded and compacted with unpoisoned fuel. A sleeve, not shown in Fig. III-1, was used to support the cladding in the region of the plenum. A perforated disk of stainless steel was welded to the lower end of the sleeve and served to prevent the powder from falling into the plenum or becoming loose during subsequent handling operations. The rods were evacuated, backfilled with helium at room temperature to a pressure of 1 atm, and sealed by welding on an end plug.

The shutdown of the VBWR also interrupted irradiation on the assembly incorporating the burnable-poison rods. An average exposure of 2972 Mwd/ton was attained.[11]

The Combustion Engineering work[7–9] to date has been with boron carbide, although other poisons are presumably to be investigated. The fabrication of boron carbide–UO_2 mixtures has been studied, as well as the mechanics of boron migration. Neutron physics studies are reported in Ref. 8 to determine B_4C particle sizes that would provide desired degrees of self-shielding. These results are contained in Table III-2. It is indicated in the reference that self-shielding factors from 0.5 to 0.6 are necessary to achieve burnable-poison utilization throughout the core lifetime, and hence the larger particles in Table III-2 are of interest. However, −325 mesh particles were used for the initial studies reported in Refs. 7–10.

A number of fuel rods have been prepared by electromagnetic and pneumatic vibratory-compaction methods, using admixtures of UO_2 and B_4C. Densities from 87 to 89% of theoretical were attained with the −325 mesh B_4C particles, although it is stated in Ref. 8 that the establishment of a uniform distribution of large particles of B_4C at low concentrations may be a problem. Local boron-concentration variations of less than ±20% from nominal were maintained; this was within the prescribed limits.

Table III-2 SELF-SHIELDING OF B_4C SPHERES[8]

Average particle diameter, in.	Self-shielding factors
0.001	0.98
0.005	0.90
0.010	0.79
0.020	0.63
0.030	0.50

The addition of boron compounds to UO_2 during fabrication of sintered pellets has been studied in the past, and Ref. 6 contains a brief bibliography on the subject. Boron losses discussed in Refs. 12 and 13 occurred during fabrication of fuel plates for the SM-1 reactor (the Army Package Power Reactor)[12] and during the sintering of UO_2 pellets containing boron compounds.[13] The approach at Combustion Engineering involves consideration of the various chemical reactions in which boron and its compounds can participate, as well as experimental investigations of volatilization by heating the boron-bearing UO_2. The following reaction is believed responsible for boron volatilization:

$$UO_{2(s)} + B_4C_{(s)} \rightarrow UB_{4(s)} + CO_{2(g)} \text{ or } CO + \tfrac{1}{2}O_2$$

Subsequent dissociation of UB_4 may provide a volatile boron species, but both analytical and experimental results indicate that the formation of significant amounts of volatile boron species is improbable in an operating fuel element. An irradiation program has been formulated[10] for the testing of boron-bearing UO_2 in-pile.

Electron-Beam Welding

Fabrication of fuel-element components of substantial length by means of electron-beam welding is reported in Ref. 14. Figure III-2 illustrates the various types of weld joints

studied, and Table III-3 gives the relative sizes used. The material employed was exclusively reactor-grade Zircaloy-2.

Problems associated with each type of weld shown in Fig. III-2 are discussed, and examples are given of welds produced with the equipment used.[14] Because weldments of about 9 ft were studied, fitup, fixturing, and work-carriage operation were important, for any distortion tended to magnify the positioning error of, for example, a burn-through weld where the inner rib might not be visible. The authors conclude that the electron-beam welding process has proved highly successful. Several 9-ft-long assemblies were fabricated with the use of this process, and a number of shorter test weldments of considerable complexity are illustrated.[14] An earlier discussion of the electron-beam welding is contained in *Power Reactor Technology*, 2(2): 33-34 (March 1959).

Table III-3 DIMENSIONS OF TYPICAL WELDMENT COMPONENTS[14]

Type of joint	Part	Dimensions
1	Tubular cladding	3.070 in. OD by 0.060 in. wall
	Rib	0.062 in. thick
2	Tubular cladding	2.330 in. OD by 0.060 in. wall
	Rib	0.062 in. thick
3	Large tubular cladding	2.330 in. OD by 0.060 in. wall
	Small tubular cladding	0.565 in. OD by 0.30 in. wall
4	Both pieces of tubular cladding	0.565 in. OD by 0.030 in. wall
5	Tubular cladding	0.565 in. OD by 0.030 in. wall
	Round wire	0.072 in. diameter

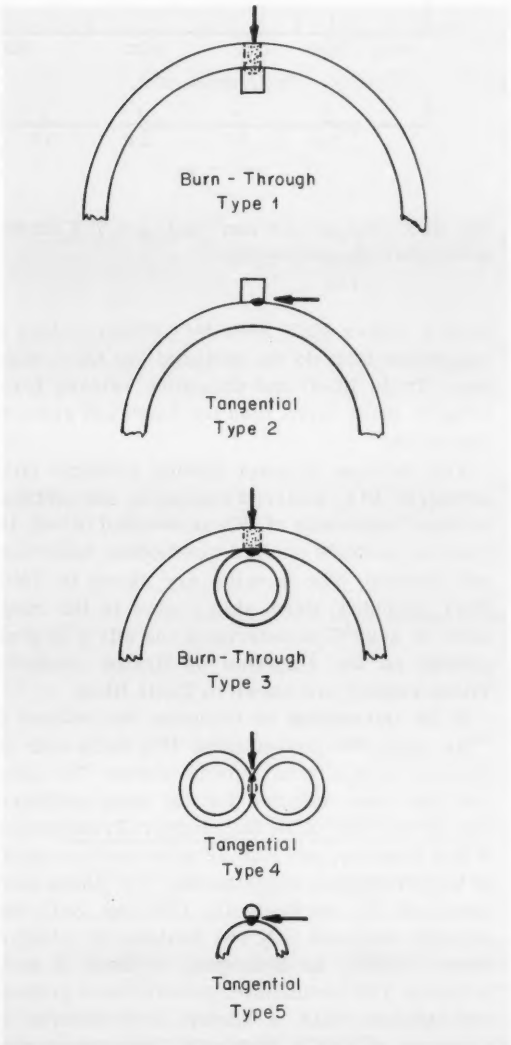

Fig. III-2 Weld-joint descriptions and designations.[14]

Irradiation Effects in UO_2

Information continues to accumulate to aid the designer in predicting the performance of UO_2-bearing fuel elements. References 15 and 16, in particular, are review articles that contain a wealth of material on UO_2 and, in the case of Ref. 15, on a number of other uranium compounds. In addition, *Reactor Materials*, 6(4), contains a feature article on the behavior of fission gases in ceramic reactor materials.

Reference 17 is a report on the emission of ^{133}Xe from irradiated UO_2 in the form of spheroids and powders. The materials are characterized in Table III-4; they were prepared as follows:

Powder specimens were prepared by precipitation of ammonium diuranate from nitrate solution and calcination at 900°C in air, followed by reduction in hydrogen at the same temperature. The preparation was divided into two portions; both were annealed in hydrogen for 5 hrs., one at 1250°C and the other at 1650°C. The latter preparation sintered during annealing and was therefore crushed to pass 400 mesh. Finally, both preparations were reduced in carbon monoxide at 800°C immediately prior to irradiation.

Sintered spheroids, Group A. These were prepared by spheroidising fragments of green compacts

of uranium dioxide in a gyratory mill. Densification was achieved by sintering in cracked ammonia at 1650°C. Finally the required size fractions were produced by sieving.

Sintered spheroids, Group B. These were prepared by blending uranium dioxide powder with binder to produce a granular mix. After sieving out the appropriate size range, the granules were densified by rotation in a gyratory mill and finally sintered.

Fused spheroids were prepared by passing fragments of sintered compacts through the flame of a plasma torch. Any material which had by-passed the torch was separated by rolling the product down an inclined plane. A portion of each of the two preparations studied was annealed in vacuo for 2 hours at 1650°C and cooled slowly in order to relieve any stress.

Table III-4 PHYSICAL PROPERTIES OF UO_2 SPHEROIDS AND POWDERS[17]

Sample type and No.	Mean radius, μ	BET* area, cm^2/g	Equivalent sphere radius, μ	Roughness factor
Sintered spheroid Group A				
A1	150	25	114	1.3
A2	40	103	29	1.5
Sintered spheroid Group B				
B1(a)	>200			
B1(b)	110	88	33	3.3
B2	150	23	125	1.2
B3	120	55	52	2.3
Fused spheroid				
F1	60	200	14	4.3
F2	60	115	25	2.4
Fused spheroid, annealed				
F1/A	60	75	38	1.6
F2/A	60	77	37	1.6
Powder				
P1		9100	0.31	
P2		1300	2.2	

*Brunauer, Emmett, Teller.

The results of the experiments are shown in Fig. III-3. It is stated in Ref. 17: "...any differences between sintered compacts of gram size, sintered spheroids of about 50 microgram size and fine powders are experimentally undetectable." The fractional release of xenon, to a first approximation, is proportional to the product of the diffusion coefficient, the square of the sample density, and the square of the BET surface area. The powdered materials

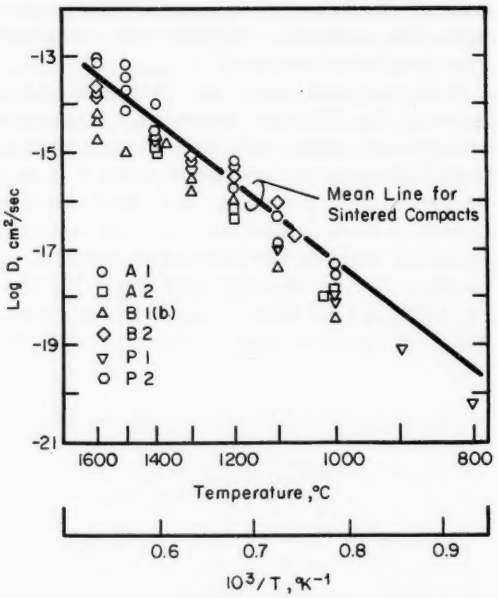

Fig. III-3 Plot of log D (cm^2/sec) vs. $1/T$°K for sintered spheroids and powders.[17]

have a larger BET area by several orders of magnitude than do the sintered and fused samples (Table III-4) and therefore release fractionally more xenon than the fused and sintered materials.

The release of other fission products from powdered UO_2, sintered compacts, and sintered or fused spheroids of UO_2 is detailed in Ref. 18. Fission products studied were iodine, tellurium, and cesium. The results are shown in Table III-5. Samples were also heated in the range 2000 to 2200°C to determine the effect of grain growth on the emission of fission products. These results are shown in Table III-6.

It is interesting to compare the release of ^{133}Xe from the conventional UO_2 fuels with the release from zirconia-urania plates. The latter fuel has been selected for the seed portion of the second core of the Shippingport Pressurized-Water Reactor, and Ref. 19 presents the results of the irradiation experiments. The plates were prepared by mechanically blending ZrO_2 and slightly enriched UO_2 and heating the blend at about 1700°C, in hydrogen, to form a solid solution. The comminuted powders were pressed into plates, with a binder, and sintered in hydrogen at 1750°F. Table III-7 lists the properties of the ZrO_2-UO_2 plates along with those of

Table III-5 EMISSION OF FISSION-PRODUCT[18] IODINE, TELLURIUM, AND CESIUM FROM UO_2

(Results Expressed as the Ratio $\sqrt{D_i'/D_{Xe}'}$)

Sample No.	Density, g/cm³	Surface area, cm²/g	Temp., °C	I	Te	Cs
Powder						
P/2		1,300	1,400	0.98	1.05	0.9
Sintered compact						
S/1	6.40	23,000	930*	0.55		0.45
S/2	6.75	19,200	1,000	0.9	1.1	>0.03
S/3	7.07	17,200	1,000	0.7	0.4	0.3
S/5	8.85	7,800	1,000	1.3	0.9	0.9
			1,000	0.7		
			1,200	0.7	0.8	0.8
			1,200	0.6		
			1,200	0.8	0.8	
S/7	8.15	1,370	1,200	1.3	1.9	0.6
			1,600	1.1	1.1	0.9
S/8	8.50	730	1,600*	1.1	1.1	0.3
			1,600*	1.5	1.5	0.7
S/9	10.3	140	1,000	3.9	2.8	2.4
			1,000	6.3	4.9	5.1
			1,200	2.9	3.9	1.4
			1,400	2.3	2.7	1.4
S/19		~100	1,600*	1.3		2.3
S/18	10.3	10	1,600*	4.4	10	6.3
S/14	10.8	5	1,600*	2.5	11	0.8
S/15	10.16	4	1,300	7.3	6.7	15.2
Sintered spheroid						
A1		25	1,200	2.1	2.6	1.0
			1,400	5.3	6.3	4.6
			1,600	2.7	10.5	0.6
			1,600	4.1	14.0	2.5
			1,600	3.5	21.0	0.8
			1,600	1.4	21.0	0.6
A2		103	1,400	2.5	3.3	2.5
Fused spheroid						
F2/A	10.6	77	1,200	2.0	5.7	1.0
			1,600	4.1	16.1	1.8

*Data obtained from a single analysis at the end of a 2-hr run.

Table III-6 FISSION-PRODUCT AND URANIUM EMISSION FROM UO_2 DURING GRAIN GROWTH[18]

(Sample No. S/13, Surface Area 7 cm²/g, Density 10.7 g/cm³)

Temperature, °C (±50°C)	Time, hr	Fraction released of								
		^{133}Xe	^{131}I	^{132}Te	^{137}Cs	^{89}Sr	^{140}Ba	^{106}Ru	^{144}Ce	U
2000	2.1	0.05	0.14	0.18	0.11	0.09	0.05	0.01	0.02	
2000	4.5	0.34		0.59	0.12	0.14	0.17	0.12	0.05	0.04
2050	1.5	0.23		0.66	0.21	0.19	0.20	0.22	0.08	0.10
2150	1.5	0.16	0.19	0.39	0.06	0.15	0.15	0.15	0.06	
2200	1.5	0.72		0.68	0.11	0.52	0.54	0.63	0.25	0.26
2200	5.0	0.99		0.94	0.33	0.83	0.74	0.78	0.47	0.45

Table III-7 CHEMICAL AND PHYSICAL PROPERTIES OF SINTERED ZrO_2-UO_2 PLATES[19]

Nominal composition	Isotopic analysis, at.% ^{235}U	Chemical analyses Wt.% U	Wt.% Zr	Ppm Al	Ppm Fe	Ppm Si	Density, % of theoretical	Grain size, μ	Roughness factor	Geometrical size, in.
ZrO_2–26 wt.% UO_2	3.75	22.7	54.9	39	180	170	98.0	10 to 25	0.9	1.5 by 0.25 by 0.05
ZrO_2–35 wt.% UO_2	3.75	31.0	47.9	120	350	64	96.5	9 to 18	1.2	1.5 by 0.25 by 0.05
UO_2	0.71	88.1		10	21	20	97.0	20 to 100	2.2	1.5 by 0.25 by 0.10

some plates made only of UO_2. The plates were sealed in quartz tubes and irradiated at nominal room temperature in the Brookhaven Research Reactor. The ^{133}Xe was then collected in charcoal traps during isothermal high-temperature anneals.

Diffusion coefficients for the various materials tested are shown in Fig. III-4. The slightly irradiated ZrO_2-UO_2 solid solutions exhibited higher ^{133}Xe release rates, diffusion coefficients, and activation energies than unalloyed UO_2. Microstructure was determined both before and after irradiation. In the as-fabricated condition, the 26 wt.% material showed only a single phase present (face-centered tetragonal), whereas the 35 wt.% material showed two phases (major phase was equiaxed face-centered tetragonal, and minor phase was transformed tetragonal). The phase transformations during irradiation and the post-irradiation heat-treatment are discussed in Ref. 19. This discussion would be of interest to the specialist.

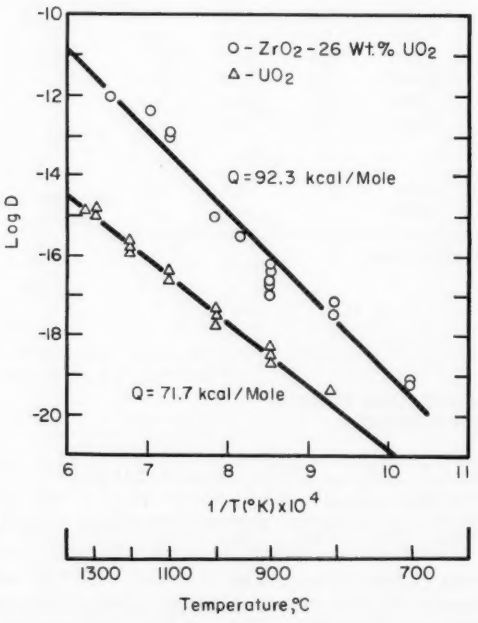

Fig. III-4 Variation of D with temperature: comparison[19] of cubic UO_2 and tetragonal ZrO_2–26 wt.% UO_2.

A number of Hanford reports deal with the change in physical properties of UO_2 under irradiation.[20–22] These reports contain much specialized information but are also of general interest. The melting point of UO_2, for example, depends on irradiation.[20] Samples of irradiated UO_2 from 0.005 to 11.3 at.% uranium were obtained from a variety of test capsules with different fabrication and irradiation histories. Aliquots of tens of milligrams were heated in a resistance furnace in direct contact with a tungsten heating element. The aliquots were observed through an external microscope, and the temperatures were measured with an optical pyrometer. Crystal growth and vaporization were observed photographically.

A melting point of 2790 ± 20°C was observed for 95% dense UO_2 that was pressed and sintered in hydrogen for 12 hr at 1750°C. Figure III-5 illustrates the behavior of the melting point with irradiation. Although there is considerable scatter of the data, a justification for the shape of the curve at exposures less than 0.4 at.% burnup is given.[20] Measurements were also made on nonstoichiometric UO_2, and these data are contained in Ref. 20. References 21 and 22 report physical property data for irradiated and nonirradiated polycrystalline and single-crystal UO_2.

Reference 23 is related to Ref. 20 and is cited here for completeness, although it is not concerned with irradiated UO_2. It reports on the density changes exhibited by UO_2 upon melting. Single crystal pins of UO_2 were heated in sealed tungsten capsules. With the use of ^{60}Co source and photographic film, the density of the crystals was determined radiographically.

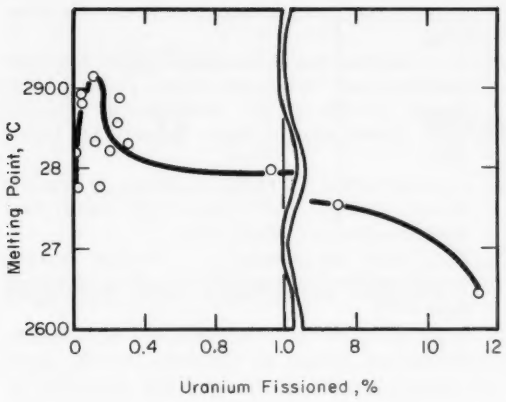

Fig. III-5 Melting point vs. in-reactor exposure[20] for irradiated UO_2.

Data were taken at temperatures from 1280 to 3100°C, and the results are shown in Fig. III-6. The density of the solid at 2800°C was determined to be 9.67 ± 0.13 g/cm^3, and that of the liquid was determined to be 8.7 ± 0.16 g/cm^3. The coefficient of expansion of the molten UO_2 was 3.5×10^{-5}/°C between 2800 and 3100°C. An empirical formula is presented for specific volume as a function of temperature between 0 and 2800°C.

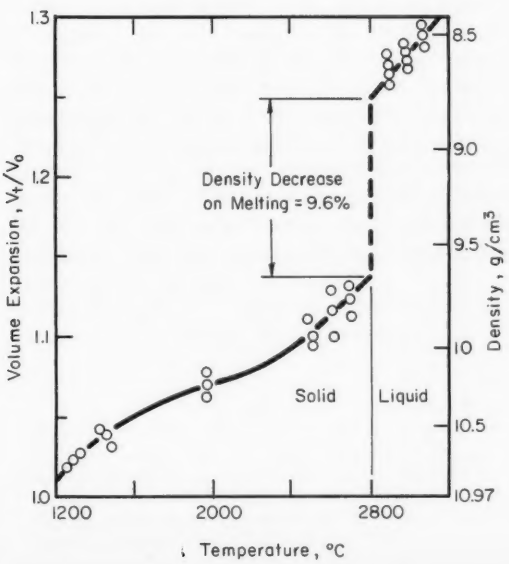

Fig. III-6 Volume and density change[23] of UO_2.

References

1. H. E. Williamson, J. P. Hoffman, C. J. Baroch, and T. J. Pashos, Comparative Performance of Similar Zircaloy- and Stainless-Steel-Clad Fuels in the VBWR, *Trans. Am. Nucl. Soc.*, 7(1): 105 (June 1964).
2. T. J. Pashos, W. H. Arlt, C. J. Baroch, and H. E. Williamson, The Intergranular Corrosion of Stainless Steel Cladding in Water Reactor Environments, *Trans. Am. Nucl. Soc.*, 7(1): 119 (June 1964).
3. R. N. Duncan, C. J. Kubit, D. R. McClintock, and W. R. Smalley, The Formation and Release of Helium from UO_2 Fuel During Irradiation, *Trans. Am. Nucl. Soc.*, 7(1): 89-90 (June 1964).
4. S. Katcoff, Fission-Product Yields from Neutron-Induced Fission, *Nucleonics*, 18(11): 201-208 (November 1960).
5. C. J. Baroch, Design and Fabrication of Fuel Rods Clad with Stainless-Steel-Lined Zircaloy-2, USAEC Report GEAP-4555, Vallecitos Atomic Laboratory, Feb. 7, 1964.
6. S. Y. Ogawa and H. E. Williamson, Design and Fabrication of Special Assembly 12-L. Two Designs for Utilizing Boron as Burnable Poison, USAEC Report GEAP-4312, General Electric Company, Atomic Power Equipment Department, July 15, 1963.
7. G. Zuromsky, R. C. Brayer, W. C. Taylor, and W. P. Chernock, Burnable Poison Additions to UO_2, Quarterly Progress Report for Period Ending March 31, 1963, USAEC Report CEND-179, Combustion Engineering, Inc., April 1963.
8. G. Zuromsky, R. C. Brayer, and W. P. Chernock, Burnable Poison Additions to UO_2, Summary Report, July 1, 1962–June 30, 1963, USAEC Report CEND-181, Combustion Engineering, Inc., November 1963.
9. R. C. Brayer and W. P. Chernock, Burnable Poison Additions to UO_2, Progress Report, Period Ending December 31, 1963, USAEC Report CEND-203, Combustion Engineering, Inc., January 1964.
10. R. C. Brayer and W. P. Chernock, Burnable Poison Additions to UO_2, Progress Report, Period Ending March 31, 1964, USAEC Report CEND-3107-210, Combustion Engineering, Inc., April 1964.
11. C. L. Howard (Comp.), Fuel Cycle Program—A Boiling Water Reactor Research and Development Program, Fourteenth Quarterly Progress Report, October–December 1963, USAEC Report GEAP-4481, General Electric Company, Atomic Power Equipment Department, Jan. 7, 1964.
12. Oak Ridge National Laboratory, Army Package Power Reactor Project Annual Progress Report for Period Ending January 31, 1960, USAEC Report ORNL-2907, Apr. 4, 1960.
13. G. L. Ploetz and H. G. Sowman, Burnable Poison Additives to Uranium Dioxide, USAEC Report

KAPL-1447, Knolls Atomic Power Laboratory, Nov. 17, 1955.

14. R. F. Klein, Electron Beam Welding of Nuclear Fuel Cladding Components, USAEC Report HW-79143, Hanford Laboratories, October 1963.
15. J. B. Melehan, V. W. Storhok, R. J. Burian, M. Kangilaski, and R. A. Wullaert, The Effect of Nuclear Radiation on Ceramic Reactor-Fuel Materials, Report REIC-27, Battelle Memorial Institute, Radiation Effects Information Center, June 30, 1963.
16. B. G. Childs, Review Article, Fission Product Effects in Uranium Dioxide, *J. Nucl. Mater.*, 9(3): 217 (August 1963).
17. D. Davies and G. Long, The Emission of Xenon-133 from Lightly Irradiated Uranium Dioxide Spheroids and Powders, British Report AERE-R-4347, June 1963.
18. D. Davies, G. Long, and W. P. Stanaway, The Emission of Volatile Fission Products from Uranium Dioxide, British Report AERE-R-4342, June 1963.
19. J. C. Clayton, The Evolution of Xenon-133 from Slightly Irradiated Zirconia-Urania Plates, USAEC Report WAPD-TM-313, Westinghouse Electric Corp., Bettis Atomic Power Laboratory, August 1963.
20. J. A. Christensen, Irradiation Effects on Uranium Dioxide Melting, USAEC Report HW-69234, Hanford Laboratories, March 1962.
21. J. L. Bates, Microhardness of Uranium Dioxide, USAEC Report HW-77799, Hanford Laboratories, June 1963.
22. J. L. Bates, J. A. Christensen, and J. L. Daniel, Irradiation Effects in Uranium Dioxide Single Crystal, USAEC Report HW-73959, Hanford Laboratories, September 1962.
23. J. A. Christensen, Thermal Expansion of Uranium Dioxide, USAEC Report HW-75148, Hanford Laboratories, Oct. 4, 1962.

Section

IV

Power Reactor Technology

Materials

Boron for Control Rods

That boron is still the most important control material is borne out by the number of power reactors in which it is used as a neutron absorber and by the amount of work reported on its properties. Several recent reports give further information on its use as a control absorber.

The Pathfinder nuclear superheat reactor, one of the more interesting concepts presently in the late development stage, has boron in both the boiler and superheat control rods. [The Pathfinder design was reviewed in *Power Reactor Technology*, 7(3).] The boiler control rods[1] are cruciform with a blade thickness of $\frac{1}{4}$ in. They are made of type 304 stainless steel containing 2 wt.% natural boron. The blade surfaces are bare to the coolant water. The overall poisoned length of the blades is 72 in., and additional short nose and tail sections are of 304 stainless steel. The superheater control rods, unlike the boiler rods, are not required to scram and are expected to be fully withdrawn from the core during normal operation. These are cylindrical rods, $\frac{3}{4}$ in. in diameter, consisting of a core of 304 stainless steel containing 2 wt.% natural boron and a mechanically bonded cladding of 304L stainless-steel tubing 0.020 in. thick. The poisoned length is again 72 in., and the rods have a short nose of 304 stainless steel and a gas space above the poison at the top of the rod.

The mechanical properties of the two boron–stainless-steel alloys are as follows:

	Boiler rod	Superheater rods
Tensile strength, psi	82,300	94,200
Yield strength, psi	42,700	64,100
Elongation, %	7.9	11.5
Rockwell B hardness	96.8 ± 3	
Impact strength, ft-lb	6.5 ± 5	

Impact strengths on the boiler material were determined on unnotched specimens. Similar specimens of boron-free 304 stainless steel gave impact values of 27.7 ft-lb.

The cruciform boiler blades were assembled in special fixtures by manual arc welding with the use of coated E-308-16 rods. The blades were subsequently stress relieved at high temperature. Stress relief is of obvious importance for such a component, but the selection of a suitable temperature demands a choice between moderate temperatures, which require long treatment times and introduce the danger of sensitization, and higher temperatures, with the attendant difficulties of distortion during cooling. Specific data on the stress-relief procedure for the Pathfinder rods would be of interest.

Analysis showed that distortion of the rods due to thermal gradients in the rod channels would not be excessive. Calculated impact stresses for the boiler rods at a maximum velocity of 22 in./sec at scram gave a maximum value of 5980 psi. In test a prototype boiler rod underwent 990 scram cycles and 22,388 cycles through a 6-ft stroke. Because the prototype differed from the reactor rods in that it did not have the 304L stainless-steel tip at the contact end, impact conditions were particularly severe, but dye-penetrant inspection showed no cracks in the unirradiated prototype. The superheat control rod, although not intended to undergo scram operation, was also tested for 20 scram cycles with no adverse effects.

Since the ex-pile behavior of the rods appeared to be satisfactory, a literature search was conducted to supply data from which the operating behavior could be predicted. The tabular data, as compiled in Ref. 2, are given in Tables IV-1 and IV-2. The hardness of boron stainless steel was also found to increase rapidly up to 8×10^{19} neutrons/cm^2 (nvt) and

Table IV-1 MECHANICAL PROPERTIES OF UNIRRADIATED AND IRRADIATED BORON STAINLESS STEEL[2]

Wt.% boron*	Test temperature, °C	Core at.% burnup† or nvt dose	Yield strength, psi	Tensile strength, psi	Elongation, %	Ref.
0	23	0	37,500	90,000	50	2
0	23	2.7×10^{20} nvt	82,000	104,000	40	2
1.0^{10}	23	0	93,400	121,000	15.6	3
1.0^{10}	23	0.7	149,500	153,500	3.4	3
1.0^{10}	23	1.1		137,100	1.6	3
1.8^{N}	23	0	41,300	84,200	8	4
1.8^{N}	23	0.5	136,000	151,000	0.5	4
1.8^{N}	315	0.5	85,500	119,000		4
2.0^{10}	23	0		88,400	8.1	5
2.0^{10}	23	0.3		93,300	0.5	5
2.0^{10}	23	0.8		78,800	0.4	5
2.04^{N}	23	0	47,000	89,000	5.4	4
2.04^{N}	23	0.6	97,800	120,000		4
2.04^{N}	315	0.6	71,300	106,000		4

*Superscripts refer to whether the boron was natural (N) or enriched to 93% in the ^{10}B isotope (10).

†Core at.% is the concentration of one particular element or isotope in terms of all the atoms in the boron–stainless-steel alloy.

Table IV-2 IMPACT STRENGTH OF UNIRRADIATED AND IRRADIATED BORON STAINLESS STEEL[2]

Wt.% boron	Test temp., °C	Core at.% burnup or nvt dose	Unirradiated ft-lb	Irradiated ft-lb	Ref.
0	23	3.0×10^{20} nvt	15.9	15.7	4
1.8^{N}	23	0.3	1.0	0.44	4
1.8^{N}	315	0.3	1.0	0.35	4
2.0^{10}	23	0.8	4.4	0.16	5
2.0^{10}	315	0.8	2.3	0.24	5
2.04^{N}	23	0.6	0.64	0.22	4
2.04^{N}	315	0.6	0.64	0.05	4

then remain nearly constant at higher doses. No correlations between hardness and mechanical properties were found in the literature, but the notch sensitivity of the material was emphasized. Although the tables indicate that losses in both elongation and impact resistance are large for relatively small burnups, the Pathfinder discussion places considerable emphasis on the fact that, in use, control-rod boron is burned preferentially from the surface to the center. The figures given in Ref. 2 are for an average burnup of 1 at.% in the boron-containing portions of the rod; at this average burnup the surface burnup would be 1.3 at.% and the center only 0.6 at.%. The designers would thus expect the rod to retain more ductility at the center, although the tables indicate that even this ductility would be quite limited. In this regard the method of fabrication of the control rod may be quite important. The Pathfinder rod design is such that no stress raisers or notch formers are introduced at the surface. With spot-welded designs, if cracks are initiated at these welds on the surface, propagation through even a low-burnup central region would seem possible.

Crack initiation at spot-welded areas is likely, as shown by some EBWR experience in which 60% of the spot welds showed $\frac{1}{4}$-in. or larger cracks in 2 wt.% boron stainless steel at only 0.4 at.% burnup. Cracks were also initiated in the weld areas of Dresden control rods employing stainless steel with 2 wt.% boron. The welds in this core were fusion welds of the general type used in Pathfinder, but the boron stainless steel was cold rolled rather than annealed, and the Pathfinder stress relief is expected to provide crack resistance.

The data on swelling as provided by the literature survey[2] are presented in Fig. IV-1. Because the data were taken from various sources employing different experimental techniques, the spread in values is not unexpected. The points grouped at 1 core at.% burnup show a swelling rate of between 1 and 4% between 450 and 600°F. For temperatures above 600°F, swelling behavior was inferred from work on

postirradiation annealing. These data are given in Fig. IV-2 and are pertinent to superheat control-rod behavior. The swelling at 600°C, for instance, would be assumed to be equal to the sum of the volume increase at lower temperatures (Fig. IV-1) plus the volume increase on annealing (Fig. IV-2).

From the literature survey it was concluded that 1 core at.% burnup is the threshold for observable effects under Pathfinder conditions and that cracking should not occur below 1.5 core at.% burnup. Swelling of from 2 to 3 vol.% is to be expected per 1 core at.% burnup in the boiler rods, with possibly larger rates of swelling in the higher temperature superheater rods. Burnup limits of 1 core at.% were set for the boiler control rods and ½ core at.% for the superheater.

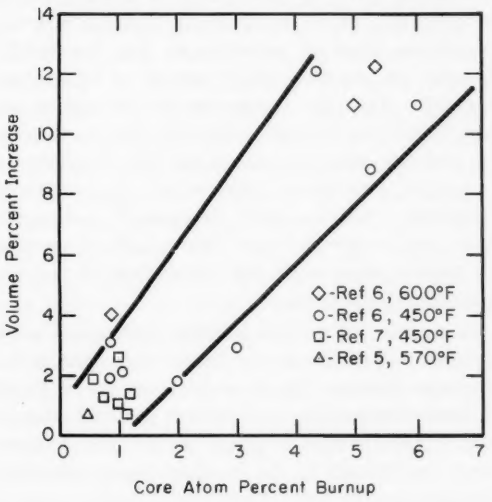

Fig. IV-1 Volume percent increase vs. core atom percent burnup for irradiated boron stainless steel.[2]

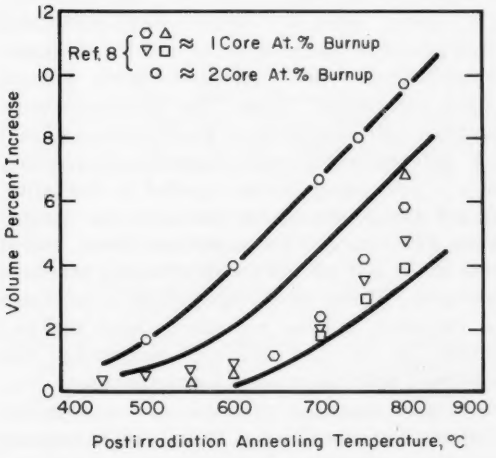

Fig. IV-2 Volume percent increase vs. postirradiation annealing temperature for 1 and 2 core atom percent burnup.[2]

For control-rod applications, boron may also be used in the form of boron carbide, B_4C, which is presumably more stable than the elemental form. A report from Atomics International[9] describes work on the compatibility of boron carbide with copper, types 430 and 304 stainless steels, and AISI 4130 steel at temperatures from 750 to 1300°F. Diffusion couples of B_4C and the alloy under study were prepared by hot-pressing the powdered carbide into a cavity in the alloy under vacuum. The sealed couples were then soaked at the test temperatures for periods up to 10,000 hr. Compatibility was determined by metallographic examination and hardness traverses. Copper and type 430 stainless steel were compatible with B_4C for 10,000 hr at 1300°F, whereas type 304 stainless steel was compatible for the same period at 1100°F but not at 1300°F. The 4130 steel was compatible for 10,000 hr at 750°F but not at 950°F and above. Also, with copper and types 430 and 410 stainless steels, little or no difference occurred in the behavior of normal B_4C (21.7% carbon), hypostoichiometric B_4C (18% carbon), and hyperstoichiometric B_4C (28% carbon) under similar but shorter tests.

The results of irradiation of boron carbide and zirconium boride dispersions in Zircaloy-2 and aluminum oxide have been reported by Battelle.[10] Pellets of Al_2O_3 containing B_4C, and hot-extruded pellets of Zircaloy-2 containing either B_4C or ZrB_2, were irradiated in the 450 to 500°F temperature range to ^{10}B burnups of 81 to 96%. The alumina pellets showed excessive cracking and poor corrosion resistance in water at 600°F. The Zircaloy-2 containing B_4C was superior to the materials containing ZrB_2 with regard to radiation stability and swelling. Both types of Zircaloy-2 pellets showed good gas retention and corrosion behavior.

Boron carbide might be usable as a burnable poison in the form of solid bodies, or lumps, as well as in the dispersion form. Reports from Westinghouse[11,12] discuss the fabrication of wafers of high-density B_4C, and B_4C plus silicon

carbide, and their subsequent irradiation. The preparation of the compacts by hot pressing is described in detail in Ref. 11. The need to develop a product that could cover a wide range of ^{10}B contents led to a study of enriched boron, depleted boron, and natural boron in the form of B_4C. Also studied were mixtures of B_4C and SiC. High densities (99%) were sought and obtained because of the requirement for corrosion resistance and gas retention. Both B_4C and B_4C-plus-SiC pellets of high density were shown to have excellent corrosion resistance to 680°F water ex-pile. Because the pellets were intended for use in the Shippingport PWR compartmental fuel elements, methods of diffusion bonding and gas-pressure bonding were developed to seal the Zircaloy-2 compartments around the B_4C pellets. During bonding the pellets were coated with carbon to prevent interaction between the pellet and the cladding. [The compartmented fuel plates for Shippingport were discussed in *Power Reactor Technology*, 7(2).]

Clad elements were irradiated in 450 to 510°F water to depletions as high as 97% of ^{10}B atoms.[12] Swelling and buckling of the pellets occurred within the compartments, and the B_4C-plus-SiC elements showed greater swelling, due to excessive cracking, than the B_4C elements. Irradiation reduced the corrosion resistance of the B_4C elements to the point that all intentionally defected elements showed a complete loss of poison. Although B_4C elements would permit higher ^{10}B loadings than are possible with boron stainless steel, the plasticity and deformation of the carbide under irradiation and its loss of corrosion resistance in-pile raise some question as to the application of B_4C elements.

Transition Joints of Zircaloy to Stainless Steel

For pressure tubes and similar applications within reactor cores, Zircaloy is, of course, extremely attractive because of its low cross section and other properties. Satisfactory methods for joining Zircaloy to stainless steel or other alloys would make it possible to secure the advantage of neutron economy in the core, and at the same time much cheaper and more readily fabricated materials could be used in regions where their cross sections are of little importance. One of the more interesting methods for joining Zircaloy to stainless steel, particularly for tubular products, is the technique of coextrusion, or tandem extrusion. The tandem extrusion method for preparing a Zircaloy–stainless-steel joint was reviewed in *Power Reactor Technology*, 6(2): 51-52. The method consists in the extrusion of a canned composite fillet made up of a cone-shaped length of stainless steel followed by a cone of Zircaloy canned in mild steel. For the production of tubes, the composite fillet is pierced for a mandrel as in conventional tube extrusions. Extrusion temperatures must be selected so that the "stiffnesses" of the two alloys match as closely as possible. But the temperatures cannot be so high that there is interaction between the alloys or that the beta transition for the Zircaloy is exceeded. Interfaces between the Zircaloy and stainless steel in such extrusions are quite thin, just a few microns thick, and no trouble is experienced with the formation of nickel-zirconium eutectics.

A number of tandem tubular extrusions were prepared for Savannah River Laboratory by Nuclear Metals. These extrusions were found to have satisfactory mechanical and other properties when tested ex-pile.[13] Some of the results were mentioned in the earlier *Power Reactor Technology* review. Data have now become available on the properties of such joints tested after irradiation.[14] In the work reported, six tandem-extruded joints prepared by the methods described in Ref. 15 were irradiated at 50°C to exposures as high as 7.8×10^{20} neutrons/cm^2 (>0.1 Mev). Integrated fluxes were calculated from previous measurements, and the specimen temperatures were calculated from gamma fluxes and coolant flows. The specimens were mounted with longitudinal loading bolts so that the differential thermal expansion on heating, plus a preloading stress applied to the bolts, placed the joints under stresses that ranged from 3800 psi for the specimen under lowest load to 20,500 psi for the most highly stressed specimen. Three of the specimens were tested as extruded, but the remaining three had received 15, 18, and 20% cold reductions. The unworked specimens were approximately 1.9 in. in outside diameter with 0.2-in. walls. In the cold-worked specimens these measurements decreased slightly. Postirradiation measurements showed a maximum diameter decrease of 13 mils. Interface lengths were from 9 to 12 in. Four of the irradiated joints showed no

defects, but some evidence of corrosion attack was found at the internal joint interfaces on the two remaining specimens. The penetration along the interface was as much as 10 mils. The two specimens that had been fabricated by a technique (not described) designed to prevent this difficulty did not show attack. The bond interfaces exhibited no changes due to irradiation.

One as-extruded and one cold-worked specimen were tensile tested. At the limit of the machine, the 56,000-psi nominal stress placed on the as-extruded tube was not sufficient to cause it to fail. Instead, deformation apparently occurred in the Zircaloy. The cold-worked specimen had a slightly thinner wall, so that failure was achieved at a nominal stress of 91,000 psi. The failure occurred in the Zircaloy at the grips. The strength up to the point of failure was similar to values previously found for unirradiated material, so that either no strengthening of the Zircaloy due to irradiation was indicated or the grip failure was below the true strength of the material. The tests show promising behavior for the tandem-extruded joints at the test temperatures under moderately high irradiation levels, but extrapolation of this behavior to much higher temperatures would probably be unwise.

The preparation of coextruded tubular joints and other coextrusion-joining techniques for bonding dissimilar metals is described in a recent review paper.[16]

References

1. D. A. Patterson, D. A. Nehrig, R. H. Klumb, and T. E. Peterson, Pathfinder Atomic Power Plant. Boron-Stainless Steel Control Rods for Pathfinder Reactor. Final Summary Report, USAEC Report ACNP-63001, Allis-Chalmers Mfg. Co., Feb. 15, 1963.
2. D. A. Patterson and D. A. Nehrig, Burnup Limits for Pathfinder Two Weight Per Cent Natural Boron-Stainless Steel Control Rods, USAEC Report ACNP-63006, Allis-Chalmers Mfg. Co., Dec. 19, 1963.
3. W. O. Schaffnit, Radiation Damage Studies of Boron Stainless Steel, Final Report, USAEC Report IDO-16502, Phillips Petroleum Co., Jan. 28, 1959.
4. General Electric Company, Atomic Power Equipment Department, Survey of the Physics, Metallurgy, and Engineering Aspects of Reactor Control Materials, USAEC Report GEAP-3183, June 12, 1959.
5. J. D. Eichenberg, The Effect of Irradiation on the Properties of Boron–Stainless-Steel Powder Dispersion Samples, USAEC Report WAPD-160, Westinghouse Electric Corp., Bettis Plant, Jan. 2, 1957.
6. W. E. Ray, The Effects of Neutron Capture on Reactor Control Materials, Report-11708, Dresser Products, Inc., 1960.
7. W. E. Ray, W. A. Neisz, and H. W. Cooper, Discrete Fixed Poison Rods Containing Boron, *Nucl. Sci. Eng.*, 4(3): 386-401 (September 1958).
8. W. V. Johnston and J. E. Noonan, Reactor Technology Report No. 8, Metallurgy, The Effect of Temperature on the Volume and Structural Stability of Irradiated Boron-Containing Materials, USAEC Report KAPL-2000-5, pp. 35-92, Knolls Atomic Power Laboratory, March 1959.
9. R. D. Hahn, Compatibility of Boron Carbide with Potential AOMR Control Rod Cladding Materials, USAEC Report NAA-SR-8702, Atomics International, Mar. 1, 1964.
10. R. J. Burian, E. O. Fromm, and J. E. Gates, Effect of High Boron Burnups on B_4C and ZrB_2 Dispersions in Al_2O_3 and Zircaloy-2, USAEC Report BMI-1627, Battelle Memorial Institute, Apr. 24, 1963.
11. S. F. Kaufman, Fabrication Development of Boron Carbide and Boron Carbide + Silicon Carbide Mixtures for Possible Application as Lumped Burnable Poisons in PWR-2, USAEC Report WAPD-244, Westinghouse Electric Corp., Bettis Atomic Power Laboratory, January 1964.
12. R. G. Gray and L. R. Lynam, Irradiation Behavior of Bulk B_4C and B_4C + SiC Burnable Poison Plates, USAEC Report WAPD-261, Westinghouse Electric Corp., Bettis Atomic Power Laboratory, October 1963.
13. J. W. Joseph, Jr., Evaluation of Tandem-Extruded Joints Between Zircaloy and Stainless Steel, USAEC Report DP-723, Savannah River Laboratory, June 1962.
14. J. W. Joseph, Jr., Irradiation of Tandem-Extruded Joints Between Zircaloy and Stainless Steel, USAEC Report DP-859, Savannah River Laboratory, October 1963.
15. W. B. Tuffin, A. R. Gilman, and S. Isserow, Tubular Stainless Steel-Zircaloy Transition Joints Prepared by Tandem Extrusion, USAEC Report NMI-7216, Nuclear Metals, Inc., Feb. 2, 1962.
16. P. Loewenstein and W. B. Tuffin, Metallurgical Bonding of Dissimilar Metals by Co-Extrusion, American Society for Metals Technical Report W4-3.2, 1964.

Section

V

Power Reactor Technology

Containment, Radiation Control, and Siting

Effect of Fission-Product Release

A report on the environmental hazard from fission-product releases has been issued by the United Kingdom Atomic Energy Authority.[1] The fission products included in the study are the same volatile fission products that would be expected to be released during a uranium fire, but they should not be much different from those expected during a fuel melt. The percentages of each isotope released are estimates obtained primarily from the Windscale accident.[2] The isotopes and elements involved and the percentage release of each used in the investigation are shown in Table V-1.

One part of the investigation was devoted to the determination of how the radioactivity would be dispersed in the atmosphere, with particular regard to conditions in the United Kingdom. The investigation indicated that Pasquill's extension of Sutton's theory of turbulent diffusion was the better representation of the dispersion, particularly at large distances. Briefly, Pasquill's method reduces the lateral and vertical spread of the Sutton theory cloud after a travel of 1 mile from the release point. For comparison of the effects of meteorological stability on the dispersion of radioactivity, two stability conditions were included in all environmental hazards evaluations. One was an average United Kingdom weather condition, and the other was an inversion condition, which in most cases represents the worst condition as far as dispersion is concerned. The effects of ground deposition on the cloud dosage and the amount of deposited activity were also investigated and included in the environmental hazard evaluations. Tests have shown that values for the "velocity of deposition" are in the range of 0.01 to 5 cm/sec, where the velocity of deposition, V_g, is defined as

$$V_g = \frac{\text{total deposited activity per unit area of ground}}{\text{cloud dosage}}$$

Analysis of the Windscale accident led to deposition velocities of 0.1 to 0.5 cm/sec. Any possibility of underestimating the cloud dosage was avoided by choosing a deposition velocity of 0.1 cm/sec for both stability conditions. For average weather conditions, the cloud dosage is indistinguishable from the $V_g = 0$ condition. For inversion conditions, deposition reduces the cloud dosage no more than a factor of 4 or 5 at 60 miles. In the deposited-activity calculations, deposition velocities were selected to give the maximum deposition at each particular distance from the release point. Deposition velocities used were 1 cm/sec for average weather conditions and 0 to 1 cm/sec for inversion conditions.

From the calculated cloud and ground concentrations, the following determinations were made:

1. Dosage as a function of distance from gamma and beta radiation released external to an individual from the cloud
2. Dosage from activity deposited on the ground
3. Dosage from activity deposited on the individual's skin
4. Internal dose rate from inhaled iodine, including the contribution from ^{132}Te
5. Hazards from food exposed to ^{131}I deposition, such as green vegetables
6. Hazards of consumption of milk and eggs that had been contaminated with ^{131}I
7. Inhalation and ingestion hazards of ^{137}Cs
8. Inhalation and ingestion hazards of ^{89}Sr and ^{90}Sr

9. A tentative assessment of the inhalation and ingestion hazards from ^{106}Pu, ^{140}Ba, and ^{144}Ce

10. Possible hazard from inhaled insolubles ^{89}Sr, ^{106}Ru, and ^{144}Ce

On the basis of the Medical Research Council-recommended dosages during emergencies (where available), the maximum permissible concentrations are reported for airborne radioactive hazards. Also reported are the ground concentration levels to give the maximum emergency dose rates either from direct contact or by eating foodstuffs that have been contaminated. Included are descriptions of the actions required to safeguard the public from the hazards brought on by the activity release.

Table V-1 ELEMENTS OR ISOTOPES UNDER INVESTIGATION[1]

Element or isotope	Amount released, %
Bromine, Krypton, Xenon	60
^{132}Te	15
^{131}I, ^{132}I, ^{133}I, ^{134}I, ^{135}I	25
^{89}Sr, ^{90}Sr	0.1
^{106}Ru	4
^{137}Cs	15
^{144}Ce	0.15
^{140}Ba	0.2

In summary, the most important isotope related to public health hazards following a reactor accident is ^{131}I. Therefore all the other activities are reported in terms of the ^{131}I activity. Because ^{131}I has a half-life of eight days, the deposition dose will have decayed sufficiently in a few weeks to permit reoccupation of most of the affected area except those portions which are contaminated by ^{137}Cs and ^{90}Sr. The ^{137}Cs and ^{90}Sr portions of the area are expected to be much smaller than the portions affected by the ^{131}I release.

All calculated data on the external and internal hazards and on the areas of food contamination are presented in terms of the distance affected by each isotope. Since the amount released depends on a number of variable factors, the magnitude of the release of all isotopes is specified for several levels of ^{131}I, ranging from 1 to 10^5 curies. The consequences of the various releases are discussed. In view of the maximum amount of ^{131}I that can accumulate in a reactor, it is evident that a complete release would be disastrous, and assurance of some retention of fission products is a matter of considerable importance.

Effect of Temperature on Fission-Product Deposition

A report has been published on the development of an analytical model to calculate the steady-state deposition of fission products from gas streams onto surfaces.[3] Included in the analytical procedure are the effects of nonisothermal regions on the steady-state deposition rate. A computer code is described which is used to evaluate the equations (derived in the report) representing the deposition. The report also gives sample results that are compared with experimental data. In general, the agreement of the experimental and analytical results for relative deposition in nonisothermal regions was reasonably good for ^{95}Zr, ^{103}Ru, ^{141}Ce, ^{140}Ba, and ^{132}Te. The experimental data for the deposition of ^{131}I were higher than was estimated by roughly a factor of 10. Although the reason for this disagreement was not fully explained in the report, the author states that it may have been caused by compound formation resulting from collision of iodine with the cold wall, with subsequent rapid condensation or deposition.

References

1. J. R. Beattie, An Assessment of Environmental Hazard from Fission-Product Releases, British Report AHSB(S)R-64, May 16, 1961.
2. H. J. Dunster, H. Howells, and W. L. Templeton, District Surveys Following the Windscale Incident, October 1957, *Proceedings of the Second United Nations International Conference on the Peaceful Uses of Atomic Energy, Geneva, 1958*, Vol. 18, pp. 296-308, United Nations, Geneva, 1958.
3. M. N. Ozisik, Effects of Temperature on Fission-Product Deposition, USAEC Report ORNL-3542, Oak Ridge National Laboratory, March 1964.

Section

VI

Power Reactor Technology

Components

Pumps

The design and test of a diaphragm pump for use with liquid metals are described in Ref. 1. This type of pump is often used as a feed pump, where its high-pressure and low-capacity characteristics make it suitable for feeding solutions or slurries into the reactor system. Figure VI-1 is a schematic illustration of the pump as used for pumping liquid metals. The particular application of this pump was in the laboratory to pump a lead-bismuth eutectic within a test loop, although the pump is expected to have value for reactor applications.

The prime mover for the pump was a pulse generator utilizing hydraulic fluid to transmit the pulses to the first diaphragm. A NaK intermediate system then transmitted the pulses from the first diaphragm to the remote high-temperature diaphragm assembly, in which the diaphragm served to separate the NaK from the process fluid, which was lead-bismuth eutectic in the application described in Ref. 1. The remote head was designed to meet four requirements:

Operation at 300 to 600°C
No external or internal leakage of fluids
Ease of disassembly
Continuous operation for extended periods of time

As illustrated in Fig. VI-1, the remote head was of bolted construction and was designed to operate at 50 psig discharge pressure and 816°C. The diaphragm was 0.030 in. thick and was of type 446 stainless steel, as were the rest of the remote high-temperature components. Polished, raised bearing surfaces ensured adequate sealing between the rather massive components of the remote head and the diaphragm itself. The remote head was entirely immersed in a liquid bath for temperature-control purposes.

A key component of the pump was the valve assembly, which contained ball type check valves and seats. The 0.75-in.-diameter balls were of type 440 stainless steel, and the valve body was type 446 except for some type 316 tie bars. As illustrated in Fig. VI-1, the valve was operated with the direction of flow from top to bottom. This was done because the balls were of lower density than the pumped fluid (lead-bismuth eutectic) and thus would be normally positioned on the valve seats when the pump was not operating. The pressure-time curve was designed to be sinusoidal in nature so as to reduce accelerations of the fluid at the beginning and end of each stroke and promote quiet operation.

The pump was operated continuously for 5376 hr without difficulty at a eutectic temperature of 575°C, an outlet pressure of 20 psig, and a flow rate of 0.6 gal/min. On two occasions, however, the temperature was briefly reduced because of failure of the cooling-water supply to the low-temperature head. Postoperation examination revealed slight wear on the valve seats, but they still maintained a tight seal.

An interesting pump described in Ref. 2 is capable of pumping boiling fluids without damage due to cavitation or noise. Although the tests described in the reference were nominally at standard conditions, the operating principles seem equally applicable at elevated pressures and temperatures. Figure VI-2 gives cross-sectional views of the device.

The following quotation[2] serves to define the operating principles of the pump (the figure numbers have been changed to be consistent with this section):

> This pump is a two-stage centrifugal-displacement unit with one rotating element—a one-piece centrifugal rotor-impeller.[P] The first stage in-

[P] U. S. Patents Nos. 2,940,657 and 3,102,083.

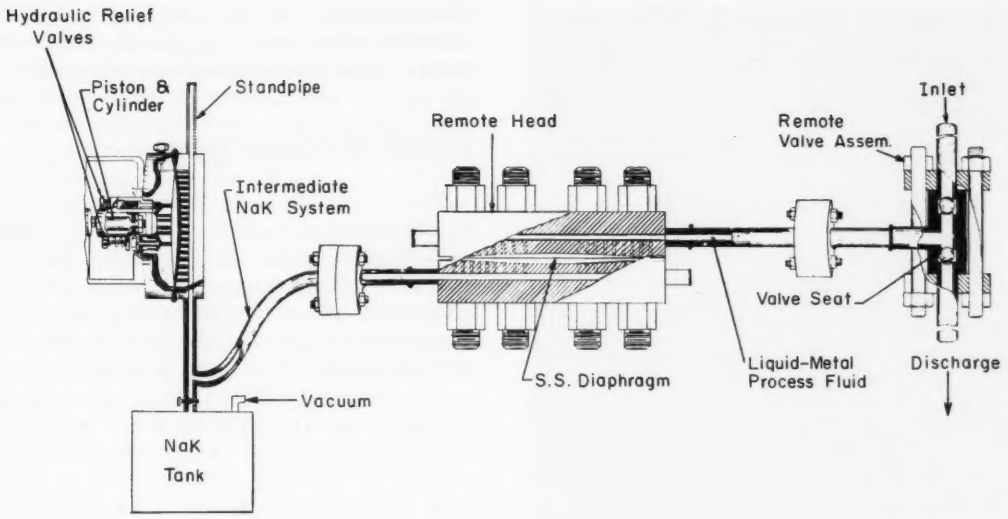

Fig. VI-1 Schematic illustration of a two-stage diaphragm pump.[1]

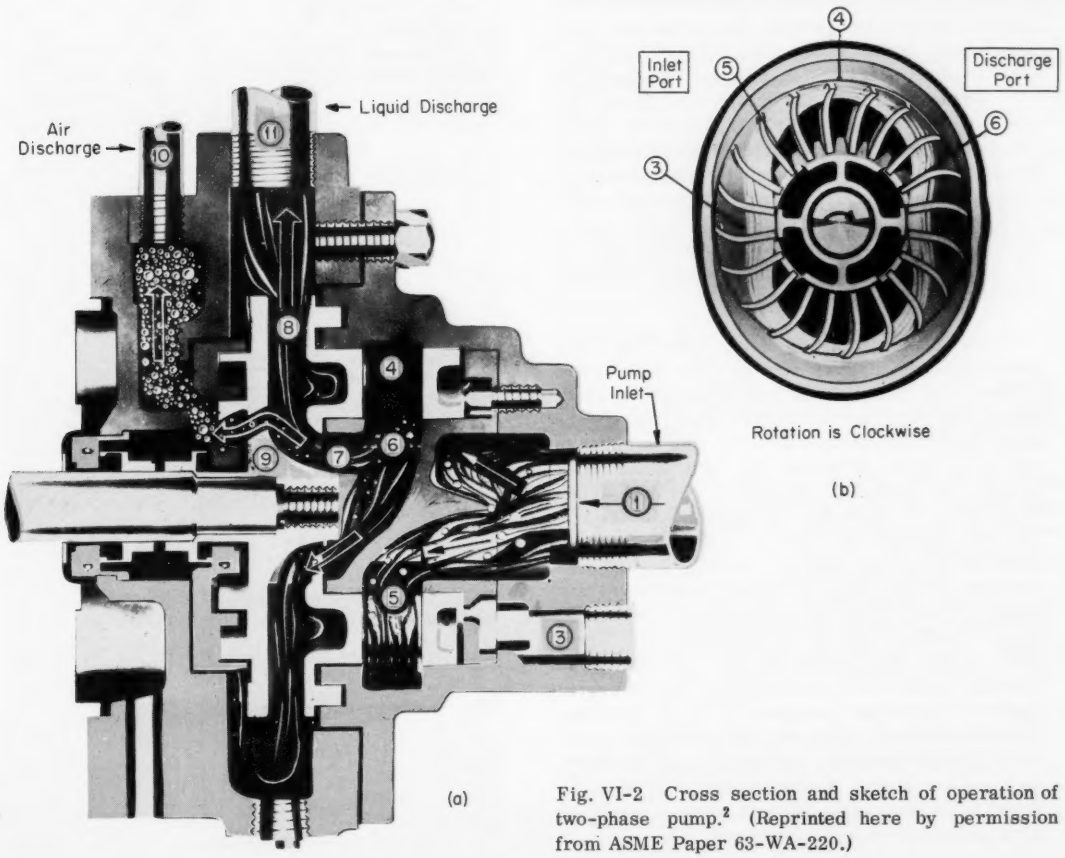

Fig. VI-2 Cross section and sketch of operation of two-phase pump.[2] (Reprinted here by permission from ASME Paper 63-WA-220.)

cludes a liquid-ring-principle compressor while the second stage is a centrifugal liquid pump. The unit has one inlet and two discharge connections, one for the second-stage discharge of liquid and the other for the interstage discharge of air or vapor. Other connections provide for liquid make-up when required, drains, and so on, Fig. [VI-2, part *a*].

The centrifugal-displacement action of a typical liquid ring compressor as used in the first stage is shown in Fig. [VI-2, part *b*]. A series of buckets in the rotor is full of liquid when leaving the minor radius of the casing, as shown at 3. The rotor throws this liquid out and into the casing as at 4, much as in a standard centrifugal pump, but after this, the similarity between the two ends. The central inlet to the rotor is ported instead of being open continuously, as in a centrifugal, and the outer casing curves inwardly to direct the liquid back into the rotor instead of delivering it to the conventional centrifugal pump casing discharge.

The centrifugal kinetic energy imparted by the rotor to each bucket of liquid in traveling from position (3) to (4) at first creates an outward piston or displacement action in each bucket. This action draws gas, vapor and/or liquid into the rotor as it passes the open inlet port (5). This liquid and vapor are trapped within each bucket and carried around from the inlet port position (5) to the discharge port (6). During the transit, the accelerated liquid ring, after passing station (4) is directed by the casing back into the rotor, where it expends its acquired liquid kinetic energy in compressing the trapped charge in each bucket and in discharging this centrally through the discharge port (6). Thus, a semi-positive displacement action is centrifugally obtained that will pump fluids of widely differing densities.

The staged relationship of the liquid ring to the centrifugal impeller, as well as other details, are shown in the cross section Fig. [VI-2, part *a*]. Fluid enters the pump at its inlet (1). This fluid may be in its liquid or gaseous state or it may be mixed in any proportion. It enters the first stage rotor through the stationary inlet ports (5), as just described, and is discharged through the central ports (6), directly into the inlet (7) of the second stage impeller (8). In this impeller, the fluid is first centrifuged. The gas and residual noncondensables are separated and escape from the center of the second stage impeller through rotating ports (9). From here the gas and noncondensables are discharged through casing connection (10). The separated liquid is discharged peripherally by the impeller (8) into the volute casing and thence to higher pressure through discharge connection (11). Provision is made for adding cooling liquid at (3) when no liquid is included at the inlet (1), as when operating as a gas compressor vacuum pump.

The advantages of this pump are compared to those of other types of pumps, and a brief history of operating experience is included.

Heat Exchangers

The fabrication of the primary heat exchanger for the Molten-Salt Reactor Experiment (MSRE) is discussed in Ref. 3. The molten fuel of the MSRE is pumped through the shell side of the exchanger, while nonfuel-bearing molten salt circulates through the tube side. Details on the heat exchanger are given in Table VI-1.

The major problem in the design of the heat exchanger seems to have been the tube-to-header joint, which experience had shown to be subject to cracking during cyclic service at high temperatures. In the final joint design,

Table VI-1 DESIGN DATA[3] FOR THE MSRE PRIMARY HEAT EXCHANGER

Structural material	INOR-8
Heat load, Mw	10
Shell-side fluid	Fuel salt
Tube-side fluid	Coolant salt
Layout	25% cut, cross-baffled shell and U tube
Baffle pitch, in.	12
Tube pitch, in.	0.775
Tube	
Outside diameter, in.	0.5
Wall thickness, in.	0.042
Active shell length, ft	6
Average tube length, ft (approximately)	14
No. of U tubes	163
Shell diameter, in.	16
Overall length, ft (approximately)	8
Tube-sheet thickness, in.	1½
Design temperature, °F	1300
Design pressure	
Shell, psig	75
Tube, psig	125
Terminal temperatures	
Fuel salt, °F	Inlet 1225; outlet 1175
Coolant salt, °F	Inlet 1025; outlet 1100
Exchange geometry	Parallel and counter flow
Effective log mean temperature difference, °F	133
Active heat-transfer surface area, sq ft	259
Fuel-salt holdup, cu ft	6.1
Pressure drop	
Shell side, psig	24
Tube side, psig	29

shown in Fig. VI-3, both welding and brazing are used so as to remove stress concentration near the weld area and provide support at the base of the weld. In addition, the brazing will reinforce defective welds, should any occur during fabrication.

The brazing alloy was 82 wt.% gold–18 wt.% nickel, and the welding electrode was thoriated tungsten. A number of test specimens were made so that optimum welding and brazing conditions could be studied, and the results of the tests are given in the reference. Fabrication of the full-size exchanger proceeded without apparent difficulty; Fig. VI-4 shows the exchanger positioned in the furnace pit. A cover was added and seal welded in place, and the assembly was brazed in a hydrogen atmosphere at about 1850°F. Final inspection included ultrasonic inspections in the braze areas after the tubes had been filled with water, a helium leak test, and an 800-psi hydrostatic test. No leaks were found.

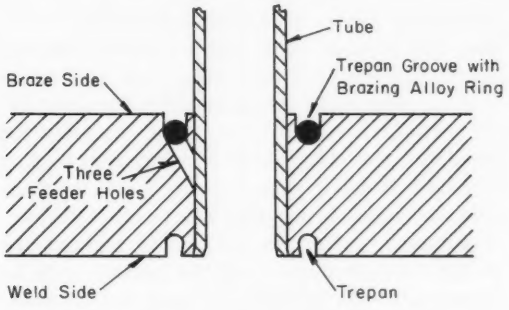

Fig. VI-3 Schematic drawing of welded and backbrazed joint design for the MSRE heat exchanger.[3]

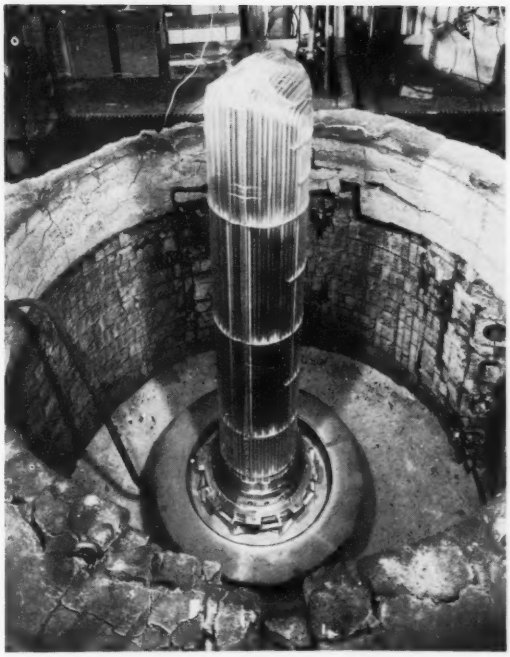

Fig. VI-4 Tube bundle of the MSRE heat exchanger positioned in furnace pit prior to brazing.[3]

REFERENCES

1. D. E. Westerheide, J. C. Clifford, and G. Burnet, Design and Test of a Diaphragm Pump for Liquid Metals, *Nucl. Sci. Eng.*, 17(4): 523-527 (December 1963).
2. H. E. Adams, Pumping Boiling Fluids When the Available Static Head is Zero or Less, Paper ASME No. 63-WA-220 presented at the Winter Annual Meeting, Philadelphia, Pa., November 17–22, 1963.
3. R. G. Donnelly and G. M. Slaughter, Fabrication of the Heat Exchanger Tube Bundle for the Molten-Salt Reactor Experiment, USAEC Report ORNL-3500, Oak Ridge National Laboratory, Dec. 9, 1963.

Section

VII

Power Reactor Technology

Design Practice

EGCR Control Rods

Control rods that are sufficiently flexible to move in bowed channels have been developed for the Experimental Gas-Cooled Reactor (EGCR). The design and thermal analysis of the rods are described in detail in Ref. 1, a recent ORNL report.

The requirement for a rod capable of moving in a bowed passage is brought about by the dimensional changes that are anticipated in the graphite-moderator structure of the EGCR. The 21 control rods, which are placed on 24-in. centers throughout the core, move in 4-in.-diameter channels. The channels are located principally at intersections of graphite columns. Some of the physical relations that exist between the core, the pressure vessel, and a control rod and its drive mechanism are illustrated in Fig. VII-1. Although restraint bands are shown around the graphite columns that form the moderator structure, the control-rod channels will become bowed because of nonuniform graphite shrinkage induced by fast-neutron flux gradients across the core. If the graphite blocks do not crack, the restraint bands should limit the maximum bow to about 1 in.; the blocks may crack, however, and an offset in the rod channel could result. In addition to the irradiation-induced dimensional changes, thermal and pressurization effects may cause misalignment of the channels.

The required diameter for the EGCR rods is 3.25 in. Their normal rate of movement is 1.8 in./min, and the maximum velocity reached during the free-fall portion of a scram is about 18 ft/sec. As shown in Fig. VII-1, the rods are suspended on stainless-steel cables that are connected to drive mechanisms located near the top extension of the rod nozzles. A shroud tube, hung from the nozzle at the pressure-vessel head, guides each control rod into its core channel and holds one portion of the rod shock absorber. Consequently the shock load involved in stopping a free-falling control rod is borne by the pressure vessel.

The rod design, which evolved from considerations of the rather stringent design requirements, is a particularly interesting one. An articulated design was adopted to achieve a very long rod capable of moving in a bowed channel. Boron carbide (B_4C) was chosen as the nuclear poison, principally because of the required 20-year lifetime of the rod. Also, to avoid the problems that may occur with external cooling of rods that can become eccentric in their channels, the rods are provided with internal, forced-circulation cooling. In addition to meeting the design requirements that the control rods be compatible with the high-pressure-helium reactor environment and that the cladding material be compatible with the core and shroud structural materials, the rod designers were called on to provide a diffusion barrier (see Sec. IV of this issue of *Power Reactor Technology*) between the boron carbide poison material and the rod cladding material to prevent the high-temperature reaction that occurs between boron and nickel. The final design of the rod, shown in Fig. VII-2, is described in the next paragraph by a paraphrased excerpt from Ref. 1.

The 3.25-in.-diameter rod has a poisoned length of about 15 ft and an overall length of about 20 ft. The rod is made up of four segments that are supported by an internal rod of type 347 stainless steel; the bottom three segments, which comprise the poison section of the rod, contain annular rings of hot-pressed B_4C. The B_4C is contained in type 304 stainless-steel-cladding tubes, and all surfaces of the stainless steel which contact the B_4C are copper plated to prevent the high-temperature boron-

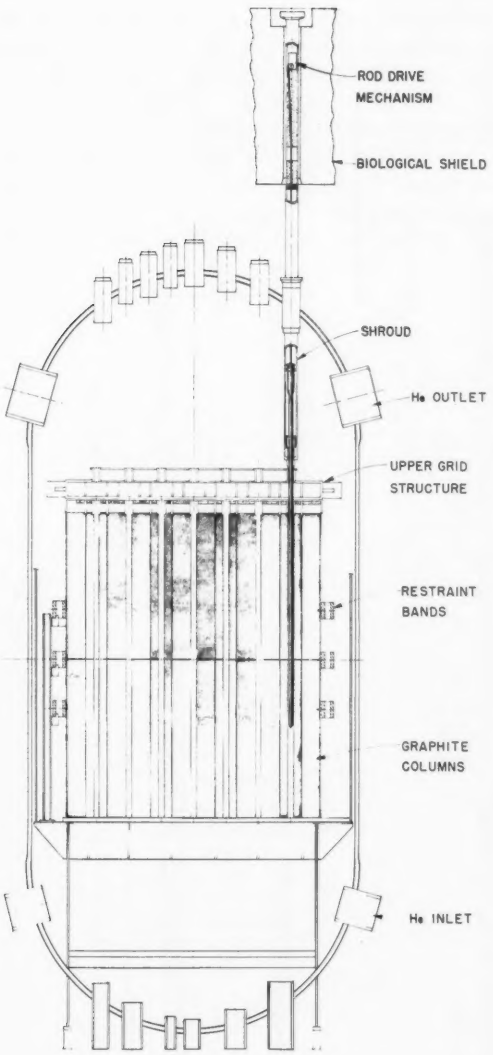

Fig. VII-1 Vertical section through the EGCR core.[1]

nickel reaction mentioned in the preceding paragraph. Flexibility of the overall assembly is achieved by elastic bending of the central rod between spacer support plates, whereas the segments of the rod can move relative to one another by means of connecting ball-and-socket joints. One face of each ball-and-socket joint is overlaid with Hastelloy C to prevent self-welding. The woven stainless-steel filter attached to the top of each poison segment of the rod vents the inner volume of the segment to the reactor, thereby equalizing pressures and avoiding the pressure differentials that could exist because of helium-gas generation in the B_4C during irradiation. The rod segments are kept in contact at their ball-and-socket joints by a top Inconel X compression spring; the joints maintain an essentially leaktight flow channel for the internal, forced-circulation coolant. The Inconel X spring and a top slip joint accommodate the relative movement that will occur between the central support rod and the tubing caused by differential thermal expansion during normal operation.

The forced-circulation helium coolant for each rod assembly enters the control-rod nozzle at the top, flows down over the rod-drive mechanism, then down the shroud, and into the center of the control rod. The wire-brush seal, shown at the top of the assembly in Fig. VII-2, prevents bypassing of the cool helium directly into the top plenum of the reactor and ensures that it flows into the center of the rod assembly. Tests of a mockup control rod showed that these wire brushes and the ball-and-socket joints between rod segments are effective seals and that the rod coolant is channeled down the interior of the rod as intended.

No major problems were encountered in manufacturing the 21 rods required in the EGCR. The finished rods weighed between 137 and 142 lb.

SRE Rod Drop-Time Measurement

A system has been developed for determining the scram, or drop, times of the safety rods in the Sodium Reactor Experiment (SRE). Total drop time of the top-driven SRE rods consists of two components: the time during which the rod is in free gravity fall into the core, and the time during which a snubbing effect slows and stops the rod at the end of the fall. If the free-fall component of total drop time is measured and then compared with calculated free-fall time, mechanical interference with rod insertion, such as that caused by warpage of the thimble in which the rods move, can be detected. Satisfactory operation of the piston-cylinder snubber, which must stop the rods without damaging them, can be verified by measuring the second, or snubber, component of total drop

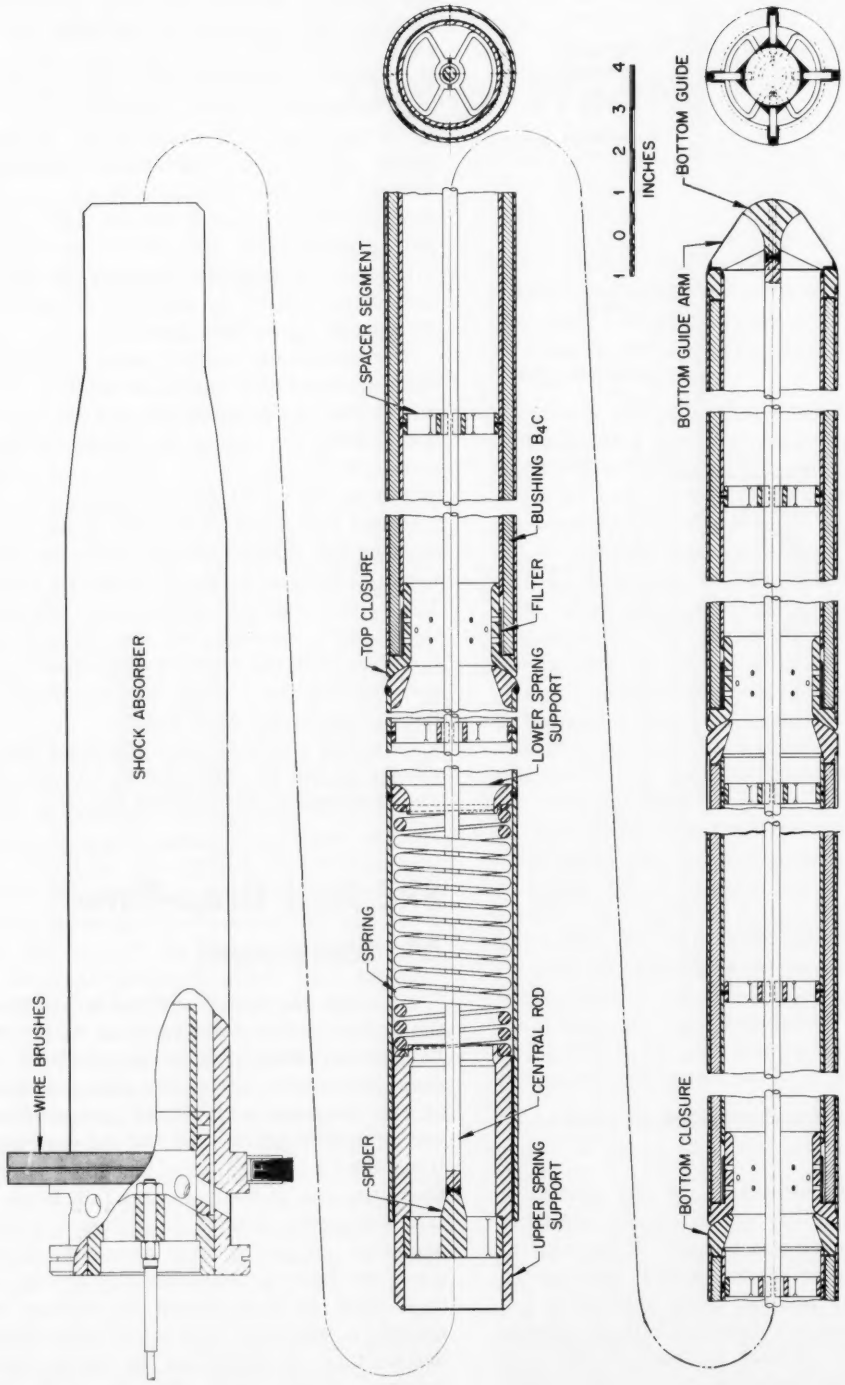

Fig. VII-2 Details and general arrangement of segmented EGCR control rod.[1]

time. The system developed for the SRE is capable of measuring each time component; furthermore, the time required is short enough that the measurements can be performed routinely.

A conceptual drawing of the SRE timing system is shown in Fig. VII-3. In this drawing a safety rod is shown held in the fully withdrawn position by an electromagnet. When the reactor is scrammed, the energizing current to the electromagnet is interrupted, and the rod, with the snubber piston at its uppermost end, falls downward into the core. As the rod nears the bottom of its stroke, the snubber piston is guided into a snubber cylinder by the tapered section of the drive housing shown in Fig. VII-3. When the rod reaches its fully inserted position, the snubber piston actuates a limit switch which indicates that the rod has reached the full-in position. As shown in the figure, the SRE timing system utilizes two timers to measure the individual components of the total scram time. When a scram is initiated and the current to a safety-rod holding magnet is interrupted, the first time-interval meter is triggered. At the entrance to the snubber cylinder, an electromagnetic pickup is actuated by the snubber piston and generates a signal that stops the first electronic timer and starts the second. The second timer is stopped when the snubber piston actuates the down-limit switch at the bottom of the snubber cylinder. Thus the free-fall component of total drop time and the snubber component of total drop time are measured.

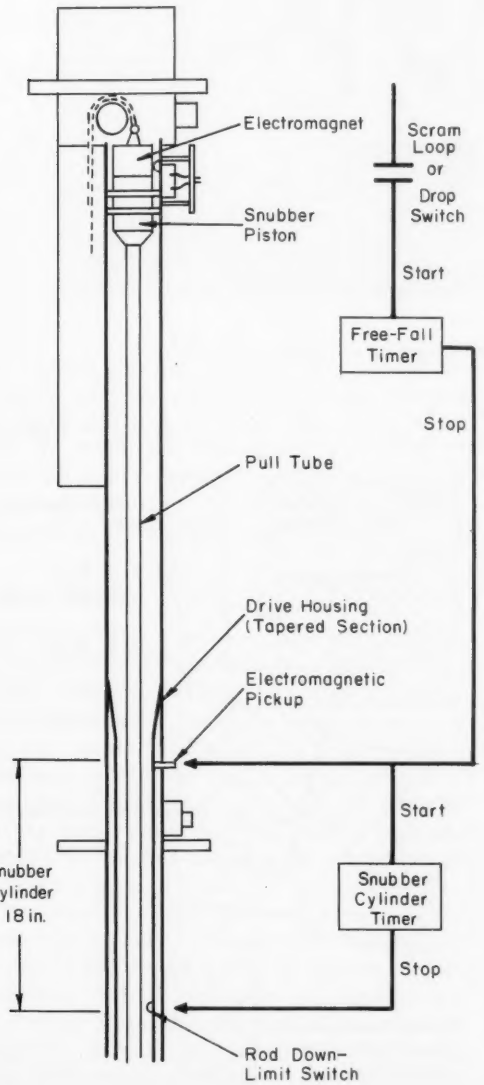

Fig. VII-3 Mark II safety rod and timing circuit of the SRE.[2]

The timing-system panel is mounted in the reactor control room, and complete drop-time measurements for the four safety rods of the SRE can be made at this panel by one person in less than 10 min. The snubber time and free-fall time are displayed directly in units of time on four-decade lighted dials on the two timers. The timing system appears to be one that would be adaptable to various reactors.

Pressure-Tube Reactor Components

Dome-Seal Tube Closure

During the period 1957 to 1958, when studies of high-performance nozzle closures for the pressure tubes of the Plutonium Recycle Test Reactor (PRTR) were undertaken, a dome type nozzle seal was conceived. The seal was subsequently developed and used in the PRTR gas loop at service conditions of 1500°F and 500 psi. Reference 3 is a description of recent work directed toward determining the suitability of the dome seal as an alternate pressure-tube nozzle closure for the heavy-water-cooled CANDU reactor. As a result of the developmental work on the dome type closure, it was concluded that

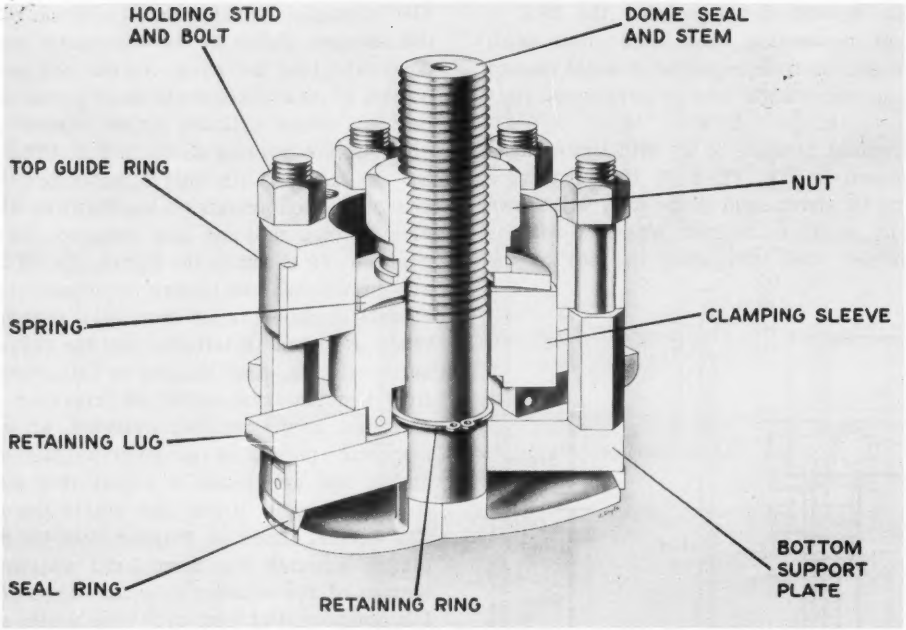

Fig. VII-4 Cutaway view of the dome seal for pressure-tube reactors.[3]

the closure is a promising type for high-pressure high-temperature water applications.

A cutaway view of the dome seal is given in Fig. VII-4. The entire assembly shown in the figure is inserted into the end of the open pressure tube to be sealed. In the simplest terms the operation of the seal can be described as follows: the large nut that is threaded to the dome-seal stem is tightened, thereby deflecting the dome and causing it to exert pressure on the seal ring. The sealing action of the assembly is illustrated in Fig. VII-5, which shows the principal components involved in the sealing process. The load exerted by the dome on the seal ring causes the ring to yield locally and effect the seal. A Belleville-spring washer installed between the dome-stem nut and the clamping sleeve, as shown in Fig. VII-4, allows the dome to expand when heated while permitting forces high enough for effective sealing in the cold condition. A schematic representation of the deflection of the dome, both with and without the Belleville spring, is shown for the cold and hot conditions in Fig. VII-6.

The dome seal did not leak during a test program that included steady-state operation, frequent assembly-disassembly operations,

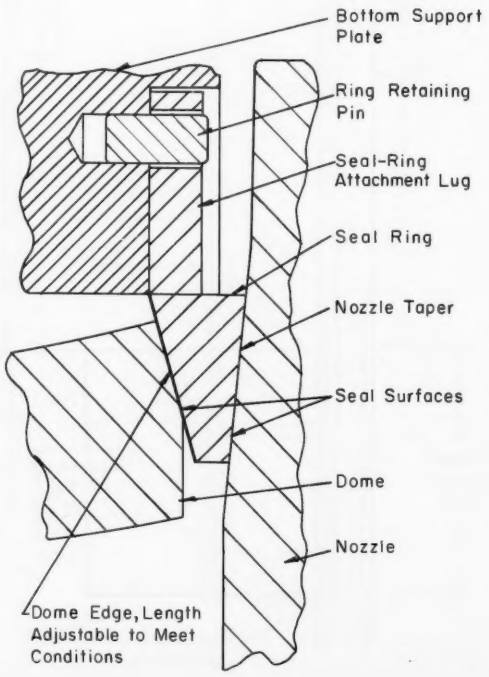

Fig. VII-5 Schematic of sealing action of the dome seal.[3]

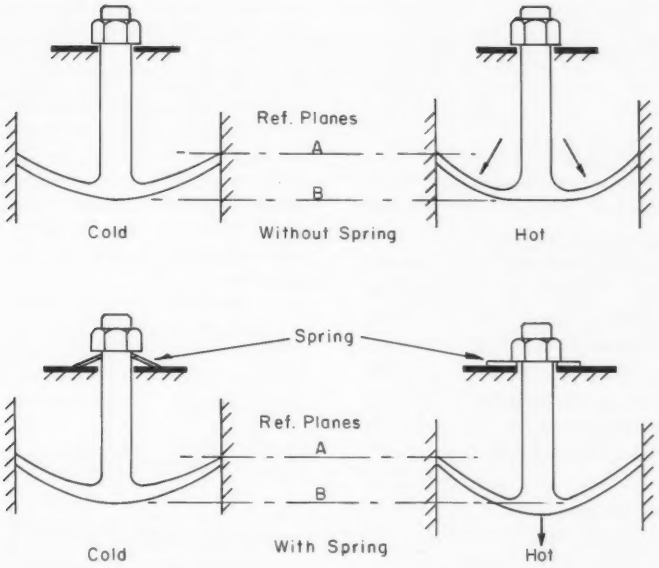

Fig. VII-6 Theory of dome deflection with and without Belleville-spring washer.[3]

and severe thermal cycling. The disassembly torques were in the same general range as assembly torques and could be varied somewhat by lubricants. The forces required to remove the seal from the nozzle were lower than expected, and they are expected to cause no operational problems.

Helium Seals

In the PRTR, a low-pressure helium atmosphere surrounds the lower, or inlet, sections of the vertically oriented Zircaloy-2 pressure tubes. The tubes penetrate the bottom of the primary shield, and a bellows type pressure-tube seal is effected at this level. Reference 4 describes a series of developmental tests that had as their objective the selection of a seal suitable for the low-pressure high-temperature application in the PRTR.

The developmental tests were concerned with seals which could withstand 4 in. Hg pressure at 480°F and which would fit into an existing assembly with a minimum of modification. Five seals were investigated: (1) a copper O-ring; (2) a Zircaloy-2 D-ring; (3) a B-F ferrule seal; (4) a stainless-steel, pressurized O-ring; (5) a Zircaloy-2 O-ring. The results of the seven tests performed (three utilized the Zircaloy-2 O-rings) are given in Table VII-1. Although the B-F ferrule seal shown in Fig. VII-7 was the most effective of those tested, the Zircaloy-2 O-ring shown in Fig. VII-8 was chosen for use in the PRTR because of its lower cost and easier installation in the existing reactor components. The following are observations on the different seal tests taken from Ref. 4.

1. Copper O-ring. Low leak rates were obtained at the beginning and ending of each cycle; maximum leak rates were at operating temperatures. Low leakage was measured during the first cycle but rapidly increased during subsequent cycles.

2. Zircaloy D-ring. Maximum leak rates were 270 and 266 liters/hr during the first two cycles. Because of these excessive rates, testing was terminated.

3. B-F Ferrule. After the first three tests, the test assembly was disassembled. Later it was reassembled and Tests 4, 5, and 6 were run. This seal had the lowest leakage of any tested. However, the shape is complex and the fabrication cost is relatively high. Maximum leak rates were obtained during the cooling portion of the cycle.

4. Stainless Steel O-ring. A good seal was obtained with the silver-coated pressurized ring during the first two cycles, but leakage increased as the number of cycles increased. Maximum leak rates were measured at steady-state conditions.

5. Zircaloy-2 O-ring. This seal had a diametrical clearance of 0.002 in. and was used with a standard PRTR flange. Leakage was low on all tests with a tendency for leak rates to decrease as cycles

Table VII-1 AVERAGE HELIUM LEAK RATES OF FIVE SEALS TESTED FOR PRTR,[4] LITERS PER HOUR

	Cycle 1	Cycle 2	Cycle 3	Cycle 4	Cycle 5	Cycle 6
Copper O-ring (standard PRTR flange; makeup torque, 30 in.-lb; 6/20/62, 6/21/62, 6/22/62; pressure, 2.0 to 3.0 in. Hg)	0.020*	2.900*	12.30*	44.50*	61.80*	
	0.180†	0.880†	2.43†	17.00†	14.05†	
Zircaloy-2 D-ring (special flange; makeup torque, 30 in.-lb; 6/5/62, 6/13/62)	55.0*	144.0*				
	141.0†	161.0†				
B-F ferrule seal (makeup torque, 15 in.-lb; 6/15/62, 6/16/62, 7/3/62; pressure, 2.0 to 3.0 in. Hg)	2.48*	1.02*	1.001*	0.075*	0.0901*	0.127*
	2.68†	1.239†	1.29†	0.381†	0.385†	0.48†
S.S. pressurized O-ring (standard flange; makeup torque, 15 in.-lb; 6/15/62, 7/2/63; pressure, 2.0 to 3.0 in. Hg)	0.248*	0.168*	13.7*	31.21*		
	0.350†	0.330†	6.70†	7.1†		
Zircaloy-2 O-ring (standard flange; ID, 2.0574 in.; 10/4/62 to 10/5/62; makeup torque, 27 in.-lb; disassembly torque, 15 to 20 in.-lb; pressure, 3.8 to 4.4 in. Hg)	1.42*	1.32*	1.12*	1.13*		0.728*
	1.61†	1.45†	1.33†	1.45†		1.00†
Zircaloy-2 O-ring (relieved flange; same O-ring as Test 5; 10/10/62; makeup torque, 30 in.-lb; disassembly torque, 15 to 20 in.-lb; pressure, 3.8 to 4.2 in. Hg)	1.830*	0.925*	0.735*	0.616*		
	1.40†	1.21†	1.11†	0.980†		
Zircaloy-2 O-ring (standard flange; ID, 2.059; makeup torque, 30 in.-lb; disassembly torque, 20 to 25 in.-lb; pressure, 3.8 to 4.2 in. Hg)	0.704*	0.680*	0.600*	0.785*		0.612*
	1.18†	0.995†	0.940†	1.07†		0.935†

*Steady-state and rising-temperature conditions.
†Falling-temperature conditions.

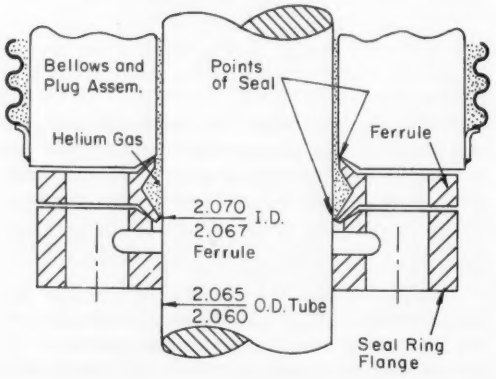

Fig. VII-7 Cross section of ferrule seal.[4]

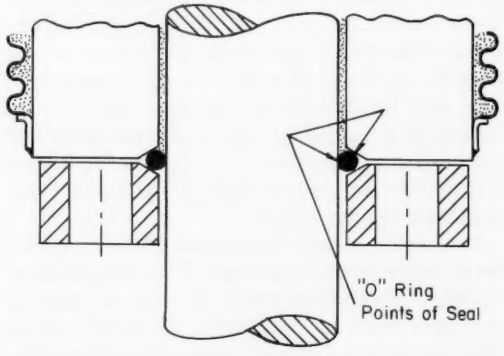

Fig. VII-8 Cross section of the PRTR Zircaloy-2 O-ring seal.[4]

increased. Small leak rates were noted during heating and steady-state conditions and maximum rates occurred during cooling.

6. Zircaloy-2 O-ring. This test was to determine the effect of a modified flange. The modification was a circumferential groove on the ID, designed to allow cantilever flexing of the flange lip. The O-ring was unchanged from Test Number 5. No significant improvement in leak rate was observed.

7. Zircaloy-2 O-ring. This test was to determine whether maximum allowable reactor tolerance conditions would adversely affect the low leak rates obtained in Test Number 5. An O-ring with a diametrical clearance of 0.015 in. was tested successfully with no significant change in results; that is, (*a*) low leak rates, (*b*) lower leak rates as cycles increased, and (*c*) maximum leakage during cooling.

Surge Suppressors in Flow-Monitor Sensing Lines

One advantage of pressure-tube reactors is the relative ease with which coolant flows and temperatures in individual process channels can be measured. In the PRTR, each of the 85 process channels is provided with flow-monitoring equipment capable of furnishing a visual readout of the flow rate in the channel, providing an electrical signal for recording, and supplying a signal to the safety circuit that initiates a reactor scram on receipt of a high-flow or low-flow signal. The flow-monitoring equipment for each process channel includes a Venturi flowmeter in the inlet piping, sensing lines containing valves, and a flow transmitter. Reference 5 gives details of an experimental program that was undertaken to devise means of reducing oscillations encountered in the PRTR flow monitors. The following quotation[5] describes the problem:

> During startup of the PRTR, it was found that the readings of flow meters on those pressure tubes which connect near the inlet of the bottom ring header were fluctuating excessively. The fluctuations were as much as ±8% which is nearly as large as the ±10% span between the high and low flow trips. When superimposed on the normal reactor flow changes, the fluctuations would cause spurious flow trips. During preliminary testing, the meter fluctuations were reduced by throttling the valves in the sensing lines from the flow venturi to the flow meter. This was recognized as being unsatisfactory for a permanent solution since this practice introduces an unknown variable lengthening of the response characteristics of the meter. It also introduces an error of unknown magnitude due to the nonuniform flow passage in the valve seat when throttled. An experimental program was therefore undertaken to determine the degree of valve throttling which might be appropriate for fluctuation suppression and to devise other and better methods of suppression.

The experimental program led to the conclusion that throttling of valves in the flow-transmitter sensing lines is not a satisfactory way of decreasing the fluctuations, principally because the flow indications are extremely sensitive to valve position and because there is a very narrow range of usable positions. A satisfactory method of damping the oscillations is to increase the hydraulic flow resistance in the pressure-sensing lines by installing (for the PRTR case) 3- to 4-ft lengths of $\frac{1}{16}$-in. tubing.

The addition of the short lengths of small-diameter tubing to the pressure-sensing lines in the PRTR flow-monitoring system has caused the flow transmitter to have time-response characteristics similar to those illustrated by curve *B* of Fig. VII-9. This curve, which is nearly critically damped, can be seen to reflect a happy medium between the time-response characteristics illustrated by curve *A*, in which the underdamped or oscillatory system has a fast response but also a very large overshoot, and the time-response characteristics shown by curve *C*, which is representative of an overdamped system in which the response is so slow that the system is unsatisfactory.

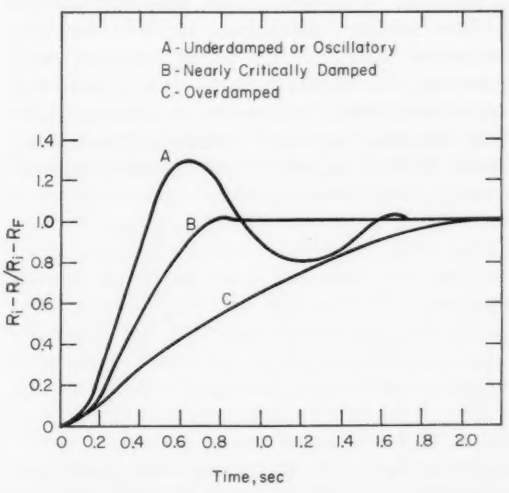

Fig. VII-9 Typical PRTR flow-transmitter response curves. R = transmitter reading, R_i = initial transmitter reading, and R_F = final transmitter reading.

Systems Design

Pathfinder Recirculation-Piping Design

A forced-recirculation mode of operation is employed for the reactor of the Pathfinder Atomic Power Plant. The recirculation system, which is described in some detail in Sec. VIII of *Power Reactor Technology*, 7(3), consists basically of three parallel coolant loops, each with a single mixed-flow centrifugal pump. Calculations and analyses to determine flexibility, vibration, and stresses in the loops are reported in Ref. 6. The majority of the information presented in the reference treats rather routine calculational methods and the results obtained by applying these methods. However, one interesting section is devoted to a description of the analysis performed to determine discontinuity stresses at dissimilar metal joints. These temperature-induced stresses occur in the primary loop piping at the junction between solid stainless-steel piping and stainless-steel-clad carbon piping. The joint was described in the above-mentioned *Power Reactor Technology* article.

LCRE Auxiliary Systems

The Lithium-Cooled Reactor Experiment (LCRE), which was to be located at the National Reactor Testing Station, was conceived as a test for a lithium-cooled high-temperature 10-Mw reactor. Reference 7 describes the functional design of the LCRE auxiliary systems and the development work and tests that were completed, in process, or planned at the time the program was canceled. The report, which is well organized and satisfyingly complete, gives the procurement and fabrication status of the auxiliary systems and includes manpower and cost expenditures and estimates. An indication of the degree of completeness which the author of Ref. 7 has attained in the report is given by the inclusion of a section in which all drawings associated with the LCRE auxiliary systems are listed, are grouped by systems, and are coded to indicate status, source, and use. The auxiliary systems include all reactor systems except the main liquid-metal coolant loops and the reactor control and safety systems.

References

1. J. W. Michel, Design and Thermal Analysis of EGCR Control Rods, USAEC Report ORNL-3503, Oak Ridge National Laboratory, March 1964.
2. J. G. Radcliff, Design and Development of the Safety-Rod Drop-Time Test System, USAEC Report NAA-SR-7880, Atomics International, Oct. 31, 1963.
3. D. H. White, Dome Seal Performance Tests, USAEC Report HW-79205, Hanford Atomic Products Operation, November 1963.
4. D. H. White, Tests on Reactor Helium Seals—PRTR Inlet, USAEC Report HW-76008, Hanford Atomic Products Operation, December 1963.
5. G. M. Hesson, W. L. Thorne, and J. M. Batch, Surge Suppressors for the PRTR Process Tube Meters, USAEC Report HW-70711(Rev.), Hanford Atomic Products Operation, May 1963.
6. D. J. Nolan and J. F. Patterson, Pathfinder Atomic Power Plant. Recirculation Piping Design, USAEC Report ACNP-63026, Allis-Chalmers Mfg. Co., Jan. 10, 1964.
7. H. J. Banach (Comp.), LCRE Auxiliary Systems Termination Report, USAEC Report PWAC-416, Pratt & Whitney Aircraft, Division of United Aircraft Corp., Mar. 9, 1964.

Section

VIII

Power Reactor Technology

Operating Experience

Moderator-Level Control

By Walter Mitchell III

Regulation of moderator height can be an attractive means of reactor control. Among the advantages enjoyed by the level-control system are its lack of strong control rods and, except for possible shim elements, any in-core hardware. Consequently local flux perturbations are small, and the reliability of the system is enhanced by not having crucial components in the reactor-core environment.

A reactor must have a fluid moderator to be able to use level control. Although several reactor types fulfill this requirement, there are many other considerations that limit the practical use of level control. A reactor that has a hydrogenous moderator, for example, is not a likely prospect for such a control scheme because the short neutron-migration length in its moderator material makes the reactivity of the system extremely sensitive to level variations. Furthermore, in a reactor without some sort of segregation between primary coolant and moderator, it is hard to assure that coolant flow is provided to the fuel elements regardless of moderator level.

The basic considerations mentioned above indicate rather strongly that the heavy-water-moderated pressure-tube reactor is the single type currently being developed which can use moderator-level control. Even within this fairly specific reactor category, however, the ease with which level control can be employed and its degree of usefulness vary. If the heavy-water-moderated pressure-tube reactor is to retain its identity as a machine in which the high-pressure components are small (i.e., pressure tubes instead of a large pressure vessel), then the temperature of the moderator must be low. If high temperatures were permitted, the moderator pressure would have to be high to prevent bulk boiling, and the moderator tank would have to embody the undesirable features of a reactor pressure vessel. Also, the usual negative reactivity effect associated with an increase in temperature indicates the desirability of a relatively cool heavy-water moderator. If it is accepted that the moderator will operate at a temperature some several hundred degrees Fahrenheit below that of the primary coolant (which must be quite hot if the plant is to produce decent steam), then there must be a thermal-insulation barrier between the two. By his placement of this insulation, the designer selects one of the two basic variations of the heavy-water-moderated pressure-tube reactor. This selection affects to some extent the ease with which moderator-level control can be incorporated in the design. One variation has internally insulated pressure tubes that are immersed in the relatively cool moderator, thereby earning the title "cool tube." The other basic variation permits contact between the hot primary coolant and the pressure tubes but limits heat conduction to the moderator by providing an insulating gap between the pressure tube and the cool moderator, which is contained in a calandria type tank. It is to this second variation that level-control schemes are more easily applied because consideration need not be given to the external cooling of pressure tubes during normal operation. Thus, for simplicity and general applicability, the heavy-water-moderated reactor using a calandria type tank with gas-gap insulation around the pressure tubes is a logical choice for reactivity control by means of moderator-level regulation.

Two operating heavy-water reactors of the type described above, the U. S.'s Plutonium Recycle Test Reactor[1] (PRTR) and Canada's Nuclear Power Demonstration[2] (NPD) reactor,

utilize moderator-level regulation as the primary means of reactivity control. In the following paragraphs the designs of these reactors are described, and operating experience with their level-control systems is discussed. Both plants are relatively small because they have thermal powers of less than 100 Mw. Units of this size can employ level-control schemes that are somewhat simpler, and at the same time more useful, than those applicable to large reactors. Large-reactor installations are discussed later in this article, with the CANDU control system used as an example.

Plutonium Recycle Test Reactor

The PRTR is a vertical pressure-tube type reactor that is moderated with heavy water and cooled by pressurized heavy water. The reactor has a thermal power of 70 Mw, and, although the plant does not produce electric power, the primary-circuit temperature and pressure conditions are typical of those which might exist in power reactors of this type. The primary coolant enters the core at 478°F, leaves at 530°F, and is maintained at a nominal pressure of 1050 psig. The arrangement of the major components of the reactor is shown in Fig. VIII-1, which illustrates the placement of the 85 Zircaloy-2 process tubes relative to the aluminum calandria type tank that contains the heavy-water moderator. In addition to the pressure tubes and 13 flux-monitor channels, the core region contains channels for 18 shim assemblies whose active elements will be described later. Full-core-length fuel assemblies are placed in the Zircaloy-2 process tubes and consist of bundles of rod type elements or of a concentric assembly containing a central fuel rod surrounded by two concentric fuel tubes. Several types of nuclear fuel material, including aluminum-plutonium alloys, UO_2, and a mixture of PuO_2-UO_2, have been used, and Zircaloy-2 has served as cladding material.

As shown in Fig. VIII-1, the calandria of the PRTR consists of several sections or compartments. The calandria is about 115 in. high and has a central, cylindrical section which contains the moderator and which is pierced by 85 vertical tubes forming dry channels for the primary-system pressure tubes. The space between the calandria tubes and the pressure tubes provides the gas-gap thermal insulation mentioned earlier. An annular compartment about 2 ft thick surrounds the 7-ft-diameter moderator portion of the calandria and contains a heavy-water reflector. The reflector and moderator systems are separate, and the reflector is held at a constant level in the reactor.

The annular reflector extends downward to a point about 2 ft above the bottom of the calandria. The bottom 2 ft of the annulus around the moderator cylinder forms a dump chamber that houses a circular weir over which the moderator flows in leaving the reactor core.[3] During an emergency shutdown of the reactor, caused by removing the heavy-water moderator from the calandria, the dump chamber serves as a temporary holdup volume that permits a rapid initial decrease in moderator level and, consequently, a rapid decrease in the reactivity of the system. Four large vertical lines connect the dump chamber to a moderator storage tank that is located beneath the reactor. Four additional lines of the same diameter connect the storage tank with the helium-gas space above the moderator in the calandria. One of the four lines that connect the dump chamber to the moderator storage tank is set flush with the base of the chamber and accommodates the normal flow of heavy water which spills over the circular weir. The other three lines are called the bottom gas lines and extend upward in the dump chamber to various heights. During normal operation these three lines equalize helium-gas pressure between the dump chamber and the storage tank. When the moderator is dumped from the calandria, the bottom lines facilitate escape of the helium from the dump chamber, thereby permitting the chamber to fill rapidly with heavy water; the lines then provide flow paths through which the moderator drains to the storage tank. The four lines that connect the moderator storage tank to the gas space above the moderator in the calandria are called the top gas lines, and each contains a fast-acting dump valve that is held closed during normal operation. The top gas lines, the bottom gas lines, and the fast-acting valves form the basis for the rapid moderator dump that scrams the reactor. During normal operation the moderator is held in the calandria by a differential gas pressure between the dump chamber and the blanket-gas space in the top of the calandria. When the fast-acting dump valves are opened, the gas pressure above the moderator in the calandria is equalized with that in the storage tank and dump chamber, and therefore the moderator falls from the calandria.

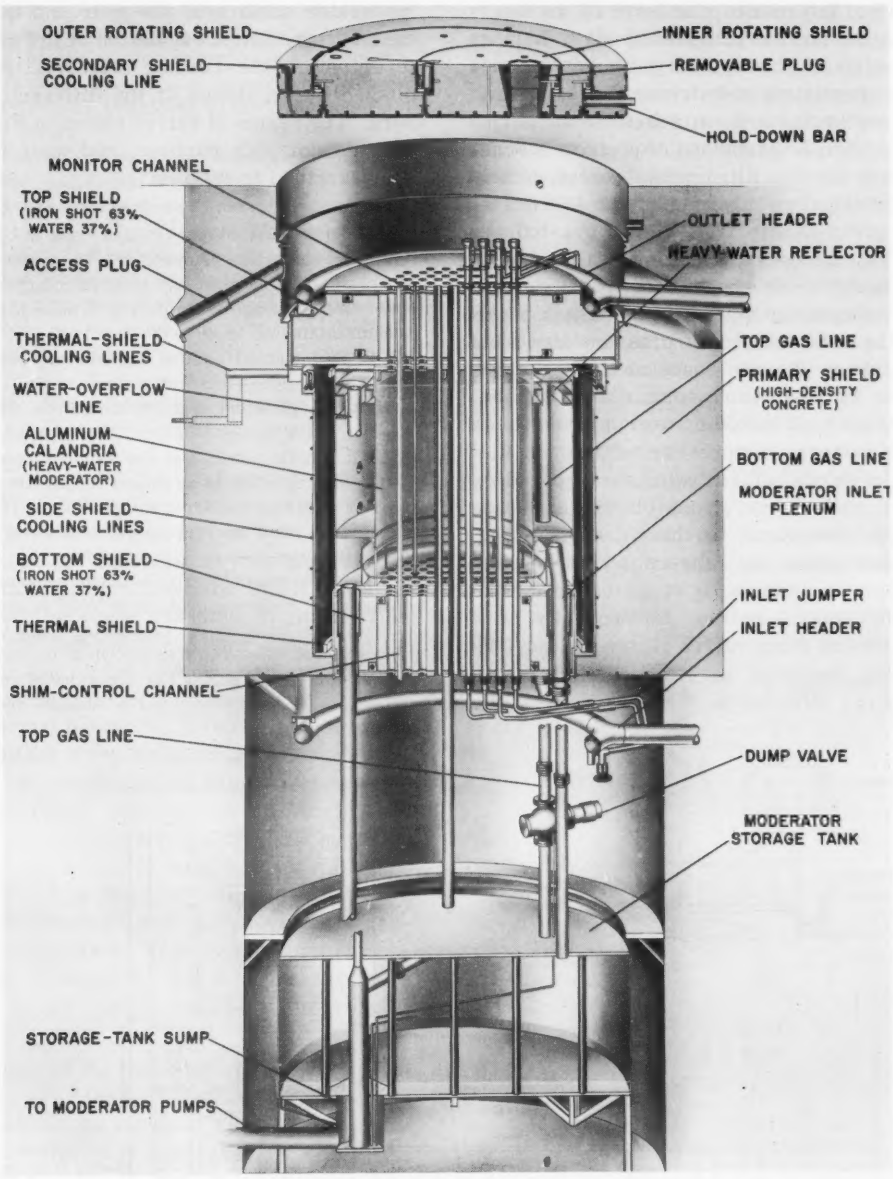

Fig. VIII-1 Cutaway view of the PRTR.[1]

The heavy-water moderator is maintained at a temperature range of 115 to 135°F by continuous circulation through a heat-removal system. Cool moderator enters the calandria at its base, picks up heat, and leaves the calandria over the weir at its base or through discharge ports in its upper regions. The warm moderator drains to the storage tank, from which it is pumped at a rate of 1100 gal/min through a heat exchanger and then returned to the bottom of the calandria. A specified minimum flow is always maintained over the weir to ensure a constant reference for static moderator level.

The differential pressure, which exerts the force necessary to hold the moderator in the calandria tank and which, as a function of its

magnitude, determines the level of the heavy water in the tank, is provided by a gas-balance control system. This system performs the same job that regulating-rod drives and safety-rod scram mechanisms do in reactors not having the moderator-level method of control. A schematic drawing that illustrates the arrangement of the principal components of the PRTR system is given as Fig. VIII-2. The gas-balance system can be operated automatically, and, in its automatic mode of operation, it has demonstrated exceptional stability at constant power level. The differential gas pressure that must exist between the gas space at the top of the calandria and the helium volume in the moderator storage tank and dump weir is provided by the gas-balance compressor shown in Fig. VIII-2. As shown in the drawing, the compressor receives helium gas from either the space above the moderator in the calandria or the helium-gas holder and delivers it to the storage tank. Excess helium gas is bypassed through the regulating control valves. Consequently, with the fast-acting dump valves closed, as they are in normal operation, the compressor creates the required differential pressure between the moderator surface at the weir and that within the reactor. Actual regulation of the moderator level within the reactor calandria is accomplished by regulation of the differential pressure. The series of valves shown in Fig. VIII-2 is used for this purpose, and their functions are described as follows:[3]

1) An automatic control valve, used in conjunction with the automatic controller. This valve can control the moderator at any level from approximately (76 cm) 30 in. above the calandria base to the maximum attainable level in the calandria.

2) Two manual control valves—a "coarse" and a "fine" valve—used in control of the reactor by manual adjustment of moderator level. The coarse valve has a capacity approximately equal to that of the automatic valve. The fine valve, of considerably smaller capacity, is provided to permit smoother level adjustment under manual control. The manual control valves are considerably slower in action than the other valves in the system.

3) A "shutdown" valve—a quick-opening valve capable of lowering moderator level to about 75 cm above the base of the calandria. This valve was provided to effect rapid shutdown of the reactor and if possible to preclude the necessity of scramming the reactor, if a short period occurs or (on auto-

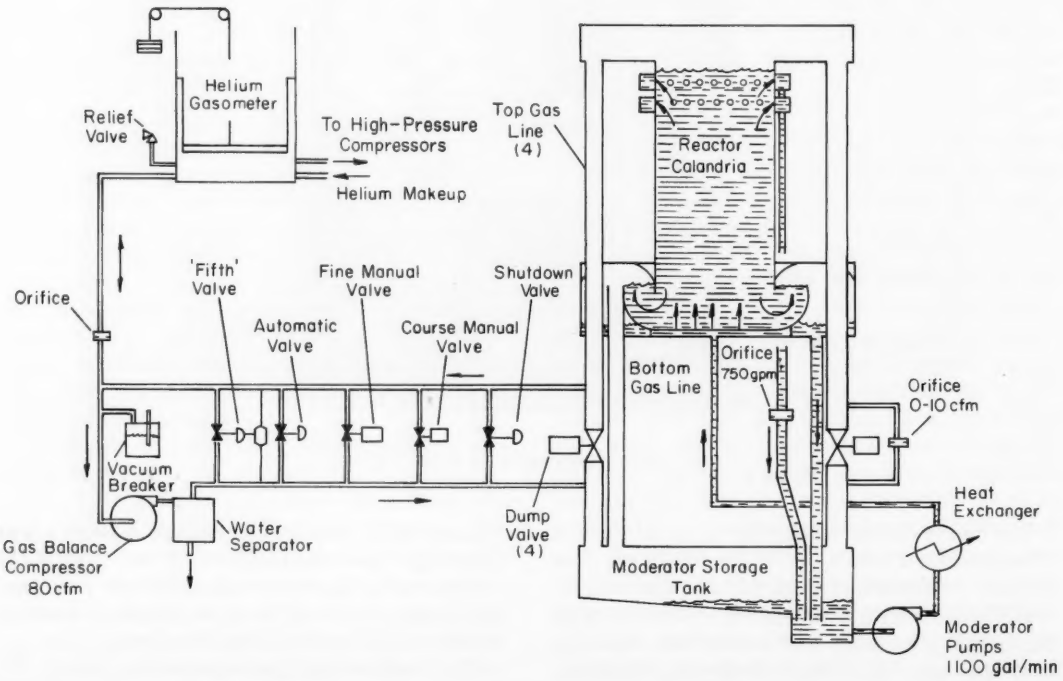

Fig. VIII-2 The PRTR moderator-level-control system.[3]

matic control) if power level varies excessively from the set point. This valve may also be opened manually by the reactor operator; in addition, it is opened (and the gas balance compressor stopped) by safety circuit interlocks at the time moderator dumping occurs.

4) A characterizing valve, referred to simply as the "fifth" valve, which is actuated in a positive feedback loop in response to the differential pressure in the gas balance system. This valve is adjusted to be fully open when pressures are equalized (i.e., when moderator is at weir level) and to be closed when moderator level reaches about 200 cm. The effects of this valve are to further limit the maximum rate of moderator rise (and thus of reactivity increase) at low moderator levels, and to extend the range of the "manual" and "automatic" control valves to lower moderator levels.

The helium gasholder (gasometer) shown in Fig. VIII-2 furnishes a pressure reference for the gas-balance system and is held at a pressure very slightly greater than the air pressure in the building that houses the PRTR. The orifice in the line to the gasholder limits the flow of gas from the reactor during dumping of the moderator but offers no appreciable resistance to the flow of gas at the flow rates that occur during normal operation. If the helium supply in the gasholder were depleted and its pressure lowered, an uncontrolled rise in moderator level could result. Although specific control interlocks are provided to prevent the depletion of the helium supply in the gasholder, a backup safety feature is provided by the installation of the vacuum breaker near the inlet to the gas-balance compressor. This vacuum breaker ensures that the system reference pressure does not fall below the pressure in the reactor building.

The design of the fast-acting dump valves that are installed in the four top gas lines deserves some attention. As shown in Fig. VIII-3, a drawing of the valve, a plug is normally held in the closed (up) position by a spring at its base. The valve plunger is not attached to the plug but is normally held free of the plug by an electromagnet located at the end of the actuator assembly. Opening of the valve is accomplished by deenergizing the electromagnet. This permits a strong spring to force the plunger against the plug, thereby overcoming the upward-acting force of the plug spring and opening the valve. The dump valves are capable of opening in 30 to 50 msec after the solenoids of the electromagnet are deenergized. The actuating plunger is recocked subsequent to opening of the valve by energizing the holding electromagnet and feeding compressed air to the bottom side of the piston; the force thus generated is capable of overcoming the downward force exerted on the pushrod by the valve-opening spring. Air pressure is bled from the cocking cylinder after the opening spring is compressed and the plunger is brought into contact with the electromagnet. The spring-loaded air piston then contracts to its normal position, leaving the valve free to open if the electromagnet is deenergized. Because failure of the cocking piston to retract could prevent or materially slow down the opening up of the valve, limit switches prevent starting of the gas-balance compressor unless the pistons of all four dump valves are in the retracted position.

Although regulating and safety rods are replaced in the PRTR by its moderator-level-control system (and its dump feature), the reactor still requires shim elements. These shim

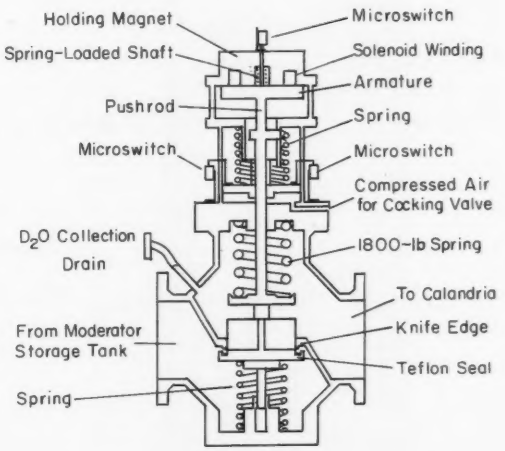

Fig. VIII-3 PRTR dump valve.[3]

elements maintain the moderator level within its normal operating range, compensate for fuel burnout, provide for xenon override, and flatten the neutron flux. The shim elements also provide for depressing the flux for experimental purposes in portions of the reactor. Operation of the units is manual, and they are not intended as a safety device. Eighteen shim assemblies[4] of the type shown in Fig. VIII-4 are provided in the PRTR core. Each of the 18 assemblies contains three Inconel elements that are "gray" to

neutrons. The basic frame, or structural members, of the shim assemblies does not move in and out of the core. Instead, the frame remains fixed in its position in the core, and the three Inconel elements are moved. Actuating force for the absorber elements is provided by electric motors that drive lead screws through suitable transmissions. The absorber elements are supported on the lead screw by recirculating-ball nuts. The overall height of the shim-rod assembly is such that the assembly extends from above the top primary shield into the bottom primary shield shown on Fig. VIII-1. The rod assembly has three basic zones that correspond to locations in the top shield, the calandria, and the bottom shield. The zone that extends through the top primary shield contains the driving head and electrical components of the control assembly. In the calandria region, the support framework provides guidance for the elements, and the lower-primary-shield zone of the assembly is used for storage of the shim elements when they are out of the core. The frame member of the shim assembly, which

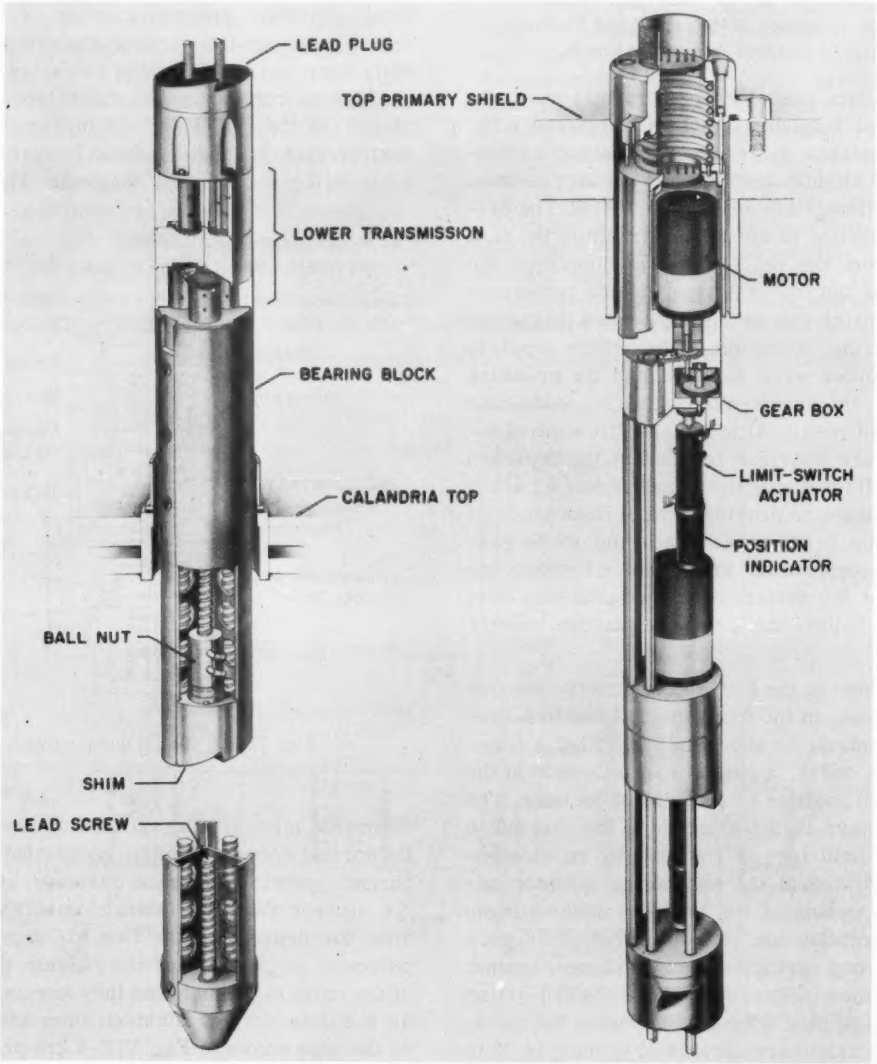

Fig. VIII-4 PRTR shim-control unit.[1]

remains in the core at all times, is fabricated from an aluminum extrusion with numerous punched holes as shown in Fig. VIII-4. The lead screws are aluminum or zirconium, and thus the absorption in the shim-assembly channel is minimized when the shim elements are in the out-of-core position. Each of the three elements in a shim assembly is 36 in. long and has an average worth of about 2 mk. Two motors are used to drive the three lead screws, and the mechanical arrangement is such that there are two mutually powered elements and one independently powered element. One of the mutually powered lead screws turns $^2/_3$ as fast as the other, so that when one of the elements is fully inserted in the core the other is immediately below it. Second-generation shim-rod assemblies[4] being developed for the PRTR will use the same lower unit (frame structure and absorber elements) as the first-generation assemblies. The driving heads, although considerably different, perform the same basic functions.

Nuclear Power Demonstration Reactor

A second reactor that utilizes moderator-level regulation as the primary means of reactivity control is the Nuclear Power Demonstration (NPD) reactor.[5,6] This reactor, which uses natural-uranium fuel and has horizontal pressure tubes, was developed and built during roughly the period that the PRTR was undergoing design and construction. Unlike the PRTR, NPD produces electric power. As its name implies, the NPD was built to prove the feasibility of the heavy-water power-reactor concept embraced by the Canadians.

The pressurized heavy-water-cooled NPD generates about 20 Mw of electric power from a thermal-power production of nearly 90 Mw and has primary coolant parameters similar to those of the PRTR. Primary coolant enters the reactor at 485°F, leaves at 530°F, and is maintained at a nominal pressure of 1040 psig. Although the appearance of NPD, as shown in Fig. VIII-5, is markedly different from that of the PRTR, the principle of operation of the moderator-level-regulation system is the same; i.e., NPD uses a gas-balance system that will be described shortly. Fuel elements in NPD consist of 7- or 19-rod bundles, with each rod containing pellets of natural UO_2 encased in cylindrical Zircaloy-2 cladding tubes. Fuel channels in the core are formed by 132 Zircaloy-2

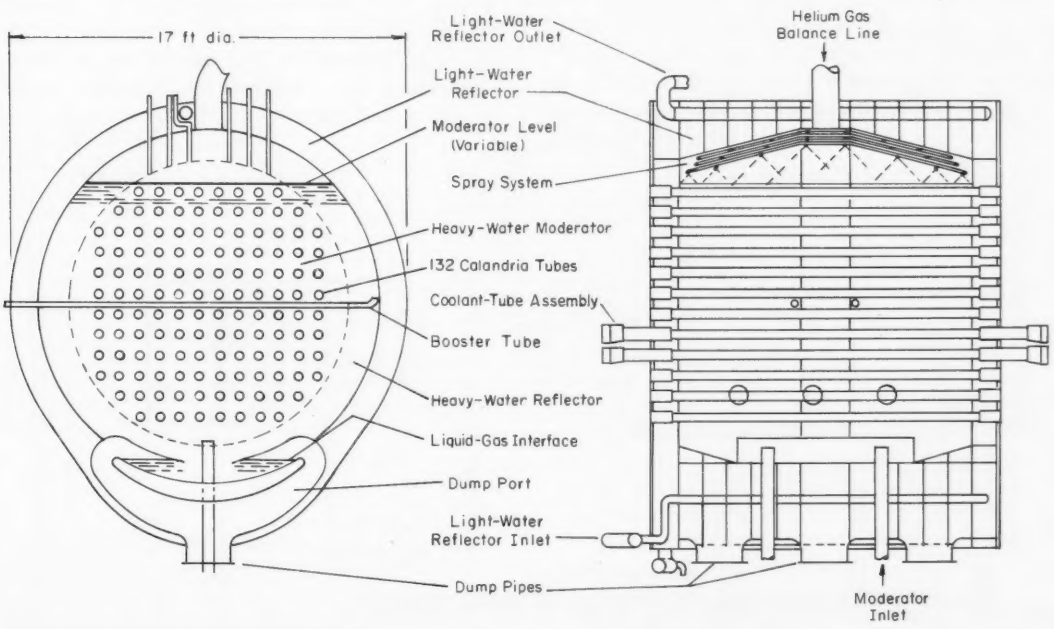

Fig. VIII-5 Vertical sections of the NPD reactor.[6]

pressure tubes, each having an inside diameter of 3.25 in. As in the PRTR, the pressure tubes penetrate the core through low-pressure calandria tubes that are part of the heavy-water core tank.

As shown in Fig. VIII-5, the calandria of the NPD reactor is a compartmented tank. However, the sections within the tank are not used to separate the moderator and reflector portions of the core as in the PRTR but, rather, to separate the two types of reflector used in NPD. As shown in the figure, the active core region of NPD is surrounded by a heavy-water reflector that is integral with, and a part of, the moderator system. It is this heavy-water reflector which the inner compartment of the calandria tank bounds, so that when the NPD moderator level is changed, the heavy-water-reflector level changes too. The incorporation of the heavy-water moderator-reflector liquid into a single system in the NPD, in which the reflector is actually quite thick (~21 in.), illustrates an interesting difference in design approach from that employed in the PRTR. In the PRTR the inner tank which surrounds the process channels and which contains the heavy-water moderator is only slightly larger than the distance across the outermost process tubes. The annular heavy-water reflector, whose level is not varied, remains in its portion of the calandria following a moderator dump and provides postdump shielding. Comparable shielding in NPD is furnished by the light-water reflector that surrounds the heavy-water moderator-reflector section of the calandria. In spite of the reactivity effects, the scheme employed in NPD appears to be the simpler one: a single heavy-water system suffices for both moderator and inner reflector, and, although a relatively large volume of heavy water must be moved to achieve a given change in moderator height, the provision of sufficient pipes, etc., to handle the relatively large flow seems to be a straightforward step.

The moderator-level-control system of the NPD reactor,[7] although utilizing the same gas-balance principle used in the PRTR, has interesting features and differences. The NPD system (shown in Fig. VIII-6) contains the same basic components as its counterpart in the PRTR: a reactor tank containing a dump region that has a relatively large volume into which heavy water can flow at the initiation of a moderator dump, large interconnecting pipes between the reactor tank and the dump or storage tank, and gas connecting lines between the top of the reactor tank and the dump tank. Fast-

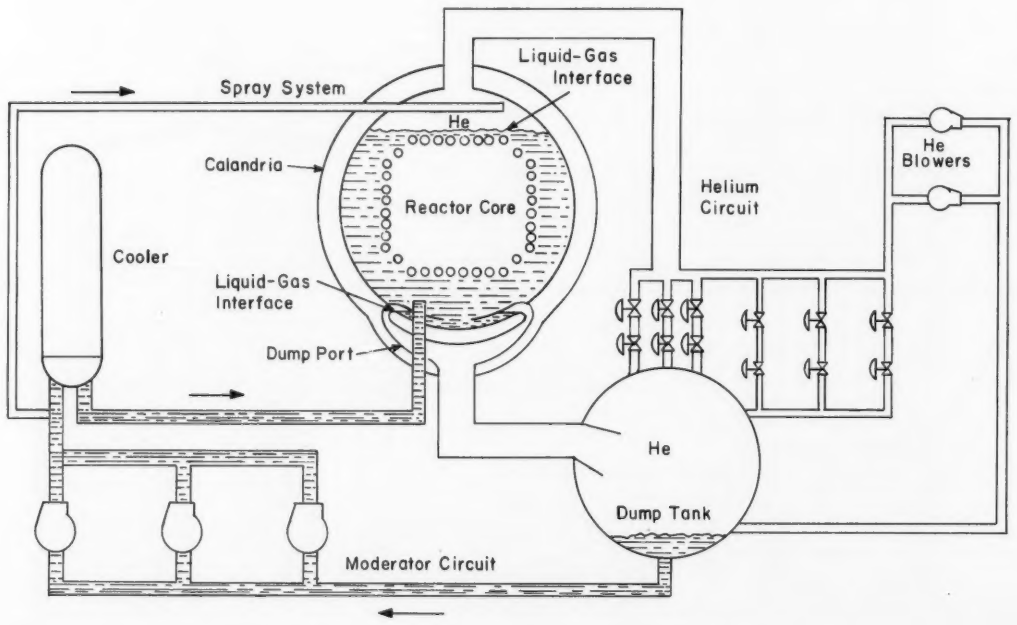

Fig. VIII-6 The NPD reactor moderator and helium systems.[7]

opening valves, which are opened to equalize pressure between the moderator and storage tanks and thereby cause the dumping of the moderator, are located in the top gas line. The pressure differential, which establishes the level of moderator in the tank, is developed around these normally closed valves by helium compressors. Since the operation of the NPD system is similar to that of the PRTR system, it will not be described here. However, the arrangement employed in valving the main gas-balance or top gas line is important. As shown in Fig. VIII-6, and as indicated in Fig. VIII-5, a single large gas line leads most of the way from the top of the calandria tank to the top of the dump tank. However, prior to entering the dump tank, the single large line branches into three parallel lines. Each of the three parallel lines is provided with two valves in series, so that, to dump the heavy-water moderator from the reactor tank to the storage tank, two valves in one of three lines must open. The opening of a single one of the three parallel lines results in a sufficiently fast lowering of the moderator level for scram purposes. The three parallel lines with double valves in each line are used in the NPD because a triplicated system[8] is employed in the scram as well as the regulating circuitry of the reactor. The triplicated safety system, which is shown schematically in Fig. VIII-7, minimizes the number of false trips and gives the advantage that all equipment can be tested routinely, one channel at a time, from the primary sensing element through to actual operation of the dump valves.

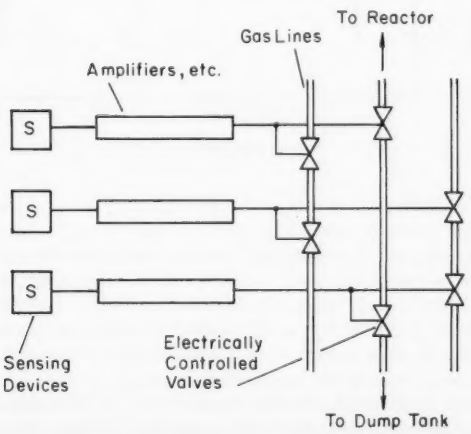

Fig. VIII-7 Triplicated system of the NPD reactor.[8]

In addition to the primary mode of reactor control, i.e., the variation of moderator level, NPD has other means of reactivity management. By virtue of the on-power refueling scheme used, the amount of excess reactivity available at any time in plant life can be held to a minimum. Although not actually a control feature as such, the on-line refueling scheme does make the job of the control-system components relatively easy once the reactor has attained an equilibrium core condition. In addition to the reactivity control methods already mentioned, NPD has the capability of changing reactivity by two other means: insertion of a booster rod and variation of moderator temperature. The booster rod, whose location is shown in Fig. VIII-5, is a fissile assembly that can be inserted into the core to give a boost in reactivity. The rod is worth 2.5 mk and, when inserted following an emergency shutdown, partially overrides xenon poison and permits the reactor to be below 60% of full power for up to 35 min while retaining a restart capability. Although moderator-temperature variation is ineffective as a control mechanism once an equilibrium fuel-burnup condition has been reached (since its reactivity coefficient is essentially zero at that condition), it is useful during the first year of operation of the reactor. With a fresh pile the temperature coefficient of reactivity for the moderator is -0.04 mk/°F. The effect of this characteristic can be used to good advantage as a reactivity shim during refueling and to further extend the poison override times up to a maximum of about 55 min.

Operating Characteristics

PRTR OPERATING EXPERIENCE

After more than two years' operating experience with the PRTR moderator-level-control system, its users report[3] that the system has proved to be a safe, reliable, and satisfactory means of reactor control. With the exception of level instabilities that occurred and were corrected during a short period early in the operating life of the reactor, the moderator-level-control system has met or exceeded design requirements for both the regulating and the safety modes of operation.

Control-System Characteristics. Startup tests performed with the PRTR verified the control-system characteristics that were pre-

dicted in analyses and tests performed during the design of the system. The moderator level is controllable over a range of about 80 cm to the maximum capacity of the calandria, which is at a level of about 287 cm. The normal range of levels for operation of the reactor at power is 260 to 270 cm. Reactor operating procedures require that criticality be attained only at moderator levels exceeding 182 cm. The worth of the moderator as a function of its height is shown in Fig. VIII-8 for a level range of 140 to

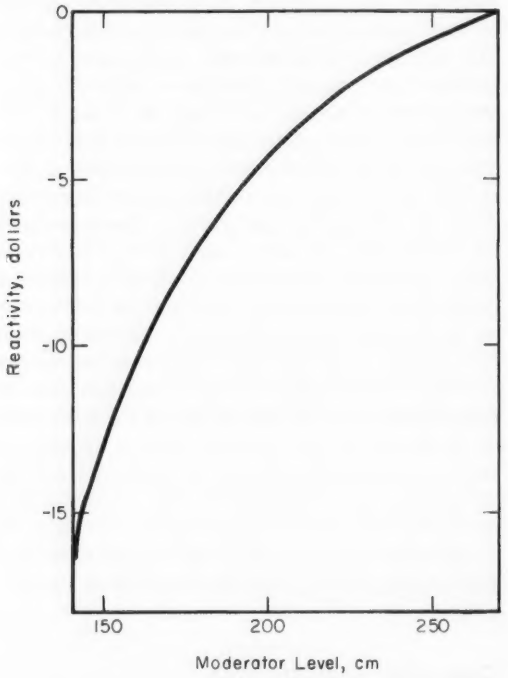

Fig. VIII-8 Reactivity variation with moderator level in the PRTR.[3]

270 cm. As can be determined from the figure, the moderator-level coefficient of reactivity is approximately 5 cents/cm in the normal range of levels for power operation.

Test data on the control system obtained during the reactor startup period show that the limiting rates of moderator-level change attainable with the system are as shown in Fig. VIII-9. One of the curves is for an increasing moderator level, and the other two curves represent level change rates corresponding to decreasing levels. The perturbations that occur in all curves at about the 220-cm level are caused by the capacity of a header located behind the moderator recirculation (outflow) ports located at that level. These perturbations, which show so clearly on the maximum rate of level-change curves, are not observed at level-change rates that normally occur in the system, and, furthermore, do not affect control of the reactor.

For the limiting level change rates shown in Fig. VIII-9, there are corresponding limiting rates of change in reactivity. Figure VIII-10 shows the limiting rates of reactivity change attainable with the PRTR control system. As shown in the figure, the maximum reactivity change rate at a moderator level of around 182 cm, which is the minimum criticality level as set by reactor operating procedures, is slightly more than 2 cents/sec, and the maximum rate at the normal range of levels for operation at power is about 1 cent/sec.

Although the PRTR control system had been operated principally in a manual mode up to the

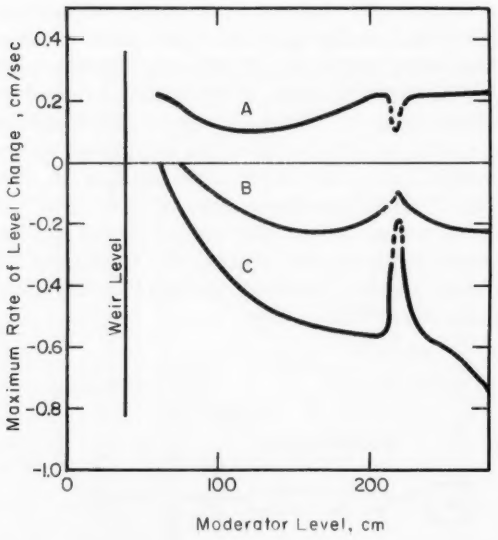

Fig. VIII-9 Limiting rates of moderator-level change with control system in the PRTR.[3] *A*, all control valves closed, increasing level. *B*, automatic or manual valve open, decreasing level. *C*, automatic and shutdown valves open, decreasing level. ("Fifth" valve is operating in all cases.) The spikes that appear in these curves are due to effects of the header volume behind the top discharge orifices. These are seen only in maximum-change-rate tests, such as produced the data, and never in actual operation where rates of level change (at this level) are well below maximum.

time of writing of Ref. 3, indications were that the stability of control would be very good in both manual and automatic modes of operation. During all phases of reactor operation under the manual option, the system provides stable control, and the limited experience obtained with the automatic controller indicates that it will provide a marked improvement and smoothness and precision of control over the manual mode at the power levels (2 to 70 Mw) at which it had been used. Although the stability of the system is entirely acceptable, minor fluctuations in moderator level (which may represent wave action at the surface rather than true variation in level) do tend to obscure measurements of reactor noise and make period measurement involving long periods difficult.

The moderator-dump feature of the PRTR control system has been demonstrated to be a rapid, reliable, and essentially fail-safe means of reactor scram. Figure VIII-11 shows the height of moderator as a function of time after tripping the reactor safety circuit. The curve shown in the figure is a composite drawn from data obtained from timed tests performed during the reactor startup. Since the times are given as time after tripping of the safety circuit, they include delays in the safety circuit and in opening of the dump valves. The decrease in reactivity, which occurs as a result of the lowering of the moderator level in the calandria, is related to the time after tripping the safety circuit by the curve shown in Fig. VIII-12. The design requirements for the safety system specified a 2-ft decrease in level from normal operating levels within 1 sec after tripping of the safety circuit. The reactivity associated with this decrease in level is about 3 dollars

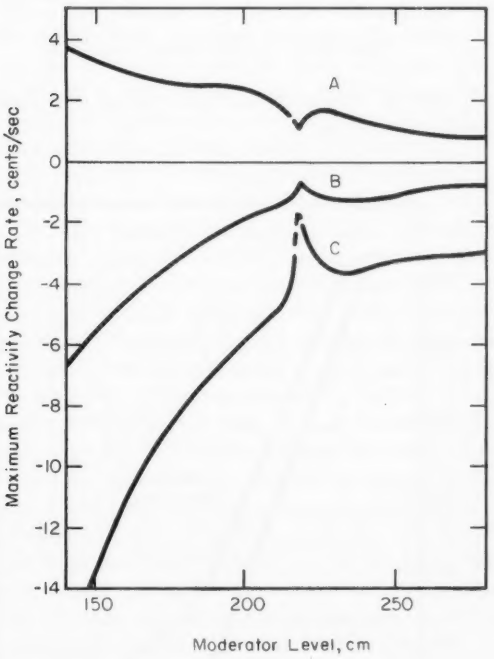

Fig. VIII-10 Limiting rates of reactivity change with control system of the PRTR.[3] *A*, all control valves closed. *B*, automatic or manual valve open. *C*, automatic and shutdown valves open. ("Fifth" valve is operating in all cases.) The spikes that appear in these curves are due to effects of the header volume behind the top discharge orifices. These are seen only in maximum-change-rate tests, such as produced the data, and never in actual operation where rates of level change (at this level) are well below maximum.

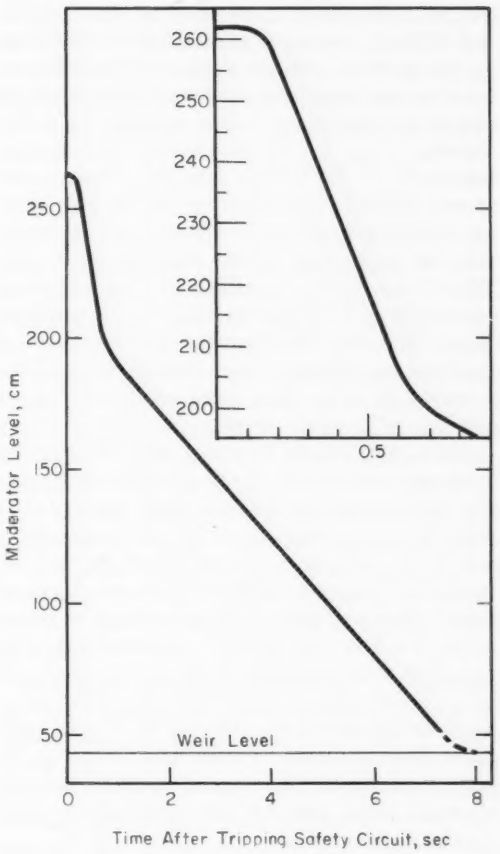

Fig. VIII-11 Typical moderator-level decrease during dump of the PRTR.[3]

and 50 cents. As can be seen in Figs. VIII-11 and VIII-12, these requirements are bettered by the system, with the required 2-ft change in level accomplished in less than 0.7 sec. At the end of the first second after tripping the safety circuit, where the reactivity decrease was required to be about 3 dollars and 50 cents, the actual reduction amounts to about 5 dollars. Although the moderator rate of level decrease may be somewhat slower than shown in Fig. VIII-11 for cases in which the moderator is dumped from levels below the normal operating range, the net rate of reactivity decrease is as great as that shown in Fig. VIII-12 owing to the increase in moderator-level coefficient of reactivity at the lower levels.

Although the dump time and effectiveness just discussed are based on the satisfactory operation of all four moderator dump valves, it is interesting to note that failure of some of the valves to open does not materially affect the initial (and most important, of course) rate of dump. Tests showed that the design requirement of a 2-ft drop within 1 sec could easily be met with two valves operating and could almost be met with only a single operable valve. Figure VIII-13 shows the difference in moderator level as a function of time after tripping the safety circuit for the normal, or four-valves-working, case and for the situation in which only one valve opens.

Problems During Early Operation. Early in the control-system test period, oscillations occurred in the moderator level.[3] These oscillations, which were up to 2 cm in height, were stopped by the addition of a water separator to the discharge of the gas-balance compressor, as shown in Fig. VIII-2, and by changes in the inventory of the helium gasholder and in helium-addition procedures, although the specific mechanism causing the oscillations was not identified. Subsequent to the stopping of the oscillations in moderator level, a pressurized helium system associated with the primary coolant loop was placed in service. Whenever the helium compressors in the system associated with the primary coolant loop were operated, the oscillations in moderator level recurred. Because the gasholder shown in Fig. VIII-2 is a common component of several systems, including the primary-loop helium system that was apparently causing the later oscillations in moderator level, it became evident that there was some interaction between the

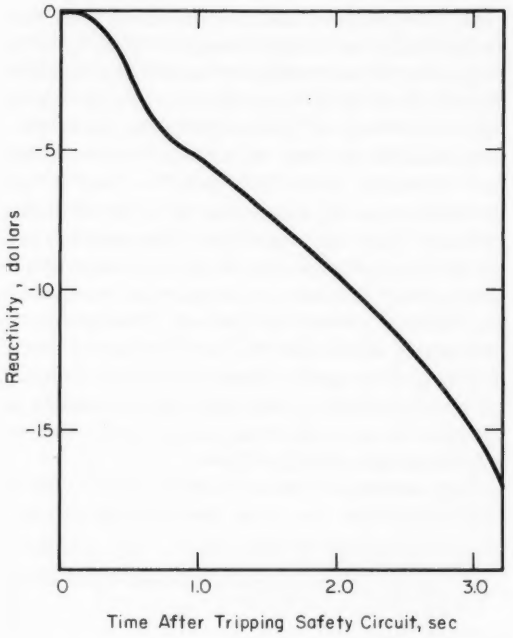

Fig. VIII-12 Reactivity decrease during moderator dump in the PRTR.[3]

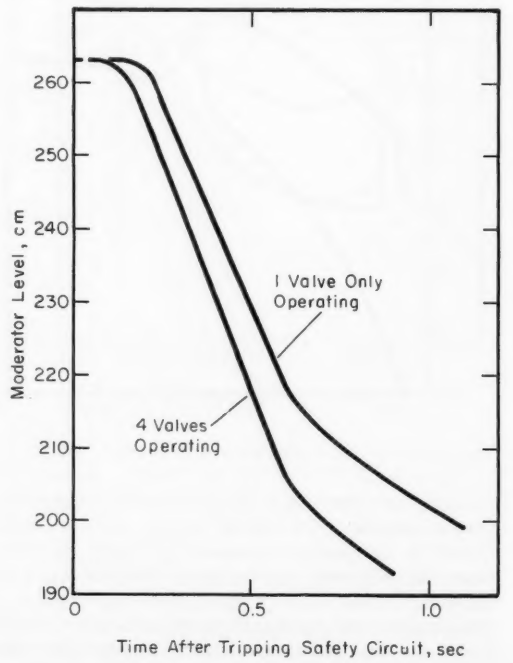

Fig. VIII-13 Effect of dump-valve malfunction on moderator dump rate in the PRTR.[3]

level-control system and other reactor systems. The causative mechanism for the second series of oscillations was determined to be fluctuations in pressure within the helium gasholder, which resulted in fluctuations in moderator level. Significant oscillations in moderator level were eliminated by modifying the gasholder cover so that the gasholder gave relatively even response to changes in inventory, and by replacing a common manifold that had served the control system as well as the primary loop system with a separate line from the gasholder to the level-control system. This latter step was taken as a precaution against pressure pulsations from other sources.

With the helium-gasholder arrangement used in the PRTR level-control system, a decrease in gasholder pressure is accompanied by a corresponding decrease in gas pressure within the reactor calandria. This decrease of pressure within the calandria results in an increase in the differential pressure between the calandria and the moderator storage tank and causes an increase in moderator level. On two separate occasions, spontaneous rises in moderator level were caused by rather sudden decreases in helium pressure in the gasholder. These spontaneous rises in level illustrate rather dramatically the strong interaction that can exist between remotely related systems. The first spontaneous rise in moderator level occurred during a critical test that was made at a time when modifications to the ventilation-exhaust system of the containment vessel were being carried out. A containment valve was closed to seal off the exhaust duct during the modification, and the ventilation supply fan was left in operation, causing the containment-vessel pressure to increase gradually. Consequently helium pressure in the gasholder increased gradually (not at a rate sufficiently fast to decrease the differential pressure across the calandria tank but, rather, so slowly that the level-control system did not "feel" the increase). When work on the containment exhaust system was completed, the valve that had been closed to seal off the exhaust duct was opened, and building pressure rapidly dropped to normal. The gasholder pressure decreased with the building pressure, thereby increasing the differential pressure across the calandria and causing a rapid rise of the moderator level of about 1 cm, followed by a slower rise to about 2.5 cm. The shutdown valve of the level-control system was opened, and the rise in moderator level stopped. On another occasion a spontaneous rise in moderator level of about 8 cm occurred. This time the reactor was ready for startup, and the control valves had been closed, but the gas-balance compressor had not been started. The rise, which had again been caused by changes in helium pressure in the gasholder, was stopped by opening the control valves. In the second instance, the sudden change in gasholder pressure had apparently been caused by the rather rapid charging of the helium into the gasholder and the inability of the pressure-relief mechanism of the gasholder to prevent an overpressure upon the injection of such large amounts of helium. Consequently the gasholder pressure increased slowly for some time, again causing no discernible change in the differential pressure across the reactor calandria. Then the gasholder inventory was rapidly reduced, probably by starting the helium compressors, thus relieving the overpressure condition and causing a rapid increase in calandria differential pressure.

A number of steps were taken to prevent the recurrence of spontaneous moderator-level rises such as those described above. These steps included the procedural requirement that the air pressure in the containment vessel must be less than atmospheric pressure by at least 0.3 in. H_2O before reactor operation is permitted. This provision prevents the occurrence of a sudden decrease in containment-vessel pressure (and, consequently, gasholder pressure) due to venting to the atmosphere. The only other step that will be mentioned here is the one taken to prevent a transient rise in moderator level caused by a rupture of the gasholder or its connecting piping. The magnitude of such a rise is limited by keeping the operating pressure of the gasholder to a value of 1 in. H_2O or less above the building pressure.

Some difficulty was encountered with leakage through the dump valves in the top helium-gas lines. This leakage caused the rate of rise of moderator level during startup to markedly decrease, and, often, the moderator could not be raised above a level of about 150 cm. Although the results of such a leak do not present a hazard, it is conceivable that a sudden stoppage of the leak could cause an increase in the differential pressure across the calandria tank and a subsequent rise in moderator level. Therefore startup procedures were specified which re-

quired that the rate of rise of moderator level during startup be within prescribed limits. A program of planned maintenance of the valves has essentially eliminated the leakage problem.

NPD OPERATING EXPERIENCE

The moderator-level-control system of NPD has performed its functions satisfactorily.[7,9–11] Utilization of the system has proceeded somewhat differently than in PRTR, in that NPD's automatic-control mode of operation was brought into use immediately after first achieving criticality. This early use of the automatic system is not too unexpected, however, since the NPD design incorporates the triplicated-components arrangement in the regulating as well as in the safety portions of the system. Another factor that probably hastened the use of the automatic system was that manual control of moderator level, which was carried out with five of the valves shown in Fig. VIII-6 in an equilibrium position and the sixth valve used for fine control, proved to be simple but slow.

Apparently the NPD control system was brought into service with a minimum of difficulty. The object of the load-following scheme used in the on-power mode of operation of NPD is to have the reactor follow changes in turbine load so that constant steam pressure is maintained at the turbine throttle valve. The reactor satisfactorily assumes load at the limiting rate of 20% full load/min; it shuts down to a low power, without excessive steam bypass, on a loss of electrical connection to the grid or loss of the turbine. Early experience with the system can probably be summarized best by the following sentence from Ref. 7: "Perhaps the most difficult commissioning operation was bringing the triplicated input signals into sufficient agreement."

It is shown by measurements that the installed blower capacity of the NPD level-control system, in conjunction with the piping arrangement employed, can cause a maximum rate of rise of moderator level which corresponds to a rate of reactivity increase at cold, clean critical conditions of slightly less than 0.3 mk/sec. At this rate, it takes 12 min to fill the calandria tank, and the rate of reactivity increase at full-tank conditions is 0.06 mk/sec. Moderator dump tests showed that with two out of three protective channels in operation (that is, with only one gas-balance line opening), reactivity could be reduced 5 mk in the first second and 15 mk in 2 sec. The dump valves had fully opened 0.3 sec after receiving a trip signal. Table VIII-1 is a comparison of pertinent design and measured parameters in NPD, and Fig. VIII-14 shows the variation of moderator temperature coefficient with fuel irradiation. As mentioned earlier, the coefficient is essentially zero with equilibrium fuel burnup, and Ref. 11 contains a statement that there is no detectable change in

Table VIII-1 COMPARISON OF DESIGN AND MEASURED PARAMETERS IN NPD[9]

Parameter	Design value	Measured value
Clean critical level	89.3 in.*	97.5 in.
Moderator temp. coefficient	−0.06 mk/°F	−0.04 mk/°F
Heat-transport system temp. coefficient	−0.024 mk/°F	−0.02 mk/°F
Light-water reflector savings	3 mk	3.6 mk
$\Delta k_{eff}/k_{eff}$		
For clean critical condition to full tank	37 mk	39 mk
For enriched booster	2.5 mk	2.4 mk
Dump rate in first second	3 mk†	5 mk

*Error due to underestimate of depleted uranium; now reconciled.

†Conservative value; measured results more favorable.

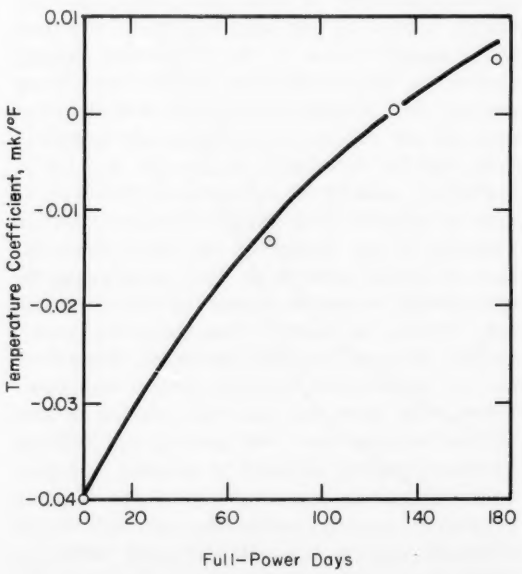

Fig. VIII-14 Variation of moderator temperature coefficient with fuel irradiation in the NPD reactor.[11]

moderator temperature coefficient with changes in moderator level. The value of 39 mk, shown in Table VIII-1 as the measured value of reactivity change from the clean critical moderator level to full tank level, corresponds to a change in level from 97.5 in., as indicated in Table VIII-1, to a full tank height of approximately 173 in.

Large Reactors

The operating experience gained with the reactor control systems of PRTR and NPD has shown the suitability of moderator-level control for small, heavy-water-moderated pressure-tube reactors. The NPD system, in particular, rather epitomizes the useful application of moderator-level control by its extreme simplicity and almost complete lack of ancillary systems, components, or gadgets for reactor control. Despite the obvious utility of moderator-level control in NPD, however, its use in future reactors is by no means certain because there appears to be no great demand for reactors of the NPD type and size and because moderator-level-control systems lose a great deal of their attractiveness when applied to large reactors. A brief discussion of the CANDU reactor,[6,12,13] which qualifies as both a large reactor and one which uses moderator-level control, serves to illustrate the complications which occur in larger reactors and which begin to nullify the advantages of a concept that is simple in practice as well as in principle in smaller reactors.

The 200-Mw(e) CANDU is similar in appearance to the NPD reactor. It utilizes a calandria pierced by horizontal process tubes, is fueled with rod type bundles containing natural UO_2, is moderated by heavy water, and is cooled by pressurized heavy water. Nominal coolant temperature at the reactor inlet is 480°F, that at the reactor outlet is 560°F, and the primary coolant pressure is about 1400 psi. As in NPD, emergency shutdown is accomplished by a moderator dump system operating on the gas-balance principle.[14] In a sense, moderator-level control is also used in CANDU, since after a shutdown the reactor must be brought back to critical by raising the moderator. However, the use of level control alone can result in the requirement that the reactor operate for significant periods at reduced power output because of xenon oscillations induced by flux distortions resulting from operation at low moderator levels. In CANDU, cadmium sulfate will be added to the moderator to permit operation at full tank at all times.[14] This moderator-poison expedient will be employed at times prior to the full build-in of xenon or if fuel reactivity is higher than usual. As the xenon builds up after an extended shutdown, the cadmium in the moderator will be removed by ion exchange.

CANDU is provided with four small absorber rods, moving in two through tubes, to give a means of local control in each of the four quadrants of the reactor.[14] These absorbers, which can be moved collectively or independently, will be used to adjust the overall reactivity as well as to exert local influence on the flux in any particular quadrant.

The last accessory control mechanism that will be described for CANDU consists of booster rods similar to the rod installed in NPD. The CANDU system consists of eight booster elements that are capable of moving independently in four through tubes.[14] The proposed total worth of the eight elements, when fully inserted, is about 10 mk. The worth of the rods is expected to be sufficient to give the reactor restart capability after being shut down for about 30 min from equilibrium full power or to allow power to be reduced to about 65% for an indefinite period.

With the exception of the on-line refueling process that is a feature of the CANDU design, all the reactivity-control methods will be integrated into an automatic system. When we consider the several major control devices which will be parts of this system, and which have been mentioned previously, it is obvious that the rather simple concept of moderator-level control loses a great deal of its simplicity when applied to reactors in the CANDU size range. The CANDU case is an example of the simple concept being a little too simple to meet the requirements of a large core, and it is unfortunate that the uncomplicated implementation of the scheme, as exemplified by the NPD system, is not applicable to the larger reactors.

References

1. N. G. Wittenbrock, P. C. Walkup, and J. K. Anderson (Eds.), Plutonium Recycle Test Reactor Final Safeguards Analysis, USAEC Report HW-61236, Hanford Atomic Products Operation, Oct. 1, 1959.

2. I. N. MacKay, The Canadian NPD-2 Nuclear Power Station, in *Proceedings of the Second United Nations International Conference on the Peaceful Uses of Atomic Energy, Geneva, 1958,* Vol. 8, pp. 313-321, United Nations, New York, 1958.
3. J. F. Fletcher and R. I. Smith, Moderator Level Control in the Plutonium Recycle Test Reactor, USAEC Report HW-79669, Hanford Atomic Products Operation, December 1963.
4. D. E. Rasmussen and L. D. Gustafson, The PRTR and PRCF Control and Safety Rod Drives, ASME Paper 62-WA-235, November 1963.
5. Reactors on the Line NPD, *Nucleonics,* 20(11): Reactor File ... No. 13.
6. *Directory of Nuclear Reactors, Vol. IV, Power Reactors,* International Atomic Energy Agency, Vienna, 1962.
7. W. S. Brown, Reactor Control of NPD, paper presented at the Winter Meeting of the American Nuclear Society, Washington, November 1962.
8. G. C. Laurence, Reactor Safety in Canada, *Nucleonics,* 18(10): 73-77 (October 1960).
9. L. G. McConnell, Commissioning and Initial Operation of NPD, in The Eighth AECL Symposium on Atomic Power, Held at Chalk River, Ontario, September 24, 1962, Canadian Report AECL-1599, September 1962.
10. L. G. McConnell, Initial Operating Experience with the "NPD" Reactor, in *Operating Experience with Power Reactors,* Vol. I, pp. 139-150, International Atomic Energy Agency, Vienna, 1963.
11. A. C. Whittier, Nuclear Performance of NPD, in ANS Topical Meeting on Nuclear Performance of Power-Reactor Cores, September 26–27, 1963, Sponsored by the Northern California Local Section of the American Nuclear Society, USAEC Report TID-7672, pp. 95-122, February 1964.
12. Atomic Energy of Canada Ltd., Douglas Point Nuclear Generating Station, Canadian Report AECL-1596.
13. C. E. Benyon, Douglas Point: The CANDU Reactor, in The Ninth AECL Symposium on Atomic Power at Toronto, Ontario, September 23, 1963, Canadian Report AECL-1807, pp. 25-30.
14. E. Siddall, Reactivity Control in the CANDU Reactor, in Papers Presented by A.E.C.L. to the International Conference of the Canada Nuclear Association, Held at Ottawa, Ontario, May 28–30, 1962, Canadian Report AECL-1962 (Paper I), Atomic Energy of Canada Ltd., February 1963.

Section

IX

Power Reactor Technology

Specific Reactor Types

Heavy-Water Reactors

Large-Plant Studies

The design of the Carolinas-Virginia Tube Reactor (CVTR) was reviewed in *Power Reactor Technology*, 6(4). This plant was designed as the prototype of a full-scale plant, and Ref. 1 is a report on a study of the larger plant. The CVTR was designed to produce 17 Mw(e), whereas the large plant nominally produces 300 Mw(e).

Although the CVTR had not produced a significant amount of operating experience at the time Ref. 1 was issued, the influence of the small reactor can be seen in the design of the large reactor, especially in the following areas:

1. The pressure-tube reactor concept (cold-tube design)
2. Heavy water as moderator and coolant
3. Pressure-tube joints, including a Zircaloy–stainless-steel joint
4. Fuel-assembly design
5. Stagnant-water (D_2O) baffle design for thermal insulation
6. Primary-system temperatures and pressures
7. Primary-system pressure drop
8. The basic reactor layout (e.g., moderator tank and header-cavity layout)
9. Refueling method
10. Closed-system ventilation of the vapor container with D_2O recovery

A set of four large plants (cases) was studied using four different fuel assemblies, as shown in Table IX-1. Design data on cases II and IV are presented in Table IX-2.

The CVTR and the large plant are both U-tube designs, although the CVTR uses a gasketed joint and the large plant uses a coextruded Zircaloy–stainless-steel transition joint. Each plant has a mechanical joint for pressure-tube closure without seal welding. The CVTR fuel element is about 8 ft long, and the large plant is fueled with a 13- to 16-ft-long fuel element, possibly made of subassemblies. Cross-sectional views of the 19- and 37-rod fuel bundles and pressure tubes are shown in Fig. IX-1.

Table IX-1 FUEL ASSEMBLIES SPECIFIED FOR LARGE-PLANT STUDIES

Case	Rods/cluster	Fuel
I	19	Natural UO_2
II	19	Enriched UO_2
III	37	Natural UO_2
IV	37	Enriched UO_2

Steam conditions of the CVTR secondary plant were dictated by the existence of a steam plant previously constructed. The large plant was designed with a primary-system pressure of 1000 psia for the natural-uranium reactor and 1500 psia for the enriched-uranium reactor. The lower pressure was selected to minimize the wall thickness of pressure tubes and fuel-rod cladding for the reactor using natural uranium, whereas the upper pressure is identical with that of the CVTR. There are some differences between the refueling concept for the large plant and that of the CVTR. The CVTR is refueled by removing the pressure tubes (from which the fuel elements have been removed) from the reactor during one of the refueling steps and replacing them by fully loaded pressure tubes, whereas the large plant would be refueled without moving the pressure tubes except in the case of pressure-tube damage. The two plants also differ in the method of pressure-tube support. The CVTR supports the pressure tubes on a core support plate by means of jumper blocks and support columns.* However,

*Figure III-7 of the previously mentioned CVTR review illustrates the method of pressure-tube support.

Table IX-2 CVTR LARGE-PLANT DATA: 300 Mw(e) NOMINAL POWER[1]

	Case II (enriched)	Case IV (enriched)
Heat output, Mw(t)		
From core	1136	1136
From fuel rods in maximum-power U tube	4.72	8.69
Coolant flow, lb/hr		
Total coolant flow rate	38.3×10^6	38.3×10^6
Flow per maximum-power U tube	147,200	272,300
Pressure, psia		
System pressure minimum (U-tube exit)	1480	1480
U-tube pressure drop	105 ± 5	105 ± 5
Steam pressure	481	481
Hot-channel factors		
Heat flux (F_q)	3.10	3.10
Radial	1.50	1.42
Axial	1.62	1.62
Maximum-to-average rod in cluster	1.18	1.25
Flux (F_q^E) engineering	1.08	1.08
($F_{\Delta H}^E$) engineering	1.05	1.05
Flow effectiveness*	1.05	1.05
Heat transfer		
Active core surface area, sq ft	32,748	32,197
Average flux, Btu/(hr)(sq ft)	124,600	124,600
Maximum steady-state flux, Btu/(hr)(sq ft)	386,000	386,000
Average film coefficient in maximum-power tube, Btu/(hr)(sq ft)(°F)	9900	10,000
Minimum DNB ratio at full power	2.3	2.3
Temperatures, °F		
Moderator, average	155	155
Moderator, inlet	130	130
Coolant, inlet-to-pressure tubes	488	488
Coolant, discharge from pressure tubes	570.8	570.8
Saturation temperature	592.7	592.7
Fuel-rod surface, maximum steady	602	602
Maximum center temperature at 100% power	3930	3930
Fuel rod		
Outside diameter, in.	0.54	0.54
Pellet diameter, in.	0.5	0.5
Cladding wall thickness, in.	0.0163	0.0163
Fuel length per rod, ft	16.04	16.03
Rod lattice, in.	0.672	0.672
Rods per assembly	19	37
Pressure tube		
Total No. of pressure tubes	760	384
No. of U-tube assemblies	380	192
No. of fuel elements	760	384
Inside diameter, in.	3.959	5.303
Wall thickness, in.	0.207	0.277

*Ratio of hot-tube enthalpy rise to corewise average enthalpy rise. Dependent on timewise nuclear factor for low-power tubes.

the major difference between the CVTR and the large plant is the number of pressure tubes, the number being larger by an order of magnitude in the large plant. This increased number results in a greatly increased jumper stack height (Fig. IX-2). In the large plant the pressure tubes are supported on the top neutron-shield tank to minimize stresses due to thermal

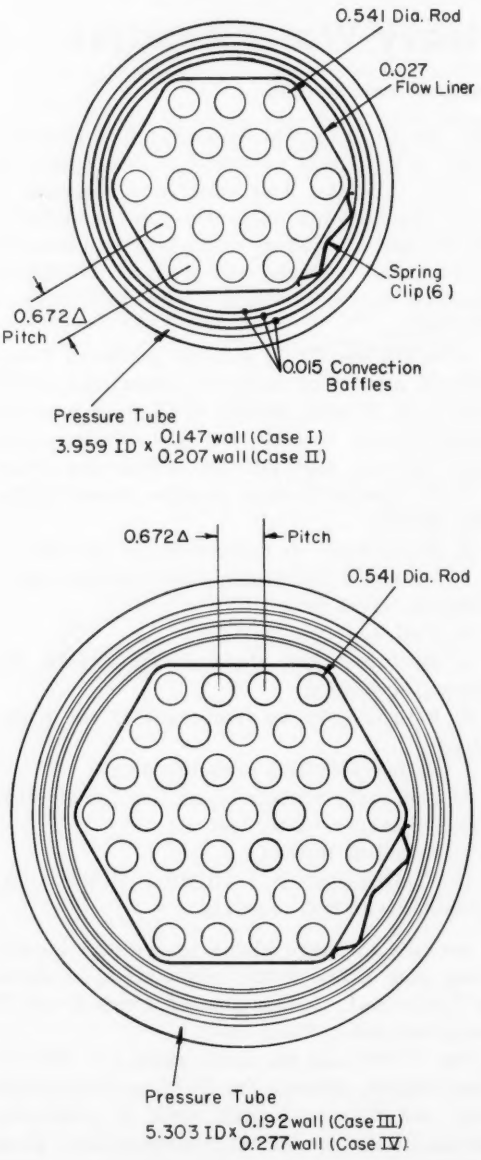

Fig. IX-1 Cross section of pressure tubes containing 19- and 37-rod fuel clusters (dimensions in inches).[1]

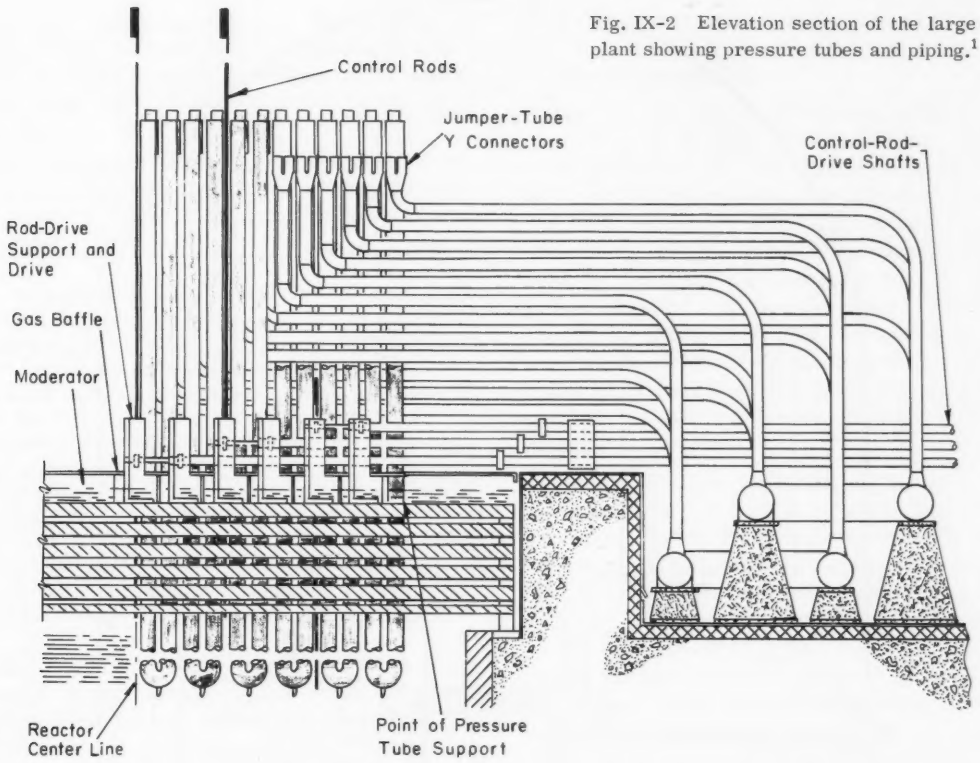

Fig. IX-2 Elevation section of the large plant showing pressure tubes and piping.[1]

expansions. It is noted in Ref. 1 that the U-tube design for the pressure tubes is not necessarily the best arrangement for the large plant. Advantages and disadvantages of U tubes relative to through-tubes and bayonet or reentrant tubes are also discussed. The U-tube design does confine all the jumper tubes and their associated joints to the top of the reactor where they are probably more readily accessible, and it avoids penetrations of the moderator tank below the D_2O level. But the U tubes also have an inherently large pressure drop (because they constitute a two-pass system) and are expensive.

Figure IX-3 is a schematic diagram of the equipment arrangement in the vapor container. The reference contains some cost data on the large-plant designs and the following quotation probably best serves to illustrate the results:[1]

> An estimate of the cost of each of the four large plants was made primarily to indicate areas where improvements must be made to lower costs. Since no concerted effort was made to achieve optimum conditions or designs, it was anticipated that the estimated costs of these four plants would be higher than estimates by others in the industry for comparable plants. Thus comparisons should be made with caution.

The costs for each of the four plants are listed below.

Item	Cost* mills/kw-hr			
	Case I	Case II	Case III	Case IV
Plant	6.06	5.89	5.53	5.27
D_2O	1.53	1.48	1.42	1.32
D_2O losses (2% per year)	0.24	0.23	0.22	0.20
Fuel cost	3.74	2.15	3.85	1.98
Operation & maintenance	0.80	0.80	0.80	0.80
Total	12.37	10.55	11.82	9.57

*Costs based on 14.5% yearly rate on capital investment and 13.0% yearly rate on the D_2O.

The fuel assemblies for each of these four cases are described in Table IX-1. Although comparisons of cost data are often not significant, there are a few comparisons of important design parameters that probably can be made with validity. These comparisons are illustrated in Table IX-3. The data for the Canadian, Du

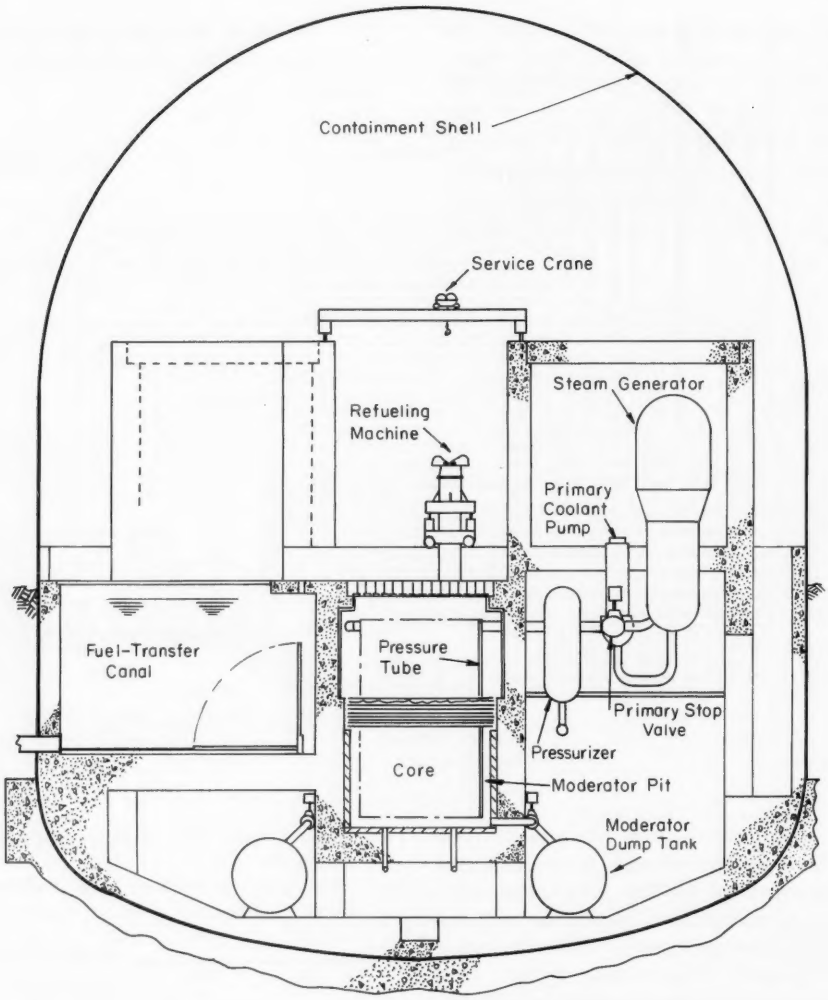

Fig. IX-3 Elevation section of vapor container.[1]

Table IX-3 COMPARISON OF DESIGNS FOR LIQUID D_2O-COOLED REACTORS

	Canadian	Du Pont	AEPSC-GNEC	Westinghouse case IV
Gross power, Mw(t)	1570	1838	1850	1135
Total D_2O inventory, metric tons	350	325	390	485
Maximum heat flux, Btu/(hr)(sq ft)	330,000	850,000	620,000	386,000
Uranium inventory, metric tons	95.7	27.1	51.4	76.7
Average specific power, Mw(t)/metric tons of U	16	68	36	14.8
No. of pressure tubes	387	226	560	384 (192 U tubes)
Average power/pressure tube, Mw(t)	4.1	8.1	3.3	3.0

Pont, and American Electric Power Service Corporation–General Nuclear Engineering Corporation (AEPSC-GNEC) designs were taken from Table IX-1, *Power Reactor Technology*, 7(1): 88.

The relatively high D_2O inventory of the U-tube design results from a large number of pressure tubes with a large tube-to-tube spacing:[1]

> The quantity of heavy water in the reactor is very large, with the consequence that the inventory charges are very high. This is brought about by the large quantity of pressure tubes and the large spacing between the pressure tubes. The spacing of the U-tubes is governed by mechanical considerations concerned with locating all the jumper tubes and pressure tube supports. It is apparent that the design of the entire upper region of the pressure tube including the jumper tubes and the arrangement of the jumper tubes, control rods, supports, etc., must be carefully engineered to give the proper balance between D_2O inventory and pressure drop without mechanical interference.

The other large heavy-water study to be considered is the organic-cooled design by Combustion Engineering, Inc.[2,3] The study was reviewed briefly in *Power Reactor Technology*, 7(1): 95-97, and this review will emphasize some of the technical details of the concept. The characteristics of the plant are summarized in Table IX-4. The reactor, shown in its containment building in Fig. IX-4, has 600 pressure tubes, each containing five fuel elements (Fig. IX-5). Interestingly, a two-pass flow through the core is used, as in the CVTR [this is shown in Fig. IX-7, *Power Reactor Technology*, 7(1)]; although the CVTR uses a U tube, the organic-cooled design connects the two passes via a lower, interpass header, so that the allocation of pressure tubes to the two passes can be made for optimum thermal performance. The fuel element contains 37 rods, but not all are of identical size. Thirty-one rods have an outside diameter of 0.513 in., and the remaining rods have an outside diameter of 0.313 in. to achieve a circular configuration. Rod-to-rod spacing is maintained by small square "wires" wound helically around each rod. These wires are extruded as an integral part of the cladding tube, which is sintered aluminum (SAP), XAP-001. Each rod was designed to be freestanding, and the assembly is secured by stainless-steel bands around the outside of the bundle. The bundle was designed with staggered ends (Fig. IX-5) that intermesh with the adjacent bundles to minimize end flux peaks and orient the elements azimuthally.

The pressure tubes are of composite design, consisting of an inner liner, a gas gap, and the outer pressure tube. The inner liner is XAP-001, and the pressure tube is Zircaloy-2. Both are designed to withstand the internal organic pressure. Inert gas is fed to the annular region between the liner and pressure tube to serve as an insulator and permit the Zircaloy-2 tube to operate in contact with the relatively cold moderator. Pressure-breakdown seals are provided at each end of the inner liner, and any gas leaking into the coolant is removed in the purification system.

Table IX-5 lists data similar to those presented in Table IX-3. The organic-cooled reactor does achieve a significant reduction of the D_2O inventory, as might be expected. On the other hand, it has the lowest power-removal rate per pressure tube, which possibly is due to the rather poorer heat-transfer capabilities of the organic coolant relative to water. There are many design variables, however, and it probably is misleading to attribute a specific performance characteristic to a single design variable. The average specific powers of the Canadian, the Westinghouse, and the Combustion Engineering designs are comparable; the relatively high specific powers of the Du Pont and AEPSC-GNEC designs are probably due to the different fuel-element designs. The Canadian, Westinghouse, and Combustion Engineering designs utilize solid pellets, whereas the Du Pont design specifies coaxial cylinders of fuel (UO_2) of relatively thin oxide sections, and the AEPSC-GNEC design specifies hollow, sintered pellets of UO_2. The Du Pont fuel element is shown and discussed in *Power Reactor Technology*, 7(1): 95. The coaxial design is mentioned in Ref. 1 as a fertile area for further study. In Ref. 2 it is recognized that the 37-rod fuel element may not be an optimum one, and the coaxial design and several others are discussed.

Reference 2 includes power cost estimates. Results are summarized in Table IX-6. Note that the organic-cooled heavy-water-moderated reactor (OHWR) was designed to operate on either enriched or natural fuel. It is stated in Ref. 2 that the resultant plant, therefore, cannot be considered as an optimum design for operation with only one type of fuel.

Table IX-4 500-Mw(e) D_2O-MODERATED ORGANIC-COOLED REACTOR-PLANT CHARACTERISTICS[2]

General		
Reactor type	D_2O moderated, organic cooled	
Steam-cycle type	Nonreheat with turbine moisture extraction	
Total fission power, including moderator heat loss, Mw	1550	
Station net output, Mw(e)	Enriched	512.2
	Natural	510.3
Net plant efficiency, %	Enriched	33.05
	Natural	32.92
Fuel and core		
Type of fuel	UO_2	
Fuel density, % of theoretical	91	
Design burnup, Mwd/metric ton	Enriched	20,000
	Natural	5,000
Cladding material	XAP-001	
Cladding thickness, in.	0.010 and 0.016	
Fuel-rod outside diameter, in.	0.313 and 0.513	
No. of fuel rods/bundle	6 plus 31	
Overall length of fuel bundle, in.	40	
No. of bundles/pressure tube	5	
Pressure tubes		
Number	600	
Lattice arrangement	Square	
Pitch, in.	$9\frac{3}{4}$	
Material	Zircaloy-2 and XAP-001	
Outside diameter, in.	$4\frac{1}{32}$	
Wall thickness, in.	Zircaloy-2, 0.036; XAP, 0.062	
Insulation material	0.100 in. inert-gas annulus	
Core length, in.	192	
Core equivalent diameter, in.	269	
Radial-reflector thickness, in.	12	
Axial-reflector thickness, in.	12	
Total UO_2 loading, lb	246,000	
Type of control unit	Hy-Ball	
No. of control units	200	

Nuclear fuel inventory and burnup	Enriched	Natural
Uranium total, metric tons	98.7	98.7
Initial enrichment, wt.% ^{235}U	1.25	0.7115
Discharge enrichment, wt.% ^{235}U	0.05	0.30
Discharge plutonium, g/kg of U initial	6.09	3.23
Design life, Mwd/metric ton of U	20,000	5000

Nuclear fuel inventory and burnup	Enriched	Natural
Fuel conversion ratio by weight for gross lifetime		
Total plutonium generated/^{235}U lost	1.40	1.24
Fissionable plutonium generated/^{235}U lost	1.23	1.06
Fuel conversion ratio by weight for net lifetime, plutonium remaining/^{235}U lost	0.51	0.79
Lifetime energy-production fractions		
^{235}U fission	0.49	0.64
^{238}U fission	0.01	0.01
Plutonium fission	0.50	0.35
Thermal		
Average heat flux, Btu/(hr)(sq ft)	115,000	115,000
Maximum heat flux, Btu/(hr)(sq ft)	298,400	352,500
Maximum cladding-surface temperature, °F	< 850	< 850
Maximum UO_2 fuel temperature including all hot-spot factors, °F	< 3450	< 3750
Primary coolant system		
Coolant material	Santowax OMP, 10% high boilers	
Total coolant flow, lb/hr	42,900,000	
Reactor inlet temperature, °F	536	
Reactor outlet temperature, °F	760	
Reactor pressure drop (header to header), psi	223	259
No. of loops	4	
Coolant inventory, lb	790,000	
Makeup, lb/day	7200	
Blanket gas	Nitrogen	
Materials in contact with coolant	Carbon steel, XAP-001, S.S.	
Moderator system		
Medium	D_2O	
Moderator-tank inlet temperature, °F	130	
Moderator-tank outlet temperature, °F	190	
Design temperature, °F	250	
Total flow rate, lb/hr	4,350,000	
System design pressure, psig	150	
Blanket gas	Helium	
Materials in contact with moderator	S.S., Zircaloy	
Total inventory, lb	519,000	
Makeup, lb/year	5000	
Cooling arrangement	Nonregenerative	

Thermal Breeder Reactors

Two recently published studies deal with the subject of D_2O reactors and their potential as breeders or near breeders.[4,5] These studies are of particular interest because one examines the thorium-^{233}U system[4] and the other considers the uranium-plutonium system.[5]

No reactor designs, as such, are presented in Ref. 4. The reference is more a discussion of the philosophy behind the thermal breeder reactor. The reactors that are discussed are D_2O-moderated and D_2O-cooled machines fueled with the coaxial fuel elements of either metal or oxide, clad in a zirconium alloy.[6] A brief description of the preliminary designs is given in Table IX-7. The thorium-fueled reactor has a number of somewhat unusual features. An outer ring of pressure tubes is placed in the

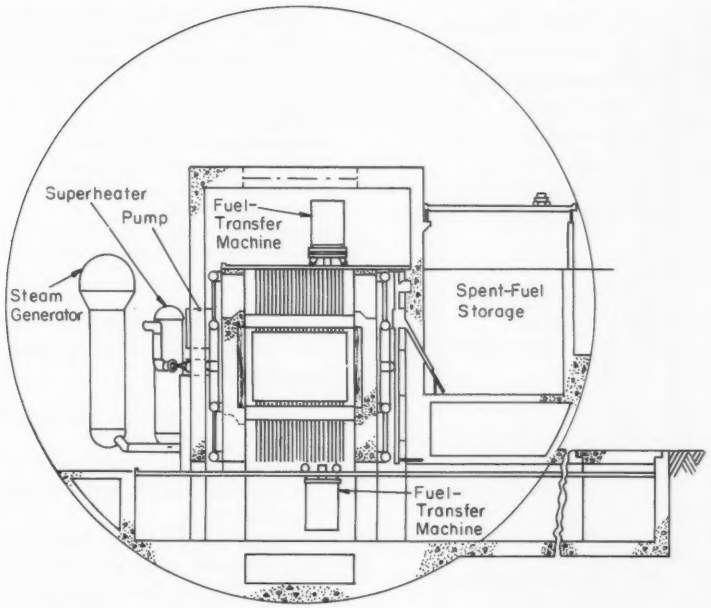

Fig. IX-4 Reactor plant elevation.[2]

reflector region to serve as a converter blanket and is fueled with thorium containing, initially, no fissile isotope. Short elements of uranium-free thorium also are placed at the top and bottom of the fuel column in the axial reflector region, and some of the control rods are fabricated of thorium.

The following quotation[4] serves to highlight the discussion presented in Ref. 4 on breeding in thermal reactors:

> In considerations of breeding in thermal reactors with the thorium-^{233}U fuel cycle, a clear distinction must be made as to the significance of the following four factors: breeding ratio, doubling time, conservation of fuel resources, and fuel economics. A high breeding ratio is of value only if it leads to a short doubling time; a short doubling time serves little purpose if it does not conserve fuel resources; and fuel conservation itself is of questionable value unless for some postulated set of economic conditions this conservation leads to lower fuel cycle costs.
>
> The D_2O-moderated thermal breeders discussed in this report are based on consideration of all four of these factors. The reactors do not represent the maximum possible breeding ratio or the minimum doubling time achievable with solid-fueled D_2O reactors. Instead, they represent a judgment of the compromises that will be necessary to achieve excellent conservation of fuel resources while retaining those features of D_2O reactors that are essential to low-cost power generation in the near future. It will be shown that the breeding gain in any of the D_2O systems considered is too small to be an important factor in fuel cycle costs during the next 50 years or so.

A fixed-fuel reactor employing thorium as the fertile material suffers from the immobility of ^{233}Pa, which may absorb neutrons prior to decay to ^{233}U. This has led to reactor concepts in which the thorium would be placed in a "blanket" where a low neutron flux would minimize ^{233}Pa losses. This principle is employed to some extent in the design shown in Table IX-7, but its use is limited by the economic disadvantages of devoting D_2O moderator and reactor volume to blanket functions, or even to power-producing functions when the specific power is low. Also, resonance absorption in ^{233}U causes significant reductions in eta and the breeding ratio.[4] Consequently the highest breeding ratios are apt to be obtained with moderator/fuel ratios higher than those which currently give the best economic performance. Taken together, these reasons have led the authors of Ref. 4 to deemphasize breeding and to emphasize low inventory and long fuel life, at least for the near future.

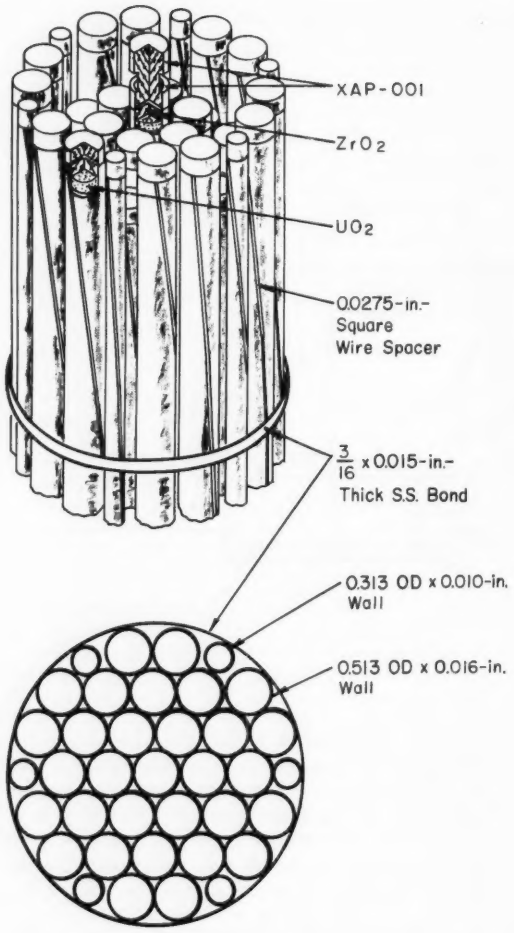

Fig. IX-5 Perspective and cross-sectional view of 37-rod fuel element.[2]

Table IX-5 COMPARATIVE DESIGN DATA FOR THE HEAVY-WATER-MODERATED ORGANIC-COOLED REACTOR: ENRICHED-FUEL DESIGN

Gross power, Mw(t)	1550
Total D_2O inventory, metric tons	235
Maximum heat flux, Btu/(hr)(sq ft)	352,500
Uranium inventory, metric tons	98.7
Average specific power, Mw(t)/metric ton of U	15.7
No. of pressure tubes	600
Average power/pressure tube, Mw(t)	2.6

The following reactor system is postulated for the orderly development of D_2O-thorium breeders:[4]

Until 1975, all new reactors are H_2O converters with Pu recycle.

From 1975 to 1985, all new reactors are D_2O converters operating on uranium fuel with Pu recycle.

In the years 1985 to 2000, all new reactors are D_2O-thorium reactors with a conversion ratio of 1.00. The old D_2O converter reactors remain on uranium fuel with Pu recycle.

After the year 2000, all new reactors are D_2O-thorium breeders, with an effective breeding ratio (including reprocessing losses) of 1.05. This breeding ratio leads to a doubling time of 32 years, which will meet the estimated growth of nuclear power beyond the year 2030.

In Fig. IX-6 are shown the uranium and thorium requirements for the above system (termed "D_2O-thorium" in the figure) and for three other systems that were postulated and discussed in a previous article in *Power Reactor Technology*, 6(4). Subject to the assumptions used in deriving the data shown in Fig. IX-6, it is evident that the D_2O-thorium system will be more conserva-

Table IX-6 OHWR TOTAL-ENERGY-GENERATION COST SUMMARY[2]

(Costs Are in Mills/kw-hr at 90% Plant Factor)

	Natural fuel with private ownership	Enriched fuel	
		Government ownership	Private ownership
Capital	2.99	2.99	2.99
Amortization of initial core fuel and fabrication	0.23	0.20	0.25
Fuel cycle	1.88	0.77	0.72
Heavy water (at $24.50/lb)			
Amortization charge	0.43	0.43	0.43
Losses (1% of inventory)	0.03	0.03	0.03
Organic makeup	0.12	0.12	0.12
Operation and maintenance	0.36	0.36	0.36
Nuclear liability insurance	0.08	0.08	0.08
Total	6.12	4.98	4.98

Table IX-7 DESCRIPTION OF 1000-Mw(e) PRELIMINARY DESIGNS OF D_2O-MODERATED POWER REACTORS[4]

Fuel	UO_2	Th metal
Initial enrichment, wt.%	1.2 (^{235}U)	1.5 (^{233}U)
Reactor coolant	Liquid D_2O	Liquid D_2O
Lattice pitch, in.	10	10
No. of fuel positions	489	678
Core radius, ft	10.8	12.6
Core length, ft	15	15
Coolant inlet temp., °C	264	264
Coolant outlet temp., °C	304	304
Maximum heat flux, pcu/(hr)(sq ft)	434,000	340,000
No. of coolant loops	8	8
Throttle steam pressure (saturated), psia	495	500
Net plant efficiency, %	26.7	26.1
Net power production, Mw(e)	1000	981
D_2O inventory, tons	660	872
Thorium or uranium inventory, metric tons	64.5	103
^{233}U or ^{235}U inventory, kg	765	1540

tive of uranium resources for the next century than will the other systems.

Fuel-cycle cost data are given in Table IX-8. In any of the cases estimated, it appears that breeding is a relatively small economic factor in fuel-cycle costs and that an attractive way to reduce near-term costs is to increase the exposure in the thorium fuel even at the expense of reduced conversion ratios. It is also indicated that thorium-fueled D_2O reactors still have an attractive fuel-cycle cost even if the cost of natural uranium should increase to $100 per kilogram. The use of uranium in the thorium fuel cycles having breeding ratios of 1.00 or greater is not obvious from Table IX-8, but the uranium is used as a source of ^{235}U for startup of the fuel cycle. As the cost of uranium increases to a high value, the inventory charge for the uranium becomes the major component of the fuel-cycle cost.

The breeding potential of thermal reactors fueled with plutonium is described in Ref. 5. The reference, primarily the result of a physics study, considers the breeding ratio in infinite homogeneous systems, presents a conceptual design for a plutonium-fueled D_2O-moderated thermal power reactor, and treats the buildup of higher plutonium isotopes and their effect on conversion ratios. The details of the various calculational procedures will not be discussed here; however, they would be of interest to the specialist. The author considers D_2O-, H_2O-, graphite-, and beryllium-moderated reactors and concludes that heavy water is the most desirable moderator and that it is essential to keep the moderator at a low temperature. The moderator temperature and resulting neutron temperature have a large effect on the value of eta of plutonium. Figure IX-7 gives $\bar{\eta}$ as a function of moderator temperature for two different values of moderating power per plutonium atom.

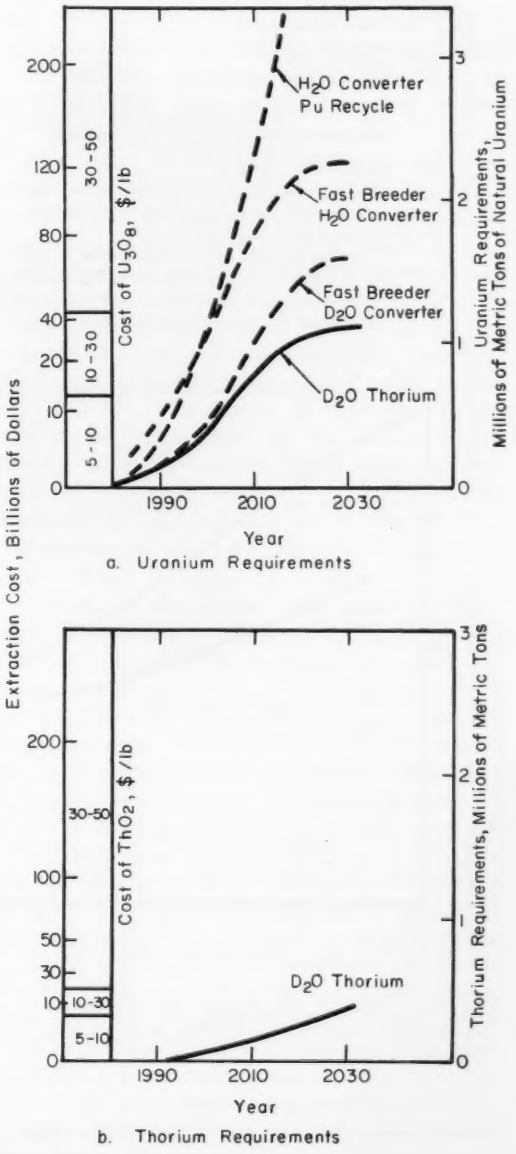

Fig. IX-6 Uranium and thorium requirements for the D_2O-moderated power reactors through 2030 A.D.[4]

Table IX-8 ESTIMATED FUEL-CYCLE COSTS FOR D_2O REACTORS[4]

	Current costs				Future costs		
Fuel	UO_2	Th	Th	Th	Th	Th	Th
Equivalent breeding ratio*		1.00	1.05	1.00	1.00	1.05	1.00
Uranium cost, $/kg of uranium	13	13	13	13	100	100	100
Thorium cost, $/kg of thorium		20	20	20	20	20	20
Exposure, 10^3 Mwd/metric ton	14	15	15	30	15	15	30
Costs, $/kg of fuel							
Fabrication	22	30	30	30	30	30	30
Shipping	2	5	5	5	5	5	5
Reprocessing		35	35	35	10	10	10
Burnup or credit	49	0	−3.6†	0	0	−27†	0
Subtotal, $/kg	73	70	66	70	45	18	45
Subtotal, mill/kw-hr†	0.81	0.74	0.70	0.37	0.48	0.19	0.24
Uranium inventory charge, mills/kw-hr‡,§	0.05	0.15	0.15	0.15	1.12	1.12	1.12
Thorium inventory charge, mill/kw-hr‡	0	0.05	0.05	0.05	0.05	0.05	0.05
Total, mills/kw-hr	0.86	0.94	0.90	0.57	1.65	1.36	1.41

*Includes allowance for reprocessing and refabrication losses; "equivalent breeding ratio" equals breeding ratio in reactor − 0.01.

†At net thermal efficiencies shown in Table IX-7.

‡At a charge rate of 10% per year; total inventory assumed 50% greater than reactor inventory.

§It is assumed that ^{233}U is worth only the cost of the natural uranium required to produce it and that 3 kg of ^{233}U can be obtained from 1 metric ton of mined uranium.

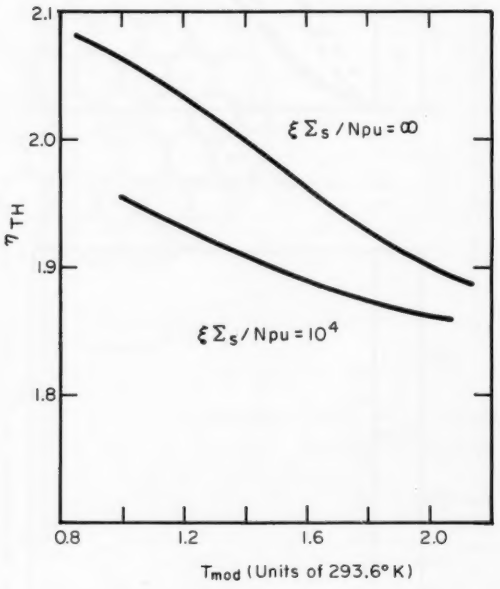

Fig. IX-7 Effect of moderator temperature on thermal average value of eta of ^{239}Pu (heavy-water moderator).[5]

Since moderator temperatures of the order of room temperature are indicated, the author concludes that the reactor should be a heterogeneous one of the pressure-tube type.

The limiting value of the attainable breeding ratio is given by

$$\bar{\eta}\epsilon - 1$$

where $\bar{\eta}$ is the number of neutrons produced per neutron absorbed in the fuel and ϵ is the fast fission factor, including $(n,2n)$ reactions. It is shown[5] that values of epsilon approaching 1.1 are necessary to obtain high conversion ratios in the plutonium-fueled thermal reactors and that these values are obtained only with close-packed large-diameter clusters of metallic (uranium-plutonium) fuel elements. The use of oxides reduces epsilon considerably. The use of large-diameter fuel clusters is reconciled with the usual heat-transfer requirement of large surface areas by conceiving the rod bundle as a cluster of at least 91 fuel rods, each having a diameter of about 0.4 in. Plutonium-bearing fuel elements were discussed in Sec. IV of *Power Reactor Technology*, 7(2), and although the uranium-plutonium type elements have not undergone extensive experimentation, the experience to date has been mixed.

The coolants considered in the study were D_2O, helium, and steam, and Table IX-9 summarizes the conversion ratios calculated to be attainable in these reactors. The choice of beryllium as a pressure-tube material has quite an effect on the attainable conversion

Table IX-9 ESTIMATES OF FINAL CONVERSION RATIOS IN URANIUM-PLUTONIUM HEAVY-WATER SYSTEMS[5]

(Beryllium Pressure Tubes, Zircaloy-2 Cladding)

Type	Initial conversion ratio	Operating conversion ratio	Final conversion ratio	Specific power, Mw/kg of plutonium (central channel)	Channel power, Mw(e)	Pumping power, % of channel electric power
D_2O coolant	1.0415	0.9784	0.9184	5.5	2.87	1.74
Steam coolant	1.0645	1.0014	0.9414	0.83	0.277	12.0
Helium coolant	1.0439	0.9808	0.9208	1.74	0.59	8.5

ratios, since they would decrease about 8% if Zircaloy-2 were employed. Beryllium cladding, in the case of the helium-cooled reactor, would increase the initial conversion ratio about 5% over the data shown in Table IX-9. If allowances were made for such items as leakage, extra parasitic absorption, and control requirements, the author concludes that reactors could be designed to yield conversion ratios of about 0.90.

Pressurized-Water Reactors: Chemical Shim

The use of soluble neutron absorber in the primary coolant system seems destined to play an increasing role in the control of reactivity in pressurized-water reactors. Although first used as an emergency shutdown measure to "back up" the control-rod system in water-moderated reactors, the soluble-absorber concept was extended, in the Yankee reactor design, to provide the normal cold shutdown margin. Because of a number of uncertainties about its behavior under conditions of power operation, dissolved absorber has up to now been restricted to use for shutdown in routine applications; it has, however, been used at full power during relatively short tests in the BORAX-II, BORAX-III, EBWR, and Yankee reactors. Also, it has been in use during several months of power operation in the Saxton reactor. The potential advantages for reactivity shimming by dissolved absorber under power are such that an extensive development effort has been directed toward that end. The application poses safety questions that have been investigated generally and in sample reactor designs. These questions will have to be answered specifically for any reactor intended for operation with dissolved absorber. It seems highly probable that this will be done and that reactivity control by dissolved absorber, otherwise known as chemical shim, will come into general use for pressurized-water reactors.

The main development effort on chemical shim has been made at the Westinghouse Atomic Power Department (WAPD), under AEC contract, as part of the AEC's Large Reactor Development Program. A survey paper on the subject was published in a recent issue of *Nucleonics*.[7] This, and a number of topical reports that have become available from the WAPD project, forms the basis for the review that follows. The review is restricted to the application and behavior of the chemical-shim system in the operating reactor, and it will not consider related plant-design questions, such as methods of fuel handling for a reactor that depends on dissolved absorber for shutdown.

The direct advantage of chemical shim is the reduction of the number and size of control rods required for the reactor installation. Although this effect is desirable in itself, the more important result is the improvement in spatial distribution of power (and hence in average power density in the core) that can be realized by minimizing the number and size of control rods in the core. The total improvement may be made up of several increments, but the main opportunity for improvement arises because a change in the concentration of dissolved absorber does not strongly affect the spatial power distribution, whereas a change in the number of control rods inserted, or in the depth of insertion of a bank of control rods, may influence the distribution profoundly. To realize the importance of this effect, one must consider the power distribution over the entire life of the core rather than at some particular instant in the life. In designing a control-rod installation, the designer can usually achieve a rather favorable power distribution for one particular condition of reactivity by utilizing

those control rods which must be in the core to flatten the distribution. Inevitably, however, the control rods must be moved as the reactivity changes (because of fuel burnup or other effects), and the power distribution then becomes less favorable. If, instead of control rods, dissolved absorber is used to compensate for reactivity changes, the initial flattening of the power distribution can be accomplished by spatial variations in fuel enrichment or by other permanently installed spatial variations of core composition. Since the concentration of dissolved absorber is changed during reactor operation to compensate reactivity changes, the effect on power distribution is relatively small because the change in concentration is distributed uniformly over the core volume, and the initial favorable power distribution is preserved reasonably well.

At the present time, at least, the complete replacement of control rods by dissolved absorber is not contemplated. The rapid-scram requirement cannot easily be met by a soluble absorber system. At this time it does not seem desirable to make rather frequent large changes in the dissolved absorber concentration, as would be necessary, for example, if it were used to compensate the reactivity changes associated with power changes. The optimum division of the control function between control rods and soluble absorber will no doubt vary from one reactor design to another. The question is discussed later in this review, but at this point, for purposes of orientation, the system described in Ref. 8 may be considered briefly. That system, which probably represents about the minimum use of control rods likely in the near future, incorporates rods for the dual purpose of covering the power defect and the power maneuvering requirements and of providing rapid power-reduction capability. The required reactivity capability of the rod installation for these purposes is estimated to be 4.4% k_{eff}. An installation of 24 cruciform rods in the 8-ft-diameter core is calculated to provide this strength with a stuck-rod margin of 1 rod; the total worth of the 24-rod installation is 6.6% k_{eff}. The installation in the core is illustrated in Fig. IX-8. The soluble absorber shown in the figure (2000 ppm boron) has a reactivity worth[9] of 14 to 15% k_{eff} at room temperature and a worth of 18 to 19% k_{eff} at 522°F.

In the following sections some of the specific characteristics and problems of the chemical-shim concept are discussed at greater length, under appropriate headings.

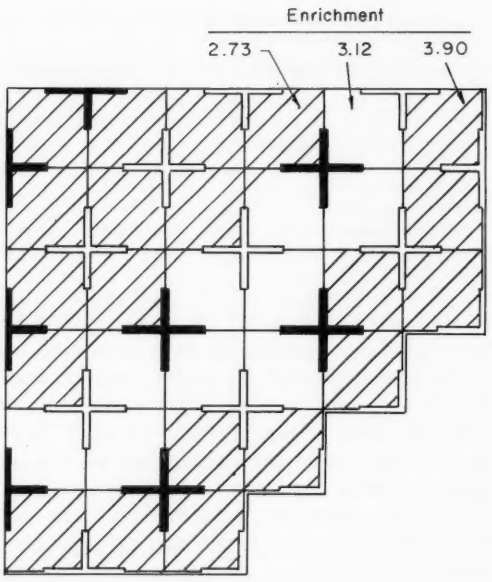

Fig. IX-8 Quarter-core diagram of control-rod installation in a reactor utilizing chemical shim.[8] The core, fueled with UO_2 clad in stainless steel, is intended for an output of 825 Mw(t). Its effective diameter is 98 in., and its height is 105 in. The equivalent H_2O/uranium volume ratio at room temperature is 3.34.

The solid cruciforms represent absorbing control rods, and the open cruciforms represent fueled "fixed followers," fueled with UO_2 of 2.73% enrichment. The absorbing control rods have a total worth of 6.6% in the hot reactor. The calculation is made for the case of 2000 ppm of dissolved boron in the water; under this condition k_{eff} for the hot, rodded core is 0.975.

Reactor Physics Effects

The most obvious question related to the reactor physics of chemical shim is how much dissolved absorber may be required to compensate a given excess reactivity. The major variables affecting this relation are the water/fuel ratio of the core, the fuel enrichment, and the reactor temperature. Calculations for three representative cores for large pressurized-water reactors are given in Ref. 9; the pertinent characteristics of these cores are summarized in Table IX-10. Figure IX-9 shows the calculated reactivity worth of the dissolved absorber (natural boron) as a function of the absorber con-

Table IX-10 CHARACTERISTICS OF PRESSURIZED-WATER REACTOR CORES USED IN ANALYSIS OF DISSOLVED-BORON REACTIVITY EFFECTS[9]

	Core 1	Core 2	Core 3
Water/UO_2 volume ratio (68°F)	1.7:1	1.7:1	1.4:1
Water/U* volume ratio (68°F)	3.4:1	3.4:1	2.9:1
^{235}U enrichment, wt.%†			
Inner	2.56	2.94	2.94
Middle	2.93	3.36	3.36
Outer	3.66	4.20	4.20
Average	3.05	3.50	3.50
Fuel-rod pitch, in.	0.553	0.553	0.554
Pellet diameter, in.	0.375	0.375	0.393
Cladding thickness, in.	0.015	0.015	0.015
Material volume fractions‡ (68°F)			
UO_2	0.33590	0.33590	0.36866
304 stainless steel	0.08612	0.08612	0.09138
H_2O	0.56412	0.56412	0.52325
Void	0.01386	0.01386	0.01671
Core height, ft	8.5	8.5	8.5
Core diameter, ft	8.1	8.1	8.1
Extrapolation distance, cm	7.5	7.5	7.5
Thickness of steel baffle around core, in.	0.6	0.6	0.6
H_2O reflector thickness, in.	4	4	4

*It is assumed that $\rho_{H_2O} = 1.0$ g/cm^3 and $\rho_U = 18.7$ g/cm^3.

†Each core has three radial zones of enrichment, of equal volumes. The enrichments in the inner, middle, and outer zones are in the ratios 7:8:10.

‡This includes structure and additional water associated with typical cores.

centration in the coolant-moderator. Curves are given for the three reactors of Table IX-10, at room temperature and at operating temperature.

The curves in Fig. IX-9 illustrate some effects besides the obvious relation between boron content and reactivity. It is clear, for example, that the effectiveness of the boron decreases slightly as the fuel enrichment is increased. This is to be expected because the more highly enriched fuel competes more favorably against the boron for the absorption of neutrons. A larger effect, however, is the effect of water/fuel ratio. The "wetter" core (No. 2) is affected considerably more than the "drier" core (No. 3) by a given concentration of boron in the water. The major part of this effect is due to the simple fact that a given concentration represents a greater total amount of boron in the wetter core.

Since the amount of boron in the core is proportional to the amount of water in the core (for a given boron concentration), it is clear that the thermal expansion of water which accompanies a rise in temperature will remove some boron from the core. This effect gives rise to a positive component of the temperature coefficient of reactivity in cores utilizing soluble absorber. The effect is apparent in Fig. IX-9, since the curves for 522°F lie well below the curves for 68°F. In reactor 3, for example, the reactivity effect of 2000 ppm of boron at 68°F is 15.8% k_{eff}, whereas the effect of the same concentration at 522°F is only 12.3% k_{eff}. The positive component of the coefficient increases with the concentration of dissolved absorber and places a limit on the amount of dissolved absorber that may be used without encountering a net positive temperature coefficient of reactivity. This limiting concentration of dissolved absorber depends on the reactor temperature, the enrichment, and the fuel/water ratio. However, the two latter variables do not affect strongly the positive-coefficient limit on the amount of reactivity that can be compensated by dissolved absorber. The latter point is illustrated by Fig. IX-10, which, for two different reactors, shows little difference in the value of "cumulative boron worth" at which the temperature coefficient of reactivity changes sign. The operating temperature, on the other

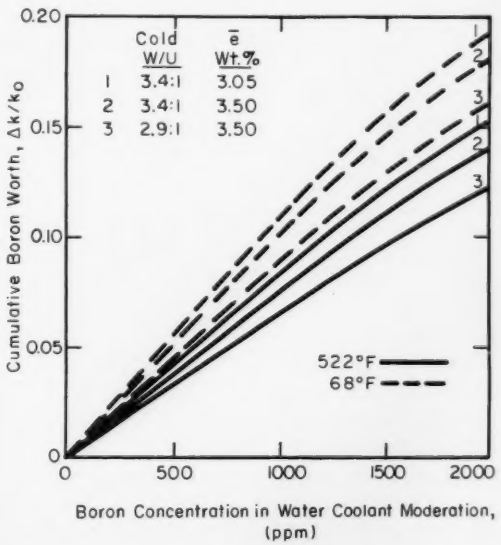

Fig. IX-9 Calculated reactivity worth of dissolved natural boron in three pressurized-water reactors.[9] The reactors are those described in Table IX-10.

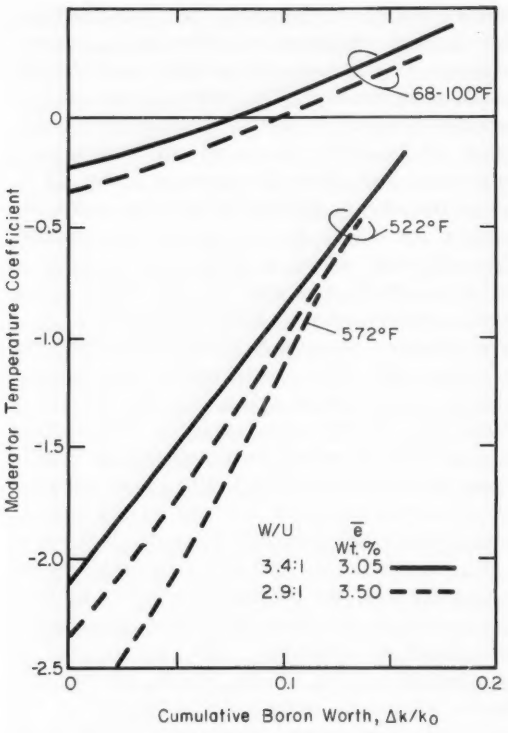

Fig. IX-10 Variation of moderator-temperature coefficient of reactivity with cumulative reactivity worth of dissolved boron in pressurized-water reactors.[9] The characteristics of the two reactors considered are given in Table IX-10.

Although the two reactors differ considerably in the reactivity effect of a given concentration of boron (see Fig. IX-9), their temperature coefficients of reactivity do not differ much if both have the same amount of reactivity compensated by dissolved boron.

hand, has a large effect. Figures IX-9 and IX-10 indicate that substantial reactivity compensation can be accomplished with soluble poison over a wide range of reactor-design variables without encountering the undesirable condition of a positive temperature (or void) coefficient of reactivity. The dissolved absorber will, however, reduce the value of the negative temperature coefficient as well as the temperature defect of reactivity from room temperature to operating temperature. These changes may affect the details of the reactor control system.

The degree of improvement in power distribution which can be achieved by the use of chemical shim depends on the specific reactor design and on the degree of design refinement which the designer is willing to invest in for the sake of a good power distribution. These considerations apply whether the reactor is controlled by chemical shim or by some competing reactivity-control method. As an example of the improvement achievable with chemical shim, Ref. 7 compares a rod-controlled case with an otherwise identical case in which chemical shim is used. The rod-controlled core is reported to have a maximum/average power-density ratio of 2.5, which is said to be 50% higher than the ratio for the chemical-shim case. This implies a maximum/average ratio of 1.67 for the latter. Even the ratio for the rod-controlled case is considerably lower than the design ratios attained in current practice. Apparently the ratios quoted are not intended to be the worst that might occur over the core lifetime but are simply comparative values for cases in which there are no partially inserted control rods—hence the quite low axial maximum/average ratios. The low ratios are also due partly to a radially zoned fuel loading, with fuel of three different enrichments, and apparently also to the assumption of fueled followers on the control rods which virtually eliminate the local power peaking in fuel elements adjacent to control-rod channels. Fueled followers for cruciform rods are not used in current design practice, but presumably they can be developed.

Pending the adoption of fueled control-rod followers or other methods of dealing with the power peaking introduced by water channels, it is interesting to see whether the chemical shim itself will reduce this local peaking effect because of the additional neutron absorption that it introduces in the water. It is indicated in Ref. 10 that there is a significant, but not large, improvement. Theoretical and experimental investigations of power peaking in fuel elements adjacent to representative water channels are reported in terms of a relative power-peaking factor.[10] This factor is the ratio of the local power density near a perturbation of the core composition (such as a water channel) to the power density that would exist at the same position if the composition were locally uniform. Typically, the relative peaking factor with 970 ppm of natural boron in the water was 97 to 98% of the factor when no boron was present (e.g., a peaking factor of 1.24 was reduced to 1.20 by the boron). Also investigated in the analysis was the effect of increased water

temperature on the peaking factor. In the no-boron case, the peaking factors at 543°F ranged from 94 to 96% of those at room temperature.

As previously mentioned, control rods are to be used in conjunction with chemical-shim control, and part of this complement of control rods will remain in the core during normal operation. If the rods are partially inserted from one end of the core, they will produce a significant distortion of the axial power distribution, even though the total inserted worth may be relatively small. Figure IX-11, from Ref. 11, is a very instructive diagram that illustrates the effects of partially inserted control-rod banks in large water-moderated cores, regardless of whether chemical shim is employed in addition to the control rods. When a control rod, or a control-rod bank, is partially inserted from one end of the core, it skews the axial power distribution, causing the position of maximum power density to shift from the center plane of the core to a position farther from the end at which the rods enter. This skewing affects the axial maximum/average ratio, and its severity is, of course, dependent on the reactivity worth of the partially inserted control-rod bank. The solid curves in Fig. IX-11 show the calculated axial maximum/average ratio as a function of the degree of withdrawal of the control-rod bank for rod banks of different total worths. Also shown are lines of constant inserted worth. These lines define the depth of insertion that must be used with the various control-rod banks to compensate for a specified amount of reactivity. The figure also shows lines of constant differential worth, i.e., the amount of reactivity change represented by a 1-in. change in rod-bank withdrawal. For a particular installation, the requirements of the control system may set lower limits on both the inserted worth and the differential worth of the partially inserted rod bank when it is at the position corresponding to normal reactor operation. Figure IX-11 would indicate that, if the differential worth requirement is the more important one, a more favorable power distribution can be obtained by employing a rod bank of relatively high total worth, whereas, if the inserted-worth requirement is the more important one, a more favorable power distribution may be obtained by use of a bank of relatively low total worth. It is understood, of course, that the designer has a good deal of flexibility in the selection of the worth of the partially inserted rod bank, regardless of the total worth of the complete control-rod installation; i.e., he can divide the total complement of control rods into a number of banks and withdraw one bank at a time in sequence. When this is done, the radial power distribution will also be affected if any one or more of the banks of rods is fully inserted under the condition of interest.

A further significant point brought out in Ref. 11 is that a very substantial difference may exist, in a large pressurized-water reactor, between the axial power distributions at full power and zero power. The major source of this difference is the Doppler effect in the oxide fuel, which causes a larger reactivity loss in the hotter fuel, i.e., in the fuel with the higher power density, and therefore tends to flatten the power distribution. Additional, but smaller, effects are present because of the slight variation in equilibrium xenon poisoning with power density and possibly because of the effect of the water temperature rise in traversing the coolant channels (the latter effect is not mentioned in Ref. 11). Shown in Fig. IX-12 are the calculated axial power distributions for the zero-power case and the full-power case. Because of the relatively long thermal time constant of the fuel elements, the changes in power distribution do not immediately follow the changes in fission power level.[11]

Control Requirements and Characteristics

The various requirements for control rods in a chemical-shim reactor, in which the adjustment of dissolved absorber is done relatively slowly, are discussed in Ref. 8. The estimated ranges for various requirements are given in Table IX-11, as well as the requirements for a "reference" core. This reference core, which was mentioned in a previous paragraph, has a rod installation that provides 4.4% reactivity worth plus a stuck-rod margin. The various items listed in Table IX-11 are defined below.

Hot-to-Power Reactivity Swing. This reactivity component is often referred to as the power defect of reactivity and is the amount of reactivity that must be added to raise the reactor power from the hot zero-power condition to full operating power. It is assumed that the power increase takes place over a period of time that is long relative to the thermal time constant of the fuel, but short relative to the xenon half-life. In the reactors considered here, the power defect is due almost entirely to the Doppler effect.

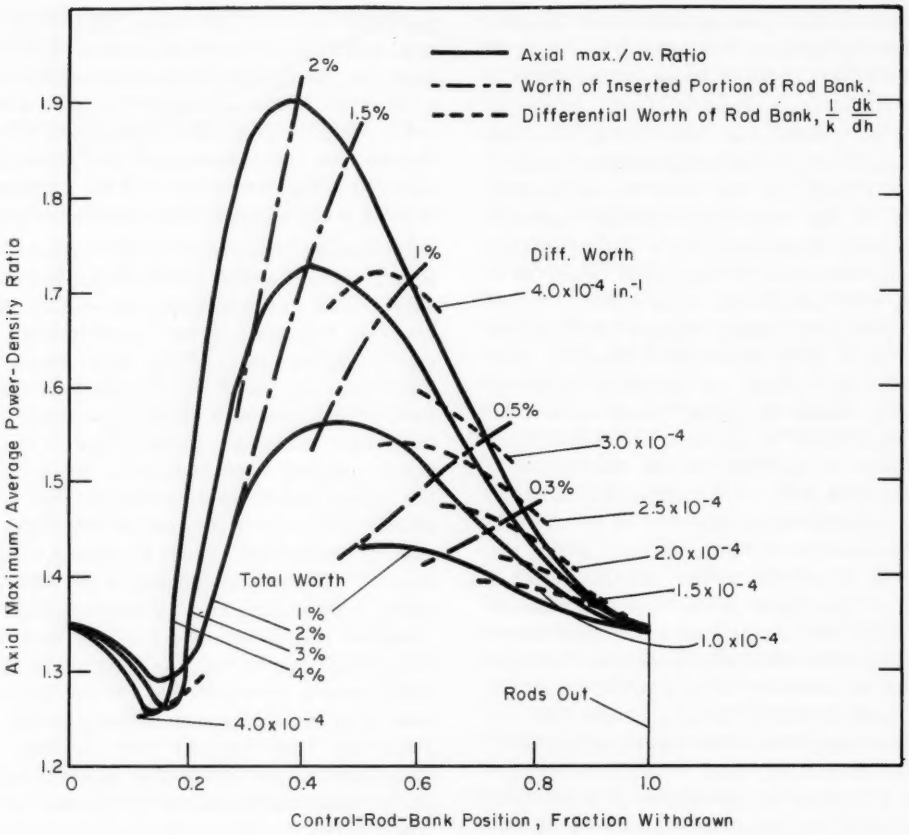

Fig. IX-11 Effect of reactivity worth and depth of insertion of control bank on axial maximum/average power-density ratio.[11] Four different rod banks are considered separately, each composed of unspecified numbers of control rods but worth 1, 2, 3, and 4% k_{eff}, respectively. Each solid curve shows the variation of the axial maximum/average ratio as one of the banks is withdrawn progressively from the core. When the bank is either fully inserted or fully withdrawn, it has a negligible effect on the ratio, which then has the value 1.35 for the particular reactor considered. When a bank is withdrawn only slightly, it decreases the maximum/average ratio slightly, for the beneficial effect of increasing the relative reactivity near one end of the core is more important than the accompanying adverse asymmetry effect. For larger degrees of withdrawal the asymmetry effect becomes large, and there is a strong concentration of power in the unrodded end of the core and a large increase in the maximum/average ratio. The effect increases greatly as the reactivity work of the partially inserted rod bank is increased.

The broken lines on the plot are loci of equal reactivity worth of the inserted portions of the partially inserted rod banks. The dashed lines are loci of equal differential worths of the partially inserted rod banks. The differential worth is the reactivity change produced by a 1-in. change in the position of the partially inserted bank.

The curves shown are qualitatively representative for any large reactor. The quantitative relations will vary greatly with individual core characteristics and especially with the length of the core as measured in neutron-migration lengths; the effects of partially inserted rods on peaking factors will increase as the core becomes longer.

The above curves were computed for a pressurized-water reactor with stainless-steel-clad UO_2 fuel rods, under full-power operation at a temperature of 543°F. The enrichment was 3.25 wt.% ^{235}U, the ratio of water to equivalent uranium metal was 3.4 at room temperature, and the active core length was 104.6 in. The thick axial reflectors were of water containing some structural material. The average power density corresponds to a total power of 825 Mw(t) from a core of about 8.1 ft diameter.

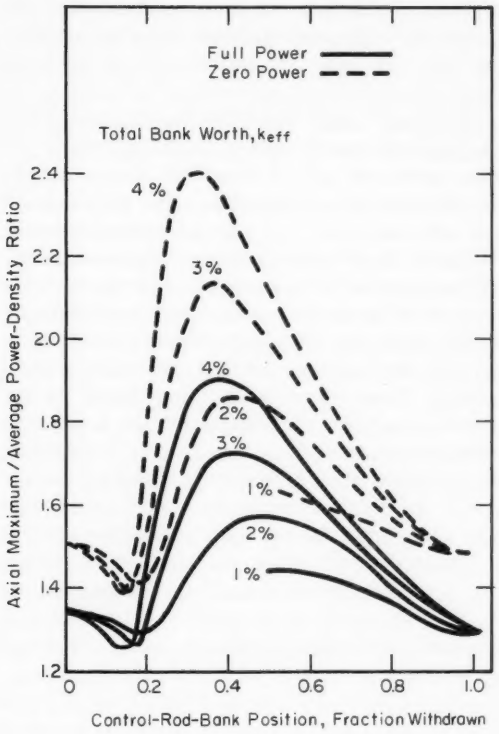

Fig. IX-12 Axial maximum/average power-density ratios as functions of partial rod-bank insertion, at full power and zero power.[11] The reactor considered is the same as that of Fig. IX-11, and the solid curves are the same as in Fig. IX-11. The dashed curves show the maximum/average ratios for the same reactor at zero power, with all other conditions the same.

Control-Rod "Bite." As illustrated in Fig. IX-11, the differential worth of a control rod or a control-rod bank is small unless the bank is inserted to some substantial depth in the reactor core. The control-rod bite refers to the amount of reactivity that must be compensated by the partially inserted rod bank in order that its differential worth may be great enough to cope with the expected rates of change of reactivity.

Control-Rod Dead Band. This item might be called, more appropriately, the chemical-shim dead band. It is the range of mismatch that is allowed between the nominal reactivity compensation by the chemical-shim system and the actual compensation. A dead band of 0.35% k_{eff}, in the reference reactor, corresponds to about 50 ppm of boron or a temperature change of approximately 15°F.

Void Content. The void content corresponds to a small amount of statistical boiling which might be allowed in the pressurized-water reactors. The reactivity change of 0.05% indicated for the reference core corresponds to about one-third of 1% of void in the core.

Concurrent Reactivity Insertion. This component of control-rod worth is provided to compensate any accidental reactivity insertion or combination of concurrent insertions that may be conceivable. The 0.8% reactivity estimated for this contingency in the reference core is considered to be made up of 0.4% due to the sudden opening of a loop containing an inadequate amount of boron, plus 0.4% due to the release of plated-out boron from the core.

Power Shaping. This adjustable reactivity component would be used for any shimming of the power distribution which might be done by means of control rods.

Variable Temperature Control. This adjustable reactivity component would be needed if it were desirable to increase the average coolant temperature as power level is increased.

Equilibrium Xenon. Unless the reactor is used strictly as a base-load plant, it is questionable whether it would be desirable to control the changes in xenon poisoning by chemical shim. If this were not done, control rods would have to be provided to control all or part of the equilibrium xenon and possibly some transient xenon.

Shutdown Margin. The shutdown margin considered in Table IX-11 includes only that amount of reactivity reduction which is required to reduce the power level at a sufficiently high rate in the event of scram — the stuck-rod margin is considered as a separate item, outside the scope of the table. In Ref. 8 it is pointed out that a shutdown margin, in addition to the reac-

Table IX-11 REACTIVITY CONTROL REQUIREMENTS FOR A CHEMICAL-SHIM CORE[8]

Control requirements	Δk, %	
	Approximate range	Reference core
Hot-to-power component	1.5 to 2.5	2.0
Control-rod bite	0.4 to 0.6	0.5
Control-rod dead band	0.3 to 0.4	0.35
Void content	0 to 0.1	0.05
Concurrent reactivity insertion	0.4 to 2.6	0.8
Power shaping	0 to 2.0	0
Variable temperature control	0 to 1.5	0
Equilibrium xenon	0 to 3.0	0
Shutdown margin	0 to 2.0	0
Total	2.6 to 14.7	3.7*

*The actual control-rod specification for the "reference" case was arrived at by increasing this value 20%, to a total of 4.4% Δk to account for uncertainties and assumptions in the analysis. These include loss in rod worth because of the change in core spectrum with lifetime, power redistribution during lifetime, depletion of poison material in the control rod, and possible error in rod-worth calculations.

tivity compensation corresponding to the power defect, may not be necessary because of the rather long thermal time constant of the oxide fuel elements. If we visualize the rapid scram, from full-power operation, of a number of control rods corresponding to the power defect, it is clear that momentarily the reactor will be subcritical by an amount nearly equal to the power defect. During the time (a few seconds) required for the fuel elements to cool down enough to make the reactor nearly critical again, the power will have decayed substantially.

In the specific case of the reference core described in Table IX-11, the situation during full-power operation would presumably be as follows. The control rods would normally be partially inserted, as a bank, to a depth such that the inserted worth of the bank is about 0.68% k_{eff}. This would correspond to the control-rod bite plus about half of the dead band. At this point (if the stuck-rod margin is ignored) the remaining worth of the bank, available on full insertion, would amount to about 3.02%, the hot-to-power component plus the components for concurrent reactivity insertion and void content plus about half the dead band. There would be no shutdown margin if the need for shutdown should occur at a time when a rod is stuck and the rods happen to be operating at the high-reactivity end of the dead band and concurrent reactivity insertions have occurred to use up all the 0.8% rod worth provided for that eventuality. From the power-distribution angle, it is important to note that, although a total rod worth of 4.4% is provided, only about 0.7% k_{eff} remains in the core under full-power operation (compare Fig. IX-11).

A study is reported in Ref. 12 on the effectiveness of control-rod scram in a chemical-shim reactor. The accidents considered were initiated by various accidental reactivity insertions by the control rods and by assumed breaks in the secondary steam line which would add reactivity by lowering the temperature of the primary circuit water. The power transients were terminated by the normal scram system, initiated either by overpower or low-pressure signals. The capability of the scram system was assumed to be a reactivity worth of 2.15%, inserted completely in 1.5 sec after initiation of the scram. This worth is stated to represent the conservative limit for the minimum absolute scram worth from full power, to be available at any time during core life. It is not clear from the reference whether the study is intended to be consistent, in detail, with the reference core of Table IX-11; but it would be consistent if the scram were assumed to occur when the control-rod bank is near the outer limit of the dead band.

The very large reduction in the moderator temperature coefficient of reactivity which results from the use of dissolved absorber represents a striking departure from the behavior that has characterized past pressurized-water reactors. In the past the strong temperature coefficient of reactivity, which produces a high degree of automatic load matching in pressurized-water systems, has been utilized to simplify certain features of the overall plant-control system. Some departures from these established practices will no doubt be necessary when chemical shim is used, and, in addition, the situation may be complicated by the rather large change in temperature coefficient that will occur over the core lifetime as the amount of dissolved absorber is changed. Although these considerations may dictate new approaches to plant control, it is unlikely that they will present feasibility problems. Some of these questions are considered in Ref. 12.

Water Chemistry

The work at WAPD has confirmed the choice of boric acid, arrived at earlier in investigations at the Argonne National Laboratory,[19] as the best available soluble absorber for chemical-shim use. References 13 to 19 cover various aspects of the behavior of boric acid solutions in the reactor environment and its effects on such important processes as corrosion and the deposition of corrosion products. These reports cover literature research, laboratory tests, and in-pile loop experiments. Much detailed information is included. Here the discussion will be limited to the most general results and the principles of operation of the chemical-shim system.

Operation with dissolved boric acid poses the following basic problem: to provide a means for varying the boric acid content in a controlled manner from a concentration of practically 0 to 1000 or so ppm and, at the same time, to maintain the rigid standards of *p*H control and purity (with respect to unwanted contaminants) which are normally sought in pressurized-water-reactor operation.

No report has been noted that gives detailed descriptions of methods for adjusting the con-

centration of boric acid in a chemical-shim application, but it is clear from Ref. 7 and from implications of the other references that the intention is to use the straightforward method of feed and bleed; i.e., the basic method is to increase the boron content by introducing into the reactor a more concentrated solution and to decrease the boron content by introducing pure water or a solution of lower concentration. Coolant must, of course, be bled from the reactor system to make room for the liquid added. This effluent may be discarded, in which case it adds to the waste-disposal load, or it may be processed by distillation, and the concentrate and/or distillate may be recycled to the reactor as needed for subsequent adjustments of concentration. As pointed out in Ref. 7, the latter method will probably prove more attractive in most cases.

With control of the boron content by the purely mechanical means of feed and bleed, it is feasible to maintain water purity with respect to unwanted contaminants in the normal way, by ion exchange, provided suitable resins are used which will not remove the boron. In this connection it must be noted also that the addition of alkali in the form of LiOH or KOH has been found beneficial for the reduction of corrosion-product deposition. The concentration used is low, of the order 10^{-4} M or about 2 ppm for LiOH. However, it is necessary to select ion-exchange resins that will preserve both the boron and alkali contents while removing other impurities.

An experimental program showed the effectiveness of the ion-exchange process in boric acid solutions, both with and without the presence of alkali.[15] For this experiment the alkali used was KOH, rather than LiOH, the favored additive for reactor use. The effectiveness of the ion-exchange process was evaluated for cesium, manganese, cobalt, and iodide ions to show that efficient ion exchange of either cation or halogen anion contaminants may be accomplished in boric acid solutions by the use of a mixed-bed resin in the potassium borate form (or in the hydrogen borate form if no alkali is used in the system). The resins used for the tests were Rohm & Haas nuclear grade ^{77}Xe cation-exchanger resin and ^{78}Xe anion-exchanger resin. The anion resin (^{78}Xe) was converted to the borate form by shaking with boric acid solution until an equilibrium boron concentration of 1000 ppm was obtained. When the potassium form of the cation resin (^{77}Xe) was desired, the conversion was made by shaking the resin with a solution containing KOH and 1000 ppm of boron. The indications are that the same general principles would be applicable when lithium hydroxide is used and that ion exchange will be effective for the removal of those impurities important in reactor operation.

Aside from the problems of maintaining water purity, pH, and boron content, the water chemistry problems that may be visualized in chemical-shim control have to do with corrosion, the behavior of corrosion products, and hideout of the boron. These questions are considered briefly below.

Corrosion. The corrosion tests to date have shown that there are no gross effects of the dissolved boron on corrosion rates and that most materials that are satisfactory in neutral or high-pH water at high temperature are also suitable for use in boric acid solution.[7] Out-of-pile tests have been made on core components and have shown no adverse effects. The corrosion problem is, of course, one which can be fully assessed only by observation over long periods of time. Long-term tests are now under way on typical materials of construction in out-of-pile loops, and the results of one such test are described in Ref. 20. The experiment consisted in exposing a number of nuclear reactor structural materials to a partially neutralized 600°F solution of boric acid for a period of nine months. The materials included a number of stainless steels, Inconel, Inconel X, a number of braze materials, Zircaloy-4, and nickel-plated silver-indium-cadmium. The results, in general, indicated that all but three of the materials behaved satisfactorily. Zirconium-beryllium braze on Zircaloy-4, nickel plate on silver-indium-cadmium, and thick layers of Nicrobraz 50 on type 304 stainless steel exhibited excessive corrosion, cracking, and/or pitting. Such long-term tests, and experience with reactor operation, will be necessary to show whether the presence of boric acid produces a significant effect on corrosion, but the evidence to date seems sufficient to eliminate the direct problem of corrosion as a feasibility problem.

Deposition of Corrosion Products. There are two possible adverse effects from the deposition of those corrosion products which do occur in any high-temperature water system. If they are deposited on the fuel elements, they may interfere with heat transfer or coolant flow, and, if they are deposited at points in the coolant system where access is important, they may add greatly to the troublesome radioactivity levels. Tests appear to indicate that the presence of boric acid does increase the deposition of corrosion products, but they have shown also that an increase of pH by the addition of alkali is effective in reducing both the release of corrosion products from their

point of formation and their deposition at other points. The indication to date is that, with suitable *p*H control, operation will be acceptable.

Hideout. In its broadest sense the term hideout of boron refers to the possible deposition of boron from solution onto solid surfaces in the coolant system or in deposits of corrosion products that are attached to surfaces. It is conceivable that the boron might subsequently reenter solution at some later time as a result of some change in water chemistry or operating conditions. Such uncontrolled behavior of the boron would, of course, be undesirable in any case since it would throw an uncertainty into the accounting of reactivity, which is important to reactor operation and safety. It would be particularly undesirable if the deposition occurred on the fuel plates or other parts of the reactor core structure, for a subsequent removal of such boron would then cause an increase of reactivity. The term hideout is sometimes used in a restricted sense to apply only to this latter possibility.

Tests and experience to date have indicated that boron does not deposit from solution onto clean surfaces, but there are indications that there may be a certain amount of deposition into corrosion products that may be adhering to surfaces. Out-of-pile investigations of such deposition are reported in Refs. 16 and 17, and both in- and ex-pile results are reported in Ref. 21. In the first investigation,[16] finely divided synthetic corrosion products were agitated in a high-temperature solution of boric acid containing 1000 ppm of boron, and the inclusion of the boron in the settled-corrosion-product sludge was measured. These tests indicated that the inclusion was of the order of 3 mg of boron per gram of synthetic corrosion product. In another portion of the program, the deposition of boron in a stable corrosion-product film was investigated, and in this case the deposition was only about 0.3 mg of boron per gram of corrosion product.

The experiments reported in Ref. 17 were made by a radiotracer technique that allowed the deposition of solute on selected surfaces to be followed continuously during the experiment. In this work it was necessary to utilize sodium as a stand-in for boron since there is no radioactive isotope of boron. The tests indicated that there was no deposition in the absence of boiling, although on fouled surfaces the deposition will occur when there is either subcooled or bulk boiling. However, there appeared to be a minimum thickness of fouling necessary to cause the deposition. This thickness was about 0.3 to 0.4 mil. When such deposition occurred, it appeared to be proportional to the rate of evaporation at the surface.

Reference 21 is a report on a study of the interaction of stainless-steel corrosion products with boric acid solutions at normal and elevated temperatures, utilizing both in- and ex-reactor experiments. The ex-reactor experiments substantiate the results given in Ref. 16, with boron absorptions ranging from about 1.5 to about 4 mg of boron per gram at 600°F, depending on the crud makeup and other experimental details. It is concluded, however, that the borate is not permanently incorporated in the crud, but can be desorbed, with the crud behaving as an amphoteric ion exchanger; i.e., in solutions of high alkalinity, little or no adsorption would occur, whereas, in acidic media, adsorption would occur to an extent determined by the borate-ion concentration and the solution *p*H. The in-pile capsule tests also indicated that reversible adsorption occurred. These latter tests indicated higher uptakes of boron compared to the ex-pile experiments, but this was believed to be due to boiling in the crud layer at the bottom of the capsule rather than as a specific result of a radiation-induced reaction. The point was not resolved, however, and further complications were noted in that the original magnetite crud had transformed to gamma ferric oxide under irradiation. No instances of rapid release of boron from a surface have been reported. In Ref. 8 the rapid release of boron from fuel plates is considered as a hypothetical means of reactivity insertion in estimating the required strength of the control-rod system for a chemical-shim reactor. In that study it is stated that the maximum amount of reactivity associated with plateout of boron would be limited to 1.2% k_{eff} by continuous evaluation of core reactivity and the initiation of remedial action if the 1.2% level is reached. It is considered inconceivable[8] that more than one-third of the deposited boron could leave the core rapidly.

Although the laboratory type tests may be useful and necessary, they are not as effective as actual reactor operation for establishing the feasibility and practicability of chemical-shim control with boric acid. For this reason, the results of operation of the Saxton reactor with chemical-shim control are of particular interest. This type of operation was begun in May 1963 and was scheduled to continue[22] through August 1964. Mention is made in Ref. 1 that the reactor has been operating for several months with a boron content of approximately 1000 ppm, both with and without nucleate boiling in the core. A test[23] of the predictability of the chemical-shim effect is shown in Fig. IX-13. The crucial factor in the test is the degree to which the theoretical predictions of control-rod position agree with those actually observed. As may be seen from the figure, the agreement is good, even after a reasonably long period of operation that involved a shutdown and a subsequent rise in power level to the point where a substantial fraction of the core area was involved in nucleate boiling. The difference between the predicted and observed control-rod position amounts, on the average, to 0.15% k_{eff}

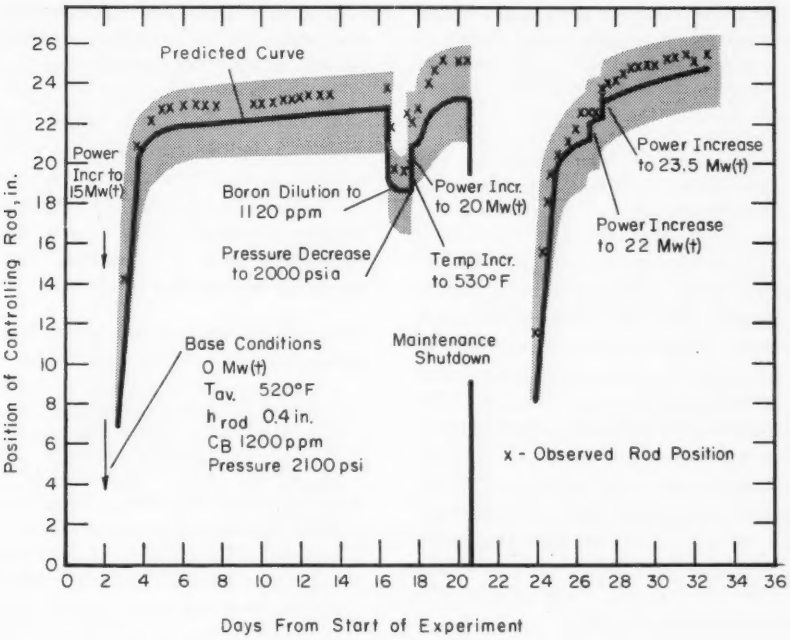

Fig. IX-13 Predicted and observed control-rod positions of the Saxton boron experiment.[23]

and is within the band of uncertainty of the calculations.

Pressurized-Water Reactors: Natural-Circulation Startup

As nuclear power becomes of age, it may be expected that refinements will be made to help reduce the capital cost of the reactor plant components. One possible refinement is discussed in Ref. 24. Although the main purpose of the reference is to describe a computer code for analyzing natural-circulation operation of a pressurized-water reactor, the reason behind the study is of more general interest and will be discussed briefly.

The startup of a power reactor usually requires operation of the primary coolant pumps, both to ensure flow through the reactor core and to help elevate the system temperature. If the pumps are of the constant-speed variety, both the coolant mass flow rate through the pumps and the pump power consumption are considerably higher at the cold, startup condition than at the high-temperature condition of normal reactor operation. One way to provide for this increased flow is to install pumps based on the capacity required during reactor startup. Unfortunately, if the primary coolant pump specified is a canned-motor pump, this solution is likely to be an expensive one for a large plant. The proposed Ravenswood Nuclear Generating Unit, for example, called for five canned-motor pumps with a design capacity of about 60,000 gal/min.[25] According to the estimates of the *Cost Evaluation Handbook,* each pump would have cost[26] approximately $500,000, and, since the cost of canned-motor pumps varies almost directly with capacity (see Fig. 321-1 of Ref. 26), the designer would be reluctant to base his pump specifications on the startup condition. Reference 24 suggests the following operating technique to avoid this penalty:

> ... A method has been proposed that permits optimum design for normal steady state operating conditions and prevents the overheating of the circulating pumps during initial cold conditions. In this method, pump operation is required only for the period of time necessary to bring the reactor power level to a heat production rate consistent with the safe plant heat-up rate. This rate is determined by the thermal stress limitations of the components within the reactor coolant system. The

power level is of the order of two percent of the reactor full power rating. Power to the pumps is then shut off and the plant heat-up is continued. As the pumps coast down, the forced circulation ceases and an adequate coolant flow is maintained by natural circulation. The operation of the pumps will be resumed when coolant temperatures (hence coolant densities) are such that continuous operation of the pumps is permissible.

The objective of the study, which required the development of the computer code, was to predict the system behavior during the proposed procedure. The code is presented in Ref. 24 and is applied to the startup problem of a large pressurized-water reactor. The particular problem studied gave results indicating the establishment of adequate coolant flow during plant heatup with natural circulation. This method of startup requires a spring-loaded check valve to ensure that the valve remains at least partially open when low flow exists in order to reduce flow resistance during natural-circulation cooling.

Pressurized-Water Reactors: The Large Power-Reactor Program

The objective of the Large Power Reactor (LPR) Program is to determine the potential of a seed-blanket reactor for application in a large central-station power plant [about 500 Mw(e)]. The research, engineering, and design work that is being conducted under the program has been described in a set of interim reports.[27–29] An earlier report on the economic potential of the seed-blanket reactor[30] gives a useful discussion of the general relation in the neutron-physics design of seed-blanket reactors. This report was reviewed in *Power Reactor Technology*, 4(3): 38-41.

Conceptual designs of large reactors utilizing several different fuel cycles have been developed,[27,28] all having the following major design features:

1. All use rod type oxide fuel elements, jacketed in Zircaloy-4 and of full core length.
2. The core is composed of a number of identical modules, each comprising a central seed, a surrounding blanket, and means for reactivity control.
3. Control of reactivity during operation is accomplished by relative motions of portions of the seeds, which vary the neutron leakage from the seeds.
4. The cores have small length/diameter ratios (ranging from 0.53 to 0.62) and are installed in spherical pressure vessels that are welded in the field. Core reloading does not require removal of the vessel head but is done through nozzles in the head. The nozzles also serve as entries for the control mechanisms.

The significance of the seed-blanket program has been summarized as follows:*

During the earlier phases of the LPR program, seed-blanket reactors using natural uranium in the blanket were studied. Nuclear calculations confirmed by critical experiments indicate that a uranium converter-burner core can be designed to produce over 65% of the total core energy from its natural uranium blanket. While the fuel cycle cost for such a core is about 10% higher than that for slightly enriched cores, its fuel utilization is about 20 to 40% better, as indicated in Table [IX-13].

While these results were promising, it became clear as the work progressed that large seed-blanket reactors using thorium fuel have high potential for (1) low power generation cost in a long-lived, thorium converter-burner design and (2) high fuel utilization in a converter-recycle design. For application in the near future, when the technology of thorium fuel reprocessing and remote fabrication of radioactive fuel has yet to be developed on a practical basis, the thorium seed-blanket converter-burner design is more attractive. This core provides a competitive power generation cost and better fuel utilization when compared to other water cooled reactors. Further, when the problems associated with recycling of irradiated fuel are solved on a practical basis, the thorium converter-recycle design appears capable of breeding.

Accordingly, a core design has been developed consisting of a thorium seed-blanket converter-burner core with a central region of breeder type fuel assemblies. Such a core would have about the same low fuel cycle cost as the converter-burner core, yet would be capable of demonstrating the breeding potential of the thorium converter-recycle design. This would make it possible to demonstrate breeding at an early date without having the power generation cost significantly dependent on the practicality of chemical reprocessing and remote fabrication of radioactive fuel elements.

*We are grateful to the Naval Reactors Branch of AEC's Division of Reactor Development for this summary.

Successful operation of a thorium seed-blanket reactor containing a central breeder region will constitute a major advance in reactor technology through the demonstration of breeding in the central region of the core. The thorium seed-blanket concept is the only known approach for extending fuel utilization of light-water reactors significantly beyond today's value of 1 to 2% of the potential energy in the mined ore. The thorium seed-blanket concept is expected to provide a means for ultimately making available for power production about half the energy in the fertile thorium fuel reserves.

A diagram of a core cross section for the uranium converter-burner design is shown in Fig. IX-14. Each of the 37 modules consists of a seed with stationary and moving parts for reactivity control, an annular blanket, and three outer blanket assemblies of chevron-shaped cross section. Each module contains also, on its axis, a round absorbing control rod for shutdown. In the pressure-vessel head, a port provided above each module is of sufficient diameter to pass the seed and annular blanket. The assembly, consisting of the seed, the shutdown rod, and the drive mechanism for the shutdown rod and the movable seed portions, is hung from a shoulder near the top of the fuel port and can be lifted out as a unit for refueling. The annular blanket is also hung from the port and can be lifted out separately. The chevron blanket sections are supported by the fixed bottom plate of the core. They can be removed individually through the fuel port after the removal of the annular blanket section. The arrangement of the core in the pressure vessel is indicated in Fig. IX-15.

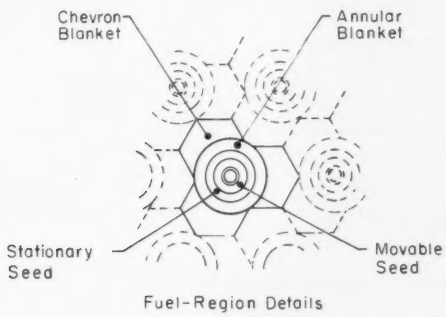

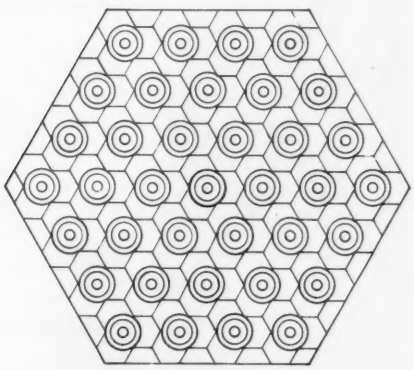

Fig. IX-14 Uranium converter-burner reactor concept.[28] Equivalent diameter = 15 ft.

The control of reactivity by "seed leakage" is to be accomplished by dividing the (nominal) seed into two coaxial parts, the inner of which is movable axially, and dividing each of the coaxial parts lengthwise into seed and blanket regions, as shown in Fig. IX-16. When the inner section is moved so that its seed portions are adjacent to the seed portions of the outer, fixed section, the fission neutrons produced in seed fuel will have the maximum probability of being absorbed in other seed fuel, i.e., the neutron leakage from the seed will be minimized, and the reactivity will be maximized. When the seed portions of the two blanket sections are mutually adjacent to blanket portions, the reactivity will be minimized. The range of reactivity adjustment available from seed movement is expected to be at least enough to compensate for fuel burnup, and hence it is expected that the parasitic loss of neutrons to absorbing control rods can be avoided.

Rod type fuel elements of full core length (8 ft) are contemplated for both the seed and blanket regions. The axial seed-blanket segmentation is to be obtained by appropriately segmented pellet loadings of the seed elements. The fuel-rod design is based on self-standing Zircaloy-4 cladding. The fuel rods are supported mechanically by a bottom grid assembly and by spring collars located at intervals along the rod length. The spring-collar design, illustrated in Fig. IX-17, is such that rubbing contact occurs only between the collars. The design of the collars is similar in principle (but different in detail) to that used successfully on a special assembly of blanket-rod elements (SABRE) which was tested in the Shippingport core. In the test assembly, the fuel rods were arranged in a square lattice to suit the basically square Shippingport geometry rather than in the tri-

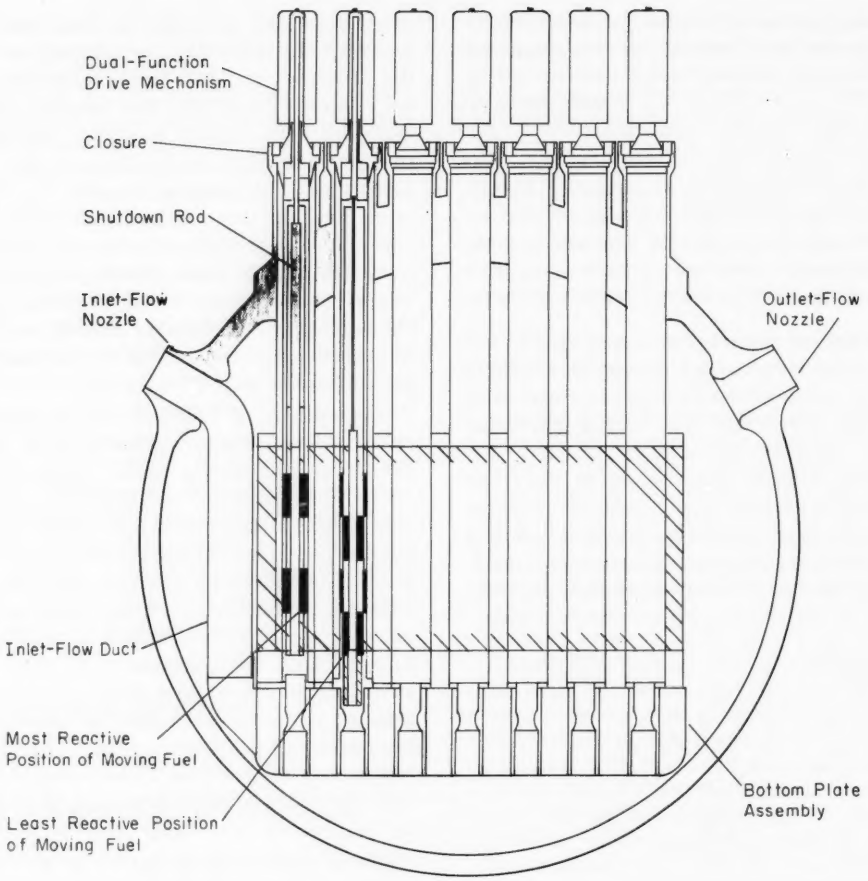

Fig. IX-15 Uranium converter-burner reactor concept (core and vessel elevation).[28]

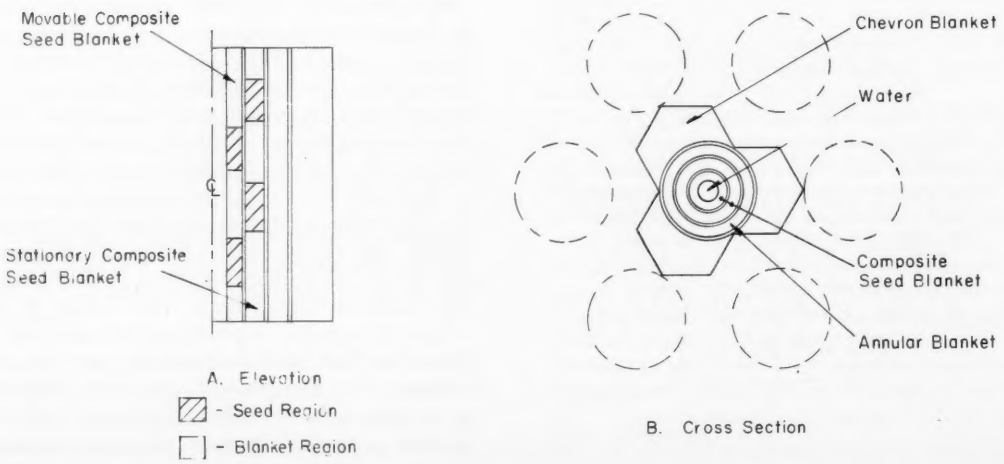

Fig. IX-16 Schematic of the uranium converter-burner unit cell.[28]

angular lattice that is contemplated for the large power reactor. The collar material is Inconel X. The seed rods in this particular LPR uranium converter-burner design are 0.25 in. in diameter. They are spaced 0.085 in. apart and are supported laterally at intervals of 12 to 20 in. The blanket rods are 0.50 in. in diameter. They are spaced 0.175 in. apart and are supported laterally at 24- to 36-in. intervals in the annular region and at 48-in. intervals in the chevron regions. The blanket fuel is natural UO_2, whereas the seed fuel is highly enriched UO_2 combined with a diluent, probably ZrO_2.

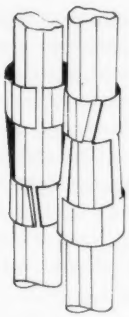

Fig. IX-17 Spring-collar fuel-rod spacers.[28]

A three-pass coolant flow is used: the coolant flows upward through the seed region, downward through the annular blanket, and finally upward through the chevron blanket sections. The flow boundaries are provided by the walls of the several regions in each individual fuel module.

It is proposed that the 24-ft-ID reactor pressure vessel be welded up in the field from the prefabricated sections illustrated in Fig. IX-18. The bottom section and the barrel-stave side sections are visualized as hot pressings, whereas the top section would be a forging or a welded assembly of smaller forgings. The inlet and outlet nozzles, which are designed with reinforcements both inside and outside the

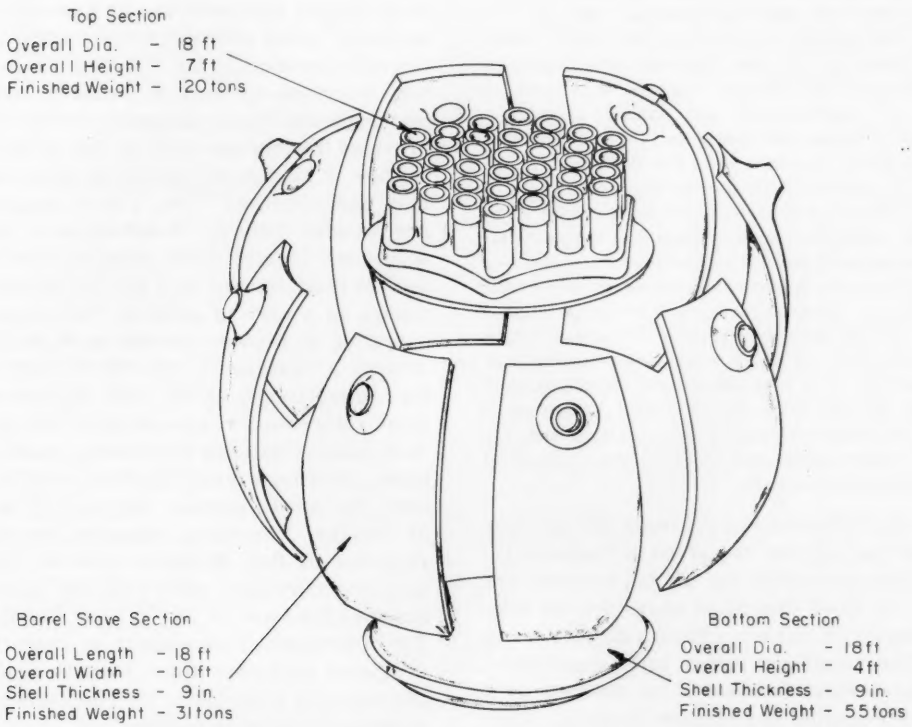
Top Section
Overall Dia. - 18 ft
Overall Height - 7 ft
Finished Weight - 120 tons
Barrel Stave Section
Overall Length - 18 ft
Overall Width - 10 ft
Shell Thickness - 9 in.
Finished Weight - 311 tons
Bottom Section
Overall Dia. - 18 ft
Overall Height - 4 ft
Shell Thickness - 9 in.
Finished Weight - 55 tons

Fig. IX-18 LPR reactor vessel concept.[28] Prefabricated sections are suitable for field erection. The finished vessel is 24 ft in inside diameter, overall height is 28 ft 4 in., and weight is 425 tons without internals and mounting skirt.

shell, would be forgings strength welded into the barrel-stave sections. It is expected that type A-302B steel would be used for the plate sections and type SA-306 for the forgings; the internal cladding would be weld-deposited stainless steel. Stress relieving in the field is visualized by the use of strip heaters or by utilizing a part of the reactor containment structure, lined temporarily with firebrick, as a furnace.

The pressure vessel is a rather impressive structure. The thinking behind this development has been summarized as follows:*

> Pressure vessels for large capacity reactors (greater than about 300 MWe) probably cannot be shipped by rail (regardless of whether spherical or cylindrical in shape) since the minimum clearance dimensions will likely exceed minimum railroad clearances (about 15 feet) even along selected routes. The LPR vessel has therefore been designed for field erection, so as to remove any restrictions on site location posed by pressure vessel shipment limitations. Further, recognizing the operational limitations that would be imposed on a cylindrical pressure vessel by neutron irradiation over a 30 year plant lifetime, the spherical shape was adopted to introduce a thick water shield (about four feet at core midplane) which reduces the lifetime fast neutron exposure to an nvt of 1.5×10^{17} neutrons/cm^2 and actually permits a decreased vessel wall thickness. The benefits from such a design are obvious. For example, (1) the resultant shift in NDT (nil ductility temperature) over 30 years of operation will be less than 50°F; (2) the spherical vessel concept has the potential for accommodating still higher power reactors — a 30 foot diameter spherical vessel would have a wall thickness of about 11 inches and would be suitable for a 1000 to 1500 MWe reactor in contrast with a cylindrical vessel which would have walls 14 to 16 inches thick for a 1000 MWe plant; (3) still another benefit derived from the spherical design as a result of minimum wall thickness is capability for rapid vessel heatup and cooldown rates compared with cylindrical vessels.

The characteristics of reactors that use four different fuel cycles are given in Table IX-12. The design principles for all the reactors are similar to those described above for the uranium converter-burner, although differences in qualitative detail and rather large quantitative differences enter because of the differences in fuel programming and blanket material. When thorium is used as the blanket fuel, the seed must initially produce nearly all the reactor power. Hence the ratio of seed volume to blanket volume must be much larger than when the blanket is composed of natural uranium. This characteristic is illustrated in Fig. IX-19, which is a diagram of the core cross section for the thorium converter-burner (compare Fig. IX-14).

The last two columns of Table IX-12 apply to recycle reactors that use very "dry" blankets. In these designs most of the bred fertile isotope remains at the end of blanket life (rather than being burned in place) and is extracted and recycled to the seed. The Bettis reports indicate that the use of the low hydrogen/fuel ratio in the blanket, coupled with the variable-geometry control method that does not introduce parasitic neutron-absorbing poisons into the core, favors very high conversion ratios.

Considerable attention has been given in the studies[27,28] to the analysis of the ^{233}U-thorium recycle case, and the conclusion is that breeding may be feasible on that cycle with the seed-blanket approach. In the past generalized analyses[31] have indicated that breeding is theoretically possible in the ^{233}U-thorium-H_2O system, provided the neutron losses to structural materials and fission products are kept low and provided the thermal-neutron flux on the fertile isotope is kept relatively low to minimize neutron absorption by ^{233}Pa. These requirements are usually difficult to satisfy in a practical solid-fuel reactor. The analysis reported in Ref. 28 indicates that they are not satisfied well enough in a core of uniform fuel composition, operating at a power density of 60 kw/liter, to achieve a conversion ratio above unity except for impractically short fuel exposures. The same reference contains analyses that show the seed-blanket reactor to perform considerably better, yielding average conversion ratios above unity for seed exposure lifetimes up to about 12 months. The more extensive investigation reported in Ref. 29 finds cases in which the average conversion ratio remains above unity for seed lifetimes as long as about 30,000 EFPH. The anticipated performance is characterized in a paper presented at the Third United Nations International Conference on The Peaceful Uses of Atomic Energy as follows:[32]

> ... The most meaningful way of describing a breeder performance appears to be by the fissile inventory ratio, i.e., the ratio of total fissile fuel

*Quoted from a summary by the Naval Reactors Branch of AEC's Division of Reactor Development.

in the core at any time to that at start of life. In a typical case with 2100 kg of ^{233}U in the seed the calculated core endurance is about 15,000 EFPH and the end-of-life value of the fuel inventory ratio exceeds 1.01. If reprocessing losses are about $\frac{1}{2}$ to 1%, this core would then be self-sustaining. As the seed fuel inventory is increased, the values of the fuel inventory ratio decreases slowly but endurance increases rapidly...

Some of the reasons for the higher conversion performance of the seed-blanket reactor are readily apparent. Thus, if the blanket is reprocessed at a relatively low value of fission depletion, high fission-product concentrations will occur only in the seed, where the fissile isotope is in a high enough concentration to compete favorably with them for neutrons. Moreover, the thermal-neutron flux may be kept low in the blanket, and the fast-fission effect may be accentuated, by employing a low coolant/fuel ratio there, since the power density in the blanket is low in any case. These observations imply some of the limitations that are imposed on other performance characteristics when very high conversion ratio is sought. The most important of these appears to be a low ratio of blanket power density to seed power density.

The preceding quotation is consistent with the concept of a "hold-its-own" or self-sustaining reactor — one which does not diminish the resource of fissile isotope, but which does not expand the resource significantly either. In an

Table IX-12 CORE CHARACTERISTICS FOR FOUR 500-Mw(e) SEED-BLANKET CONCEPTS[28]

	Uranium converter-burner	Thorium converter-burner	Uranium converter-recycle	Thorium converter-recycle
Reactor power, Mw(t)	1650	1720	1730	1750
Pressure, psia	2000	2000	2000	2000
Reactor inlet temperature, °F	537	515	515	515
Pressure at turbine throttle, psig	700	600	600	600
Pumping power, % of gross	3.3	4.4	5.3	6.2
Coolant flow rate, 10^6 lb/hr	70	120	95	120
Core				
Pressure drop, psi	80	50	135	100
Diameter, ft	15	15	13.7	13
Active height, ft	8	8	8	8
Average power density, kw/liter	42	42	50	56
Seed				
Volume % of core	10	30	24	40
Power density, kw/liter*	170	140	160	140
Moderator/water ratio	0.7	0.7	0.7	0.7
Fuel-rod diameter, in.	$\frac{1}{4}$	$\frac{1}{4}$	$\frac{1}{4}$	$\frac{1}{4}$
Fuel-rod spacing, in.	$\frac{3}{32}$	$\frac{3}{32}$	$\frac{3}{32}$	$\frac{3}{32}$
Equivalent full-length fuel rods	16,600	50,000	37,000	55,000
Fuel loading, kg of ^{235}U	1000	4500		
Seed lifetime, EFPH	10,000	70,000	10,000	7000
Average depletion, 10^{20} fissions/cm^3	7	22	7	4
No. of seeds/blanket	7	1	6	3
Peak depletion, 10^{20} fissions/cm^3	20	30		
Wt.% UO_2 in seed fuel	32	35		
Blanket				
Blanket fuel	UO_2	ThO_2	UO_2	ThO_2
Power density, kw/liter*	33	33	27	23
Hydrogen/fuel atom ratio	3.5	4.5	0.8	0.6 to 0.7
Water/UO_2 or ThO_2	1.5	1.75	0.35	0.25
Fuel-rod diameter, in.	$\frac{1}{2}$	$\frac{5}{8}$	$\frac{3}{4}$	$\frac{3}{4}$
Fuel-rod spacing, in.	$\frac{3}{16}$	$\frac{5}{16}$	$\frac{1}{32}$	$\frac{1}{32}$
Total No. of fuel rods	42,000	21,400	26,000	20,000
Fuel loading, metric tons	100	68	138	100
Blanket lifetime, EFPH	70,000	70,000	60,000	21,000
Average fuel depletion, Mwd/metric ton of fuel	30,000	36,500	10,000	2000
Average blanket power fraction (over blanket life), %	65	50	32	13

*At maximum power fraction.

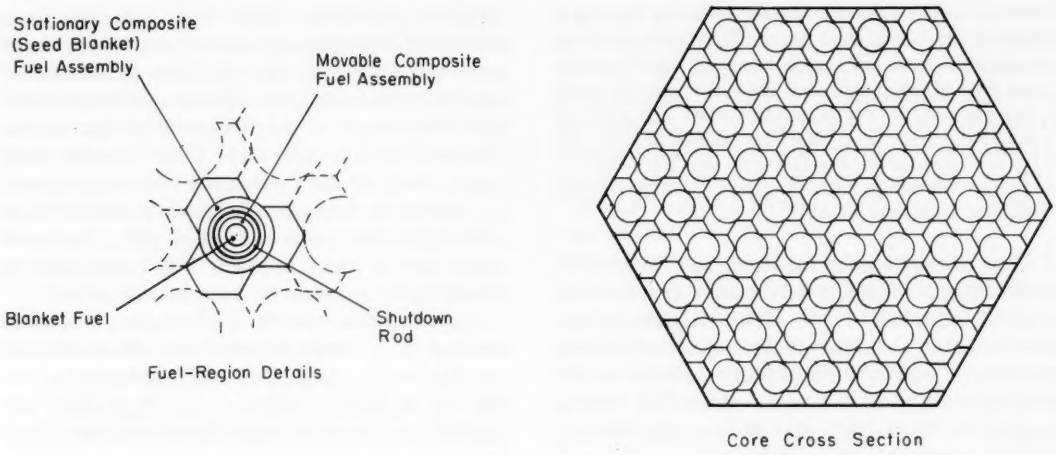

Fig. IX-19 Thorium converter-burner reactor concept.[28]

Table IX-13 COMPARATIVE PERFORMANCE OF WATER-COOLED CONVERTER-BURNER REACTORS[27]

	Potential energy from nuclear fuel mined,* %	^{235}U destroyed,† g/Mwd(t)	Fissionable Pu or ^{233}U remaining, g/Mwd(t)	Fissionable material‡ consumed, g/Mwd(t)	Uranium reprocessed to recover bred fuel, g/Mwd(t)	Natural-uranium input to diffusion plant, g/Mwd(t)	Fuel cost,§ mills/kw-hr
Uranium converter-burner cores							
Seed-blanket	1.4	0.59	0.15	0.44	21	100	2.3
Slightly enriched spectral shift	1.2	0.82	0.37	0.45	39	180	2.1
Slightly enriched poison control	0.9	0.88	0.28	0.60	40	200	2.1
Thorium converter-burner cores							
Seed-blanket	1.4	0.63	0.24	0.39	12	160	1.8

*Includes plutonium or ^{233}U credit.

†Grams per thermal megawatt-day of energy produced by reactor.

‡Assumes ^{235}U in tailings can be utilized; otherwise comparison would indicate the uranium seed-blanket core to be still more favorable.

§The costs given in this table are solely for the purpose of comparing the various reactor concepts on a consistent basis and should not be construed as actual fuel costs.

expanding nuclear power industry, the problem of supplying the inventory of fissile isotope for the increasing number of power reactors is an inherent part of the fuel-supply problem, the importance of which has been recognized in the general breeder-development effort by a strong emphasis on breeding gain and the attainment of short doubling times. Although a reactor which breeds even by a small margin is obviously better than a reactor with a low conversion ratio, opinion varies as to the unique significance of a hold-its-own reactor (of infinite or very long doubling time) in relation to the nuclear fuel supply problem. The question is too complex to be treated here, but some aspects of it have been explored in a previous review of nuclear fuel utilization in *Power Reactor Technology* [6(4): 1-39 (Fall 1963)].

The fuel-utilization characteristics of the nonrecycle seed-blanket reactors are also emphasized.[27,28] Table IX-13, from Ref. 27, gives a comparison with other pressurized-water types.

All entries in the table are self-explanatory except, perhaps, the first column. The number given is the amount of energy derived from unit quantity of virgin natural uranium, expressed as a percentage of the energy that would be available if all the uranium were consumed via conversion of ^{238}U to plutonium and subsequent fission. The total potentially available energy is taken as 915,000 Mwd/metric ton of natural uranium. In arriving at the numbers in the first column, credit is given for the fissile isotope discharged from the nonrecycle reactors by assuming it to be equivalent to ^{235}U.

In the case of the uranium converter-burner, the seed-blanket core shows a higher percentage energy extraction than the spectral-shift core (1.4% vs. 1.2%). Almost all the difference appears to be due to the smaller losses in the diffusion-plant tailings in the seed-blanket case (because much of the energy is produced in the natural-uranium blanket), since the specific net consumption of fissile isotope (fourth column of Table IX-13) is nearly the same in the two cases. In comparison to the conventional poison-control core, the seed-blanket core shows a considerable increase in the percentage energy extraction. This is due partly to the lower tails losses and partly to a lower specific net consumption of fissile isotope.

In a previous issue of *Power Reactor Technology*, the efficiency of fuel utilization has been considered in terms of the specific utilization, Υ, defined as the energy produced per net gram of fissile isotope made unavailable. This quantity may be derived for the several reactor types from Table IX-14, from Ref. 28. Not all

Table IX-14 CHARACTERISTICS OF VARIOUS WATER-COOLED REACTORS USED AS BASIS FOR FUEL-COST CALCULATIONS[28]

	Seed-blanket thorium burner	Seed-blanket uranium burner	Spectral-shift-controlled uranium burner	Poison-controlled uranium burner	Spectral-shift-controlled thorium converter
Nuclear design data obtained from	Bettis calculations	Bettis calculations	AEEW-R-174*	AEEW-R-174*	BAW-1241†
Nuclear constants calculated by	MUFT-KATE codes	MUFT-KATE codes	Adaptation of MUFT-KATE codes	Adaptation of MUFT-KATE codes	BPG code
Type of core cycle	Batch	Batch	Fuel shuffling	Fuel shuffling	Batch
Water/UO_2 volume ratio		1.5 (blanket)	2.0	2.0	
Cladding material	Zircaloy	Zircaloy	Zircaloy	Zircaloy	Zircaloy
Average fuel burnup, Mwd/metric ton of fuel	40,000 (blanket)	30,000 (blanket)	25,000	24,000	21,500
Initial enrichment, % ^{235}U in fuel	93/0	93/0.7	3.5	3.5	3.3
Final enrichment, % ^{235}U in fuel	78.9/0	90/0.7	1.51	1.43	1.61
Grams of ^{235}U consumed/Mwd	0.66	0.61	0.82	0.88	0.92
Grams of ^{239}Pu + ^{241}Pu or ^{233}U discharged/Mwd	0.24	0.14	0.37	0.28	0.65
Net grams of fissionable material destroyed/Mwd	0.42	0.47	0.45	0.60	0.27
Fuel-rod diameter, in.	0.250/0.625	0.250/0.500	0.400	0.400	0.436
Maximum linear heat rating, kw/ft	15.0	15.0	15.0	15.0	10.5
Overall power-peaking factor	3.7/2.4	3.7/4.2	1.9‡	3.0	1.57‡
Fuel residence time, days at 80% load factor	3650/3650	521/3650	883	1339	843
Total feet of fuel rod for 500-Mw(e) core	400,000 (seed) 171,000 (blanket)	133,000 (seed) 356,000 (blanket)	215,000	340,000	305,000
Kw-hr/core × 10^{10}	3.5	3.5	0.848	1.285	0.810

*D. Hicks, Light Water Lattice Calculations in the U.K., British Report AEEW-R-174, April 1962.

†Based on design and compositions of first core for potential plant given in the report by D. Mars, Spectral Shift Control Reactor Design and Economic Study, USAEC Report BAW-1241, Babcock & Wilcox Co., December 1961.

‡Assumes extensive fuel zoning (USAEC Report BAW-1241).

the reactors listed are identical to those represented in Table IX-13. The values of Υ and Υ_r (the specific utilization in the reactor, without regard to diffusion-plant losses) derived from Table IX-14 are given in Table IX-15.

It has been pointed out before [*Power Reactor Technology*, 6(4): 1-37] that in an expanding nuclear power industry the inventory requirements of the nuclear plants may be as important as the actual consumption of nuclear fuel. Estimating from the characteristics quoted in Refs. 27 and 28, and allowing for an ex-reactor inventory equal to 1.5 years of throughput, we can conclude that the seed-blanket uranium converter will require about 0.4 metric ton of natural uranium to supply the inventory for each thermal megawatt of installed capacity. This is about the same as the specific inventory requirement of conventional slightly enriched pressurized-water reactors. The requirement of the seed-blanket thorium converter-burner is considerably higher, amounting to about 0.66 metric ton of natural uranium per thermal megawatt. The very long seed life (10 years) of this reactor is purchased partly at the expense of a large loading of ^{235}U, which accounts for the rather high inventory requirement. The inventory component of the fuel cost (i.e., the use charge) has been computed for this reactor in Ref. 28 as 0.56 mill/kw-hr on the basis of the 4.75% per year "government-ownership" use-charge rate.

Although Refs. 27 and 28 are not intended to give a complete evaluation of the seed-blanket concept, they do indicate its areas of strength and weakness. In the areas of strength, there is the possibility of superior neutron-physics performance in comparison to other pressurized-water types and the possibility of greater operating convenience and higher plant availability. This is due to the very long life of the blanket, the relatively long life of the seed, and the ease of seed refueling. On the other hand, the concept results in a relatively low average power density in the core, apparently an inherent result of the necessity for producing a substantial fraction of the power in a small fraction of the core volume (i.e., in the seeds).

The use of highly enriched fuel in the seed is characteristic of the seed-blanket concept. Except for the fuel cost estimates reported in the references cited, it is difficult to evaluate the long-range economic implications of this feature, for it has not previously been used in

Table IX-15 SPECIFIC FUEL UTILIZATIONS COMPUTED FROM DATA OF TABLE IX-14

	Seed-blanket thorium burner	Seed-blanket uranium burner	Spectral-shift-controlled uranium burner	Poison-controlled uranium burner	Spectral-shift-controlled thorium converter
Grams of ^{235}U consumed/Mwd (total)	0.66	0.61	0.82	0.88	0.92
Grams of ^{235}U consumed/Mwd (from enriched fuel	0.66	0.44*	0.82	0.88	0.92
Grams of ^{235}U discarded/Mwd in diffusion plant tails† = $B[0.25/(0.72 - 0.25)]$	0.35	0.23	0.44	0.47	0.49
Grams of $^{239}Pu + ^{241}Pu$ or ^{233}U discharged/Mwd	0.24	0.14	0.37	0.28	0.65
Net grams of fissile isotope destroyed/Mwd = $A - D$	0.42	0.47	0.45	0.60	0.27
Specific utilization of fissile isotope in reactor, Υ_r, Mwd/net grams of fissile isotope destroyed (= $1/E$)	2.38	2.13	2.22	1.67	3.71
Net grams of fissile isotope made unavailable/Mwd (= $A + C - D$)	0.77	0.70‡	0.89	1.07	0.76
Specific utilization of fissile isotope in fuel cycle, Υ, Mwd/net grams of fissile isotope made unavailable (= $1/G$)	1.30	1.43‡	1.12	0.94	1.32

*Assuming an average of 65% of the energy produced in the blanket. The consumption of about 1.26 g of ^{235}U (by fission and neutron capture) yields 1.0 Mwd of energy. If 35% of the power is generated in the seed, the specific consumption of ^{235}U in the seed is $0.35 \times 1.26 = 0.44$ g/Mwd of total core power.

†Assuming tails enrichment of 0.25% ^{235}U.

‡Neglecting the discard of any ^{235}U that may be left in the discharged blanket.

commercial reactors, and consequently there is no generally available body of cost information.

At this stage of development, the recognition of these advantages and limitations of the concept cannot serve as an evaluation, but only as an indication of the probable directions of further development.

References

1. R. G. McGrath (Ed.), Carolinas Virginia Tube Reactor. Large Plant Study, USAEC Report CVNA-184, Westinghouse Electric Corp., Atomic Power Division, June 1963.
2. Combustion Engineering, Inc., Nuclear Division, Organic Cooled, Heavy Water Moderated Reactor Power Plant Conceptual Design and Evaluation, Volume I, Evaluation of the Concept, and Volume II, Reference Plant Design, USAEC Report CEND-175, Vols. I and II of two, March 1963.
3. R. J. Rickert, Fuel Cycle Economics of Large D_2O Moderated, Organic Cooled Power Reactors, *Combustion*, 35(10): 20 (April 1964).
4. D. F. Babcock, R. R. Hood, and D. S. St. John (Comps.), Thorium-Fueled D_2O-Moderated Power Reactors, USAEC Report DP-864, Savannah River Laboratory, December 1963.
5. S. G. Sharma, Plutonium-Fueled Thermal Reactors with High Conversion Ratios (thesis), USAEC Report BNL-7355, Brookhaven National Laboratory, March 1963.
6. D. F. Babcock, R. R. Hood, L. Isakoff, J. C. Jensen, D. S. St. John, and J. W. Wade, An Evaluation of Heavy-Water-Moderated Power Reactors, Status Report as of March 1963, USAEC Report DP-830, Savannah River Laboratory, June 1963.
7. P. Cohen and H. W. Graves, Jr., Chemical Shim Control for Power Reactors, *Nucleonics*, 22(5): 75-82 (May 1964).
8. D. L. Miller, Control Rod Requirements in a Chemical Shim Core, USAEC Report WCAP-3727, Westinghouse Electric Corp., Atomic Power Division, August 1963.
9. P. G. Lacey, Reactivity Dependence upon Moderator Temperature and Boron Concentration in Large PWR Cores Controlled by Chemical Shim, USAEC Report WCAP-3720, Westinghouse Electric Corp., Atomic Power Division, November 1962.
10. P. G. Lacey, Fine Structure Power Peaking in a Critical Experiment Mockup of a Chemical Shim Core, USAEC Report WCAP-3723, Westinghouse Electric Corp., Atomic Power Division, March 1963.
11. H. Aisu, R. F. Barry, and P. G. Lacey, Load Variation Restrictions in a Chemically Poisoned Large PWR Core, USAEC Report WCAP-3724, Westinghouse Electric Corp., Atomic Power Division, March 1963.
12. J. S. Moore and B. H. Axelson, Reactor Control and Protection System Study for Chemical Shim Operation of a Large Closed Cycle Water Reactor, USAEC Report WCAP-3714, Westinghouse Electric Corp., Atomic Power Division, October 1962.
13. D. E. Byrnes and W. E. Foster, Literature Values for Selected Chemical/Physical Properties of Aqueous Boric Acid Solutions, USAEC Report WCAP-1570, Westinghouse Electric Corp., Atomic Power Division, January 1961.
14. D. E. Byrnes, Some Physicochemical Studies of Boric Acid Solutions at High Temperatures, USAEC Report WCAP-3713, Westinghouse Electric Corp., Atomic Power Division, September 1962.
15. W. D. Fletcher, Ion Exchange in Boric Acid Solutions with Radioactive Decay, USAEC Report WCAP-3716, Westinghouse Electric Corp., Atomic Power Division, November 1962.
16. W. D. Fletcher, A. Krieg, and P. Cohen, The Behavior of Austenitic Stainless Steel Corrosion Products in High Temperature Boric Acid Solutions, USAEC Report WCAP-1689, Westinghouse Electric Corp., Atomic Power Division, December 1960, Revised May 1961.
17. L. F. Picone, D. D. Whyte, and G. R. Taylor, Radiotracer Studies of Hideout at High Temperature and Pressure, USAEC Report WCAP-3731(Rev.), Westinghouse Electric Corp., Atomic Power Division, June 1963.
18. L. F. Picone, The In-Pile Test of Chemical Shim, USAEC Report WCAP-3729, Westinghouse Electric Corp., Atomic Power Division, June 1963.
19. C. R. Breden and A. Abers, Corrosion and Stability Tests on Chemical Poisons in High-Temperature Water, USAEC Report ANL-5147 (Rev.), Argonne National Laboratory, Sept. 1, 1953.
20. D. D. Whyte, A Long Term Corrosion Test of Reactor Structural Materials in a Chemical Shim Solution, USAEC Report WCAP-3737, Westinghouse Electric Corp., Atomic Power Division, March 1964.
21. W. D. Fletcher, Interactions Between Stainless Steel Corrosion Products and Boric Acid Solutions, USAEC Report WCAP-3730, Westinghouse Electric Corp., Atomic Power Division, March 1964.
22. D. R. Rees and E. U. Powell, Saxton Tests Lead Toward Better Water Reactors, *Nucl. Eng.*, 21(11): 72-77 (November 1963).
23. S. Bartnoff, J. Weisman, A. J. Impink, W. H. Layman, and D. E. Hetrick, The Saxton Experiment on Chemical Shim Control, *Trans. Am. Nucl. Soc.*, 6(2): 305-306 (November 1963).
24. A. N. Nahavandi, B. H. Axelson, G. B. Killinger, and A. H. Killinger, A Digital Computer Analysis of Closed Cycle Water Nuclear Power Plant Start-Up Using Natural Circulation (THERMO-

SYPHON Code), Vols. I and II, USAEC Report WCAP-3722, Westinghouse Electric Corp., Atomic Power Division, February 1962.

25. Westinghouse Electric Corp. and Stone & Webster Engineering Corp., Consolidated Edison Company of New York, Inc. Ravenswood Nuclear Generating Unit A, Preliminary Hazards Summary Report, Vol. I, USAEC Docket No. 50-204, Exhibit A.
26. U. S. Atomic Energy Commission, *Nuclear Power Plants Cost Evaluation Handbook*, Vol. 3, Mar. 15, 1962.
27. Westinghouse Electric Corp., Large Power Reactor Program Interim Report, USAEC Report WAPD-LPR-141, Bettis Atomic Power Laboratory, July 1963.
28. Westinghouse Electric Corp., Large Power Reactor Program Interim Report Supplement, The Design of Seed-Blanket Cores, USAEC Report WAPD-LPR-154, Bettis Atomic Power Laboratory, July 1963.
29. Westinghouse Electric Corp., Report on Large Power Reactor (LPR) Program, USAEC Report WAPD-LPR-181, Bettis Atomic Power Laboratory, December 1963.
30. F. Schwoerer, Economic Potential of the Seed-Blanket Reactor, USAEC Report WAPD-237, Westinghouse Electric Corp., Bettis Atomic Power Laboratory, December 1960.
31. J. Chernick and S. O. Moore, Breeding Potential of Thermal Reactors, *Nucl. Sci. Eng.*, 6(6): 537 (December 1959).
32. A. Radkowsky, G. W. Harding, and R. G. Luce, Seed and Blanket Reactors, Paper A/Conf 28/P/208, presented at the Third United Nations International Conference on the Peaceful Uses of Atomic Energy, Geneva, September 1964.

Index

Power Reactor Technology

Volume 7

Note: The page range for each of the four issues of Vol. 7 is as follows: No. 1, pages 1 to 106; No. 2, pages 107 to 200; No. 3, pages 201 to 327; and No. 4, pages 329 to 432.

A

Absorbers, iodine removal by, 58
Accidents, fission-product release, environmental hazards, 370-1
  maximum credible, for New Production Reactor, 267
Algae, control in fuel-transfer canal at Consolidated Edison Thorium Reactor, 313
Aluminum, reactivity effects in ZPR-III assembly, 11
Aluminum alloys (Al-Pu), spike enrichment element for Plutonium Recycle Test Reactor, 169, 181
Aluminum oxide systems (Al_2O_3-B_4C), irradiation testing, 367
Aluminum systems (Al-Al_2O_3)
  See Sintered aluminum powder
Ammonia, synthesis using reactor heat, economics, 1-3
Annealing, postirradiation, of boron-containing stainless steels, 366-7
Atmosphere, fission-product dispersal after accidental release, 370
Autocorrelation function, reactor noise analysis studies, 249-50

B

Baffles, stagnant heavy-water design for thermal insulators, 401
Barium-140, deposition from gas stream onto surfaces, temperature effects, 371
  emission from irradiated uranium dioxide, 361
  release during uranium fire, 370-1
Belleville-spring washers
  See Washers
BEPO reactor
  See Reactors (BEPO)
Beryllium, reactivity effects in ZPR-III assembly, 11
Beryllium oxide, reactivity effects in ZPR-III assembly, 11
  subcritical assemblies of, hafnium control studies, 10-11
Bibliographies, neutron thermalization, 331
Big Rock Point Power Reactor
  See Reactors (Big Rock Point Power)
Bismuth alloys (Bi-Pb) (liquid), expansion, reactivity effects in fast reactors, 122
Bismuth alloys (Bi-Pu), preparation and testing, 182
Blankets
  See Breeding blankets
Boiling burnout, correlations, comparison of Russian and U. S. data, 223-35
  limits for reactors, 14-26
  in multirod geometries, 154-65
  in steam-water mixtures, 335-52
Boiling Nuclear Superheater Reactor
  See Reactors (BONUS)
Boiling-water reactors
  See Reactors (boiling-water)
Bonding, gas-pressure, tubular fuel elements, 237-8
  uranium dioxide-fueled rods, 238-41
BONUS Reactor
  See Reactors (BONUS)
BORAX-II Reactor
  See Reactors (BORAX-II)
BORAX-III Reactor
  See Reactors (BORAX-III)
BORAX-V Reactor
  See Reactors (BORAX-V)
Boric acid, chemical-shim use in pressurized-water reactors, 411-21
  shielding-solution use in ML-1 Reactor, 219
Boron, burnable-poison use, in experimental fuel assemblies, 34-5
  in fuel elements, 356-8
  control-rod use, 365-8
  cross-section change with burnup in reactors, 216-18
  dissolution in coolant for control of pressurized-water reactors, 411-21
Boron carbide, burnable-poison use in fuel elements, 358
  control-rod use, 367-8
  in Experimental Gas-Cooled Reactor, 376-7, 378
  corrosion, 367-8
Boron carbide (Zircaloy-2-clad), irradiation testing, 368
Boron carbide systems (Al_2O_3-B_4C), irradiation testing, 367
Boron carbide systems (B_4C-Cu), corrosion testing, 367
Boron carbide systems (B_4C-SiC), corrosion, 367-8
Boron carbide systems (B_4C-SiC) (Zircaloy-2-clad), irradiation testing, 368
Boron carbide systems (B_4C–stainless steel), corrosion testing, 367
Boron carbide systems (B_4C–steel), corrosion testing, 367
Boron carbide systems (B_4C–Zircaloy-2), irradiation testing, 367
Brazing, heat exchanger for Molten-Salt Reactor Experiment, 374-5
Breeder reactors
  See Reactors (breeder)
Breeding blankets, lifetime estimation for Shippingport core 2, 200
  management, 128
  power contributions during operation of Shippingport core 1, 195
  Shippingport core 2 design, 197-8
Breeding potential, fissile isotopes in various reactors, 113
Breeding ratios, effects of structural materials in fast reactors, 131-3
  fast reactors with metal, oxide, and carbide cores, 114-17
  plutonium-uranium heavy-water systems, 411
British Experimental Pile O
  See Reactors (BEPO)
Bromine, release during uranium fire, 370-1
Buckling, determination for heavy-water lattices, 212-14
  measurement in substitution critical experiments, 4-5
Buildings, Big Rock Point comparison with Humboldt Bay plant, 78-9
  BONUS Reactor containment, 308
  containment at low pressures, 54-5
  New Production Reactor, 267
  Pathfinder Reactor containment, 290
  reinforced concrete, stress analysis, 54-5
Burnout, comparison of Russian with U. S. data, 223-35
  DNB-2 curve significance, 335-43
  limits for boiling-water reactors, 14-26
  multirod geometry studies, 154-65
  in nonuniformly heated channels, 343-52
  rod-bundle geometry studies, 226-7
  test device, 15
  tubular geometry studies, 227-34
Burnup
  See also Core life
  fuel assemblies, in Fuel-Cycle Program, 28-31
  in High-Power-Density Development Project, 38-39, 42, 44
  fuel-element studies for Shippingport core 2, 197, 199-200
Butterfly valves
  See Valves

C

Cadmium, cross-section change with burnup in reactors, 216-18
Cadmium alloys (Ag-Cd-In), cross-section change with burnup in reactors, 216-18

Cadmium alloys (Cd-Eu), burnable-poison use studies, 217
Canada, comparison with United States in heavy-water reactor development, 87-95
Canals
  See Fuel-transfer canals
CANDU Reactor (Canada)
  See Reactors (CANDU) (Canada)
Carolinas-Virginia Tube Reactor
  See Reactors (Carolinas-Virginia Tube)
Cerium-141, deposition from gas stream onto surfaces, temperature effects, 371
Cerium-144, emission from irradiated uranium dioxide, 361
  release during uranium fire, 370-1
Cerium alloys (Ce-Co-Pu) (liquid), properties, 182-3
Cermets, plutonium-containing, fabrication and testing, 183
Cesium-137, evolution from irradiated uranium dioxide, 360-2
  release during uranium fire, 370-1
Circuits (electric)
  See Electric circuits
Chromium, neutron-physics effects in fast reactors, 128-33
Cladding
  See also specific cladding materials, e.g., Stainless steels (304) and Zircaloy-2
  boron incorporation for burnable-poison use, 357-8
  failure, effects of uranium dioxide core melting, 46-8
  fuel assemblies, testing in VBWR, 27-34
  sintered aluminum powder use, for fuel elements, 242
    in organic-cooled heavy-water-moderated reactor design, 95, 405
    in WR-1 reactor, 324-5
  stainless steel, failure on fuel elements in Vallecitos Boiling-Water Reactor tests, 354-5
  Zircaloy-2 system with stainless-steel inner lining, 356
  Zircaloy-2 use for boron carbide systems, 368
  Zircaloy-4 use for Shippingport core 2 fuel elements, 197
Coal, gasification by reactor heat, economics, 1-3
Cobalt alloys (Ce-Co-Pu) (liquid), properties, 182-3
Cobalt alloys (Co-Pu), preparation and testing, 182
Cobalt alloys (Co-Pu) (liquid), properties, 182-3
Coke, iodine removal by, 58
Compaction, explosive, of tubular fuel elements, 237-8
  vibratory, annular multitube fuel elements, 241-2
  uranium dioxide fuel rods, 238-41
Components, 60-9, 269-75, 372-5
  See also specific components, e.g., Pumps, Steam generators, and Valves
  of fuel assemblies, functional description, 38, 43
  fuel-handling equipment, 68
  of transducers, limitations on use in reactors, 52-3
Computer programs, AIM-5, graphite-moderated critical assembly studies, 9
  BICEP, graphite-moderated critical assembly studies, 9
  BPG, diffusion-equation coefficient studies for Spectral Shift Control Reactor, 212
  CINDER, time-dependent fission-product concentration studies, 215-16
  fission-product deposition from gas streams, 371
  FORM, graphite-moderated critical-assembly studies, 9
  GAM-I, critical configurations studies, 6
  MUFT-KATE, nuclear constant calculations for seed-blanket reactors, 429
  PDQ-4, perturbation analysis for Spectral Shift Control Reactor, 212
  period-meter output studies during reactor startup transients, 51
  radiation-effects studies of transducer materials, 53
  reactor noise analysis, 248
  REPAD, Doppler effects on neutron absorption resonance, 329-30
  STEWPOT, graphite-moderated critical assembly studies, 10
  TEMPEST, critical configurations studies, 6, 9
  THERMO-SYPHON, pressurized-water reactor natural-circulation studies, 421-2
  THERMOS, heavy-water lattice studies, 7
  TKO, perturbation analysis for Spectral Shift Control Reactor, 212
  TYCHE, fission-neutron age studies, 331
Condensers, BONUS Reactor, 307
  comparison of Big Rock Point with Humboldt Bay plant, 79-81
  Pathfinder Reactor, 289-90
Conferences, fuel management, 201
  Tripartite Organic-Cooled Heavy-Water Reactor Meeting, 324
Construction practices, 70-84, 276-312
Containers, stainless-steel, criticality measurements of uranium and plutonium solutions, 5-6
Containment, 265-7, 370-1
  BONUS Reactor, 307-9
  comparison of Big Rock Point with Humboldt Bay plant, 79
  large heavy-water pressure-tube reactor, 404
  leak studies with concrete buildings, 54-5
  New Production Reactor, vented-containment concept, 265-7
  Pathfinder Reactor, 290-1
Contamination, environmental, from uranium fire, 370-1
  fossil-fired superheaters, 314
  turbines in superheater reactors, 310
Control-rod drives, 272-5
  Big Rock Point Reactor, 82
  electrical switch problems in Consolidated Edison Thorium Reactor, 314
  Heavy-Water Components Test Reactor, problems of, 316-17
  Pathfinder Power Reactor, 274-5
Control rods, BONUS Reactor, 301-3, 306
  boron use, review of, 365-8
  Experimental Gas-Cooled Reactor, design, 376-7, 378
  flexibility for travel in bowed channels, 376-7, 378
  hafnium, studies in BeO subcritical assemblies, 10-11
  hydraulic actuator, 271-4
  materials for, cross-section vs. burnup data, 216-18
  Pathfinder Reactor, 282-4, 288
  pressure-balanced type for Experimental Organic-Cooled Reactor, 274
  requirements in reactors using chemical shim in primary coolant, 415-18
  shim assemblies for Plutonium Recycle Test Reactor, 390
  Shippingport Reactor, neutron-exposure effects, 195-6
  Sodium Reactor Experiment, drop-time studies, 377, 379
  withdrawal program for large multiregion reactor, 331-2
Control systems, 51-3, 248-63
  augmentation in boiling-water reactors by boron steel poison slabs, 207
  chemical shim in primary coolant of pressurized-water reactors, 411-21
  comparison of Big Rock Point with Humboldt Bay plant, 81-3
  Consolidated Edison Thorium Reactor operating experience, 314
  moderator-level control, 385-99
  noise-analysis studies, 248-63
Converter reactors
  See Reactors (converter)
Coolants
  See also specific coolants, e.g., Sodium (liquid) and Water
  expansion, reactivity effects in fast reactors, 118-22
  flow-rate measurement in Plutonium Recycle Test Reactor, 383
  quality control, in reactors using dissolved chemical shim, 418-21
  in Shippingport plant, 196
Cooling systems, comparison of Big Rock Point with Humboldt Bay design, 70-3, 76-9
  Consolidated Edison Thorium Reactor, purification problems, 314
  design variables, effects on burnout in boiling-water reactors, 15
  organic-cooled heavy-water-moderated reactor, 96
  pressure control in Pathfinder Reactor, 288
  recirculation-piping design for Pathfinder Reactor, 384
Copper, mesh, iodine removal by, 58
Copper systems (B_4C-Cu), corrosion testing, 367
Core design, BONUS Reactor, 303-6
  comparison of Big Rock Point with Humboldt Bay plant, 73-6
  evaluation of Zircaloy use in N. S. *Savannah* Reactor, 322-4
  fast-breeder reactor for water desalinization, 138-9
  NPD Reactor, 391
  Pathfinder Reactor, 284-8
  Plutonium Recycle Test Reactor, 387
  seed-blanket reactor, 423-4, 427-8
  thermionic water-cooled reactor, 103
Core life
  See also Burnup
  extension in boiling-water reactors by control augmentation techniques, 207
  plutonium-uranium mixtures in water-moderated reactors, 203-5
Corrosion, alumina–boron carbide pellets, 367
  boron carbide, 368
  boron carbide–copper couples, 367
  boron carbide–stainless-steel couples, 367
  boron carbide–steel couples, 367
  control in reactors using boric acid shim in primary coolant, 419-20
  fuel assemblies tested in VBWR, 29-30, 38, 40, 354-5
  stainless-steel fuel-element cladding in VBWR tests, 354-5
  welds on Shippingport control-rod assemblies, 196
Corrosion products, buildup in coolant pumps of Plutonium Recycle Test Reactor, 315-16
  deposition in reactors using chemical shim in primary coolant, 419-20
Cracking, fuel assemblies tested in VBWR, 38, 40
  spot welds in boron-containing stainless steels, 366
  stainless-steel fuel-element cladding in VBWR tests, 354-5
Critical assemblies, beryllium oxide-moderated types, 10-11
  fast-neutron types, 11-12, 211-12
  graphite-moderated type, 8-10, 209-10
  heavy-water type, 7-8, 209, 213-14

Critical assemblies (Continued)
light-water-moderated types, effects of variation of ^{240}Pu concentration, 207-8
noise analysis, 252
solution type, 5-6
zirconium hydride types, 211
Critical assemblies (Peach Bottom), thorium resonance-capture studies, 10
Critical assemblies (ZPR-III), comparison of experimental parameters with calculations, 211-12
reactivity-worth determination for various materials, 11
Critical assemblies (ZPR-VII), uniform lattice experiments, 7-8
Critical experiments, 4-13
BORAX-V reactor, 206
Critical mass, fast reactors, 114-16, 131-3
Criticality, plutonium-solution studies, 5-6
^{235}U aqueous solutions, 6
uranyl fluoride solutions, 6
Croloy alloy, evaluation for gas-heated steam-generator construction, 65
Cross sections, data for zirconium, 331
fission products, calculations of change with time, 215-16
neutron, Doppler effects in reactors, 329-30
neutron absorption, for gold, 10
for thorium, 10
neutron capture, in fast reactors, 111-12
for materials in fast reactors, 128-33
for reactor poison materials, 216-18
neutron fission, in fast reactors, 111-12
$^{16}O(n,p)^{16}N$ reaction, measurement, 220

D

D-ring seals, for helium retention in Plutonium Recycle Test Reactor, 381-3
Damping oils, radiation effects on use in reactor instruments, 52-3
Demineralizers, comparison of Big Rock Point with Humboldt Bay plant, 79-81
Density, plutonium carbide–uranium carbide fuel materials, 180
uranium dioxide, changes during melting, 362-3
uranium dioxide fuel elements, effects on exposure lifetime in Shippingport core 2, 199
Departure from nucleate boiling
See also Burnout
burnout-limit studies, 18-26
DNB-2 curve significance, 335-43
Desalinization, economic aspects, 138-44
heavy-water reactor cost studies, 87
Design practices, 70-84, 276-312, 376-84
Dielectrics, radiation effects on use in reactor instruments, 52-3
Diffusion coefficients, fission products in uranium dioxide plates, 362
Diffusion length, thermal neutrons in water, 146-8
Diffusion parameters, thermal neutrons, in graphite, 151-2
in heavy water, 151
in water, 148-50
DNB
See Departure from nucleate boiling
Dome seals
See Seals
Doppler effect, effect on neutron-absorption resonance in SPERT reactor, 329
reactivity effects in fast reactors, 122-4
Dose (radiation)
See Radiation dose
Douglas Point Station
See Reactors (CANDU)
Dounreay Fast-Breeder Reactor
See Reactors (Dounreay Fast-Breeder)
Drive mechanisms
See Control-rod drives
Dry wells, Humboldt Bay Reactor containment-system design, 79
Dual-purpose plants, electricity generation and water desalinization, 87, 142-4
Ductility, boron-containing stainless steel, 365-6
Shippingport pressure vessel, fast-neutron effects, 193
Dump valves
See Valves
Dysprosium, cross-section change with burnup in reactors, 216-18

E

Economics, 1-3, 138-44
CANDU Reactor, fuel management, 202-4
canned-motor pump costs, 421
dual-purpose electric power and water desalinization plants, 142-4
electrical revenue effects on cost of water desalinization by reactors, 144
fuel cycles for heavy-water–thorium breeder reactors, 410
heavy-water reactors, review of recent developments, 86-7, 89, 96
large heavy-water pressure-tube reactor, 403
large organic-cooled heavy-water-moderated reactor, 405, 408
Lithium-Cooled Reactor Experiment auxiliary systems, 384
organic-cooled heavy-water-moderated reactor, 408
pressurized-water reactors with natural circulation, 421-2
seed-blanket reactor designs, 429
SENN Reactor, effects of partial reloading scheme, 202
solid-fuel gasification, 1-3
water desalinization, 138-44
Zircaloy use in core structure of N.S. *Savannah* Reactor, 322-4
Eggs, expected contamination from released fission products, 370-1
Electric circuits, period meters, 51-2
servomechanisms, 53
switches, problems in control-rod drive of Consolidated Edison Thorium Reactor, 314
Electrical insulation
See Insulation (electrical)
Electromagnetic pumps
See Pumps
Electron-beam welding, fuel-element components, 358-9
Enrico Fermi Fast-Breeder Reactor
See Reactors (Enrico Fermi Fast-Breeder)
Equipment, for fuel handling, 68
Erbium, cross-section change with burnup in reactors, 216-18
Erbium systems (Er-Eu), burnable-poison use studies, 217
Erbium systems (Er-Gd), burnable-poison use studies, 217
Europium, cross-section change with burnup in reactors, 216-18
Europium systems (Cd-Eu), burnable-poison use studies, 217
Europium systems (Er-Eu), burnable-poison use studies, 217
Europium systems (Eu-Gd), burnable-poison use studies, 217
Experimental Breeder Reactor II
See Reactors (Experimental Breeder, II)
Experimental Organic-Cooled Reactor
See Reactors (Experimental Organic-Cooled)
Explosive compaction, tubular fuel elements, 237-8
Exponential experiments, 4-13
Extrusion, tandem, stainless-steel-to-Zircaloy transition-joint preparation, 368-9

F

Fabrication
See also specific processes, e.g., Bonding, Extrusion, and Swaging
fuel assemblies for boiling-water reactors, 27-42
novel methods for fuel elements, 237-46
Feedwater systems, BONUS Reactor, 307
comparison of Big Rock Point with Humboldt Bay plant, 79-81
Pathfinder Reactor, 289-90
Fermi Fast-Breeder Reactor
See Reactors (Enrico Fermi Fast-Breeder)
Ferrule seals, for helium retention in Plutonium Recycle Test Reactor, 381-3
Filters, 55, 58
for fuel-transfer canal at Consolidated Edison Thorium Reactor, 313
Fires, uranium, fission-product dispersal, 370-1
Fission gases
See also specific isotopes, e.g., Iodine-131 and Xenon-133
pressure determination in uranium dioxide-filled fuel rods, 43-5
release, by irradiated plutonium carbide–uranium carbide fuel materials, 181
by irradiated plutonium oxide–uranium oxide systems, 178
Fission products
See also specific isotopes, e.g., Cesium-137 and Strontium-90
containment in New Production Reactor accident, 266-7
deposition from gas stream onto surfaces, temperature effects, 371
effects on breeding ratio in fast reactors, 116
environmental hazards, 370
evolution from irradiated uranium dioxide, 359-62
time-dependent concentration calculations, 215-16
turbine contamination problems in superheater reactors, 310
Flowmeters, damped signals for, using surge suppressors in Plutonium Recycle Test Reactor, 383
Fluid flow, 14-26, 154-65, 335-52
axial- vs. cross-flow in steam generator design, 65
rate measurement in flow channels of Plutonium Recycle Test Reactor, 383
Fluoride ion, effects on Zircaloy-2 corrosion, 356
Foils, ^{197}Au, resonance capture studies, 10
cadmium-covered gold, flux-traverse measurements in heavy-water lattices, 7
^{55}Mn, resonance-capture measurements, 10
^{232}Th, resonance-capture measurements, 10
vanadium, resonance-capture measurements, 10
Food, expected contamination from released fission products, 370-1
French reactors
See Reactors (Rapsodie) (France)
Fretting corrosion, Zircaloy-clad fuel rods in VBWR tests, 29-30
Fuel assemblies, Big Rock Point Power Reactor, variations of basic design, 37
BONUS Reactor boiler, 296-8
BONUS Reactor superheater, 298-301
comparison of Big Rock Point with Humboldt Bay design, 73-6

Fuel assemblies (Continued)
components, functional description of, 38, 43
design for boiling-water reactors, 27-38
fabrication for testing in VBWR, 27-38
geometric effects on burnout, 23-6, 154-65
irradiation testing in VBWR, 27-38
large heavy-water pressure-tube reactor, 401-2
Pathfinder Reactor boiler, 279-80
Pathfinder Reactor superheater, 279, 281-2
uranium dioxide-fueled, fabrication and testing, 27-50
Fuel-Cycle Program, 27-34
fuel-element cladding tests in VBWR, 354-5
fuel-element fabrication for irradiation testing in VBWR, 356, 357
Fuel cycles, 201-5
CANDU Reactor, 202-4
costs, for Canadian and U. S. heavy-water reactors, 89, 97
for heavy-water–thorium breeder system, 410
fast reactors, 124-6
plutonium, review of developments, 167-83
plutonium-uranium mixture in water-moderated reactors, 203-5
seed-blanket reactor designs, 429
SENN Reactor, 202
Fuel elements, 27-50, 167-83, 237-46, 354-63
See also Fuel assemblies
aluminum-plutonium, plutonium-content determination from reactivity coefficients, 208
annular multitube type, novel fabrication techniques, 241-2
boron-containing types, 356-8
containers, evaluation of Zircaloy use in N.S. *Savannah* Reactor, 322-4
design problems for superheater reactors, 310
Experimental Boiling-Water Reactor, plutonium-bearing type, 172
fabrication by novel methods, 237-46
handling equipment, 68
internal pressure, contributions of fission-product helium, 455-6
organic-cooled heavy-water-moderated reactor, 408
Pathfinder Reactor, end-closure fabrication, 245-6
plutonium-bearing, review of development, 167-83
Plutonium Recycle Test Reactor, 167-73
Rapsodie Reactor, 167-9
rejuvenation without reprocessing, 172-3
rods, design for heavy-water reactors, 93
rods fueled with uranium dioxide, novel fabrication techniques, 238-41
Shippingport core 2 design, 197-8
stainless-steel-cladding failure in Vallecitos Boiling-Water Reactor irradiations, 354-5
thermionic water-cooled reactor, 102, 103-4
tubular, design for heavy-water reactors, 94
tubular, novel consolidation and bonding methods, 237-8
uranium dioxide, core-melting effects on cladding failure, 46-8
Zircaloy-2-clad, stainless-steel-lined types, 356
Fuel-transfer canals, Consolidated Edison Thorium Reactor, water clarity and leakage problems, 313
Fuels
See also specific fuel materials, e.g., Plutonium oxide (PuO_2) and Uranium oxide (UO_2)
cost bases used in CANDU Reactor design, 202
costs for seed-blanket reactor designs, 429
expansion, reactivity effects in fast reactors, 118
management studies, 201-5
plutonium-bearing, review of developments, 167-83

G

Gadolinium, cross-section change with burnup in reactors, 216-18
Gadolinium systems (Er-Gd), burnable-poison use studies, 217
Gadolinium systems (Eu-Gd), burnable-poison use studies, 217
Gas, pipeline, economics of synthesis using reactor heat, 1-3
Gasification, solid fuels by reactor heat, economics, 1-3
General Electric Test Reactor
See Reactors (General Electric Test)
Geometrical configurations, effects on burnout in multirod fuel assemblies, 23-6, 154-65
rod-bundle burnout correlations, 226-7
shielding studies, 220
tubular burnout correlations, 227-34
Gold, absorption cross section, 10
foils, use in flux-traverse measurements in heavy-water lattices, 7
Gold-197, foils, resonance-capture studies, 10
Gold alloys (Au-Ni), brazing alloy use in heat exchanger for Molten-Salt Reactor Experiment, 375
Graphite, neutron-diffusion parameters in, 151-2

H

Hafnium, control-rod studies in BeO subcritical assemblies, 10-11
cross-section change with burnup in reactors, 216-18
Halden Boiling-Water Reactor
See Reactors (Halden Boiling-Water)
Hazards
See Safety
Heat exchangers, Molten-Salt Reactor Experiment, design and fabrication, 374-5
U-tube type, for heavy-water reactors, 90-92
Heat transfer, 14-26, 154-65, 223-35, 335-52
burnout, in multirod geometries, 154-65
in steam-water mixtures, 335-52
burnout correlations, comparison of Russian and U. S. data, 223-35
burnout limits for boiling-water reactors, 14-26
comparison of Big Rock Point with Humboldt Bay plant, 76
data for large heavy-water pressure-tube reactor, 402
fuel assemblies for boiling-water reactors, 31, 36, 39-40, 42, 44
nonuniformity in heated channels, effects on burnout, 343-52
Heavy water
See Water (D_2O)
Heavy-Water Components Test Reactor
See Reactors (Heavy-Water Components Test)
Heavy-Water Lattice Project, 7
Heavy-water reactors
See Reactors (heavy-water)
Helium, content in fuel-element voids from ternary fission of ^{235}U, 455-6
seals for, in Plutonium Recycle Test Reactor, 381-3
Helium system, NPD Reactor, 392
"Hideout," boron in chemical-shim control of pressurized-water reactors, 420
High-Performance UO_2 Program, 38-50
High-Power-Density Development Project, 34-44
fabrication-process studies, 243-4
High-Temperature Gas-Cooled Reactor Experiment
See Reactors (ZENITH)
Holmium, cross-section change with burnup in reactors, 216-18
HPD
See High-Power-Density Development Project
HPP
See High-Performance UO_2 Program
Humboldt Bay Power Reactor
See Reactors (Humboldt Bay Power)
Humidity, effects on control-rod-drive switch in Consolidated Edison Thorium Reactor, 314
Hydrostatic pressing, tubular fuel elements, 237-8

I

Impact strength
See Ductility
Implosive consolidation, tubular fuel elements, 237-8
Indium, cross-section change with burnup in reactors, 216-18
Indium alloys (Ag-Cd-In), cross-section change with burnup in reactors, 216-18
In-pile loops, uranium dioxide fuel-assembly testing, 45-8
Instrumentation, BONUS Reactor, 306
comparison of Big Rock Point with Humboldt Bay plant, 81-3
Pathfinder Reactor, 288
period meters, time-constant studies, 51-2
reactor control, 51-3
Insulation (electrical), radiation effects on use in reactor instruments, 52-3
Insulation (thermal), "MinK" compressed-silica material, 326
pressure tubes, 326
Iodine, behavior in large containers, 58
deposition on laboratory surfaces, 57-8
removal from BEPO cooling system, 56
Iodine-131, deposition from gas stream onto surfaces, temperature effects, 371
evolution from irradiated uranium dioxide, 360-2
release during uranium fire, 370-1
Iodine-132, release during uranium fire, 370-1
Iodine-133, release during uranium fire, 370-1
Iodine-134, release during uranium fire, 370-1
Iodine-135, release during uranium fire, 370-1
Ion exchange, *p*H control in Shippingport reactor, 196
Iron, neutron physics effects in fast reactors, 128-33
Iron alloys (Fe-Pu), preparation and testing, 182
Iron alloys (Fe-Pu) (liquid), properties, 182-3
Iron oxides, reactivity effects in ZPR-III assembly, 11
Iron systems (Fe-PuC-UC), fabrication and testing, 183
Irradiation testing, alumina–boron carbide pellets, 367
boron carbide–Zircaloy-2 systems, 367
boron-containing stainless steel, 365-6
fuel assemblies for boiling water reactors, 27-42, 44
fuel elements in Fuel-Cycle Program, 354-5
plutonium alloys, 180-2
plutonium carbide–uranium carbide systems, 176-80
plutonium oxide–uranium oxide systems, 169-78
transition joints of Zircaloy to stainless steel, 368
type 347 stainless steel, by fast neutrons, 187-91
uranium dioxide, 359-63

Irradiation testing (Continued)
Zircaloy-2-clad boron carbide systems, 368
Zircaloy-2–zirconium boride systems, 367

J

Joints
See also Welds
stainless-steel-to-Zircaloy, 401
stainless-steel-to-Zircaloy, preparation by tandem extrusion, 368-9

K

Krypton, release during uranium fire, 370-1

L

Laboratories, iodine deposition on surfaces, 57-8
Large Power Reactor Program, 197
seed-blanket reactor studies, 411, 422-31
LCRE
See Reactors (Lithium-Cooled, Experiment)
Lead alloys (Bi-Pb) (liquid), expansion, reactivity effects in fast reactors, 122
Lead telluride, thermoelectric power unit use, 106
Leak testing, dome-seal tube closures, 380-1
Linings, stainless-steel, use under Zircaloy-2 cladding, 356
Liquid metals
See Metals (liquid) and specific metals, e.g., Bismuth alloys (Bi-Pb) (liquid) and Sodium (liquid)
Lithium, cross-section change with burnup in reactors, 216-18
Lithium (liquid), expansion, reactivity effects in fast reactors, 118-22
LP-1 pump for, 269-72
Lithium-Cooled Reactor Experiment
See Reactors (Lithium-Cooled, Experiment)
Los Alamos Molten-Plutonium Reactor Experiment I
See Reactors (Los Alamos Molten-Plutonium, Experiment I)
LP-1 pump, design, for liquid metals, 269-71
Lubricants, radiation effects on use in reactor instruments, 52-3
Lutetium, cross-section change with burnup in reactors, 216-18

M

Magneform Mark I, swaging of fuel-element cladding to core, 242-3
Magnesite, iodine removal by, 58
Magnesium oxide systems (MgO-PuO_2), fuel-use studies, 169-71
Magnetic-pulse forming machine
See Magneform Mark I
Manganese-55, foils, resonance-capture measurements, 10
Manipulators, for fuel handling, 68
Mass flow, burnout studies of nonuniformly heated channels, 343-52
Materials, 187-91, 365-9
See also specific materials
structural, effects on neutron physics of fast reactors, 128-33
Mathematics, analysis of Doppler effects on neutron-absorption resonance, 329
control-rod withdrawal program for large multiregion reactor, 331-2
reactor noise analysis, 248-63
time-dependent fission-product concentration studies, 215-16
Mechanical properties, boron-containing stainless steel, 365-6
cladding materials, 42
fuel assemblies for boiling-water reactors, 39
hafnium control rods in Shippingport, neutron-exposure effects, 195-6
transition joints of Zircaloy to stainless steel, 368
type 347 stainless steel, fast-neutron effects, 188-91
Melting, uranium dioxide in fuel elements, effects on cladding failure, 46-8
Melting point, uranium dioxide, 362-3
Metals (liquid), pump designs, 372-4
pumps for, 269-71
Methanol, synthesis using reactor heat, economics, 1-3
Milk, expected contamination from released fission products, 370-1
"MinK"
See Insulation (thermal)
ML-1 Reactor
See Reactors (ML-1)
Moderator-level control, 385-99
Moisture separators, 55
Molybdenum, neutron physics effects in fast reactors, 128-33
Molybdenum alloys (Mo-Pd-Pu-Rh-Ru-U-Zr), irradiation testing for use in Experimental Breeder Reactor II, 180-2
Molybdenum alloys (Mo-Pu-U), swelling during irradiation, 181
Molybdenum systems (Mo-PuO_2), preparation, 183
properties, 183

N

Neutron economy, heavy-water reactors, 85-6
Neutrons, age measurements in water, 331
cross sections, Doppler effects in reactors, 329-30
effects, on ductility of Shippingport pressure vessel, 193
on tensile properties of hafnium control rods in Shippingport, 195-6
energy spectra for fast reactors, 108-10
fast, effects on type 347 stainless steel, 187-91
number produced by fission of various elements by 1.5-Mev neutrons, 112
physics, considerations in large fast reactors, 107-34
pulsed-source, criticality studies on plutonium solutions, 5-6
thermal, diffusion parameters, 145-52
thermalization, 331
New Production Reactor
See Reactors (New Production)
Nickel, neutron physics effects in fast reactors, 128-33
reactivity effects in ZPR-III assembly, 11
Nickel alloys (Au-Ni), brazing-alloy use in heat exchanger for Molten-Salt Reactor Experiment, 375
Nickel alloys (Ni-Pu) (liquid), properties, 182-3
Nickel oxides, reactivity effects in ZPR-III assembly, 11
Niobium, neutron-physics effects in fast reactors, 128-33
Niobium systems (Nb-PuC-Zr), properties, 183
Niobium systems (Nb-PuO_2-Zr), properties, 183
Noise, reactor, analysis of, 248-63
NPD Reactor
See Reactors (NPD)
Nuclear Power Demonstration Reactor
See Reactors (NPD)
Nuclear reactions, $^{16}O(n,p)^{16}N$, cross-section measurements, 220

O

O-ring seals, for helium retention in Plutonium Recycle Test Reactor, 381-3
Oils, damping, radiation effects on use in reactor instruments, 52-3
Operating experience, 193-6, 276-312, 385-99
Consolidated Edison Thorium Reactor, 313-15
Experimental Boiling-Water Reactor, 317-20
Heavy-Water Components Test Reactor, 316-17
NPD Reactor, 391-3, 398-9
Plutonium Recycle Test Reactor, 315-16, 386-91, 393-8
Shippingport Pressurized-Water Reactor, 193-6
Organic compounds, radiation effects on use in reactor instruments, 52-3
Organic coolants, effects on zirconium alloys, 324-5
ORGEL Program, 97

P

Palladium alloys (Mo-Pd-Pu-Rh-Ru-U-Zr), irradiation testing for use in Experimental Breeder Reactor II, 180-2
Pathfinder Power Reactor
See Reactors (Pathfinder Power)
Pawling Lattice Test Rig
See Reactors (Pawling Lattice Test Rig)
Period meters, time-constant studies, 51-2
*p*H, control in reactors using boric acid shim in primary coolant, 418-19
control system for Shippingport coolant water, 196
Physical Constants Testing Reactor
See Reactors (Physical Constants Testing)
Physical properties, uranium dioxide, 360, 362-3
uranium dioxide–zirconium dioxide plates, 362
Physics, 4-13, 145-52, 206-20, 329-32
neutron, considerations in large fast reactors, 107-34
Plutonium, recycling in breeder reactors, equilibrium composition of fuel, 127
recycling study for water-moderated reactors, 203-5
thermal breeder reactor studies, 409-11
Plutonium-239, breeding potential in various reactors, 113
critical concentrations of aqueous solutions, 6
fission products, time-dependent concentration studies, 215-16
fission-rate measurements in graphite, 10
fission ratio to ^{235}U in graphite systems, 10
fission-ratio measurements in ZPR-III, 11
neutron capture-to-fission ratio, 111
neutron fission cross sections, 111
neutron production in fission by 1.5-Mev neutrons, 112
Plutonium-239 systems (^{239}Pu-Th), fuel cycle for breeder reactors, 124-6
Plutonium-239 systems (^{239}Pu-^{238}U), critical mass, fast reactor studies, 115
fuel cycle for breeder reactors, 124-6
Plutonium-240, concentration effects on criticality of light-water assemblies, 207-8
fast-fission bonus to breeding in various reactors, 113
fission-ratio measurements in ZPR-III assembly, 11
neutron fission cross sections, 111
neutron production in fission by 1.5-Mev neutrons, 112
Plutonium-241, breeding potential in various reactors, 113
neutron cross sections, Doppler-broadening, 330

Plutonium-241 (Continued)
neutron production in fission by 1.5-Mev neutrons, 112
Plutonium-242, fast-fission bonus to breeding in various reactors, 113
Plutonium alloys, testing, 181-3
Plutonium alloys (Al-Pu), spike enrichment element for Plutonium Recycle Test Reactor, 169, 181
Plutonium alloys (Bi-Pu), preparation and testing, 182
Plutonium alloys (Ce-Co-Pu) (liquid), properties, 182-3
Plutonium alloys (Co-Pu), preparation and testing, 182
Plutonium alloys (Co-Pu) (liquid), properties, 182-3
Plutonium alloys (Fe-Pu), preparation and testing, 182
Plutonium alloys (Fe-Pu) (liquid), properties, 182-3
Plutonium alloys (Mo-Pd-Pu-Rh-Ru-U-Zr), irradiation testing for use in Experimental Breeder Reactor II, 180-2
Plutonium alloys (Mo-Pu-U), swelling during irradiation, 181
Plutonium alloys (Ni-Pu) (liquid), properties, 182-3
Plutonium alloys (Pu-Th), preparation and testing, 182
Plutonium alloys (Pu-U), fuel-cycle studies for water-moderated reactors, 203-5
preparation and testing, 182
Plutonium alloys (Pu-Zr), irradiation testing, 182
Plutonium carbide systems (Fe-PuC-UC), fabrication and testing, 183
Plutonium carbide systems (Nb-PuC-Zr), properties, 183
Plutonium carbide systems (PuC-UC), fabrication, 175-80
properties, 180
Plutonium nitrates, criticality measurements on solutions, 5-6
Plutonium nitride systems (Pu-PuN), properties, 183
Plutonium nitride systems (PuN-W), properties, 183
Plutonium oxide (PuO_2), preparation, 167-9, 174
Plutonium oxide systems (MgO-PuO_2), fuel use studies, 169-71
Plutonium oxide systems (Mo-PuO_2), preparation, 183
properties, 183
Plutonium oxide systems (Nb-PuO_2-Zr), properties, 183
Plutonium oxide systems (PuO_2–stainless steel), preparation, 183
Plutonium oxide systems (PuO_2-UO_2), fuel-element development, 167-75
irradiation testing, 173-5
Plutonium oxide systems (PuO_2-UO_2–stainless steel), fabrication and testing, 183
Plutonium oxide systems (PuO_2-W), properties, 183
Plutonium oxide systems (PuO_2-Zr), properties, 183
Plutonium Recycle Test Reactor
See Reactors (Plutonium Recycle Test)
Plutonium systems (Pu-PuN), properties, 183
Poisons (reactor), BORAX-V critical experiments, 206
boron, incorporation into fuel elements, 356-8
use in experimental fuel assemblies, 34-5
cross-section change with burnup, 216-18
flat-region critical experiment studies, 4-5
reactor control augmentation by, 207
shim elements, for BONUS Reactor, 301-3
for Pathfinder Power Reactor, 282-4
soluble chemical-shim use in primary coolant of pressurized-water reactors, 411-21
Portable power plants
See also Reactors (ML-1)
thermionic type, design, 99-105
Power spectral density, reactor noise-analysis studies, 250-51, 254-55
Pressing, hydrostatic, tubular fuel elements, 237-8
Pressure, control in Pathfinder Reactor, 288
effects on gas-heated steam-generator design, 65
fission gases in uranium dioxide-filled fuel rods, 43-5
Pressure tubes, design for large reactor plant, 402
dome-seal tube-closure design, 379-81
insulation, 326
Pressure vessels, BONUS Reactor, 294-6, 303-6
comparison of Big Rock Point with Humboldt Bay design, 72, 79
Experimental Boiling-Water Reactor, modification for 100-Mw(t) operation, 318
Pathfinder Reactor, 284-8
seed-blanket reactor design, 425-6
Shippingport, neutron-induced embrittlement, 193
thermionic water-cooled reactor, 101, 103
Process Development Pile
See Reactors (Process Development Pile)
Process-heat reactors
See Reactors (process-heat)
Pumps, canned-motor type, costs for pressurized-water reactors, 421
canned type for high-temperature organic liquids, 67-8
electromagnetic, helical-rotor design, 65-8
for liquid metals, 269-71
diaphragm type, 372-3
two-stage centrifugal-displacement type, 372-4
primary coolant, problems in Plutonium Recycle Test Reactor, 315-16
PWL loop, uranium dioxide fuel-assembly testing, 45-8

R

Radiation control, 54-9, 265-7, 370-1
Radiation dose, environmental, from fission product release, 370-1
Radiation effects
See also Irradiation testing
transducer components, 52-3
Radiation protection standards, emergency exposure to released fission products, 371
ML-1 reactor, 218-19
Rapsodie Reactor (France)
See Reactors (Rapsodie) (France)
Reactivity, changes with burnup of poison materials, 216-18
control, in BORAX-V by poison rods, 206
by chemical shim in primary coolant of pressurized-water reactors, 411-21
control in Pathfinder Reactor, 288
effects of Doppler broadening of neutron-absorption resonance, 329
long-term effects in fast reactors, 116-17
Plutonium Recycle Test Reactor, moderator-level effects, 394-6
shutdown, determination by reactor noise analysis, 254-6
Reactivity coefficients, Consolidated Edison Thorium Reactor, 314-15
fast-reactor safety studies, 118-24
NPD Reactor, design vs. measured values, 398
Reactivity lifetime, plutonium-uranium mixtures in water-moderated reactors, 203-5
Reactivity parameters, fertile materials, 112
fissile materials, 112
Reactor control
See Control-rod drives, Control rods, and Control systems
Reactors
See also Critical assemblies
noise analysis, 248-63
Reactors (BEPO), iodine removal from cooling system, 56
Reactors (Big Rock Point Power), design comparison with Humboldt Bay Power Reactor, 70-84
High-Power-Density Development Project, 34-44
Reactors (boiling-superheater)
See also Reactors (BONUS) and Reactors (Pathfinder Power)
annular multitube fuel-element development, 241-2
Reactors (boiling water)
See also Reactors (BONUS), Reactors (BORAX), Reactors (Experimental Boiling-Water), Reactors (Halden Boiling-Water), Reactors (Humboldt Bay Power), Reactors (Pathfinder Power), Reactors SENN), and Reactors (Vallecitos Boiling-Water)
burnout limits, 14-26
comparison of Big Rock Point with Humboldt Bay design, 70-84
critical experiments, 206-7
fuel-assembly fabrication and testing, 27-44
uranium oxide fuel-life studies, 27-34
void-content measurements, 7
Reactors (BONUS), construction, 292-309
critical experiments, 5
design, 292-309
design comparison with Pathfinder Reactor, 310-12
Reactors (BORAX-II), chemical-shim use in primary coolant, 411
Reactors (BORAX-III), chemical-shim use in primary coolant, 411
Reactors (BORAX-V), critical experiments, 206
exponential experiment, void-distribution studies, 7
Reactors (breeder)
See also Reactors (converter), Reactors (Dounreay Fast-Breeder), Reactors (Enrico Fermi Fast-Breeder), Reactors (Experimental Breeder, II), and Reactors (seed-blanket)
breeding potential of various fissile isotopes, 113
fuel cycle, 124-6
fuel recycling, 127
heavy-water thorium-^{233}U system, 406-11
heavy-water uranium-plutonium system, 406-11
water desalinization by, 38-9, 141
Reactors (CANDU) (Canada), design, 89-92
dome-seal tube-closure design, 379-81
fuel cycle, 202-4
iodine removal in, 58
moderator-level control, 399
Reactors (Carolinas-Virginia Tube), power cost estimates, 86-7, 89
pressure-tube design, 326
prototype of large-reactor plant, 401-5
Reactors (Consolidated Edison Thorium), operating experience, 313-15
Reactors (converter), seed-blanket design studies, 197-8, 422-31
Reactors (Dounreay Fast-Breeder), noise analysis, 260-1
Reactors (Enrico Fermi Fast-Breeder), breeding potential of various fissile isotopes, 113
core B mockup studies in ZPR-III assembly, 11

Reactors (Experimental Boiling-Water), chemical-shim use in primary coolant, 411
operating experience at 100 Mw(t), 317-20
plutonium-bearing core fabrication, 172
Reactors (Experimental Breeder, II), breeding potential of various fissile isotopes, 113
Reactors (Experimental Gas-Cooled), control-rod design, 376-7, 378
lattice studies using Physical Constants Testing Reactor, 210
Reactors (Experimental Organic-Cooled), canned-pump development, 67-8
pressure-balanced control rod, 274
Reactors (fast)
See also Reactors (Dounreay Fast-Breeder), Reactors (Enrico Fermi Fast-Breeder), Reactors (Experimental Breeder, II), and Reactors (Los Alamos Molten-Plutonium, Experiment I)
breeding potential of various fissile isotopes, 113
critical mass, 114-16
neutron-balance studies, 113
neutron physics, 107-34
safety characteristics, 117-24
water desalinization by, 138-9, 141
Reactors (gas-cooled)
See Reactors (Experimental Gas-Cooled), Reactors (ML-1), and Reactors (ZENITH)
Reactors (General Electric Test), plutonium oxide—uranium oxide fuel irradiations, 173-5
uranium dioxide fuel-assembly testing, 45-8
Reactors (Halden Boiling-Water), noise measurements, 260
Reactors (heavy-water)
See also Reactors (CANDU), Reactors (Carolinas-Virginia Tube), Reactors (Heavy-Water Components Test), Reactors (NPD), Reactors (organic-cooled heavy-water-moderated), Reactors (Plutonium Recycle Test), Reactors (Process Development Pile), Reactors (Spectral Shift Control), Reactors (Whiteshell, No. 1)(WR-1), and Reactors (Zero Energy Experimental Pile)
large-plant designs, 401-11
review of recent developments, 85-97
Tripartite Organic-Cooled Heavy-Water Reactor Meeting, 324
water desalinization by, 87, 139-41
Reactors (Heavy-Water Components Test), drive problems for control and safety rods, 316-17
Reactors (heavy-water-moderated organic-cooled)
See Reactors (organic-cooled heavy-water water-moderated)
Reactors (High-Temperature Gas-Cooled Reactor Experiment)
See Reactors (ZENITH)
Reactors (Humboldt Bay Power), design comparison with Big Rock Point Power Reactor, 70-84
Reactors (liquid-metal-fuel), fuel-alloy studies, 182-3
Reactors (Lithium-Cooled, Experiment), auxiliary systems design, 384
Reactors (Los Alamos Molten-Plutonium, Experiment I), fuel-alloy studies, 182-3
Reactors (ML-1), shield design, 218-20
Reactors (Molten-Salt, Experiment), heat exchanger, design and fabrication, 374-5
Reactors (New Production), maximum credible accident, 267
vented-containment concept, 265-7
Reactors (NPD), moderator-level control, 391-3
operating experience with moderator-level control, 398-9
power cost estimates, 86-7, 89
Reactors (N.S. *Savannah*), evaluation of a Zircaloy core structure, 322-4
Reactors (organic-cooled)
See also Reactors (Whiteshell, No. 1) (WR-1)
Tripartite Organic-Cooled Heavy-Water Reactor Meeting, 324
Reactors (organic-cooled heavy-water-moderated)
See also Reactors (Whiteshell, No. 1) (WR-1)
design, 95-7
large-plant design, 405-6, 407, 408
Reactor (Pathfinder Power), boron control-rod design, 365-7
construction, 276-92
control-rod-drive design, 274-5
design, 276-92
design comparison with BONUS Reactor, 310-12
fuel-rod end-closure development, 245-6
lattice experiments for second-generation core, 6-7
recirculation-piping design, 384
Reactors (Pawling Lattice Test Rig), heavy-water lattice measurements, 213
Reactors (Physical Constants Testing), critical experiments, 4-5, 6
heavy-water lattice measurements, 213
lattice studies of Experimental Gas-Cooled Reactor, 210
Reactors (Plutonium Recycle Test), coolant flow-rate determination, 383
dome type nozzle seals, 379
fuel elements, 167-73
moderator-level control, 385-91
operating experience with moderator-level control, 393-8
primary coolant pump problems, 315-16
Reactors (pressure-tube)
See also Reactors (CANDU), Reactors (Carolinas-Virginia Tube), Reactors (New Production), Reactors (Plutonium Recycle Test), and Reactors (Whiteshell, No. 1) (WR-1)
component design, 379-83
large-plant design, 401-5
Reactors (pressurized-water)
See also Reactors (N.S. *Savannah*), Reactors (Saxton Power), Reactors (Shippingport Pressurized-Water), Reactors (Spectral Shift Control), Reactors (SPERT), and Reactors (Yankee Power)
chemical-shim use in coolant system, 411-21
Large Power Reactor Program, 422-31
natural-circulation startup studies, 421-2
Reactors (Process Development Pile), buckling-measurement studies of heavy-water lattices, 212-13
Reactors (process-heat), costs of heavy-water type, 87
solid-fuel gasification, economics, 1-3
Reactors (Rapsodie)(France), fuel-element development, 167-9, 181
Reactors (Saxton Power), operation with boric acid shim in primary coolant system, 420-1
Reactors (seed-blanket), economic comparison with other water-cooled reactors, 429-30
Large Power Reactor Program, design studies, 422-31
Reactors (SENN) (Italy), partial-reloading scheme, 201-2
Reactors (Shippingport Pressurized-Water), core 2 design, 197-200
operating experience over past five years, 193-6
Reactors (sodium-cooled), throttle-valve design, 271
Reactors (Sodium, Experiment), safety rod drop-time experiments, 377, 379
Reactors (Spectral Shift Control), critical experiments, 8
economic comparison with other water-cooled reactors, 429-30
lattice measurements, 212
Reactors (SPERT), Doppler broadening of neutron-absorption resonance, 329
Reactors (superheater)
See also Reactors (boiling-superheater), Reactors (BONUS), Reactors (Consolidated Edison Thorium), and Reactors (Pathfinder Power)
design problems, 310-12
Reactors (thermionic, water-cooled), design, 99-105
Reactors (University of Florida Training), noise-analysis studies, 253-4
Reactors (Vallecitos Boiling-Water), fuel-assembly testing, 27-38
Fuel-Cycle Program for fuel-element irradiation testing, 354-5, 356
Reactors (water-cooled, thermionic)
See Reactors (thermionic, water-cooled)
Reactors (Whiteshell, No. 1)(WR-1), 97
design, 324-5
pressure-tube design, 326
Reactors (Yankee Power), chemical-shim use in primary coolant, 411
Reactors (ZENITH), reactivity, temperature coefficient studies, 9
Reactors (Zero Energy Experimental Pile), heavy-water lattice measurements, 213
Recirculation system, BONUS Reactor, 306-7
Pathfinder Reactor, 288-9, 384
Recycling, plutonium, equilibrium composition of fuel, 127
Refueling, bidirectional method for CANDU Reactor, 202-4
large heavy-water pressure-tube reactor, 401-2
partial-reloading scheme for SENN reactor, 201-2
Resonance integral, fertile isotopes, 214-15
Rhenium alloys (Mo-Pd-Pu-Rh-Ru-U-Zr), irradiation testing for use in Experimental Breeder Reactor II, 180-2
Rejuvenation, fuel elements without reprocessing, 172-3
Reliability, servomechanisms, 53
Ruthenium-106, deposition from gas stream onto surfaces, temperature effects, 371
emission from irradiated uranium dioxide, 361
release during uranium fire, 370-1
Ruthenium alloys (Mo-Pd-Pu-Rh-Ru-U-Zr), irradiation testing for use in Experimental Breeder Reactor II, 180-2

S

Safety
See also Containment and Control systems
comparison of Big Rock Point with Humboldt Bay plant, 79, 81-4
fast reactors, 117-24
Shippingport shutdown record over past five years, 195
Safety rods, Sodium Reactor Experiment, drop-time measurements, 377, 379
Saline water
See Water (saline)
Samarium, cross-section change with burnup in reactors, 216-18
Santowax, pump development for, 67-8
SAP
See Sintered aluminum powder
Savannah River Plant, ventilation-filtering systems, 55
Scrubbers, iodine removal by, 57-8

Seals, distortion in coolant pumps of Plutonium Recycle Test Reactor, 315-16
dome type for pressure-tube closure, 379-81
for helium retention in Plutonium Recycle Test Reactor, 381-3
for liquid-metal pumps, 269-70
Seed-blanket reactors
See Reactors (seed-blanket)
Seed-blankets, Shippingport core 2 design, 197-8
SEF
See Steam-energy flow
SENN Reactor (Italy)
See Reactors (SENN) (Italy)
Servomechanisms, reliability studies, 53
Shielding, geometrical attenuation factors, 220
ML-1 Reactor, 218-20
^{16}N activity studies, 220
Shutdown reactivity, determination by reactor noise analysis, 254-6
Shutdowns, effects of Doppler broadening of neutron-absorption resonance, 329
six-month operating history of Consolidated Edison Thorium Reactor, 313
Silica, thermal-insulation use for pressure tubes, 326
Silicon carbide systems (B_4C-SiC), corrosion, 367-8
Silicon carbide systems (B_4C-SiC)(Zircaloy-2-clad), irradiation testing, 368
Silver, cross-section change with burnup in reactors, 216-18
Silver alloys (Ag-Cd-In), cross-section change with burnup in reactors, 216-18
Sintered aluminum powder, cladding use in organic-cooled heavy-water-moderated reactor design, 405
compatibility with organic coolants, 95
fuel-element cladding, 242
in WR-1 reactor, 324-5
Siting, 265-7, 370-1
Skin, radiation dose from released fission products, 370-1
Sodium, reactivity effects in ZPR-III assembly, 11
Sodium (liquid), expansion, reactivity effects in fast reactors, 118-22
throttle valves for, 271
Sodium void coefficient, effects of structural materials in fast reactors, 131-3
reactivity effects in fast reactors, 118-22
Space power units, design of thermoelectric type, 106
Special Power Excursion Reactor Test
See Reactors (SPERT)
Spectral Shift Control Reactor
See Reactors (Spectral Shift Control)
SPERT Reactor
See Reactors (SPERT)
Sprays, water, iodine removal from air by, 56-7
Stack disposal, BONUS Reactor, 309
Pathfinder Reactor, 292
Stainless-steel systems (B_4C—stainless steel), corrosion testing, 367
Stainless-steel systems (PuO_2—stainless steel), preparation, 183
Stainless-steel systems (PuO_2-UO_2—stainless steel), fabrication and testing, 183
Stainless steels, joining to Zircaloy, 401
by tandem extrusion, 368-9
uranium and plutonium solutions, 5-6
reactivity effects in ZPR-III assembly, 11
Stainless steels (304), cladding of fuel assemblies for boiling-water reactors, 27-34
cladding of fuel elements, failure by cracking in Vallecitos Boiling-Water Reactor tests, 354-5
ultrasonic inspection of tubing, 246
Stainless steels (304L), boron-containing, control rod use in Pathfinder Power Reactor, 365-6
boron-containing, mechanical properties after irradiation, 366-7
lining of Zircaloy-2-clad fuel elements for corrosion protection, 356
ultrasonic inspection tubing, 246
Stainless steels (316), ultrasonic inspection of tubing, 246
Stainless steels (347), fast-neutron irradiation effects, 187-91
Statistics, reactor noise analysis, 248-63
Steam, separation from water in superheater reactors, 310
Steam-energy flow, burnout-limit studies, 18-26
burnout studies of nonuniformly heated channels, 343-52
comparison of Russian and U. S. data, 225-35
DNB-2 curve significance, 335-43
multirod test-section data, 156-65
Steam generators, comparison of Big Rock Point with Humboldt Bay plant, 79-81
gas-heated types, 64-5
sodium-heated types, 60-4
Steam systems (steam-water), burnout studies, 335-52
Steel systems (B_4C-steel), corrosion testing, 367
Stress analysis, reinforced-concrete buildings, 54-5
Strontium-89, emission from irradiated uranium dioxide, 361
release during uranium fire, 370-1
Strontium-90, release during uranium fire, 470-1
Structural materials
See Materials and specific materials, e.g., Stainless steels
Superheater reactors
See Reactors (superheater)
Surfaces, laboratory, iodine-deposition studies, 57-8
Surge suppressors, for flowmeter sensing lines in Plutonium Recycle Test Reactor, 383
Swaging, fuel-element fabrication, 243-5
magnetic technique for fuel-element cladding-to-core bonding, 242-3
Swelling, boron-containing stainless steels during irradiation, 366-7
cladding materials, effects of uranium dioxide core melting, 46-8
Switches (electrical), problems of control-rod drive, in Consolidated Edison Thorium Reactor, 314

T

Tandem extrusions, stainless-steel-to-Zircaloy transition-joint preparation, 368-9
Tantalum, neutron-physics effects in fast reactors, 128-33
Tellurium-132, deposition from gas stream onto surfaces, temperature effects, 371
evolution from irradiated uranium dioxide, 360-2
release during uranium fire, 370-1
Temperature, effects on fission-product deposition onto surfaces, 371
effects on gas-heated steam-generator design, 65
thermionic emitters, effects on conversion efficiency, 105
uranium dioxide fuel-elements effects on exposure lifetime in Shippingport core 2, 199
Tensile strength, boron-containing stainless steel, 365-6
hafnium control rods in Shippingport, neutron-exposure effects, 195-6
type 347 stainless steel, fast-neutron effects, 188-91
Thermal conductivity, plutonium carbide—uranium carbide fuel materials, 180-1
uranium dioxide, temperature effects, 48
Thermal insulation
See Insulation (thermal)
Thermionic conversion, 99-106
See also Reactors (thermionic, water-cooled)
efficiency, effects of emitter temperature, 105
Thermoelectric power units, design for space application, 106
Thorium, absorption cross section, 10
cadmium ratio, ZPR-VII experiments, 8
converter-reactor studies, 422-31
fast-fission bonus to breeding in various reactors, 113
neutron production in fission by 1.5-Mev neutrons, 112
resonance-capture measurements in Peach Bottom Critical Assembly, 10
thermal breeder reactor studies, 406-10
Thorium-232, foils, resonance-capture measurements, 10
neutron fission cross sections, 111
resonance integral, 214-15
Thorium alloys (Pu-Th), preparation and testing, 182
Thorium-232 oxide, resonance integral, 214-15
Thorium Systems (^{239}Pu-Th), fuel cycle for breeder reactors, 124-6
Thorium systems (Th-^{233}U), critical mass, fast reactor studies, 115
fuel cycle for breeder reactors, 124-6
Thorium systems (Th-^{235}U), critical mass, fast reactor studies, 115
fuel cycle for breeder reactors, 124-6
Throttle valves, for sodium-cooled reactors, 271
Thulium, cross-section change with burnup in reactors, 216-18
Titanium, neutron-physics effects in fast reactors, 128-33
Trail Cable facility, uranium dioxide fuel-rod testing, 46-8
Transducers, fission-gas pressure determination in fuel rods, 43-5
limitations in nuclear reactor applications, 52-3
Transfer functions, reactor noise-analysis studies, 251-2
Tungsten systems (PuN-W), properties, 183
Tungsten systems (PuO_2-W), properties, 183
Turbines, BONUS Reactor, 307
comparison of Big Rock Point with Humboldt Bay plant, 79-81
Pathfinder Reactor, 289-90
radioactive contamination problems in superheater reactors, 310
Tubing, stainless-steel, ultrasonic inspection, 246

U

Ultrasonic testing, stainless-steel tubing, 246
United States of America, comparison with Canada in heavy-water reactor development, 87-95
University of Florida Training Reactor
See Reactors (University of Florida Training)
Uranium, converter-reactor studies, 422-31
emission from irradiated uranium dioxide, 301
Uranium-233, breeding potential in various reactors, 113
fission-rate measurements in graphite, 10
fission ratio to ^{235}U in graphite systems, 10
fission-ratio measurements in ZPR-III assembly, 11

Uranium-233 (Continued)
neutron capture-to-fission ratio, 111
neutron fission cross sections, 111
neutron production in fission by 1.5-Mev neutrons, 112
thermoelectric power supply studies, 106
Uranium-233 systems (Th-^{233}U), critical mass, fast reactor studies, 115
fuel cycle for breeder reactors, 124-6
Uranium-233 systems (^{233}U-^{238}U), fuel cycle for breeder reactors, 124-6
Uranium-234, fission-ratio measurements in ZPR-III assembly, 11
Uranium-235, breeding potential in various reactors, 113
cadmium ratio, ZPR-VII experiments, 8
critical concentrations of aqueous solutions, 6
fission products, time-dependent concentration studies, 215-16
fission-rate measurements in graphite, 10
fission ratio, to ^{239}Pu in graphite systems, 10
to ^{233}U in graphite systems, 10
to ^{238}U in heavy-water systems, 7
neutron capture-to-fission ratio, 111
neutron fission cross sections, 111
neutron production in fission by 1.5-Mev neutrons, 112
Uranium-235 systems (Th-^{235}U), critical mass, fast reactor studies, 115
fuel cycle for breeder reactors, 124-6
Uranium-235 systems (^{235}U-^{238}U), critical mass, fast reactor studies, 115
fuel cycle for breeder reactors, 124-6
Uranium-236, fission-ratio measurements in ZPR-III, 11
Uranium-238, cadmium ratio in heavy-water systems, 7
fast-fission bonus to breeding in various reactors, 113
fission ratio to ^{235}U in heavy-water systems, 7
fission-ratio measurements in ZPR-III assembly, 11
neutron capture cross sections, 111-12
neutron fission cross sections, 111
neutron production in fission by 1.5-Mev neutrons, 112
resonance integral, 214-15
Uranium-238 systems (Pu-^{238}U), fuel cycle for breeder reactors, 124-6
Uranium-238 systems (^{238}Pu-^{238}U), critical mass, fast reactor studies, 115
Uranium-238 systems (^{233}U-^{238}U), fuel cycle for breeder reactors, 124-6
Uranium-238 systems (^{235}U-^{238}U), critical mass, fast reactor studies, 115
fuel cycle for breeder reactors, 124-6
Uranium alloys (Mo-Pd-Pu-Rh-Ru-U-Zr), irradiation testing for use in Experimental Breeder Reactor II, 180-2
Uranium alloys (Mo-Pu-U), swelling during irradiation, 181
Uranium alloys (Pu-U), fuel-cycle studies for water-moderated reactors, 203-5
preparation and testing, 182
Uranium carbide systems (Fe-PuC-UC), fabrication and testing, 183
Uranium carbide systems (PuC-UC), fabrication, 175-80
properties, 180
Uranium oxide, irradiation testing, 359-63
Uranium oxide (UO_2), blanket fuel-element use in Shippingport core 2, 197-8
boron incorporation for burnable poison use, 357-8
expansion during melting, effects on swelling of cladding, 46-8
fuel-element development programs, 27-50
physical properties, 360, 362-3
plates, fission-product diffusion coefficients, 362
preparation, 167-9, 174
resonance integral for ^{238}U oxide, 214-15
thermal conductivity, temperature effects, 48
vibratory compaction in fuel-element fabrication, 237-42
Uranium oxide systems (PuO_2-UO_2), fuel-element development, 167-75
irradiation testing, 173-5
Uranium oxide systems (PuO_2-UO_2–stainless steel), fabrication and testing, 183
Uranium oxide systems (UO_2-ZrO_2), physical properties of plates, 362
plates, fission-product diffusion coefficients, 362
seed fuel-element use in Shippingport core 2, 197-8
Uranyl fluorides, critical concentrations of solutions, 6

V

Vallecitos Boiling-Water Reactor
See Reactors (Vallecitos Boiling-Water)
Valves, dump type, for moderator in Plutonium Recycle Test Reactor, 389
butterfly type, cavitation tests, 68
throttle, for sodium-cooled reactors, 271
for venting pressure from New Production Reactor containment building, 265-7
Vanadium, foils, resonance-capture measurements, 10
neutron-physics effects in fast reactors, 128-33
subtraction technique for resonance-capture measurements, 10
Vibration, coolant pumps of Plutonium Recycle Test Reactor, 315-16
Vibratory compaction, annular multitube fuel elements, 241-2
uranium dioxide fuel rods, 238-41

W

Washers, Belleville-spring type, use in dome-seal tube closures, 380-1
Waste handling and disposal
See also Stack disposal
BONUS Reactor, 309
comparison of Big Rock Point with Humboldt Bay Plant, 83-4
Pathfinder Reactor, 292
Water, corrosive effects on boron carbide systems, 367-8
iodine removal from air by sprays, 56-7
neutron-diffusion parameters in, 146-50
quality control in reactors using chemical shim in primary coolant, 418-21
separation from steam in superheater reactors, 310
Shippingport reactor, *p*H and quality control, 196
Water (D_2O), criticality studies on slightly enriched fuel rods, 7
inventory charges for large-reactor designs, 405
neutron-diffusion parameters in, 151
Water (saline), distillation, heavy-water reactor cost studies, 87
by reactors, economic studies, 138-44
Water systems (D_2O-H_2O), criticality studies on slightly enriched fuel rods, 7
Water systems (steam-water), burnout studies, 335-52
Welding, electron-beam technique for fuel-element components, 358-9
heat exchanger for Molten-Salt Reactor Experiment, 374-5
Welds, corrosion of Shippingport control-rod assemblies, 196
Whiteshell Reactor No. 1
See Reactors (Whiteshell, No. 1)(WR-1)
Windscale accident, fission-product dispersal, 370-1
Wood, shielding use during ML-1 Reactor operation, 219-20
WR-1 Test Reactor
See Reactors (Whiteshell, No. 1)(WR-1)

X

Xenon, release during uranium fire, 370-1
Xenon-133, evolution from irradiated uranium dioxide, 359-62

Y

Yield strength, boron-containing stainless steel, 365-6
cladding materials, 42
fuel assemblies for boiling-water reactors, 39
hafnium control rods in Shippingport, neutron-exposure effects, 195-6
type 347 stainless steel, fast-neutron effects, 188-91
Ytterbium, cross-section change with burnup in reactors, 216-18

Z

ZENITH Reactor
See Reactors (ZENITH)
Zircaloy, evaluation for core structure of N.S. *Savannah* Reactor, 322-4
joining to stainless steel, 401
by tandem extrusion, 368-9
Zircaloy-2, cladding of fuel assemblies for boiling-water reactors, 27-34
cladding use for boron carbide systems, 368
corrosion due to fluoride ion, 356
electron-beam welding, 359
Zircaloy-2 systems (B_4C-Zircaloy-2), irradiation testing, 367
Zircaloy-2 systems (Zircaloy-2-ZrB_2), irradiation testing, 367
Zircaloy-4, cladding of fuel assemblies for boiling-water reactors, 27-34
cladding use for Shippingport core 2 fuel elements, 197
compatibility with organic coolants, 95
neutron-physics effects in fast reactors, 128-33
nuclear data, 331
Zirconium-95, deposition from gas stream onto surfaces, temperature effects, 371
Zirconium alloys, organic-coolant effects, 324-5
Zirconium alloys (Mo-Pd-Pu-Rh-Ru-U-Zr), irradiation testing for use in Experimental Breeder Reactor II, 180-2
Zirconium alloys (Pu-Zr), irradiation testing, 182
Zirconium boride systems (Zircaloy-2–ZrB_2), irradiation testing, 367
Zirconium hydride, moderator for critical assemblies, 212
Zirconium oxide systems (UO_2-ZrO_2), physical properties of plates, 362
plates, fission-product diffusion coefficients, 362
seed fuel-element use in Shippingport core 2, 197-8
Zirconium systems (Nb-PuC-Zr), properties, 183
Zirconium systems (Nb-PuO_2-Zr), properties, 183
Zirconium systems (PuO_2-Zr), properties, 183
ZPR-III Critical Assembly
See Critical assemblies (ZPR-III)
ZPR-VII Critical Assembly
See Critical assemblies (ZPR-VII)

LEGAL NOTICE

This journal was prepared under the sponsorship of the U. S. Atomic Energy Commission. Neither the United States, nor the Commission, nor any person acting on behalf of the Commission:

A. Makes any warranty or representation, expressed or implied, with respect to the accuracy, completeness, or usefulness of the information contained in this journal, or that the use of any information, apparatus, method, or process disclosed in this journal may not infringe privately owned rights; or

B. Assumes any liabilities with respect to the use of, or for damages resulting from the use of any information, apparatus, method, or process disclosed in this journal.

As used in the above, "person acting on behalf of the Commission" includes any employee or contractor of the Commission, or employee of such contractor, to the extent that such employee or contractor of the Commission, or employee of such contractor prepares, disseminates, or provides access to, any information pursuant to his employment or contract with the Commission, or his employment with such contractor.

NUCLEAR SCIENCE ABSTRACTS

The U. S. Atomic Energy Commission, Division of Technical Information, publishes *Nuclear Science Abstracts (NSA),* a semimonthly journal containing abstracts of the literature of nuclear science and engineering.

NSA covers (1) research reports of the U. S. Atomic Energy Commission and its contractors; (2) research reports of government agencies, universities, and industrial research organizations on a world-wide basis; and (3) translations, patents, books, and articles appearing in technical and scientific journals.

Complete indexes covering subject, author, source, and report number are included in each issue. These are cumulated quarterly, semiannually, and annually providing a detailed and convenient key to the literature.

Availability of *NSA*

SALE *NSA* is available on subscription from the Superintendent of Documents, U. S. Government Printing Office, Washington, D. C., 20402, at $30.00 per year for the semimonthly abstract issues and $22.00 per year for the four cumulated-index issues. Subscriptions are postpaid within the United States, Canada, Mexico, and all Central and South American countries, except Argentina, Brazil, British and French Guiana, Surinam, and British Honduras. Subscribers in these Central and South American countries, and in all other countries throughout the world, should remit $37.00 per year for subscriptions to semimonthly abstract issues and $25.00 per year for the four cumulated-index issues.

EXCHANGE *NSA* is also available on an exchange basis to universities, research institutions, industrial firms, and publishers of scientific information. Inquiries should be directed to the Division of Technical Information Extension, U. S. Atomic Energy Commission, P. O. Box 62, Oak Ridge, Tennessee, 37831.

TECHNICAL PROGRESS REVIEWS may be purchased from Superintendent of Documents, U. S. Government Printing Office, Washington, D. C., 20402. *Isotopes and Radiation Technology* at $2.00 per year for each subscription or $0.55 per issue; the other four journals at $2.50 per year and $0.70 per issue. The use of the coupon below will facilitate the handling of your order.

POSTAGE AND REMITTANCE: Postpaid within the United States, Canada, Mexico, and all Central and South American countries except as hereinafter noted. Add $0.50 per year, or $0.15 per single issue for the *Isotopes and Radiation Technology* journal and $0.75 per year or $0.20 per single issue for the other four journals for postage to all other countries, including Argentina, Brazil, British and French Guiana, Surinam, and British Honduras. Payment should be by check, money order, or document coupons, and MUST accompany order. Remittances from foreign countries should be made by international money order, or draft on an American bank, payable to the Superintendent of Documents, or by UNESCO book coupons.

order form

SUPERINTENDENT OF DOCUMENTS
U. S. GOVERNMENT PRINTING OFFICE
WASHINGTON , D. C., 20402

Enclosed:
document coupons ☐ check ☐ money order ☐

Charge to Superintendent of Documents No._____

Please send a one-year subscription to

☐ NUCLEAR SAFETY

☐ POWER REACTOR TECHNOLOGY

☐ REACTOR FUEL PROCESSING

☐ REACTOR MATERIALS

(Each subscription $2.50 per year; $0.70 per issue.)

☐ ISOTOPES AND RADIATION TECHNOLOGY

(Each subscription $2.00 a year; $0.55 per issue.)

SUPERINTENDENT OF DOCUMENTS
U. S. GOVERNMENT PRINTING OFFICE
WASHINGTON, D. C., 20402

(Print clearly)

Name _____

Street _____

City _____ Zone ____ State _____